Z4-codes and their gray map images as orthogonal arrays and t-designs

Kusuma, Josephine

Mechanisms of Interlaminar Fracture Toughness Using Non-Woven Veils as Interleaf Materials

by
Manabu Kuwata

Queen Mary, University of London

School of Engineering and Material Science
Department of Materials

A thesis submitted for the degree of Doctor of Philosophy

2010 February

Dedicated to my parents,

Junji and Taeko

両親へ

淳二および多恵子

座右の銘

エキスパートとは、ごく限られた分野で、
ありとあらゆる間違いをすべて経験した人物である。
Niels Henrik David Bohr (1895-1961)

Abstract

The main objective of this research is to understand the mechanisms of interlaminar toughness using non-woven veils as the interleaf materials. The vacuum assisted resin transfer moulding (VaRTM) method was chosen for making specimens. Several types of non-woven veils were used as the toughening materials, because the non-woven veil was expected for good resin permeability. Three types of carbon fabrics, (plain, 5-harness satin, and unidirectional) and two types of resins (epoxy and vinyl ester) were selected for base materials.

Firstly, the Mode-I and Mode-II interlaminar toughness tests, which are double cantilever beam (DCB) and four-point end notched flexure (4ENF) tests, were carried out to evaluate the effect of toughening by the interleaf veils. The mechanisms of the improvement by the interleaf veils were evaluated by microscopy. The adhesion between veil fibres and matrix is an important factor of the improvement of the interlaminar toughness. If veil fibres have poor adhesion to resin, these fibres would be pulled out from the matrix and work as fibre-bridging. In contrast, good adhesion of veil fibres is not necessary improvement of the interlaminar fracture toughness. Because these fibres are embedded in the matrix and interleaf veil cannot contribute to suppression of the crack propagation.

The second stage of experiments was impact and compression after impact (CAI) tests. In this stage, the base materials were plain weave fabric only. Impact damage was evaluated using ultrasonic C-scan. The polyamide veils interleaved samples had superior impact and CAI resistance properties in all interleaved materials.

In the final stage, correlation between each mechanical property was analysed and discussed. It was found that the relationship between each fracture toughness is affected by fabric and resin. Moreover, this work and previous literature data were compared. It can be found that the non-woven veils are effective toughening materials.

Acknowledgments

This work was carried out at Queen Mary, University of London, Department of Materials.

A number of people offered their support to make the project a success. I would like to express my thanks to my supervisors, Professor Paul J. Hogg and Professor Ton Peijs for their useful comments, suggestions and encouragement.

I am very grateful to Cytec, Saint-Gobain Technical Fabrics, Carr Resinforcement Limited, Advanced Composite Group, Reichhold, Technical Fibre Products, and Japan Vilene for supplying materials for this research.

Many thanks also to Mr. Colin Langdown, Mr. Bill Godwin, Dr. Zofia Luklinska, Mr. Mick Willis, and Dr. Silvano C. Savona, for their support for experiment, advice, and help, and Dr. Ali Ahmadnia for his kind support and help at Brunel University.

Thanks also to my composite group colleagues for their supports and light conversations, in particular Alan, Chi, Harish, Vimal, and Doris.

Finally, I would like to thank my parents, Junji, Taeko, and younger brother, Masashi, for their support and encouragement.

Contents

List of Figures

Chapter 1

Chapter 2

Chapter 3

Chapter 4

Chapter 5

Chapter 6

Appendix A

Appendix B

Appendix C

List of Tables

Chapter 2

Chapter 3

Chapter 4

Chapter 5

Chapter 6

Appendix A

Appendix B

Nomenclature

Abbreviations

2-D : Two dimension
3-D : Three dimension
3ENF : Three-point end notched flexure
4ENF : Four-point end notched flexure
ACM : Advanced composite material
ADCB : Asymmetric double cantilever beam
BMI : Bismaleimide
CAI : Compression after impact
CC : Compliance calibration
CFRP : Carbon fibre reinforced plastic
CLS : Crack lap shear
CRS : Crack rail shear
DCB : Double cantilever beam
ECT : Edge crack torsion
EDT : Edge delamination torsion
ELS : End loaded slide
ENF : End-notched flexure
FRP : Fibre reinforced plastic
FRTP : Fibre reinforced thermo-plastic
GFRP : Glass fibre reinforced plastic
HBP : Hyperbranchedpolymer
MBT : Modified beam theory
MCC : Modified compliance calibration
MMB : Mixed-mode bending
NDI : Non-destructive identification
PA : Polyamide
PE : Polyester
PE/C : Polyester/Carbon
PEEK : Poly(ether ether ketone)
PEI : Polyetherimide
PES : Polyethersulphone
PI : Polyimide

PP : Polypropylene
PPE : Poly(2,6-dymethyl-1,4-phenylene ether)
PU : Polyurethane
PVAL : Polyvinyl alcohol
RTM : Resin transfer moulding
SCB : Split cantilever beam
SENF : Stabilised end-notched flexure
SEM : Scanning electron microscope
UD : Unidirectional
UP : Unsaturated polyester
VaRTM : Vacuum assisted resin transfer moulding
VE : Vinyl ester

Symbol

a : Delamination length
A_1 : Coefficient for MCC method
B : Specimen width
c : Lever length of the MMB test apparatus
C : Compliance
E : Flexural modulus
F : Correction for large displacement for 3ENF test
G_{IC} : Mode-I critical energy release rate
$G_{IC\text{-}NL}$: Mode-I initial energy release rate at non-linear point
$G_{IC\text{-}5\%/MAX}$: Mode-I initial energy release rate at 5% offset or Maximum load point
$G_{I\text{-}prop}$: Mode-I propagation energy release rate
G_{IIC} : Mode-II critical energy release rate
$G_{IIC\text{-}NL}$: Mode-II initial energy release rate at non-linear point
$G_{IIC\text{-}5\%/MAX}$: Mode-II initial energy release rate at 5% offset or Maximum load point
$G_{II\text{-}prop}$: Mode-II propagation energy release rate
G_{IIIC} : Mode-III critical energy release rate
h : Thickness of specimen
I : Second moment of area
L : Length of specimen
n : Coefficient for CC method
N : Correction for end block for 3ENF test
P : Load

P_C : Critical load

U : Total kinetic energy or impact energy

V_f : Volume fraction

γ : Shear strain

δ : Load point deflection

Δ : Coefficient for MBT method

Chapter 1

Introduction

1.1 What are Composites?

Composites have a very long history. In ancient Babylon, bitumen reinforced with plaited straw was made. Straw and horse hair have been used to reinforce mud bricks, improving their fracture toughness, for at least 5000 years. Almost all, natural materials which must bear load, such as wood, bone, paper, or muscle, are composites [1].

The composite materials, in particular fibre reinforced plastic (FRP), are one of the most interesting materials in both academic and industrial areas. The composite industry, however, is new. It has grown rapidly over the past 30 years with development of fibrous composites. The roots of the advanced composite materials (ACM) can be found with glass fibre reinforced plastics (GFRP) developed in World War II. In the 1950s, FRP using glass fibre and unsaturated polyester was developed [2]. In the 1960s, carbon fibre as reinforcement material was invented. Compared to glass fibres, the carbon fibres have a high elastic modulus. As a result, the FRPs have progressed dramatically as new structural materials, and fields of application have also evolved. Subsequently, the other reinforcements with high strength and elastic modulus have been developed, for example, aramid fibre, silicon carbide and so on. The matrices have also been improved.

Composites are versatile materials that are artificially made, as opposed to materials that occur naturally [3]. In addition, the constituent phases must be chemically dissimilar and separated by a distinct interface. In contrast, most metallic alloys and many ceramics do not adapt to this definition because their multiple phases are formed as a consequence of natural phenomena. Many composite materials are composed of just two phases. One is termed the matrix, which is continuous and surrounds the other phase. The other phase is called the reinforcement, which toughens the matrix. The

classification of the composite materials is shown in Figure 1.1. From Figure 1.1, the composites are arranged in three main divisions: Particle-reinforced, Fibre-reinforced, and Structural composites. There are at least two subdivisions for each main division. The dispersed phase for the particle-reinforced composites is equiaxed, i.e., particle dimensions are approximately the same in all directions. For the fibre-reinforced composites, the dispersed phase has the geometry of fibres. Finally the structural composites are combinations of composites and homogeneous materials [4].

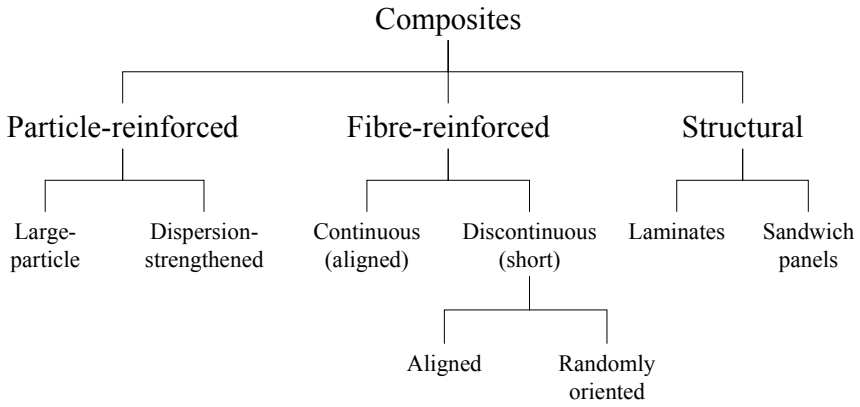

Figure 1.1 A classification scheme for the various composite types [4]

At present composite materials are used in wide variety of areas, including aerospace, ships, architectures, sports goods, energy and so on. The composite materials possess characteristics of high specific stiffness and strength, corrosion resistance, and good electrical properties. Moreover they are superior to other multipurpose materials such as metals. One major advantage of the composite materials is that they can be made according to specific needs, by selecting fibre, fibre orientation, and matrices. The FRP in structural application is superior in cost effectiveness and weight to metal materials. Consequently, FRP, especially carbon fibre reinforced plastic (CFRP), is an attractive material as an alternative to conventional materials.

The point, where the composite materials are different from the other materials, is their anisotoropy. Isotropic materials have identical properties in any direction. Metal is a typical isotropic material. On the other hand, anisotropic materials have properties such as strength and elastic modulus, which are different according to reinforcement orientation. A special case is an orthotropic material which has properties that are different in orthogonal direction. The FRP, in particular unidirectional composite, is strong anisotropy materials. Consequently, when the structure is designed using

composite materials, the anisotropy is a key consideration.

One of the major drawbacks for the FRPs, especially laminated materials, is their susceptibility to damage from external impacts. When FRP receives low velocity impact such as dropped tools, interlaminar damage, in the form of delaminations, would occur with little or no external evidence of the damage. The strength, nevertheless, may be severely reduced, in particular the compression strength. One of the goals of composite materials designers is to develop the material with damage resistance and damage tolerance.

1.2 Main Objective of Research

The overall objective was to achieve improvement of the interlaminar toughness for the composite materials using interleaf veils as toughening materials, understanding the mechanisms of the toughening by the interleaf veils, and discussing correlation between Mode-I, Mode-II, impact, and compression after impact (CAI) properties. A multitude of research for interlaminar fracture toughness has been undertaken by many researchers. To take an example, the matrices are toughened by particles or added rubber, thermoplastic films have been interleaved in interlaminar region, laminate fabrics are stitched, etc. In this research, the non-woven veils as interleaf materials have been used for the improvements of the interlaminar toughness of the composites. The interleaf techniques based on polymer films were introduced in 1980s, and interleaved composites exhibited superior fracture toughness compared to the non-interleaved cases using the same resin.

Various methods are available for manufacturing composites: Prepreg moulding, Resin transfer moulding, Autoclave method, Filament-winding method, etc. Resin transfer moulding (RTM), in particular vacuum assisted resin transfer moulding (VaRTM), has become well established in the industrial field, because the VaRTM method can provide low cost and high quality for large FRP structures [5]. However, when composites are made by the VaRTM technique, some toughening techniques, such as interleaf materials, would be restricted. Because the interleaf materials will prevent resin flow though the thickness direction. In this research, therefore, non-woven veils were used for interleaf materials. It can be expected that the non-woven veils possess good resin permeability for the VaRTM method.

Some specific objectives of this research are:

1. To examine Mode-I and Mode-II interlaminar toughness of the non-woven veil interleaved laminates by double cantilever beam (DCB) and four-point end notched flexure (4ENF) tests. Base materials are selected woven and unidirectional carbon fabrics. The interleaf veils are used polyester/carbon hybrid, carbon, polyester, and polyamide samples.
2. To determine mechanisms of the interlaminar toughening by the non-woven veils. The mechanisms of the toughening by the interleaf veils are evaluated by observation of fracture surfaces and cross-sections of damaged laminates.
3. To perform impact tests on the non-interleaved and interleaved specimens. Damage of the impacted specimens is detected using ultrasonic wave C-scan.
4. To perform CAI tests of the non-impacted and impacted specimens. The CAI behaviour with interleaf veils is evaluated and discussed using results of test and microscopy.
5. To analyse for correlation between Mode-I, Mode-II, impact resistance, and CAI properties and discuss comparison between this work and previous reference data.

The DCB and 4ENF tests were tested by tensile and compression loading, respectively. A drop-impact test was carried out followed by a CAI test performed using an anti-buckling fixture to support the plates in compression.

The work written in this thesis has been undertaken at Queen Mary, University of London (QMUL) from 2005 to 2008. This thesis is mainly an investigation into CFRP with several non-woven veils, fracture testing by double cantilever beam (Mode-I), four-point end notched flexure (Mode-II), impact, and CAI tests. Fracture mechanisms were evaluated for cross-section and fracture surface using scanning electron microscope (SEM) and optical microscopy, and impact damage area was detected by ultrasonic C-scan.

1.3 Outline of Thesis

This thesis consists of seven chapters and three appendices. Chapter 1 is an introduction to composites and the research. This chapter describes the composite materials briefly and explains objective of this work and construction of this thesis.

The literature reviews of previous researches are mentioned in Chapter 2. In this chapter, firstly characteristics of the composite materials and the RTM method are

introduced. In this chapter, details of the composites and RTM method are indicated. Secondly, various toughening techniques for the composites are reviewed. Thirdly, each toughness properties for Mode-I, Mode-II, and CAI resistance are compared using previous literature data. Fourthly, the interlaminar fracture tests are summarised. The interlaminar fracture toughness tests are divided into four types: Mode-I, Mode-II, Mixed mode, and Mode-III interlaminar toughness tests. Details of each test are mentioned in this section. Finally, the compression after impact test is reviewed and summarised. This section is divided into three part, low-velocity impact test, non-destructive investigation (NDI), and CAI test.

Chapter 3 reports on the Mode-I interlaminar toughness tests. Three types of carbon fabrics and two types of resin were chosen as the base materials. The non-woven veils as the interleaf material were 5 types. Mode-I energy release rate, G_I, was measured using the DCB test. Firstly, the Mode-I energy release rate values, G_I, for all specimens are illustrated and summarised in result section. In discussion section, mechanisms of the Mode-I toughening by the interleaf veil are evaluated and discussed using microscopy images.

Mechanisms of the Mode-II interlaminar toughening by the non-woven interleaf veils are discussed in Chapter 4. For the Mode-II tests, 4ENF test was carried out and the same materials as the Mode-I test were used. Construction of the chapter is almost the same as chapter 3. Resistance-curves (R-curves) and Mode-II energy release rate values, G_{II}, are illustrated and explained in result section. The mechanisms of the Mode-II interlaminar toughness by the interleaf veils are evaluated in discussion section.

Chapter 5 shows impact and CAI resistance properties by the non-woven veils. In this chapter, the base materials were plain weave and two types of resin. A result section is divided into three parts: Impact damage resistance, Results of compression test, and CAI strength. The impact damage of specimens was detected by ultrasonic C-scan machine. In the discussion part, the impact and CAI resistance properties are evaluated using microscopy images.

In Chapter 6, discussion and analysis of the research has been carried out. Correlations between Mode-I and Mode-II, impact, and CAI properties are evaluated: Mode-I and Mode-II, interlaminar toughness and impact resistance, both modes of

interlaminar toughness and CAI properties, and impact and CAI resistance properties. For the Mode-I and Mode-II energy release rates, initial and propagation values are used. Finally, this work and previous literature data are compared.

The toughness mechanisms of FRPs have been investigated by many methods and aspects. Of course, improvement of toughening techniques for the composite materials is developing still. Chapter 7 is final conclusions of this research and suggestion for future works.

Appendix A and B show results of the DCB and 4ENF tests, respectively. Appendix C mentions correlation between damage area and other properties.

Chapter 2

Literature Review

2.1 Introduction

Composites are comprised of more than 2 types of materials and are used in various fields of engineering. For composite materials, the interface between the composition materials divides clearly, unlike metals. They have many attractive properties, such as high specific strength and stiffness, and light weight as compared to metal materials [2]. Figure 2.1 shows a diagram of evolution for engineering materials. Composite materials started to be used rapidly after 1960s. The use of composites is expected to spread in the future. The most important properties for composite materials are high specific strength and stiffness. Table 2.1 shows properties of various materials. The strength and stiffness properties of steels are superior to most other materials, except for the composite materials. However, a drawback of steel is that the specific gravity is very high. On the other hand, composite materials have good strength and stiffness, with a low specific gravity.

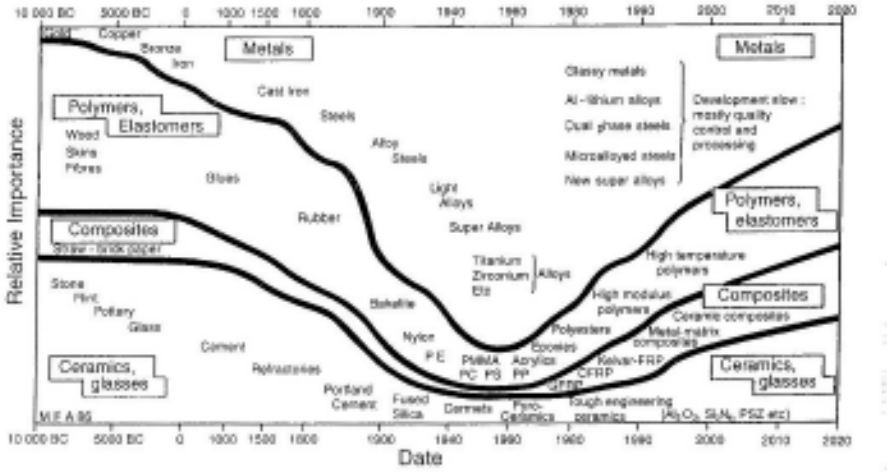

Figure 2.1 The evolution of engineering materials with time [6]

Table 2.1 Properties of various materials [7]

Material	Density [g/m^3]	Elastic modulus [GPa]	Tensile strength [MPa]
Soft steel	7.8	210	300
Structural steel	7.8	210	450
Chrome Molybdenum steel	7.8	210	1000
Aluminum	2.7	70	150
Aluminum base alloy [2017: Duralumin]	2.73	70	280
Aluminum base alloy [2024: Super duralumin]	2.77	73	450
Aluminum base alloy [7075: Extra super duralumin]	2.80	75	500
Polyethylene	0.9	0.3	10
Polyester matrix	1.3	2	40
Epoxy resin	1.3	3	50
Glass	2.2	75	50
Wood	0.5	10	100
Glass fibre	2.5	75	2500
Carbon fibre	1.7	230	3000
Aramid fibre [Kevlar]	1.4	130	2800
Unidirectional glass fibre reinforced epoxy plastic	2.0	40	1200
Unidirectional carbon fibre reinforced epoxy plastic	1.7	140	1500

2.2 Moulding of Composites

Compared to the other engineering materials, the FRPs can be moulded using a number of methods. They have various moulding methods by changing figure of reinforcement materials. The moulding techniques are of 2 types, which are open moulding (mould with only one side) and closed moulding (mould with both side). Representative FRP moulding methods are indicated as follows:

- Hand lay-up
- Spray-up
- Filament winding
- Resin transfer moulding
- Press moulding
- Drawing moulding
- Vacuum bag moulding
- Autoclave moulding

2.3 Resin Transfer Moulding (RTM) Method

Resin transfer moulding (RTM) or resin injection moulding (RIM) are methods where laminated dry fibre materials are bagged in a mould and resin is infused into the mould, as shown in Figure 2.2. The RTM method has merits of low cost, high efficiency. Especially, the RTM method has been able to mould effectively large structures [8]. The RTM technique is steadily gaining importance, as it provides cost effective and more accurate part geometries than prepreg based lay-up structures [9-10].

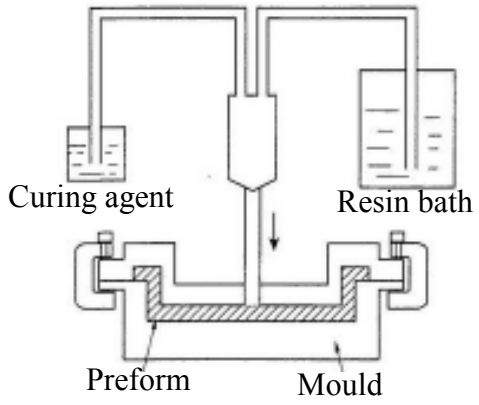

Figure 2.2 Schematic diagram of RTM method [11]

The vacuum assisted resin transfer moulding (VaRTM) method is one of the liquid moulding process that offers advantages to reduce tooling costs for large or complex composite structures [12-15]. In the VaRTM process, the dry fibrous materials, which are called the perform, are placed onto a single hard sided mould and sealed with a vacuum bag. This method is infusing resin by applying vacuum. Hence, compared to the conventional RTM method, voidless products can be produced. For the RTM method, the resin viscosity is an important factor for the injection process. If the resin

has high viscosity, the infusing process would be difficult. Therefore it is important to find the optimum moulding condition. The resin flow or distribution of voids by the VaRTM have been analysed using experimental and numerical methods [16-18].

2.4 Failure of Composites

It is necessary to distinguish fracture and failure to discuss the strength of composites. The former indicates a state where materials separation or breakup has occurred, and the latter means that the damage disappears on the surface. Generally, when the strength of the engineering materials is considered, the failure strength is used for criteria.

Although composite materials have desirable properties, the defect of the materials is their susceptibility to damage, such as impact damage. When composites, in particular the FRPs, receive impact loads, the materials can delaminate at interlaminar regions. This fracture would cause serious problems for structural materials even if the damage is barely visible on the surface. When the laminate materials are damaged from out-of-plane loads, the failure is mainly interlaminar delamination, and in-plane compression strength of this laminate reduces significantly. Consequently, a lot of research on interlaminar fracture toughness has been carried out. Figure 2.3 shows models of fracture processes for the composite materials.

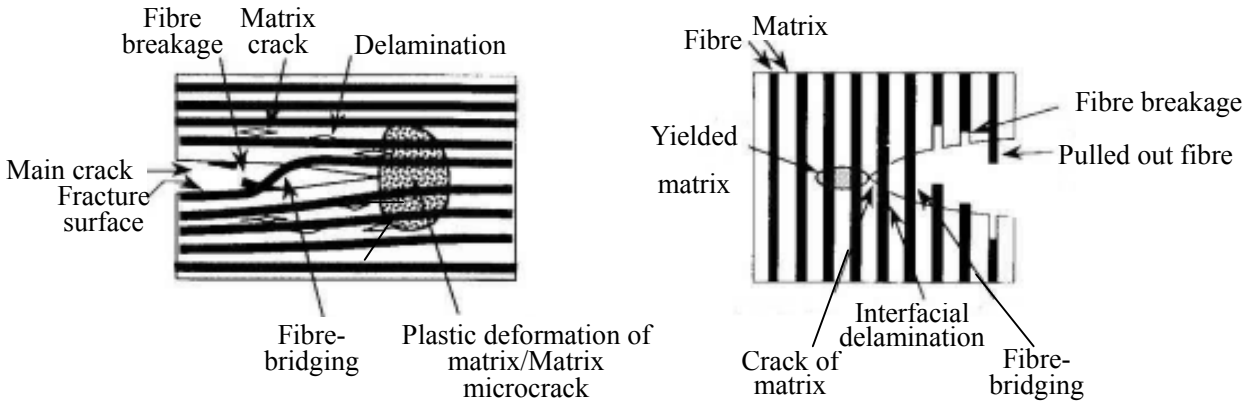

(a) Parallel fracture to fibres (b) Vertical fracture to fibres

Figure 2.3 Schematic diagram of fracture of composites [19]

2.5 Interlaminar Fracture Toughness of Composites

2.5.1 Introduction for Interlaminar fracture Toughness

Laminated materials have poor transverse or thickness-through strengths. They tend to delaminate or interlaminar separate due to external loads. The delamination is the most predominant and life-limiting failure mechanism in composite structures [20]. The delaminations occur only at interfaces between plies with different fibre orientations, not with same fibre orientations [21-22]. Improvement of the delamination resistance can be devided into two ways, improving materials and tailoring the laminate in construction [23].

2.5.2 Toughened Matrix

Matrix toughening technique is the simplest way of improving interlaminar fracture toughness. Various resins have been used as the matrix. To take an example, the thermoset resins are unsaturated polyester (UP), epoxy, vinyl ester (VE) or polyimide (PI). The UP is key material of GFRP. This resin has been used widely because of good flexibility of use and its low cost. Epoxy provides better adhesion between matrix resin and reinforcement. Moreover, it has good mechanical properties, dimensional stability, heat tolerance, electrical properties. The VE has better adhesion than the UP. Mechanical property and heat tolerance are similar to the epoxy resin. Acid and alkali resistance are very good. The PI has more heat resistance than the epoxy resin. However, this resin is quite hard to process and requires a high cure temperature (>300^{o}C).

Epoxy resin is now used widely for composite materials especially CFRP. However, FRP with unmodified epoxy has poor fracture toughness. Therefore, toughened matrices have been investigated by many researches. Rubber has been used as one of the toughening materials, typically liquid carboxyl terminated butadiene-acrylonitrile co-polymer (CTBN), as liquid rubber or addition rubber particles. The G_{IC} value of bulk resin with added rubber was significantly increased, up to a maximum 3.2kJ/m^2 [24]. The resin toughness, however, is only partially transferred to the composites, because the reinforcements restrict plastic deformation of the crack tip in matrix [25]. The G_{IC} of rubber added composites were moderately increased, up to 0.5kJ/m^2. This was due to the improvement by the rubber toughening mechanism and associated with resin film thickness [24]. Increasing resin toughness by increasing the rubber content may not lead to increase composite toughness. It is likely to weaken strength or thermal properties [26]. J. Kim *et al.* investigated modified epoxy resin using rubber, Al_2O_3 fibre or powder as toughened materials [27]. The resistance curve

(R-curve) for the rubber modified matrix composites, both with and without Al_2O_3 fibres or powder, were superior to that of the controls. However, the addition of rigid fillers to the matrix did not improve the crack growth resistance. The rubber toughening was used for not only epoxy resin but also VE resin [28].

Bismaleimide (BMI) resin has a significantly higher thermal stability than the other thermoset resins such as epoxy resin [29]. The glass transition temperature (T_g) of the BMI is approximately 230^{o}C and above. The BMI resin, however, is inherently brittle. Therefore, various approaches have been carried out on improving composites with the BMI resin. S. Chou *et al.* studied properties of three dimension (3-D) and five dimension (5-D) composites (see in Figure 2.4) with the BMI resin. Various mechanical properties such as tensile, flexure, and impact resistance are affected by weaving density. Moreover at a high temperature, which is over 250^{o}C, reduction of mechanical properties for the BMI composites was moderate [30]. S.P. Wilkinson *et al.* suggested that the BMI resins were modified using thermoplastic toughness modifiers. Poly(arylene ether sulphone) and polyimide were used as toughening materials. The modified BMI composites for Mode-I and Mode-II energy release rates indicated excellent results. Addition tougheners of 15 and 20% of maleimide-terminated poly(ether sulphone) yielded composite G_{IC} values of 0.490 and 0.735kJ/m^2, respectively. On the other hand, unmodified composite G_{IC} value was about 0.360kJ/m^2 [31].

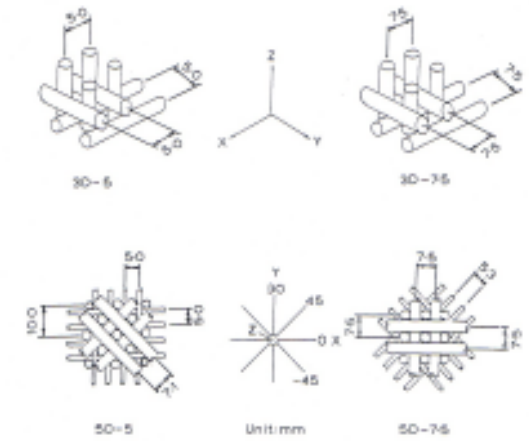

Figure 2.4 Structural geometry of three dimension (3-D) and five dimension (5-D) fabrics [30]

Modifiers for the improvement of matrices are quite a useful toughening technique. However, they may lead to degradation of thermo-mechanical properties, and mould of the composites would be difficult by high resin viscosity. Furthermore, the modifier might be filtered out during composites manufacturing. A toughener is preferred which does not affect the viscosity of the uncured resin and risk toughener segregation or filter [32]. The toughness implies energy absorption and can be achieved through various deformation mechanisms. The toughening of composites can be realised by reduction of the cross-linking density or use of plasticisers which lead to increased plastic deformation in interlaminar regions. The most effective toughening techniques, on the other hand, are induced by the addition of a second phase in the form of particles [32-34]. Toughening process is that liquid reinforcement is dissolved in matrix at uncured condition. Afterwards, phase-separation occurs during cure, as shown in Figure 2.5.

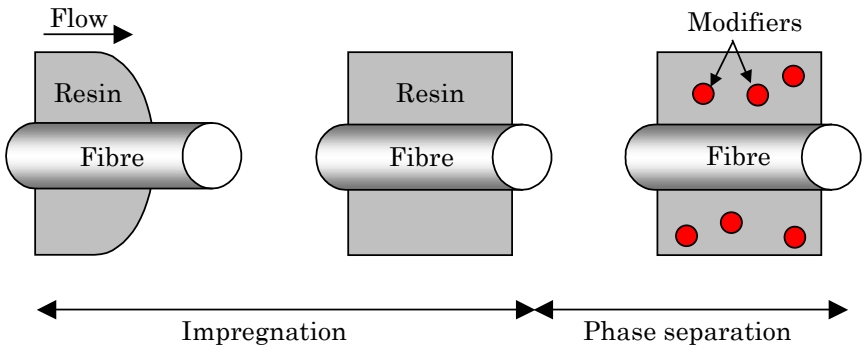

Figure 2.5 Model of phase separation process [33]

A high molecular weight toughener will facilitate control of the phase separation process. A high molecular weight, however, has a high viscosity. In order to satisfy both requirements, which are a low viscosity and a high molecular weight, a spherical molecular structure is more suitable than a linear structure. Dendritic polymers which consist of a spherical structure have a lower viscosity than linear polymers for equivalent high molecular weights [32]. Hyper-branched polymer (HBP) has similar properties to the dendritic polymer as shown in Figure 2.6. This polymer is composed of three parts: (a) A multi-functional core, (b) Several layers of monomers, (c) A multi-functional shell. The core influences the mechanical properties of the HBP, because chemical properties of hull controls the phase separation process and can be tailored for each type of resin [35]. The specific advantage of the HBP are three: (a) Their chemistry can be easily tailored to have suitable mechanical properties for

inducing the most efficient toughening mechanisms, (b) They are reactive, (c) They can readily be made compatible with the matrix [35].

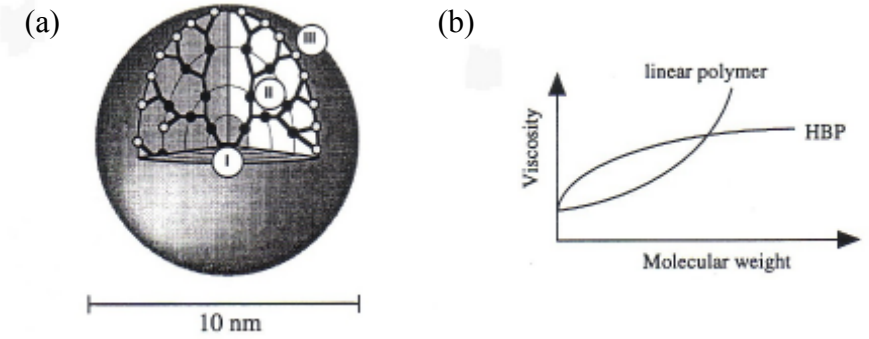

Figure 2.6 (a) A dendric hyperbranched polymer molecule with a structure composed of a multifunctional core (I), several layers of repeating units building up the bulk structure (II) and a multifunctional shell (III); (b) Viscosity behaviour as a function of molecular weight for linear polymers and hyperbranched polymers (HBPs) [32]

In some studies, the HBP modified epoxy resins demonstrate improving toughness compared with the unmodified resins. L. Boogh *et al.* indicated that a 6 times increase in the G_{IC} could be obtained for DGEBF-epoxy resin system using 5% by weight of a HBP modifier [32]. R. Mezzenga *et al.* investigated to work the structure-properties relations of the epoxy functional HBP in epoxy composite materials [33]. The HBP modifier could realise the improvement of DGEBA-based and TGMDA-based epoxy composites. These composites were able to induce more than a 2 times increase in the G_{IC} values compared to the unmodified composites. Moreover, they pronounced an effect of fibre/matrix adhesion on the interlaminar fracture toughness of the composite with the HBP modified resins. A specific amino-silane sizing improved interlaminar fracture toughness. Toughened resin using the HBP modifier can improve significantly interlaminar toughness. However, an increase in fracture toughness of the composites would not increase necessarily according to the kind of resin type. This is due to poor adhesion between the fibre and the modified resin. In order to solve this problem, the adhesion properties could be restored by using an excess of amine (hardener) [35].

Thermoplastic resins have also been developed as matrices for high performance composites. The thermoplastic resins are more ductile than the thermoset

resins. The thermoplastic matrices possess some advantages in terms of higher strain to failure and impact tolerance, recyclability, repeatability, and longer storage in comparison to thermoset matrices [34-35]. Fibre reinforced thermoplastics (FRTP) are a tougher material. Especially, the fracture toughness is superior to the FRP. The poly (ether ether ketone) (PEEK) is one of the most attractive materials with respect to interlaminar fracture toughness. Since the early 1980s, a lot of research for the PEEK composites has been undertaken [38]. The PEEK is not hydrolysed by acid or alkali, however, the T_g is 143^{o}C, and use of high temperature cannot be endured. For the Mode-I interlaminar fracture toughness, the CF/PEEK composites were significantly high G_{IC} value, around 1.7kJ/m^2. The CF/epoxy composites, on the other hand, were about G_{IC} value of 0.2kJ/m^2. P. Davies *et al.* reported that the specimens have dependence on specimen thickness by Mode-I test using the thermoplastic resin [39]. The thicker specimens are, the higher G_I values increase. This was due to increase fibre-bridging in thicker specimens. The PEEK composites with various reinforcements were evaluated. G. von Bradsky *et al.* investigated the Mode-I fracture toughness of the PEEK matrix with various base fibres, which were glass, carbon, and aramid fibres [40]. The G_{IC} value of the glass fibre and carbon fibre composites was in the range of 2.9 to 3.3 kJ/m^2, whereas that of aramid fibre composites was a lower value, approximately 1.1kJ/m^2. They mentioned that fibre/matrix adhesion is the most important factor for interlaminar fracture toughness of continuous fibre PEEK composites. The AF/PEEK composite has poorer fibre/matrix adhesion than the other fibres, therefore the G_{IC} value is quite small. R. Frassine *et al.* reported rate and temperature dependence in PEEK and polyetherimide (PEI) matrix with the carbon fibres. In comparison to the PEI-matrix composite, fracture toughness of the PEEK matrix is strongly influenced by test condition such as loading rate and temperature [38, 41]. On the other hand, although the fracture toughness of the PEI matrix is insensitive to the test condition, that of the CF/PEI composite is influenced by temperature [41-42]. There are some works using the poly-ethersulphone (PES) composites [43-44]. The crack propagation for the PES system composites was stable. T. Kuboki *et al.* examined for the Mode-I and Mode-II interlaminar toughness and impact properties of GFRP composites with isophthalic polyester and polyurethane matrices. The polyurethane-based composite showed a more stable Mode-I crack propagation than the polyester-based composite. G_{IC} value of the polyurethane-based composite was significantly high, 1.6kJ/m^2 (initial) and 3.8kJ/m^2 (propagation) [45]. Poly(2,6-dimethyl-1,4-phenylene ether) (PPE) have been exhibited interest as tough thermoplastic composite. In particular, it has high glass transition temperature (approximately T_g=220^{o}C) and excellent mechanical properties. R.W.

Venderbosch *et al.* discussed interphase behaviour of the PPE composite by using epoxy resin as a reactive solvent [46]. This tailoring dramatically improved the adhesion between the fibre and the thermoplastic matrix. As the other thermoplastic resin, there is polypropylene (PP) matrix. The PP matrix has good mechanical and chemical performance, recyclability, and low organic compound emission during moulding [47]. However, the PP matrix is quite sensitive to moulding condition, because of its semicrystalline nature. This strongly affects mechanical properties. The thermoplastic matrices are influenced by environmental condition, such as temperature, test rate and so on. The design of the thermoplastic composites, therefore, should consider conditions of test and fabrication.

2.5.3 Particles and Whiskers Modificaion

In section 2.5.2, the polymer additives as modifiers are mentioned. In this section, inorganic additives are reviewed as toughners. The addition of rigid particles, such as alumina, silica, glass beads [48-50] or block copolymer [51], has been conducted to improve the stiffness and toughness of the resin. J. Spanoudakis and R.J. Young evaluated the fracture toughness using glass particles in the epoxy resin [49-50]. They focused on the effect of particle volume fraction and size, and particle/matrix adhesion. The crack propagation behaviour can be explained as crack pinning, which is dependent on the particle volume fraction and size [49]. Moreover, the strength of the particle/matrix adhesion affects both the crack propagation behaviour and the appearance of the fracture surface [50]. The particle toughened composites can improve also post-impact compression strength [52]. V.K. Srivastava and P.J. Hogg studied damage performance using particles, which were polyethylene and $Al(OH)_3$ [53]. The G_{IC} value for particles modified composites was marginally increased. They suggested that the suppression of crack propagation by particles has the limit. On the other hand, the G_{IIC} values were significantly affected. The G_{IIC} induced by ductile thermoplastic particles was larger than that induced by hard ceramic particles. The thermoplastic particles have good fracture toughness property as modifiers [53-54].

The modifications of resin using whiskers as an alternative technique have been approached for improving fracture toughness. Silicon carbide (SiC) whiskers have been used for many studies of fracture toughness. For the whisker, the SiC whisker is the most widely used as whisker reinforcements for composites, because its physical properties are well known and the cost is not expensive [55-56]. In mid-1990s, a short fibre reinforcement technique using Kevlar fibres of 5 to 7mm length was used to

improve interlaminar fracture toughness. The fracture toughness mechanisms by the short fibre reinforcement are mainly fibre-bridging [57]. As the other short fibre reinforcements, there are alumina fibre [58], glass fibre [59], or Zylon fibre [57, 60]. L. Walker *et al.* investigated that the addition of short fibre produces a randomly oriented heterogeneous layer. This created the potential for random and disturbed crack path. On the other hand, the orientation of the whiskers was magnetically controlled to the direction of thickness [61]. The oriented whiskers improved fracture toughness due to bridging. Moreover, the short fibres absorb energy dependent upon the creation of laminate damage. Hence, overall laminate damage reduces due to the increased fracture toughness of the short fibres modified materials. Recently, nanoclay has been attempted as a reinforcement materials, interlaminar fracture toughness of the nanoclay-filled composites was significantly increased [62].

2.5.4 Fibre/Matrix Adhesions

The fibre/matrix interfaces are weaker than the matrix. Composites can fracture often in the fibre/matrix interface at an early stage [63]. The strength of the fibre/matrix adhesion affects the fracture toughness in FRPs. A strong interface bond is essential for improvement of high strength for the composite materials. However, this generally leads to a catastrophic fracture through the fibre/matrix interface [64]. On the other hand, weak interface bonding leads to fibres debonding or pulling-out from the matrix. This may contribute to the improvement of fracture toughness for composite by fibre-bridging [64-65]. Many researches have been carried out evaluating and improving the fibre/matrix adhesion. It is well-known that the surface treatment of fibres changes morphology and chemical properties of the fibre surface, and can improve the fibre/matrix interfacial bonding [66-69]. Some researchers reported that release agent as the fibre treatment was used to establish the extreme case of poor interface adhesion due to identify the pure behaviour of fibre/matrix interface [63, 70]. S.M. Lee mentioned the fibre/matrix interface strength influenced strongly the crack initiation stage, but did significantly affect the not propagation stage [63]. J. Kim and Y.–W. Mai investigated the fracture behaviour of Kevlar and carbon fibres in epoxy composites using three types of coating, which are the CTBN copolymer, polyvinyl acetate (PVA), and polyvinyl alcohol (PVAL) [71]. The CTBN and PVA coating were not improved significantly. In contrast, KFRP and CFRP with the PVAL coating improved impact fracture toughness. The PVAL coating induces an increase in the interfacial debonding and fibre pull-out. These pull-out fibres work as fibre-bridging and therefore fracture toughness can increase [64-65]. Fibre-bridging is a quite

important phenomenon for the interlaminar fracture toughness, particularly in delamination mode. The fibre-bridging occurs when fibres are pulled from one side of the delamination plane to the other side. The interlaminar fracture toughness will be increased by occurring fibre-bridging [72-74]. Figure 2.7 shows schematic of fibre bridging. However, the fibre-bridging effect may be undesirable when a relationship between matrix toughness and composite toughness is trying to be understood [72], because the damage behaviour would be complicated.

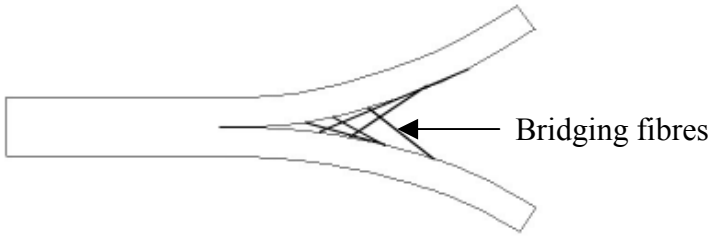

Figure 2.7 Schematic of fibre-bridging

2.5.5 Improvement of Fabric Architecture

In order to improve through-thickness strength of the composites, various woven or 3-D fabrics have been introduced. The woven fabric composites are considered for high performance applications because they have superior impact resistance and damage tolerance properties [75-77]. The woven fabrics are made by interlacing two or more sets of fibre tows or yarns. Figure 2.8 illustrates diagrams of representative woven fabrics. Orthogonal woven fabrics have good dimensional stability in the warp (the longitudinal yarns) and weft (the widthwise yarns) directions [78]. B.J. Briscoe *et al.* investigated the relationship between fabric surface properties and interlaminar fracture toughness using various aramid fabrics [79]. They found that a coarse fabric with higher areal weight had higher fracture toughness than a fine woven fabric with lower areal weight. The type of fabric weave has a small effect on fracture toughness. A rough surface of the woven fabrics creates a thicker resin-rich region than the non-woven unidirectional composites. As a result, the plastic zone can be developed ahead of the crack tip during delamination [78]. As the other fabric materials, felt composites have been suggested recently [80-82]. J. Kim *et al.* introduced carbon fibre felts produced by needle-punching the stack of loose fibre webs and woven fabrics [80-81]. They investigated the influences of weave pattern and needle-punching density using carbon fibre woven and felt composites. The felt/epoxy composite could improve interlaminar

fracture toughness and damage tolerance as compared with the woven laminates. These mechanical properties of the felt/epoxy composites improve with increasing needle-punching density.

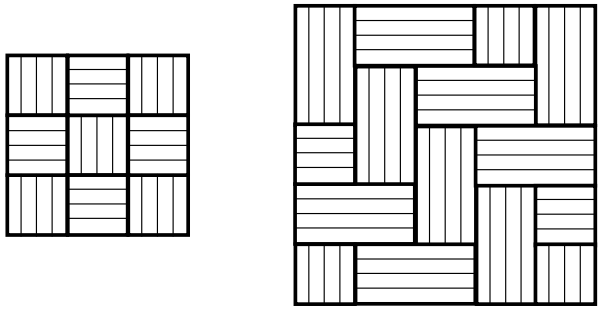

(a) Plain weave (b) 2-2 twill weave

Figure 2.8 Schematic diagrams of representative 2-D woven fabric

Alternative approaches are to the advanced fabric manufacturing technologies of knitting, braiding, through-the-thickness stitching and so on. The 3-D structure consists of in-plane yarn for stiffness and strength and z-binder yarns for through-thickness reinforcement [83-84], as shown in Figure 2.9. Figure 2.10 shows schematic diagrams of the advanced textile fabric. The 3-D composites have two important advantages compared with the traditional laminated composites. Firstly, complex shaped components, such as I-beams, stiffened panels, cylinders and nozzles, can be manufactured rapidly using a variety of fibres, and secondly, the impact resistance is improved due to presence of the reinforcement in the through-thickness direction [84-89]. The 3-D composite possesses good fracture toughness performance. K.–Y. Kim *et al.* studied to characterise delaminarion behaviour of the composites using several weft-knitted fabrics [89]. It was established that the G_{IC} values for the knitted composites were approximately 10 or 20 times higher than for the control. The G_{IC} values of the knitted composites were influenced by fibre volume fraction of the composites, or tightness factor of the knitted preforms.

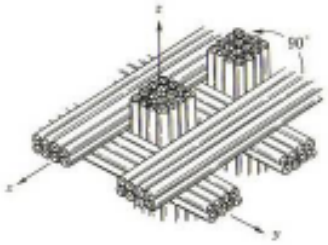

Figure 2.9 Schematic of representative 3-D fabric [2]

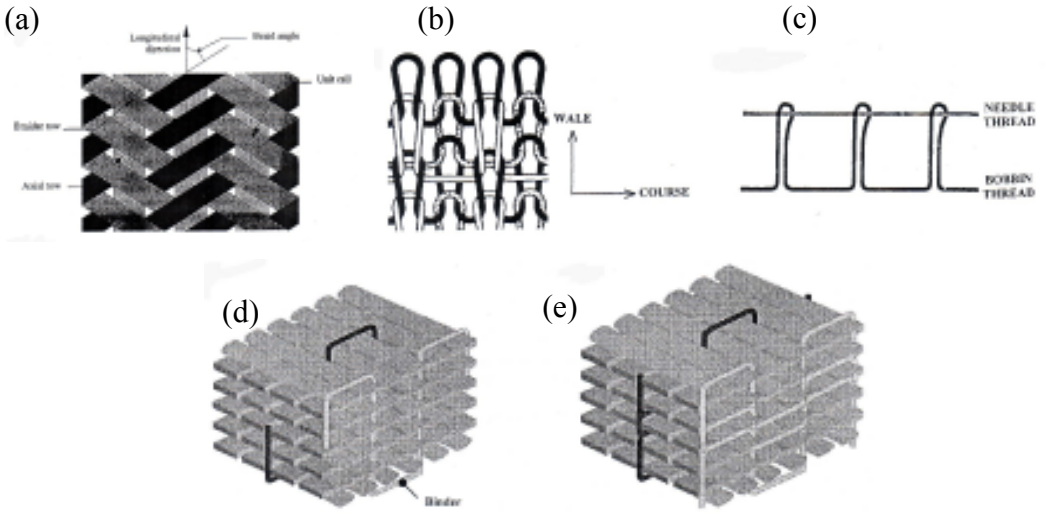

Figure 2.10 Schematic diagram of the textile fibre architectures: (a) Triaxial braided fibre. (b) Milano weft knit rib. (c) Through-the-thickness stitching pattern. (d) Orthogonally woven fibre. (e) Layer interlock woven fibre [85]

Since the 1980s, the use of through-the-thickness stitching with FRP has been developed dramatically. A large number of researches have been conducted to investigate the impact delamination resistance or damage tolerance of the composites made with a 3-D fibre structure, in which fibres extend in through-the-thickness direction. For the stitching, K. Dransfield *et al.* [90] and A.P. Mouritz *et al.* [91] reviewed the effect of stitching for the FRP from many previous researches. The merits of through-the-thickness stitching are: (1) Cost-effective method because of easy improvement of handling prior to liquid moulding, (2) Effective method to produce high in-plane and through-thickness strength, and (3) Improvement of the interlaminar fracture toughness and impact damage tolerance [91-92]. The mechanical properties of stitched composites, therefore, have been evaluated experimentally [85, 93-95] and

analytically [94, 96-100] by many researchers. The stitching technique can improve significantly interlaminar fracture toughness, in particular the Mode-I fracture. V.A. Guenon *et al.* found to a ten times increase in the Mode-I interlaminar fracture toughness for the stitched composites [93]. On the other hand, the Mode-II fracture toughness of the stitched composites is moderately improved. Parameters of stitch, such as stitch separation, stitch type, and stitch orientation affect interlaminar fracture toughness [94].

Although the 3-D woven composites have many advantages over 2-D composites, there is a disadvantage that the in-plane mechanical properties are degraded during manufacture, for example by fibre damage or fibre curvature. It is often found that the in-plane tension, compression and flexural properties of the 3-D composite are 10-40% lower than the 2-D composite with the same in-plane fibre content [80, 101]. The decreased mechanical property is due to crimping and misalignment of the load-bearing fibres by insertion of the z-binder yarns during weaving [83, 85-86, 101]. The twisted fibre yarns for reinforcement might cause a resin rich pocket and decrease some internal mechanical properties. In order to avoid this degradation the plain stitch, which is untwisted fibre roving, was introduced [102]. In the plane stitch, thread cross and resin rich pockets were not formed. The G_{IC} values were increased up to 20 times more than the control samples.

2.5.6 Geometric of Specimens

Composite materials possess quite strong anisotropic properties. The mechanical strength of composites is dependent on stacking sequence. Therefore, the fibre orientation is a significantly important factor for composite designing. Figure 2.11 shows representative fibre orientation patterns.

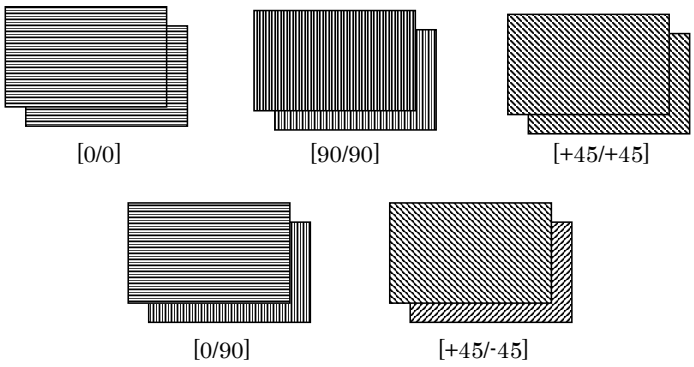

Figure 2.11 Schematic diagrams of representative fibre orientation

The mode of fracture is significantly dependent on stacking sequence and fibre orientation of composites [103]. If there are no $\mathbf{0^o}$ plies in crack propagation area, the crack tends to jump from ply to ply and as a test result it is invalid and complex [104-106]. On the other hand, the symmetric laminates minimise crack jumping [104]. When the crack was propagated between **[0/0]**, which is stacking sequence at mid-plane, the G_{IC} value was lower than stacking sequence of **[0/90]** or **[90/90]**. In the **[0/90]** and **[90/90]** specimens, ruptures of fibres or fibre-bridging were occurred. The presence of $\mathbf{90^o}$ plies in the interlaminar region influences the crack propagation behaviour [105]. Many researches for changing fibre orientation have been undertaken experimentally and analytically [106-109]. A.B. de Morais *et al.* reported the Mode-I interlaminar fracture properties for the asymmetric cross-ply $\mathbf{[0/90]_{12}}$ specimens and $\mathbf{[0/0]_{24}}$ specimens [110]. They presented crack behaviour between two neighbouring **[0/90]** interfaces, as shown Figure 2.12. A Similar zigzag propagation has been reported in [110] for plain weave specimens. A.B. Pereira and A.B. de Morais presented the results of the DCB tests for the multi-directional CF/epoxy specimens on $\mathbf{[0/\theta]}$ interfaces [111].

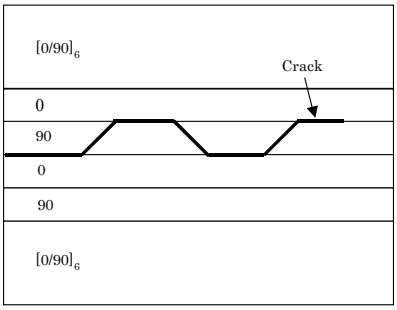

Figure 2.12 Schematic representation of crack propagation in **$[0/90]_{12}$** specimens [110]

The Mode-II interlaminar fracture is also affected by the fibre orientation in the crack propagation region. In the fracture of low angle specimens is by single interface Mode-II interlaminar cracking. The higher angle specimens, on the other hand, intra-ply cracking and multiple delamination occur [112]. S.L. Bazhenov investigated the fracture toughness of different fracture modes, which are interlaminar and intralaminar, using **[0/90]** cross ply GF/epoxy system composites [113]. Figure 2.13 shows schematic diagrams of both fracture modes.

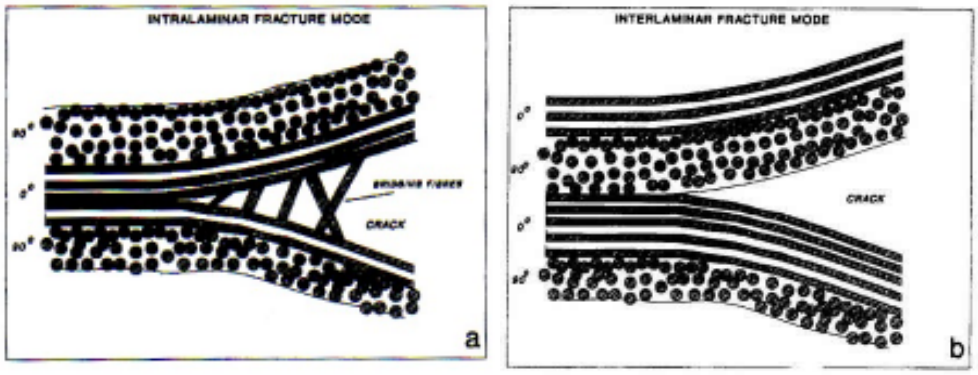

Figure 2.13 Schematic diagrams of fracture modes: (a) Intralaminar, (b) Interlaminar [113]

The thickness of the specimens also influences fracture toughness and mode. The effect of specimen size, hence, has been examined [114-119]. The thin laminates have generally superior damage resistance properties [120]. In short thick specimens, damage initiated at the edge of impact point because of locally high impact stresses. In the long thin specimens, the fracture occurred as a result of splitting between lower surface fibres. The geometrical parameters are one of the factors for dependence of

damage [121].

2.5.7 Hybrid Composites

A hybrid composite material consists of two or more types of fibre in a common matrix. The research for the hybrid composites was examined using glass/carbon or carbon/Kevlar fibres from the 1970s. The hybrid composites possess excellent properties that cannot be realised in a single fibre composite. The failure strain and strength of carbon fibre, which is low-elongation, appears to be larger in a hybrid composite than all carbon fibre composite [122]. Moreover, more cost-effective utilization of the expensive fibre, such as carbon fibres, can be expected using less expensive fibres such as the glass fibres. These merits encourage the extensive application of the hybrid composites. The glass/carbon hybrid composites have been investigated by many researchers [122-125]. P.W. Manders and M.G. Bader reviewed and discussed for strength of the glass/carbon fibres hybrid composites [122-123]. They investigated the tensile properties of the hybrid composites covering a range of glass/carbon ratios. Other combinations of fibres have been also investigated as hybrid composites. The glass or carbon fibres with thermoplastic fibres hybrid composites have been introduced [126-129]. The Mode-I and Mode-II interlaminar fracture toughness increases significantly using the thermoplastic fibres [129]. Recently, hybrid composites with non-woven tissue and natural plant fibres have been used to improve the mechanical properties [130-131]. The natural fibres can be economically and ecologically useful alternatives to reinforcement fibres in polymeric composites [131].

2.5.8 Interleaving Techniques

The interleaving technique is to insert reinforcement materials, such as thermoplastic films, at the interlaminar region. The concept of the interleaving technique is that the plastic zone in the interlaminar region can be extended [132]. The mechanisms of the interleaving technique for interlaminar fracture toughness are shown in Figure 2.14 and 2.15. As the interlaminar spacing is increased by interleaf materials, higher fracture toughness may be expected correspondingly.

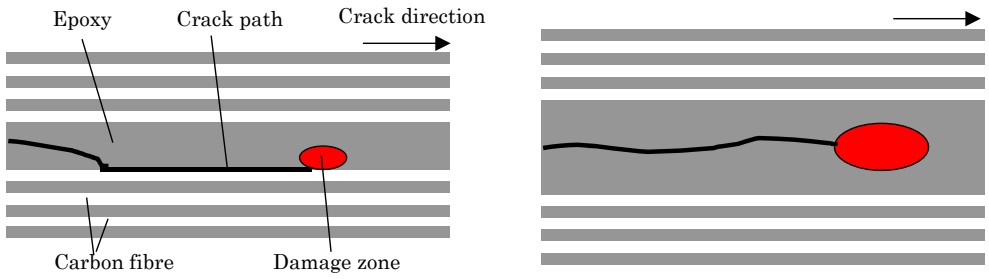

Figure 2.14 Schematic diagrams of crack growth under Mode-I loading: (a) Control sample, (b) Epoxy interleaved sample [132]

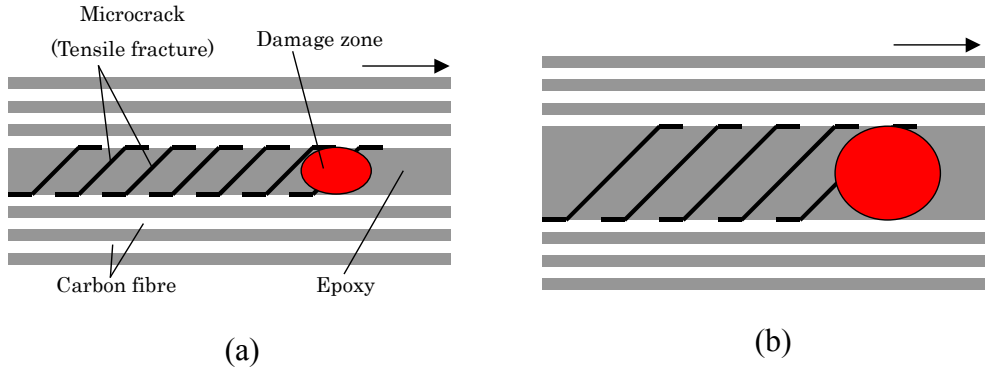

Figure 2.15 Schematic diagrams of crack growth under Mode-II loading: (a) Control sample, (b) Epoxy interleaved sample [132]

A cross-section of the interleaved laminate is shown in Figure 2.16. The interleaved composites have a superior behaviour in the CAI strength compared to the non-interleaved material. However, the major drawback of this system is a weight penalty [20]. Moreover, the mechanical properties, like flexural or thermal properties, may decrease by interleaf materials [133-134]. Therefore, interleaving techniques have to be developed without sacrificing various properties.

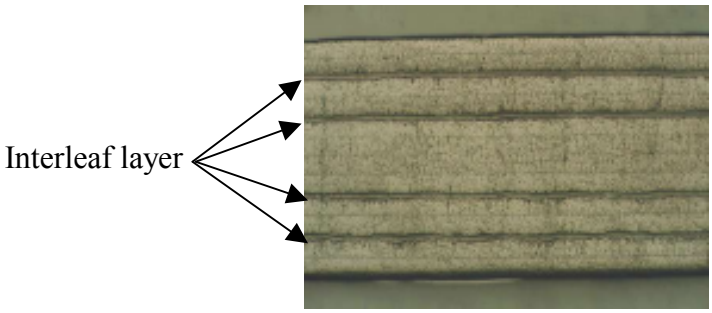

Figure 2.16 Picture of a cross-section of a interleaved laminate

In order to solve the weight penalty, a selective toughening concept has been suggested [20, 135-137]. This technique is that interleaf materials are placed at critical locations that are potential sites for premature failure. O.Ishai *et al.* evaluated the effect of the selective interleaving technique using CFRP laminates [135]. The selective toughening realised a significant effect on the Mode-I and Mode-II interlaminar fracture toughness. It improved the G_{IC} up to six times and the G_{IIC} up to four times compared with the controls. The adhesive thickness is also an important factor on interlaminar fracture toughness of the interleaved composites [137-141]. However, increasing adhesive thickness was not necessarily improving interlaminar fracture toughness [142]. There is an optimum adhesive thickness for effective improvement of interlaminar fracture toughness.

Various interleaf materials as tougheners have been developed by many researches, such as thermoplastic films [139-146], thermoset films [135-138, 142, 145], non-woven tissue veils [147-152], self-same resin interleaf materials [132, 153], and so on. F. Ozdil and L.A. Carlsson reported the Mode-I interlaminar fracture properties using thermoset and thermoplastic interleaf materials of various thicknesses [142]. The thermoplastic interleaf increased the G_{IC} value compared with the thermoset interleaf. They mentioned that the low adhesion between the interleaf/matrix causeed poor toughness. Both high toughness and good adhesion are essential to improve the interlaminar fracture toughness. A. Aksoy and L.A. Carlsson evaluated the Mode-II interlaminar fracture toughness for the thermoplastic and thermoset interleaved composites [145]. In the Mode-II fracture, the thermoplastic interleaf materials were also superior to the thermoset interleaf materials. For the thermoplastic interleaf materials, an ionomer film possesses superior fracture toughness. This is a polymer which is partially ionised by metallic ions and has been utilised as a package material

and an adhesive film [139-141]. The ionomer has high ductility and good adhesion to epoxy resin. Figure 2.17 shows the structure of ionomer. In ref [141], the G_{IIC} of the ionomer interleaved CFRP was over 9.0kJ/m^2.

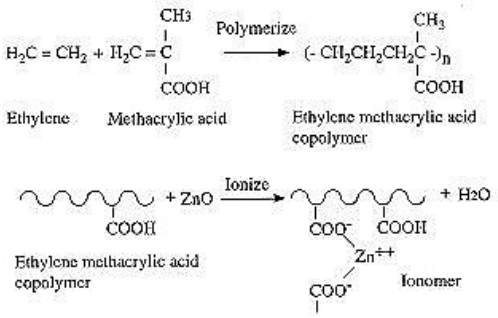

Figure 2.17 Schematic diagram of structure of ionomer [140]

The non-woven fabric or perforated films have been also used as the interleaf materials [129, 147-152]. These publications mentioned that the non-woven fabrics could improve the Mode-I and Mode-II interlaminar fracture resistance, or the impact damage. The non-woven fabrics have good permeability of the resin, therefore they may be used as the interleaf materials using liquid resin moulding, such as the RTM and VaRTM. M. Kuwata *et al.* investigated impact resistance for non-woven fabrics interleaved CFRP using the VaRTM [152]. They found that the adhesion properties between matrix and non-woven fibres are an important factor in the damage resistance of interleaved CFRP. However, research into the interlaminar fracture toughness using non-woven fabric is scarce. O. Jorgensen and A. Horsewell studied indentation failure of the interleaved CFRP experimentally and numerically [154]. The interleaf layers can contribute to toughening the interface between interlaminar regions and reduce matrix cracking. The presence of a high strain and low modulus interleaf layer may significantly improve interlaminar fracture [155]. Some researches have used self-same matrix resin-rich layers as the interleaf materials [132, 153-155]. Significant improvements in the interlaminar fracture toughness have been realised by this technique without the use of any specialised interleaf materials. In order to use same matrix interleaf, the resin rich region is enlarged in interlaminar fracture areas. A thicker resin rich layer contributes to an enlarged plastic deformation zone, and the interlaminar fracture toughness would be influenced strongly.

The interleaving technique can improve not only interlaminar toughness but

also impact tolerance and resistance [136]. J.E. Masters discussed impact and delamination resistance using the interleaving technique [143-144]. The CAI strength was increased up to 80% by the addition of the interleaf films. He evaluated a correlation between the delamination and post-impact compression resistance. The residual compression strength after impact against the Mode-I strain energy release rate shows a poor correlation, as shown in Figure 2.18 (a). In contrast, the residual compression strength against the Mode-II strain energy release rate indicates good correlation, as illustrated in Figure 2.18 (b). The extent of impact-induced delamination is a function of the critical shear strain energy release rate of the matrix.

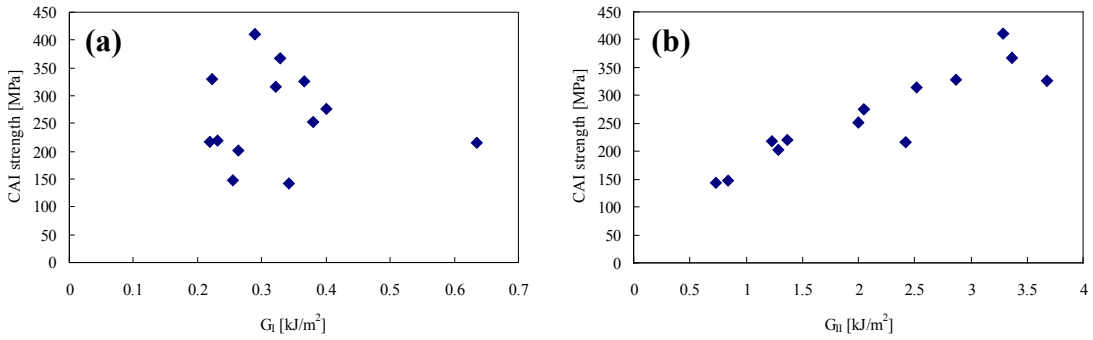

Figure 2.18 Correlation of Mode-I and Mode-II energy release rates and impact resistance: (a) Mode-I energy release rate against CAI strength, (b) Mode-II energy release rate against CAI strength [143]

The interleaved system has been used not only for interlaminar fracture toughness, but also damping performance [133-134, 156-159]. H. Kishi *et al.* evaluated damping properties of the interleaved CFRP. They focused on visco-elastic behaviour of the interleaf materials [134, 159]. The damping properties of the interleaved laminates depended not only on the visco-elastic properties of the interleaf materials, but also on the stacking sequence.

2.6 Comparison of Fracture Toughness for Previous Works

In this section, comparisons of the results from previous literatures are mentioned. Figure 2.19 plots range of G_{IC} for various resin types. For the thermoset resins, the epoxy and VE resin possess moderate fracture toughness, around 0.05 to 0.45kJ/m^2. The BMS resin possesses a wider range of the G_{IC} values compared with the other thermoset matrices. The polyester resin has the lowest fracture toughness. The toughening matrix can improve the Mode-I energy release rate. The maximum G_{IC} of

the toughened epoxy is over 5kJ/m^2. The rubber toughened resin is also significantly improved. On the other hand, the thermoplastic resins are significantly higher in the Mode-I interlaminar fracture toughness than the thermoset resins. In particular, PEEK has excellent Mode-I interlaminar toughness and over 10kJ/m^2 as a maximum value [160].

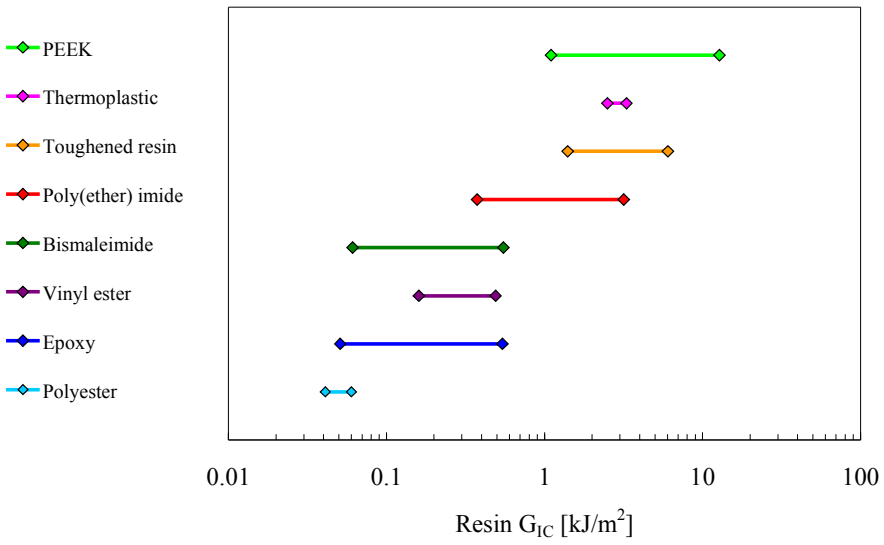

Figure 2.19 Comparison of Mode-I energy release rates for various matrices [24-25, 31, 38, 41-42, 160-163]

For the composites, the G_{IC} and G_{IIC} values of various interlaminar fracture toughness methods is compared. Figure 2.20 shows a diagram of Mode-II interlaminar toughness as function of Mode-I interlaminar toughness for the composites. For the thermoset resin system composites, whereas the G_{IC} values are relatively lower than for the other reinforced composites, the range of the G_{IIC} values is moderate, up to 3kJ/m^2. The toughened epoxy system is improved in Mode-I interlaminar toughness, but not the Mode-II interlaminar toughness. In thermoplastic resin system, the PEEK and PEI matrices show different fracture toughness behaivours. Whereas the PEEK composites have significantly superior G_{IC} values, the PEI system composites have quite high G_{IIC}. The rubber or whiskers toughened composites do not have high toughness for both fracture modes. For the interleaving, although the G_{IC} values are not improved, the G_{IIC} values are spread over a significantly wide range. The stitching technique is the most superior for both fracture modes toughness properties. In particular, the Mode-I fracture toughness is significantly high, over 9kJ/m^2 [141].

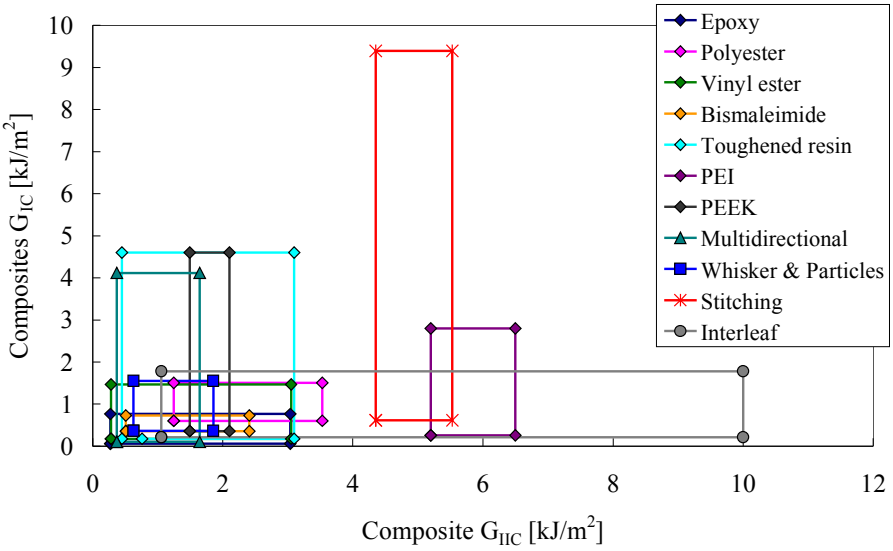

Figure 2.20 Comparison of Mode-II interlaminar toughness against Mode-I interlaminar toughness for composites [20, 27-28, 31, 41-42, 45-46, 53, 56, 89-90, 94, 102, 108, 112, 130, 141, 162]

The relationship between resin G_{IC} and composite G_{IC} is plotted in Figure 2.21. This correlation was mentioned by D.L. Hunston [25]. This figure is an addition of further data from other literatures. The general trend of relationship is not changed. With the brittle matrix the resin toughness is transferred to the composite toughness. With the tougher matrix, on the other hand, the resin toughness cannot be transferred enough. Two chain lines in Figure 2.21 indicate the relationship of resin G_{IC} and composite G_{IC} in brittle and tougher matrix region from ref [25]. The correlation in brittle and toughner matrix region is good, except for the PEEK matrix composites. The long chain line indicates a slope of 2.3. On the other hand, the short chain line is 0.31. Although the PEEK matrix has significantly high G_{IC} values, the PEEK composite is not improved much. It is thought that high Mode-I toughness characteristic of the PEEK matrix cannot be transferred to the composite by the existence of reinforcements. The blue chain line means the relationship in tougher matrix region including the PEEK matrix. The gradient of blue double line is approximately 0.1. Even if the matrix toughness is quite high, it would be significantly difficult that toughness of the matrix transfers to that of the composite materials. Because the existence of reinforcement restricts improving fracture toughness of composites [25].

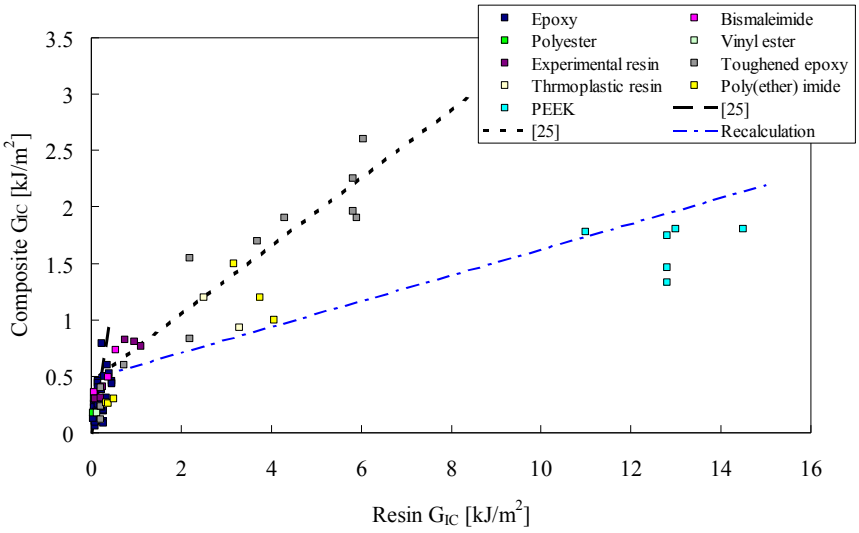

Figure 2.21 Relationship between Resin G_{IC} and Composites G_{IC} values [20, 24-25, 31, 41-42, 46, 62, 66, 72, 130, 136, 160. 162-164]

Figure 2.22 indicates the relationship of resin G_{IC} and composite G_{IIC}. The correlation does not appear clearly unlike the Mode-I interlaminar toughness. V. Altstadt *et al.* evaluated a correlation between the composite Mode-II interlaminar toughness and the resin Mode-I interlaminar toughness [165]. However, it has been shown that these properties did not correlate. Figure 2.22 indicates that there is no correlation between resin G_{IC} and composite G_{IIC} values. The composite G_{IIC} may not be affected by the matrix types.

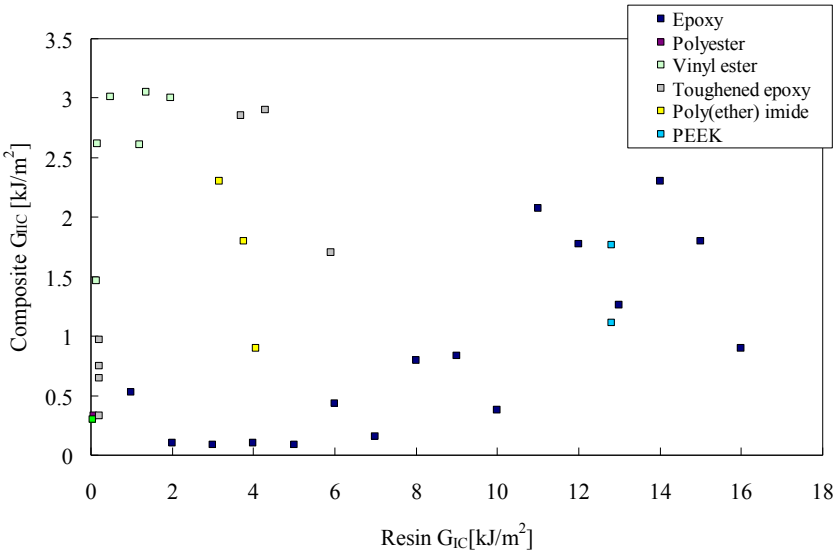

Figure2.22 Relationship between Resin G_{IC} and Composites G_{IIC} values [20, 25, 42, 46, 66, 130, 136, 162, 164]

Figure 2.23 illustrates the relationship between Mode-I interlaminar toughness and the CAI strength. The epoxy system composites have relatively higher CAI strength than the other thermoset resin system samples. Surprisingly, the stitching technique cannot improve the residual compressive strength unlike the Mode-I interlaminar fracture toughness. On the other hand, the PEEK and interleaving have significantly high CAI strength. In particular, the PEEK system composites have good mechanical properties for both of the Mode-I interlaminar toughness and the CAI resistance. Although the interleaved composites do not show a wide range of G_{IC} values, the residual compressive strength has quite a wide range and the maximum strength is over 400MPa compressive strength [143-144].

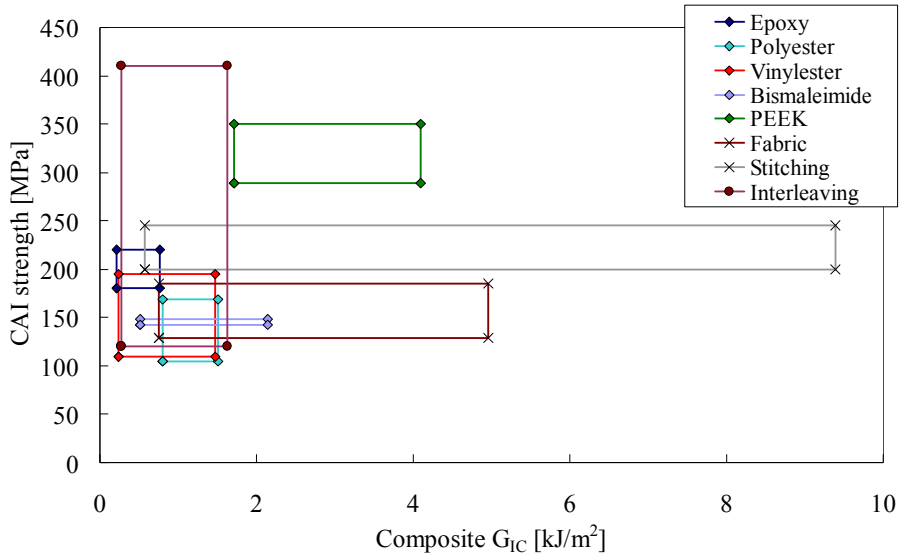

Figure 2.23 Comparison of CAI resistance against various Mode-I interlaminar toughness techniques of composites [20, 27, 31, 41-42, 45, 63, 89-90, 95, 102, 130, 143, 148, 162, 165-171]

Figure 2.24 shows the diagram of the Mode-II interlaminar toughness against the CAI strength. The tendency of the relationship between G_{IIC} and CAI strength is similar to that of G_{IC} and CAI strength. The interleaving technique has good properties of both G_{IIC} and CAI strength [143-144, 148]. Although, the PEEK-matrix composites have not got good properties for the Mode-II interlaminar toughness compared with the other toughened composites, the CAI resistance is significantly high [171]. The stitching and epoxy-matrix composites have moderate CAI resistance [95, 166, 168].

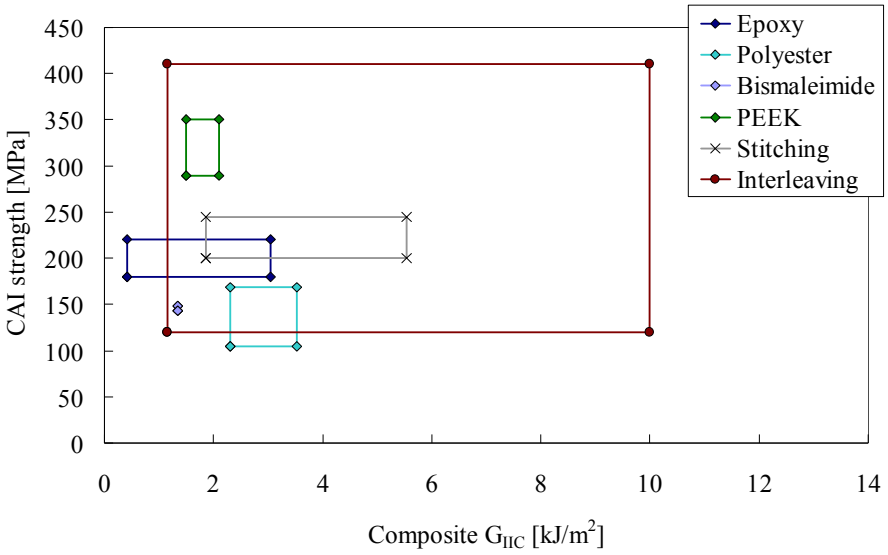

Figure 2.24 Comparison of CAI resistance against various Mode-II interlaminar toughness techniques of composites [28, 46, 53, 56, 63, 94-95, 108, 112, 141, 143, 148, 165-166, 168-172]

2.7 Interlaminar Toughness Tests

2.7.1 Introduction

FRP structures such as aeroplanes and automobiles are constructed from the laminates of stacked plies with several fibre orientations. It has been mentioned already that laminated materials are especially susceptible to damage from out-of-plane impact. In this case, the fracture mode is mainly interlaminar delamination. If the laminate composites receive impact damage, residual strength, in particular the compression properties will be significantly reduced.

For the laminated composite materials, the evaluation of the interlaminar fracture is important. There are three fracture modes for interlaminar fracture, Mode-I (Open mode), Mode-II (In-plane shear mode), and Mode-III (Out-of-plane shear mode). Figure 2.25 shows models of each fracture mode. P. Davies *et al.* summarised various interlaminar fracture toughness tests [173].

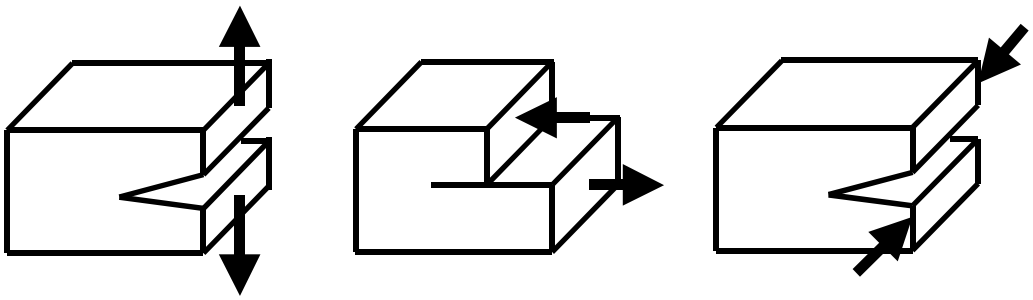

(a) Mode-I (b) Mode-II (c) Mode-III

Figure 2.25 Schematic diagrams of each fracture mode [174]

The strain energy release rate, *G*, is defined as the potential energy of dynamic system when the crack propagates per unit area. The total kinetic energy, *U*, means the energy conserved by object and external force system. The equation for calculating *G* is as follows:

$$G = -\frac{dU}{Bda} \tag{2.1}$$

where *B* is width of specimen and *da* is amount of crack propagation. The ratio of displacement, δ, and load, *P*, is called compliance, *C*. If the crack propagates under constant load, the increment of displacement is *PdC*. Therefore, the energy release rate *G* can be calculated using the following equation.

$$G = \frac{P^2}{2B}\frac{dC}{da} \tag{2.2}$$

For the strain energy release rate, initiation and propagation values are used as toughness values of the composites. They increase with growth of delamination from the initial cracks or starter film. This behaviour is often influenced by fibre-bridging. The effect of the fibre-bridging depends on laminate thickness, ply orientation and moulding condition. Therefore, the initial value of energy release rate value, G_{IC}, is the most conservative criteria [175]. The non-linearlity (NL) and the 5% offset or maximum load (5%/MAX) values are often used as the initial toughness properties. The 5%/MAX value defines initiation at the lowest displacement point among the 5% offset and the maximum load. The former is obtained by intersecting the load-displacement curve with a line corresponding to a compliance 5% higher than the initial case, as shown in Figure 2.26.

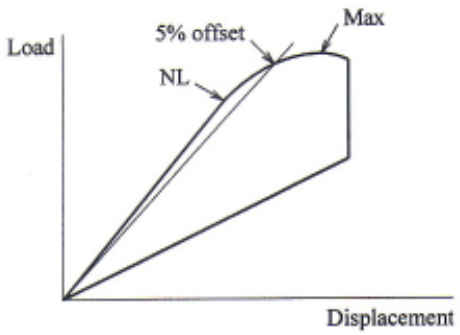

Figure 2.26 Crack initiation criteria [176]

2.7.2 Mode-I Interlaminar Toughness Test

The Mode-I interlaminar toughness tests are carried out using the double cantilever beam (DCB) test, as shown Figure 2.27. The DCB test has been standardised by JIS, ASTM, and ISO [177-179].

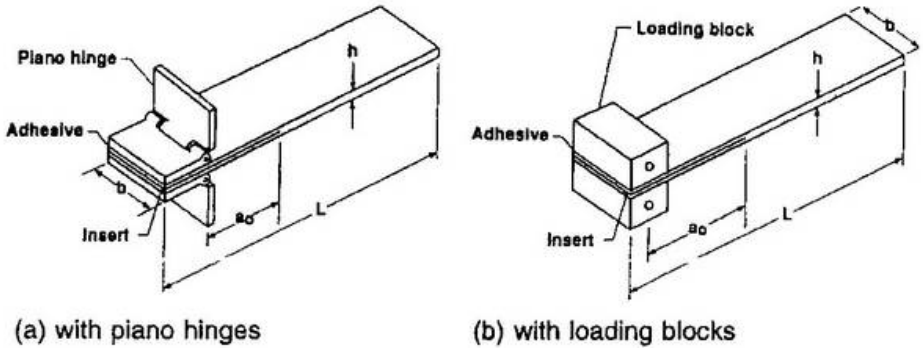

Figure 2.27 Double cantilever beam (DCB) specimens [178]

In order to introduce a starter crack, a non-adhesive film, such as Teflon, aluminum and so on, is inserted at mid-plane. Alternatively, an initiation crack is made by inserting a wedge. The DCB test has attracted attention over the 30 years. The test has been generally performed on unidirectional specimens. Round robin tests for the DCB tests have been carried out by many researchers or societies [180-182]. Various parameters for the DCB specimens, such as specimen thickness, insert film type, and with/without pre-crack have been investigated in these round robin tests [175, 182]. Many researches indicated that the G_{IC} value decreased as the starter film thickness was decreased. However if a starter film is below a certain thickness, a constant G_{IC} value was measured. The threshold thickness appeared to be approximately 15 μ m. If the

specimen is too thin or the toughness of the materials is too high, an arm of the specimens might fail in bending before the delamination grows. In order to prevent this fracture, a reinforcement panels are put on both top and bottom surfaces of the specimen [183]. The data reduction methods to obtain the critical energy release rate, G_{IC}, have been developed experimentally and analytically [184-188]. L. Ye characterised correlation between the Mode-I interlaminar toughness G_{IC} and the Mode-I critical stress intensity factor K_{IC} [189]. The calculation method of G_{IC} value has four types [185].

2.7.2.1 The Area Method

Firstly, the value of G_{IC} for the Area method is defined by

$$G_{IC} = \frac{\Delta U}{B\Delta a} \tag{2.3}$$

where B is the width of crack, ΔU is the area under the load-displacement trace, and Δa is length of crack, as illustrated in Figure 2.29. G_{IC} value is calculated by energy change ΔU with crack propagation Δa. If the load-displacement relationship in crack propagation is assumed to be linear, the G_{IC} is as follow

$$G_{IC} = \frac{P_A\delta_B - P_B\delta_A}{2B\Delta a} \tag{2.4}$$

where P is the load and δ is the displacement. Subscripts, A and B, mean the value at A and B, as shown in Figure 2.28.

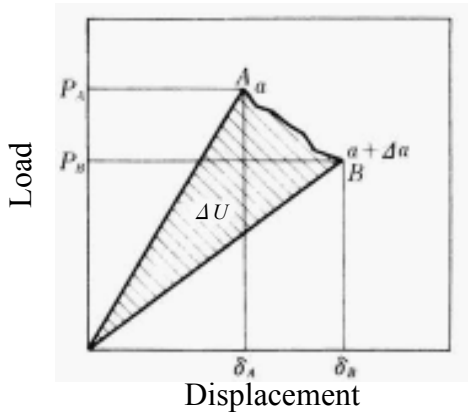

Figure 2.28 Calculation of G_{IC} by the area method [4]

2.7.2.2 The Compliance Method

The compliance method is presented as follows

$$G_{IC} = \frac{P^2}{2B}\frac{dC}{da} \tag{2.5}$$

where C is the compliance, given by

$$C = \frac{\delta}{P} \tag{2.6}$$

where δ is the displacement corresponding to load P.

2.6.2.3 The Load Method

The value of the compliance, C, from simple beam theory, is given by

$$C = \frac{\delta}{P} = \frac{2a^3}{3EI} \tag{2.7}$$

and, $I = Bh^3/12$

$$C = \frac{8a^3}{BEh^3} \tag{2.8}$$

where E is the flexural modulus, I is the second moment of area and $2h$ is the total thickness of the DCB specimen. Therefore, from Equations 2.5 and 2.8

$$G_{IC} = \frac{P^2a^2}{BEI} \tag{2.9}$$

2.7.2.4 The Displacement Method

For the displacement method, Equation 2.7 is substituted into Equation 2.9. To give G_{IC}:

$$G_{IC} = \frac{3P\delta}{2Ba} \tag{2.10}$$

2.7.3 Mode-II Interlaminar Toughness Test

As the typical Mode-II interlaminar toughness test, the end notched flexure (ENF) test has been carried out mainly. Figure 2.29 illustrates a typical ENF test configuration.

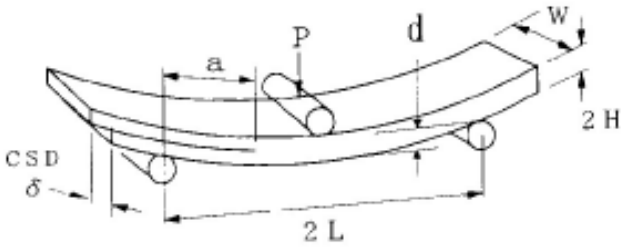

Figure 2.29 End notched flexure (ENF) test specimen [173]

The geometry of the ENF specimens is the same as the DCB specimens, and pure Mode-II deformation can be obtained by loading using a three-point bending fixture. The ENF test was standardised by JIS in 1993 [177]. Some researchers reported results of round robin tests by the ENF tests [190-191]. The Mode-II interlaminar test remains controversial, because of unstable crack propagation, friction effects, and difficulty in defining a starter defect [173]. In order to solve this problem, several Mode-II interlaminar test methods have been suggested by organisations and many researchers [173, 177, 190-192].

2.7.3.1 Three-Point End Notched Flexure (3ENF) Test

The development of the ENF specimen, as shown Figure 2.30, was based on work on the fracture of wood. The three-point ENF test (3ENF) is the most widely used Mode-II configuration [193]. The following analyses were applied [173].

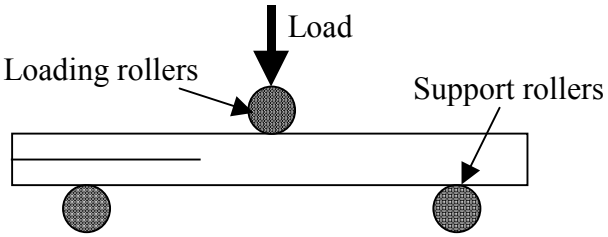

Figure 2.30 Three-point end notched flexure (3ENF) test specimen

The following analyses are applied,

Compliance method: $C = C_0 + ma^2$

$$G_{IIC} = \frac{3P^2 ma^2}{2B} \tag{2.11}$$

Simple beam theory

$$G_{IIC} = \frac{9P^2a^2}{16B^2E^1h^3} \tag{2.12}$$

Corrected beam theory

$$G_{IIC} = \frac{F}{N}\frac{9P^2a^2}{16B^2E_1h^3}\left[1+0.2\frac{E_1}{G_{13}}\left(\frac{h}{a}\right)^2\right] \tag{2.13}$$

where C is compliance, C_0 is uncracked compliance, m is an experimental parameter, a is the crack length, B is the width of specimen, E is the longitudinal modulus, h is half thickness, and F and N are corrections for large displacements. The disadvantage of this method is that propagation is unstable except for very long crack length ($a/L > 0.7$) [173].

2.7.3.2 Stabilised End Notched Flexure (SENF) Test

The Work in Japan has led to a number of procedures for stabilising the test on the ENF specimen (SENF) by feedback control of the test machine [177]. Two methods were applied in the Versailles Project on Advanced Materials and Standards (VAMAS) test program. The first is referred to as crack share displacement (CSD) control, in which CSD is measured as shown in Figure 2.31. This is then used as the input parameter fed negatively into a feedback loop and the CSD rate is kept constant.

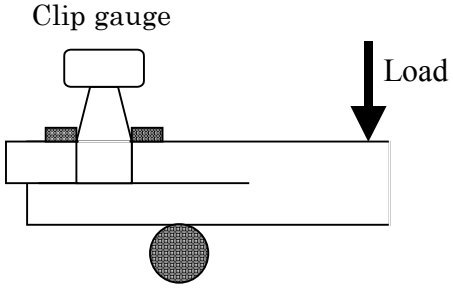

Figure 2.31 Stabilised end notched flexure (SENF) test specimen

An alternative is to use the coordinate conversion control (CCC) method [190]. In this case, the load P and cross-head displacement δ are input to a circuit which gives an output $C = \delta - \alpha P$. When C is controlled so as to increase monotonically, the crack propagation is stabilised. For both these tests, a servo-controlled test machine is needed. Two test procedures based on the SENF specimen were proposed by the JIS

group for the VAMAS exercise [173, 191].

2.7.3.3 End Loaded Split (ELS) Test

The specimen is held in a clamp which is free to slide horizontally, as shown Figure 2.32. The crack propagation along this specimen is basically stable provided the ratio of crack length to free length exceeds 0.55 [173].

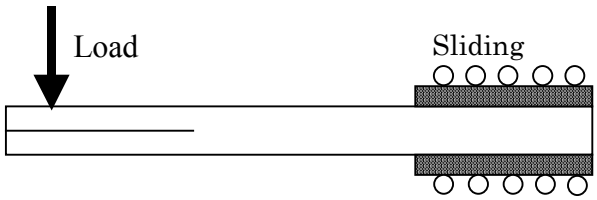

Figure 2.32 End loaded split (ELS) test specimen

The analyses are applied [191],
Simple beam theory

$$G_{IIC} = \frac{9P^2a^2}{4B^2E_1h^3} \tag{2.14}$$

Experimental compliance calibration

$$G_{IIC} = \frac{3P^2ma^2}{2B} \tag{2.15}$$

where m is the slope of a plot of compliance versus the cube of crack length.

Corrected beam theory

$$G_{IIC} = G_{IIBT}\left[1 - \theta_1\left(\frac{\delta}{L}\right)^2 - \theta_2\left(\frac{\delta l_1}{L^2}\right)\right] \tag{2.16}$$

where θ_1 and θ_2 are large displacement and loading block corrections respectively, and L is the free length of the specimen.

2.7.3.4 Four-Point End Notched Flexure (4ENF) Test

The modified version of the 3ENF configuration, as shown in Figure 2.33, was proposed by R.H. Martin and B.D. Davidson [192]. The delamination tip may be to the left of or in between the loading rollers. The connection between load fixture and the

load frame is pinned. For a pinned configuration with the delamination front within the loading roller span, the shear force is zero and the bending moment is constant. This provides a reduction of delamination face friction compared with the conventional Mode-II interlaminar tests. Therefore, crack growth in this configuration is stable. The analysis is by experimental compliance calibration only, and the slope m is determined from a plot of compliance, C, versus crack length, a. The G_{IIC} value is given by

$$G_{IIC} = \frac{P^2 m}{2B} \tag{2.17}$$

where P is the load, m is the gradient from CC curve, and B is the width of specimen.

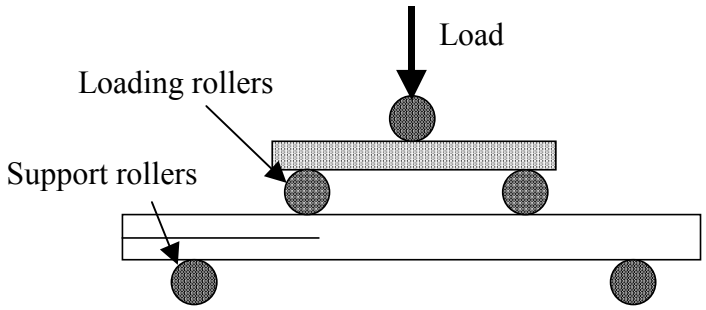

Figure 2.33 Four point end notched flexure (4ENF) test specimen

This method is new and developing. Recently, some researches using 4ENF test have been reported [94, 194-196]. Table 2.2 summarises some of the advantages and disadvantages of each test [173]. The Mode-II tests have to consider several factors, such as type of starter crack, definition of initiation, stability, friction, and data analysis.

Table 2.2 Comparison of specimens for each Mode-II test [173]

Methods	***Advantage***	***Disadvantage***
ENF	Simple The Most used	Unstable propagation
SENF	Stable propagation	Complicated Special equipment
ELS	Stable propagation	Clamping variability
4ENF	Stable propagation	Little experience and developing

2.7.4 Effect of Test Condition

Some researchers have suggested that the Mode-I interlaminer fracture toughness is loading rate sensitive [197-201]. Figure 2.34 shows rate dependency of the fracture toughness for the CFRP.

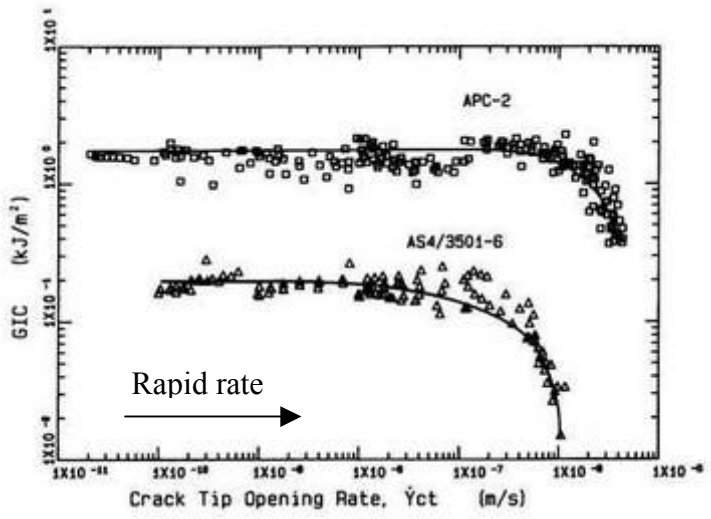

Figure 2.34 Rate dependency of Mode-I interlaminar toughness [197]

If the displacement rate is rapid, a plastic zone in the interlaminar region cannot be enlarged enough. This reflects the rate sensitivity of the matrix resin. Figure 2.35 shows the influence of rate effect on the plastic zone. In other researches, the effects of loading rate on CF/epoxy and CF/PEEK composites have been undertaken [197-201]. The test rate was 0.2 to 250mm/min. The G_{IC} value for the CF/epoxy composites were not affected strongly by loading rate. In contrast, the CF/PEEK was significantly dependent on loading rate [199]. They concluded that the dependence of rate in G_{IC} for the CF/PEEK composite is affected by transition from a ductile to brittle behaviour of the polymer in the process zone.

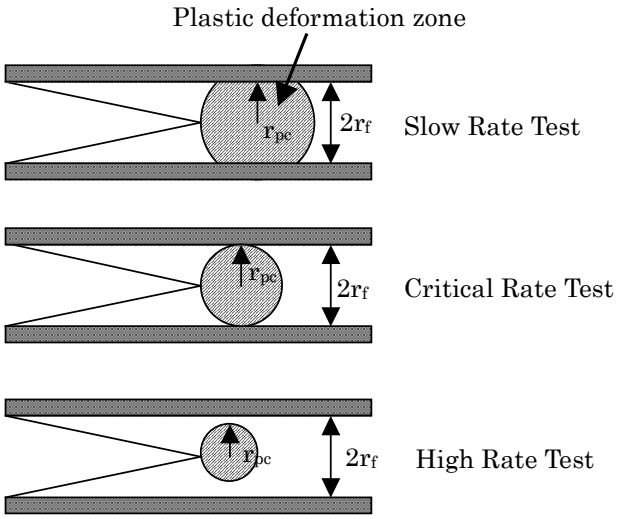

Figure 2.35 Rate effects on plastic zone size of composites [197]

Mode-II interlaminar toughness also is affected by loading rate. P. Compston *et al.* investigated loading rate dependency on the Mode-II interlaminar fracture toughness using the GF/VE composites [161]. They, however, mentioned that the displacement rate effect for G_{IIC} is not significant, as compared with the G_{IC}. It is thought that the rate effect for the Mode-II interlaminar toughness may be more complex than for the Mode-I interlaminar toughness. Moreover, test temperature also affects results [201].

2.7.5 Mixed-Mode Interlaminar Toughness Test

A Mixed-Mode bending (MMB) test was introduced in the late 1980s. Thereafter a modified method to reduce non-linearity has become the most widely used specimen for MMB test, as shown in Figure 2.36. The MMB configuration has two advantages [173]:

(i) The possibility of using the same specimen geometry as for the Mode-I tests
(ii) The means to vary simply the mixed mode ration over the whole range from pure Mode-I to pure Mode-II.

However, it has many disadvantages. It requires a complex fixture and bonded steel hinged tabs [202-203].

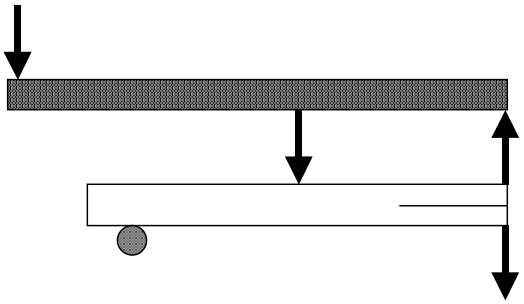

Figure 2.36 Schematic of Mixed-Mode bending (MMB) specimen

In this method the loading technique combines the DCB and ENF tests. The characteristics of the MMB test are that specimens can be the same as the DCB or ENF specimens, mode ratio can be varied continuously and does not change with crack propagation. The energy release rate for each mode is as following

$$G_I = \frac{3P^2(a+\gamma_I h)^2(3c-L)^2}{4E_L B^2 h^3 L^2} \tag{2.18}$$

$$G_{II} = \frac{9P^2(a+\gamma_{II} h)^2(c+L)^2}{16E_L B^2 h^3 L^2} \tag{2.19}$$

or mode ratio is

$$\frac{G_I}{G_{II}} = \frac{4}{3}\left[\frac{(a+\gamma_I h)(3c-L)}{(a+\gamma_{II} h)(c+L)}\right]^2, \quad c \geq \frac{L}{3} \tag{2.20}$$

where χ is the crack length correction for crack tip rotation. If the specimen is unidirectional CFRP, χ_I and χ_{II} are approximately 2 and 1, respectively. The MMB test was standardised by ASTM [204]. Many researches for the Mixed-Mode have been carried out experimentally and analytically [43, 155, 188, 200, 202-203, 205-208].

For the mixed mode specimens, several methods were suggested. Figure 2.37 show some of the specimens for the mixed mode ratio specimens, cracked lap shear (CLS), asymmetric double cantilever beam (ADCB), single leg bend (SLB) and four point bend (FPB) specimens. Table 2.3 indicates advantages and disadvantages of each mixed-mode fracture toughness test.

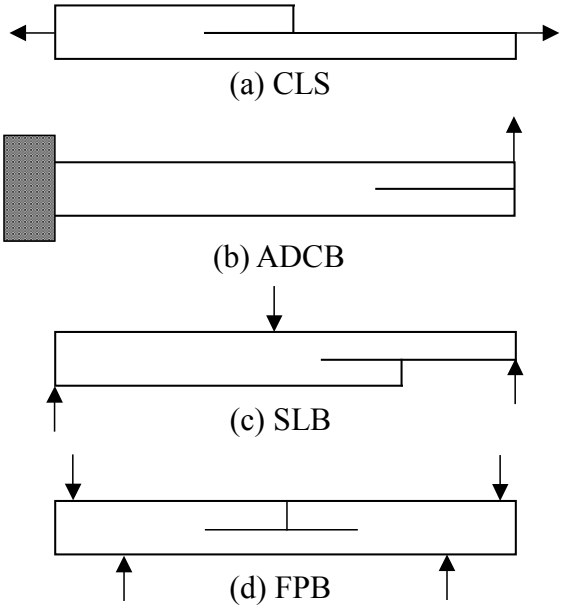

Figure 2.37 Various single Mixed-Mode (I/II) ratio specimens [207]

Table 2.3 Comparison of Mixed-Mode test method [207]

Test method	***Advantages***	***Disadvantages***
MMB	Simple specimen geometry Variable mode mix ratio	Requires complex fixture, bonded hinged tabs, and complex data reduction techniques
CLS	Simple fixture and specimen geometry Small crack opening displacement Constant mode ratio	Requires non-linear numerical analysis Large rotations at crack tip Different ply lay-ups needed for different mode ratio
ADCB	Simple specimen geometry	Requires complex fixture and bonded hinged tabs
SLB	Simple fixture and specimen geometry	Mode ratio changes with crack length Different specimen geometry needed for different mode ratio
FPB	Simple fixture and specimen geometry Constant mode ratio	Two cracks growing simultaneously at different rates Different specimen geometry needed for different mode ratio

2.7.6 Mode-III Interlaminar Toughness Test

In the late 1980s, some researches suggested the way of introducing out-of-plane shear (Mode-III) test for the composite materials. However, compared to the Mode-I and Mode-II tests, there has been little research into Mode-III Interlaminar toughness properties. Moreover, none are considered a very satisfactory method. It is also not clear whether the G_{IIIC} is an important factor. Recently, several researchers have reported work on the Mode-III test.

2.7.6.1 Cracked Rail Shear (CRS) Test

G. Becht and J.W. Gillespie suggested the cracked rail shear (CRS) specimen for the Mode-III interlaminar fracture toughness test, as shown in Figure 2.38 [209]. This test uses a two-rail shear specimen [210] and release film is used for introducing a delamination crack. The specimen is strained using two-rail test rig, and the crack is loaded in Mode-III.

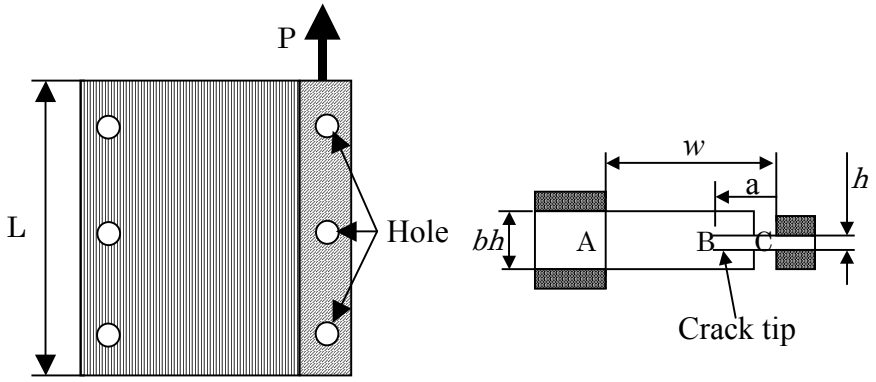

Figure 2.38 Cracked rail shear (CRS) test specimen [211]

The Mode-III interaminar toughness, G_{IIIC}, is calculated by

$$G_{IIIC} = \frac{P_C^2}{4L}\left(\frac{\gamma^{AB}}{P}\right)[b-1] \tag{2.21}$$

where P_C and P are the critical load and load respectively, L is the length, γ_{AB} is shear strain at AB cross-section, and b is the total thickness of specimen. γ_{AB} is calculated by

$$\gamma_{AB} = \frac{P}{LbhG^{AB}} \tag{2.22}$$

where G^{AB} is shear modulus at cross-section AB.

2.7.6.2 Split Cantilever Beam (SCB) Test

S.L. Donaldson suggested that the split cantilever beam (SCB) test method was used similar to the DCB specimen and loaded in the shear direction [212]. Figure 2.39 shows a schematic of the SCB specimen. The laminate material with inserted crack is adhered between two aluminum plates, and the edges of the two aluminum plates are loaded to give a parallel crack surface, as shown in Figure 2.39. P. Robinson and D.Q. Song modified the loading pattern for the SCB test [213]. They tried to eliminate the unwanted Mode-II component. The $G_{IIIC,i}$ value for crack length, a_i, at No. i followed as

$$G_{IIIC,i} = \frac{nP_i\delta_i}{2ba_i} \tag{2.23}$$

where P_i and δ_i are the critical load and displacement for crack length at No.i, respectively, b is the depth of cantilever, n is the coefficient.

Figure 2.39 Split cantilever beam (SCB) test specimen [211]

2.7.6.3 Edge Crack Torsion (ECT) Test

For this test a series of specimens with different initial film crack length is prepared [173]. The lay-up is typically: $\mathbf{[90/(+45/-45)_n/(-45/+45)_n/90]_S}$ with n=3. These are loaded in torsion by pushing down on one corner and the initial part of the load-displacement plots allows a compliance calibration to be determined of the form.

$$\frac{1}{C} = A\left[1 - m\left(\frac{a}{B}\right)\right] \tag{2.24}$$

where C is the compliance, a is the crack length and B is the specimen width. Plotting $1/C$ versus a/B gives gradient, m. the G_{IIIC} value is as followed.

$$G_{IIIC} = \frac{mP^2C}{2LB\left[1 - m\left(\frac{a}{B}\right)\right]} \tag{2.25}$$

where P is the critical load point. Figure 2.40 presents the ECT specimen.

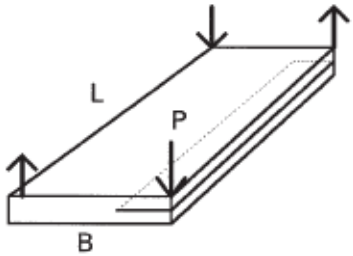

Figure 2.40 Edge crack torsion (ECT) test specimen [173]

2.8 Compression After Impact (CAI) Properties

2.8.1 Low Energy Impact

In this section, impact, damage assessment, and CAI responses are reviewed. Comprehensive reviews on impact responses of the composites can be found in various literatures [22, 214-216]. Impact damage resistance is described as "the measure of the ability of a composite structure to resist damage due to a foreign object impact" [217-218]. On the other hand, damage tolerance is defined as "the ability of a structure to contain representative weakening defects under representative loading and environment without suffering excessive reduction in residual strength, for some stipulated period of service" [215, 218-219]. The response of the composite materials to impact loading and dissipation of incident impact energy are completely different as compared to that of metal materials [216]. For low or medium incident impact energies, the metals can absorb impact energy through elastic and plastic deformation. Although the plastic deformation causes some permanent deformation, the reduction of residual strength is small. In contrast, the energy for the composite materials is largely absorbed in creating large areas of damage. Therefore, a reduction of the residual strength is higher than for metals. When the composite materials such as the laminated FRP have damage from out-of-plane impact, the composites exhibit various damages, such as intralaminar failure, delamination, and fibre failure, under the impact [22, 77, 119, 172, 215, 220]. Figure 2.41 is a schematic representation of damage modes. The intralaminar failure and delamination include matrix cracking. The matrix cracks do not significantly contribute to the reduction in residual mechanical properties of the laminate. The damage process such as the delamination, however, is initiated by the matrix cracks [21].

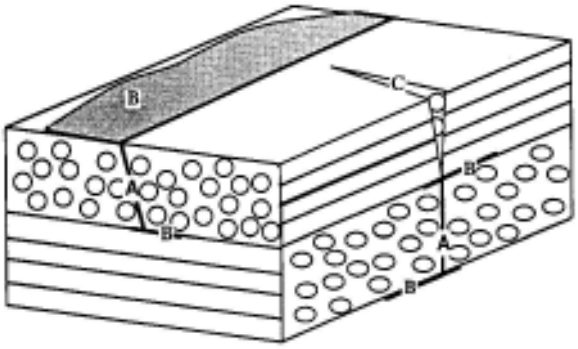

Figure 2.41 Three basic damage modes of composite laminates: (A) Intraply cracking mode, (B) Delamination mode, (C) Fibre breakage mode [22]

The matrix cracks can be divided two types: Tensile cracks and Shear cracks (see in Figure 2.42). The tensile cracks are introduced when in-plane normal stresses exceed the transverse tensile strength of the ply. On the other hand, the shear cracks are at an angle from the mid-surface, which indicates that transverse shear stresses play a significant role in their formation.

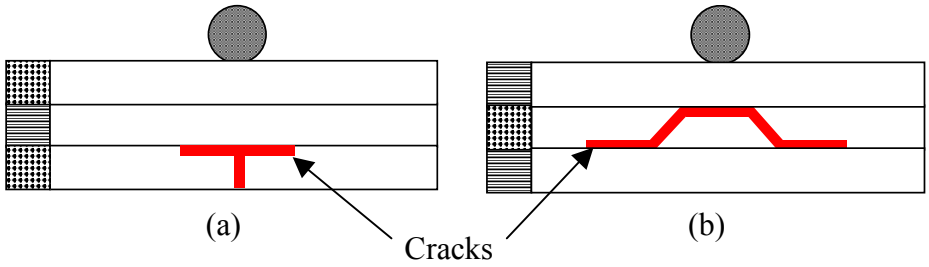

Figure 2.42 Schematic diagrams of matrix cracks: (a) Tensile crack, (b) Shear crack [21]

An impact damage develops under the impact area. The area of cracks increases with the distance from the impact point and forms the well-defined pine tree or cone [21, 166, 172, 220]. Figure 2.43 illustrates schematically impact damage for the composites. This impact event is affected by geometry of the laminates such as thickness or length [21, 121]. With thick and long laminates, the matrix cracks first occurred in the first layer impacted by the striker, because contact stresses concentrate locally. Therefore, the damage grows from the top down, as shown in Figure 2.44 (a). On the other hand, for thin and long laminates bending stresses in the back side of the laminate and matrix cracks induce in the lowest layer, as shown in Figure 2.44 (b).

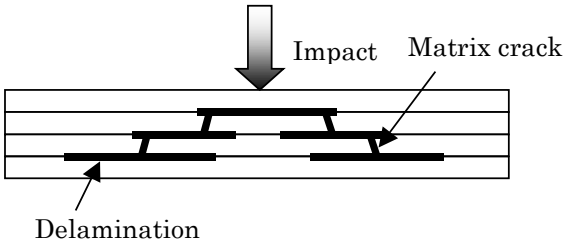

Figure 2.43 Schematic model of impact damage for laminate materials [19]

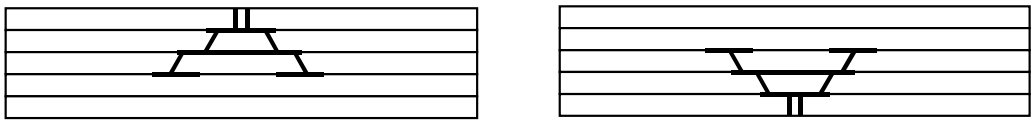

Figure 2.44 Schematic of pine tree: (a) Thick and short laminate, (b) Thin and long laminate [21]

Impacts can be divided briefly into low-energy impact and the high-energy impact [22, 119, 214-216, 221]. Figure 2.45 shows schematic diagrams of impact behaviour for low-energy and high-energy conditions. The low-energy impact loading is such that the contact time of the striker is relatively long and the target response is global, as shown in Figure 2.45 (a). Internal fracture may progress easily so that the specimen deforms over a wide range. The high-velocity impact loading, on the other hand, gives a localised damage of the target and the contact time of the striker is relatively short, as shown in Figure 2.45 (b). Under the high-energy impact, geometric parameters of the specimens, i.e. length, width and thickness, have little influence on the impact behaviour. The composite materials under the high-energy impacts are completely ruptured or penetrated by the striker [216]. In contrast, the geometric parameters of the specimens under the low-energy impact loading significantly influence results [117, 214, 216].

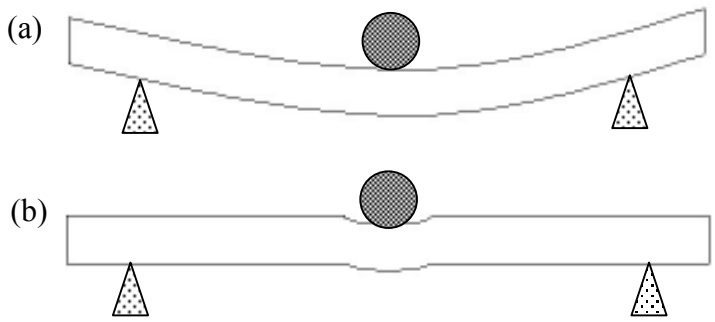

Figure 2.45 Schematic of the response to impact under (a) Low energy and (b) High energy conditions [216]

Several impact tests have been suggested and reviewed [119]. The impact damage can be divided into two conditions. One is the low-energy impact by a large mass (dropped tools) and the other is high-energy impact by small mass (runway debris, hail stones, etc.). The low-energy impact tests are generally evaluated using a swinging pendulum or a drop weight test. For example, the Charpy and Izod pendulums, and drop weight fixtures have been used for simulating the low-energy impact behaviour. In particular, the charpy impact test has been standardised by ASTM [222] for metallic materials, and JIS for CFRP [223]. The high-energy impact tests, on the other hand, have used a gas gun or other ballistic launcher. Standard impact tests for composite materials, however, are developing [214].

2.8.2 Non-Destructive Identification (NDI)

The failure for composite materials is surface failure and internal failure briefly. The surface failure appears on surface of the composite. Therefore, its detection is relatively easy. Internal failure, however, is a quite difficult issue, because the damage is normally barely visible on the surface. Consequently, the damage detection of composite materials is quite difficult. Non-destructive identification (NDI) testing plays a significantly important role in assessing damage of composite materials and supplying information on the damage behaviour. Various defects for GFRP have been defined by ASTM-D2563 [224]. The defects that require evaluation are crack, internal delamination, dry spot, foreign inclusion, void, blister, porosity, resin rich, and so on. These defects are internal defection which is target of the NDI.

The main problem of the NDI test, however, is the choice of best way to detect

damages. In GFRP, there is some degree of clearness, and the visual detection of the fracture may be easy. Meanwhile the visual observation of CFRP is significantly difficult, because of it is completely opacity. NDI for the composite materials uses the phenomenon which changes the physical property of the material by the existence of the failure. There are sound waves, X-rays, electromagnetic or thermal properties for physical characteristic using the NDI. Some detecting methods have been suggested such as ultrasonic, acoustic emission, X-ray and so on. Table 2.4 summarises types and characteristics of the NDI. It is well-known that the ultrasonic detecting is the most versatile technique. It is necessary to look for the optimum detecting method corresponding to the material because each detecting method has advantages and disadvantages.

Table 2.4 Characteristic of NDI test [225]

Properties	**Method of NDI**
Sound waves	Ultrasonic wave Acoustic Emission (AE)
Radioactive ray	X-ray
Electromagnetic	Electromagnetic wave
Thermal or kinetic	Thermography Laser-horography

Ultrasonic testing makes use of behaviour which is reflection, absorption or refraction, and mechanical oscillation at frequencies above 20kHz [225-226]. This method obtains information from the ultrasonic wave which is changed by the existence of flaws. The ultrasonic wave is transmitted through the specimen to be investigated, and the reflected signal from the specimen passes to the receiver. If a flaw is present in the specimen, the wave is reflected from the damaged area and does not reach the receiver. The lack of signal will be registered as a damage spot on the scanning image. The ultrasonic wave which propagates through solid materials exists as longitudinal, transversal, or surface waves. The ultrasonic wave used in the NDI of the composites is always the longitudinal wave. There are three ways of displaying the ultrasonic signals, which are termed A, B, and C-scan [227]. An ultrasonic A-scan refers to data presented as signal amplitude versus time. An ultrasonic B-scan is the presentation of ultrasonic data in the form of a depth profile versus position along a specimen. The C-scan gives a map view of the component showing defect areas, however obtains no information on

depth of the defect. The ultrasonic C-scan is probably the most used in the NDI test method for the composite materials [226-228].

2.8.3 Compression After Impact (CAI)

There are three types of mechanical properties, which are compression, tension, and flexure, and fatigue of post-impact residual strength. The compression and tensile strength have received large attention [21, 229]. In particular, the compression after impact (CAI) property is recognised as the most important mechanical property, because strength reductions under compressive loading are the largest [229]. The compression test for the composite materials is one of the most difficult types of testing, because of tendency for premature failure due to crushing or buckling [171]. The CAI test has been used widely as one of the important criteria for the aerospace industry. Hence, some specifications for the CAI tests have been suggested, for example NASA [230], CRAG [231], and Boeing [232]. Moreover, SACMA have standardised the CAI test method [233]. A large number of the CAI tests are currently being carried out by aerospace industries and advanced material suppliers. The full size Boeing, SACMA, and Airbus tests have the high cost of producing specimens. For example, the geometry of NASA type is 250 x 125 x 6mm, and that of SACMA is 150 x 100 x 4mm. Therefore a miniaturised version of the test coupons has been required. J.C. Prichard and P.J. Hogg developed the miniaturised CAI fixture at Queen Mary and Westfield College (QMW) [171]. The QMW test specimen consists of a plate specimen, 89 x 55mm. A summary of some of the CAI tests is indicated in Table 2.5. The CAI test consisting of mainly three processes [234]:

(1) Introducing initial delamination by impact load
(2) Inspection of interlaminar delamination by NDI such ultrasonic test
(3) Measurement of CAI behaviour and strength by compression test

In contrast, residual flexure and fatigue strength have received less attention than the other two properties [22, 220]. Flexure testing introduces a complex stress pattern in the specimens. Hence, post-impact flexure properties are very difficult to analyse. For post-impact fatigue property, it is difficult to evaluate by only few numbers of studies [229].

Table 2.5 Summary of common CAI test methods [171, 229]

Conditions	*NASA*	*Boeing*	*CRAG*	*Prichard & Hogg*
Lay-up	[45,0,-45,90]	[-45,0,45,90]	[45,-45,0,90]	$[-45,0,45,90]_{2S}$
Thickness	6.35mm	4 to 5mm	3mm	2mm
Striker diameter	12.7mm	15.75mm	10mm	20mm
Striker mass	4.5kg	4.6 to 6.8kg	As required	3.96kg
Drop height	0.63m	As needed	1m	As needed
Specimen size	h = 243–317mm w = 178mm	h = 152mm w =102mm	h =180mm w =50mm	h =89mm w =55mm
Test loading	End loading	End loading	End tabs	End loading
Loading rate	1.27mm/min	0.5mm/min	Adjusted to achieve failure in 30–90s	0.3mm/min

The delaminations at low-energy impact damage have little effect on the tensile property but significantly decrease the compression property [22, 214-216, 235]. The residual strength normally indicates as shown in Figure 2.46. As shown in Figure 2.46, the residual tensile strength is little affected at low impact energy. However, the residual tensile strength reduces rapidly after fibre fractures occur [215-216]. On the other hand, reduction of the compressive strength is rapid even at the low impact energy.

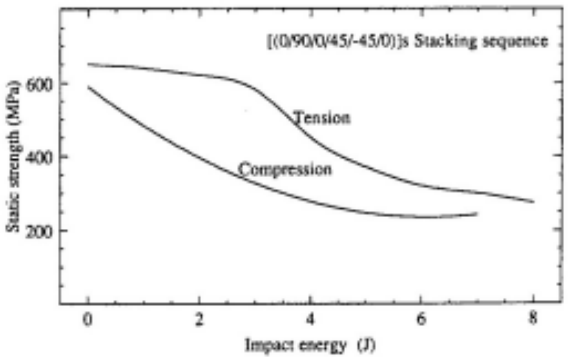

Figure 2.46 Characteristic residual strength against impact energy [215]

CAI specimens are generally flat plates although curved plates have also been evaluated for CAI properties [236-237]. Moreover, P.J. Hogg and co-workers investigated miniaturising curved specimens also [167]. Currently, the CAI test has been standardised by ASTM and JIS [238-239].

Caprino [240] suggested a model based on linear elastic fracture mechanics for predicting the residual strength, σ_r (tension and compression) of impacted notched laminates:

$$\frac{\sigma_r}{\sigma_0} = \left(\frac{C_0}{C}\right)^m \tag{2.26}$$

where σ_0 represents the strength of unnotched material, C_0, the dimension of a characteristic defect of the materials and C, the dimension of the notch. The parameters m and C_0 must be experimentally determined and depend uniquely on the examined materials. The above equation is valid for

$$C \geq C_0 \tag{2.27}$$

when $C = C_0$, the strength of notched materials is equal to its unnotched strength. From a physical point of view, Equation 2.26 indicates that the laminate strength is not influenced by notches smaller than C_0. If the relationship between the notch of dimension, C, and the impact energy, U, can be expressed by a power law, then

$$C = kU^n \tag{2.28}$$

Because of the increase of C with the increase of U, of course n must be > 0. From Equation 2.26 and 2.28, we get:

$$\frac{\sigma_r}{\sigma_0} = \left(\frac{U_0}{U}\right)^\alpha \tag{2.29}$$

where

$$\alpha = mn \tag{2.30}$$

and U_0, given by:

$$C_0 = kU_0^n \tag{2.31}$$

Equation 2.31 gives a model for predicting residual strength as a function of impact energy, U_0, and α are experimentally determined. If impact energy, U, is less than the critical energy, U_0, the residual strength is equal to the unnotched strength.

The residual compressive strength is influenced significantly by the low-energy impact. This is due to susceptibility for delamination of the composite materials. Under the compressive load, the specimen has undergone buckling failure. The buckling modes are briefly two types which are local buckling and global buckling [237]. These buckling modes are illustrated in Figure 2.47. The local mode occurs when the delamination is near the surface of the laminate and the area of the delamination is large.

The global mode, on the other hand, occurs when the delamination is deeper within the laminate and has a small area. The CAI testing has to avoid buckling failure due to the difficulty in evaluating results caused by complex fractures. Therefore, an anti-buckling rig for the CAI testing has been produced to prevent global buckling failure.

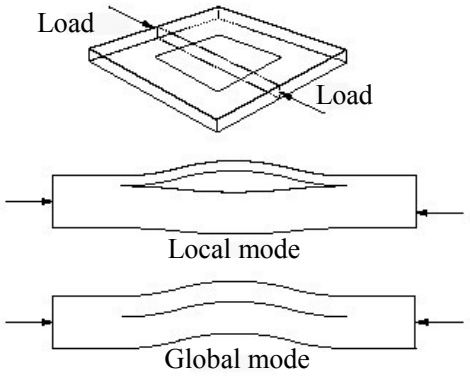

Figure 2.47 Local and global modes of delamination induced buckling [237]

2.9 Conclusions

Various aspects of the relevant literature have been reviewed, focusing on obtaining previous research of the moulding method and the interlaminar fracture toughness for composite materials. This chapter is divided into five divisions: RTM moulding methods of the composite materials, Interlaminar fracture toughness techniques, Comparison of previous researches, Various mode fracture tests, and finally Compression after impact properties.

- There are manual and automatic moulding methods of the composite materials. The hand lay-up method is the basic manual moulding technique. Moulding methods should be selected appropriately in response to the type of composite structure. In this research, the VaRTM derived from the RTM technique was chosen for moulding of the specimens. The VaRTM method is a low cost moulding process with the capability of producing huge and complex composite materials. However, the resin viscosity and permeability of the toughening materials are a significantly important factor for moulding. If the resin possesses high viscosity or the toughening materials do not have permeability, the resin injection will be significantly difficult.

- The history of research into interlaminar fracture toughness for the composite materials is long, over 30 years. One of the simplest toughening method is toughened matrix using rubber particles. Although the matrix can be improved by the rubber toughening significantly, interlaminar fracture toughness of the rubber toughnend composite is only moderately improved, because the existence of reinforcement, such as fibres, restricts extension of the plastic zone at the interlaminar region. For the other toughening techniques, there are improving adhesion between fibre and matrix, changing fibre orientation, stitching, interleaving and so on. In this work, suitable materials for the VaRTM method are focused on and the non-woven veils are chosen because of good resin permeability.

- For the Mode-I fracture, stitching, fabric improvement and PEEK resin realise high fracture toughness. The interleaving, thermoplastic resins, and stitching methods lead to superior characteristics of the Mode-II fracture toughness. For the post-impact resistance, the toughening techniques which possesses high G_{IC} values do not necessary lead to high CAI resistance. On the other hand, the relationship between the G_{IIC} and CAI values show a relatively better correlation than that between the G_{IC} and CAI values. For the resin G_{IC} and composites G_{IC}, high resin toughness does not transfer to high composites toughness necessarily, in particular PEEK composite. It is thought that the plastic zone is restricted by existence of the reinforcements. The G_{IC} value, therefore, cannot be increased largely. The relationship between the resin G_{IC} and composites G_{IIC} is not seen completely.

- Interlaminar toughness tests for each fracture mode have been suggested over many years. For the Mode-I interlaminar fracture test, the DCB test is established completely. Mode-II interlaminar fracture tests are developing and being tested. The 3ENF test is the most used for the Mode-II interlaminar fracture test. Crack propagation during testing, however, is unstable for the 3ENF test. Therefore, the other Mode-II interlaminar fracture tests have been established by researchers, which are the SENF, ELS, and 4ENF tests. Each Mode-II test has some merits and demerits. In this work, the 4ENF test was selected as the Mode-II interlaminar fracture test. The mixed-mode combined Mode-I and Mode-II interlaminar fracture tests have been also carried out and evaluated by many researchers. Finally, the Mode-III interlaminar fracture tests have had little investigation.

- Impact damage can be divided briefly into two: Low-energy and High-energy

impact. There are clear different behaviour between low- and high-energy impact damage. The low-energy impact may show barely visible damage on surface. The composites, however, would receive internal damage, such as delamination, matrix cracking, or fibre breakage. These damages cause a significant reduction of the residual strength, in particular compression strength. On the other hand, high-energy impact is basically local damage. The high-energy impact damage is not influenced by geometric parameters of the specimens, unlike the low-energy impact.

- The NDI is an important technique for assessment of the damage. Especially, the ultrasonic C-scan is the most used of the NDI methods. The NDI has several techniques, and each technique possesses merit and demerit. Hence, researchers have to select a suitable NDI method for inspection of the damaged specimens.

- There are four types of residual strength properties, such as compression, tensile, flexure, and fatigue. In particular, post-impact compression strength is the most important property, because the reduction of residual strength is the largest. CAI test has been developed from the aerospace industrial area. Various geometric parameters of the CAI specimens have been developed by researchers and industries.

Chapter 3

Toughening Mechanisms of Mode-I Interlaminar Fracture using Non-woven Veils as Interleaf Materials

3.1 Introduction

In this chapter, the main objective is to investigate the mechanisms of Mode-I interlaminar toughness for interleaved laminate composites. Several types of non-woven fabrics were chosen as the interleaf materials. The laminated specimens and the non-woven veil-interleaved composites can be made by the VaRTM technique [129, 152]. DCB tests were carried out for evaluating the Mode-I interlaminar toughness. The fracture surfaces and cross-sections of tested specimens were observed using microscopy. The mechanisms of enhancing the toughness by non-woven veils are discussed using the test results and the microscopy observations.

3.2 Materials and Experiment Methods

3.2.1 Materials Information

To investigate interlaminar toughness, three types of carbon fabrics were selected as the base materials. The carbon fabrics were plain and 5-harness satin weaves, and a unidirectional fabric. The plain weave fabric (38399 and 38422) was supplied by Carr Reinforcement Limited, in two different areal weights, 300 and 375g/m^2. A ply thickness of the plain weave fabrics is approximately 0.48 (38399) and 0.54mm (38422), respectively. The 5-harness satin weave fabric (P1726) was supplied by Cytec having an areal weight of 275g/m^2 and a ply thickness of approximately 0.35mm. The unidirectional non-crimped fabric (CT300) was supplied by Saint-Gobain Technical Fabrics having an areal weight of 615g/m^2 and a ply thickness of approximately 0.5mm. Figure 3.1 shows schematic of weave pattern for the carbon fabrics.

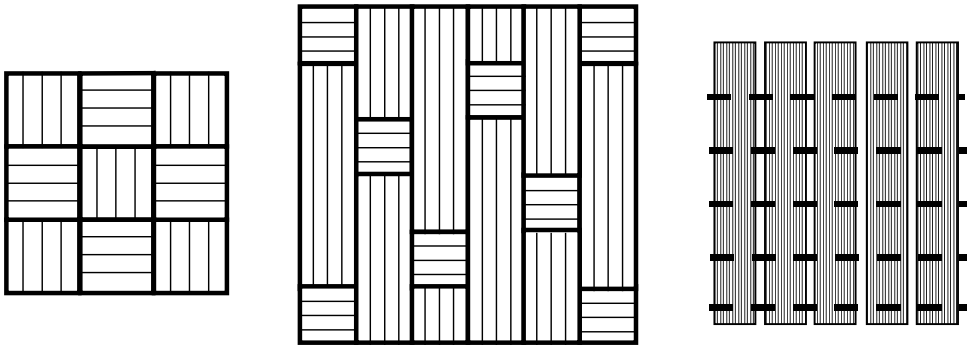

(a) (b) (c)

Figure 3.1 Schematic of weave pattern for carbon fabrics: (a) Plain weave, (b) 5-harness satin weave, (c) Unidirectional non-crimped fabric (Chain lines are stitches)

Two types of resin were used for interlaminar toughness tests, epoxy and vinyl ester and there were two types of epoxy resins. One epoxy was CYCOM 823^{R}, which was supplied by Cytec. The other epoxy was MVR444, which was supplied by Advanced Composites Group. The vinyl ester resin used DION9102-500, was supplied by Reichhold. Table 3.1 shows the characteristics of the resins.

Table 3.1 Characteristics of resins for experiments [from data sheets]

Property	**Epoxy 1^{+}**	**Epoxy 2^{++}**	**Vinyl ester***
Density (g/m^3)	1.23	1.14	1.03
Tensile strength (MPa)	80	77.6	79
Tensile modulus (GPa)	2.9	3.1	3.4
Flexural strength (MPa)	114	-	130
Flexural modulus (GPa)	3.4	-	3.25
Strain energy release (kJ/m^2)	0.9	0.3	-

+: CYCOM 823^{R}. ++: MVR444, *: DION9102-500

Five types of non-woven veils were used: two variants of Polyester/Carbon fibre hybrid (Hyb1 and Hyb2), and veils based on Carbon, Polyester (PE), and Polyamide (PA) fibres. The two types of hybrid veils differ in the polyester fibre content. Two variants of the pure polyester veils were also used with different areal weights. The hybrid, carbon, and PE1 (10g/m^2) veils were supplied by Technical Fibre Products. The PE2 (20g/m^2) and PA veils were supplied by Japan Vilene. Table 3.2 gives

characteristics of the interleaf veils. Figure 3.2 shows SEM pictures of the interleaf veils. The carbon veil is quite stiff. In contrast, the PE and the PA veils are soft materials. The hybrid veils are moderately stiff. For the structure of veils, the hybrid, carbon, and PE1 are that the individual fibres are predominantly straight. The PE2 and PA veils often exhibit bent and curved fibres. The hybrid and PE2 veils have a relatively high fibre density. Therefore, these veils are opaque. The carbon and PE1 veils have a lower areal weight and a more open structure that allows easy resin percolation. The PA veil is different from the other veils. The fibre diameter is larger than the other veil fibres. Nevertheless the areal weight of the PA veil is about 20g/m^2, it is very porous with apertures below the fibres.

Table 3.2 Characteristics of interleaf veils [from data sheets]

Properties	Hyb1^{+}	Hyb2^{++}	Carbon	PE1	PE2	PA
Areal weight **[g/m^2]**	20	20	10	13	23	21
Thickness **[mm]**	0.018	0.017	0.007	0.012	0.07	0.010
Tensile strength **[N/Length]**	-$^{\$}$	7*	8*	12*	19**	-$^{\$}$
Fibre diameter **[um]**	9 - 13	13	7	14	12	59
Content	Polyester 70%	Polyester 80%	Carbon 100%	Polyester 100%	Copolymer Polyester	Copolymer Polyamide

+: Polyester/Carbon (70:30), ++: Polyester/Carbon (80:20), *: N/15mm, **: N/5cm, $: No data

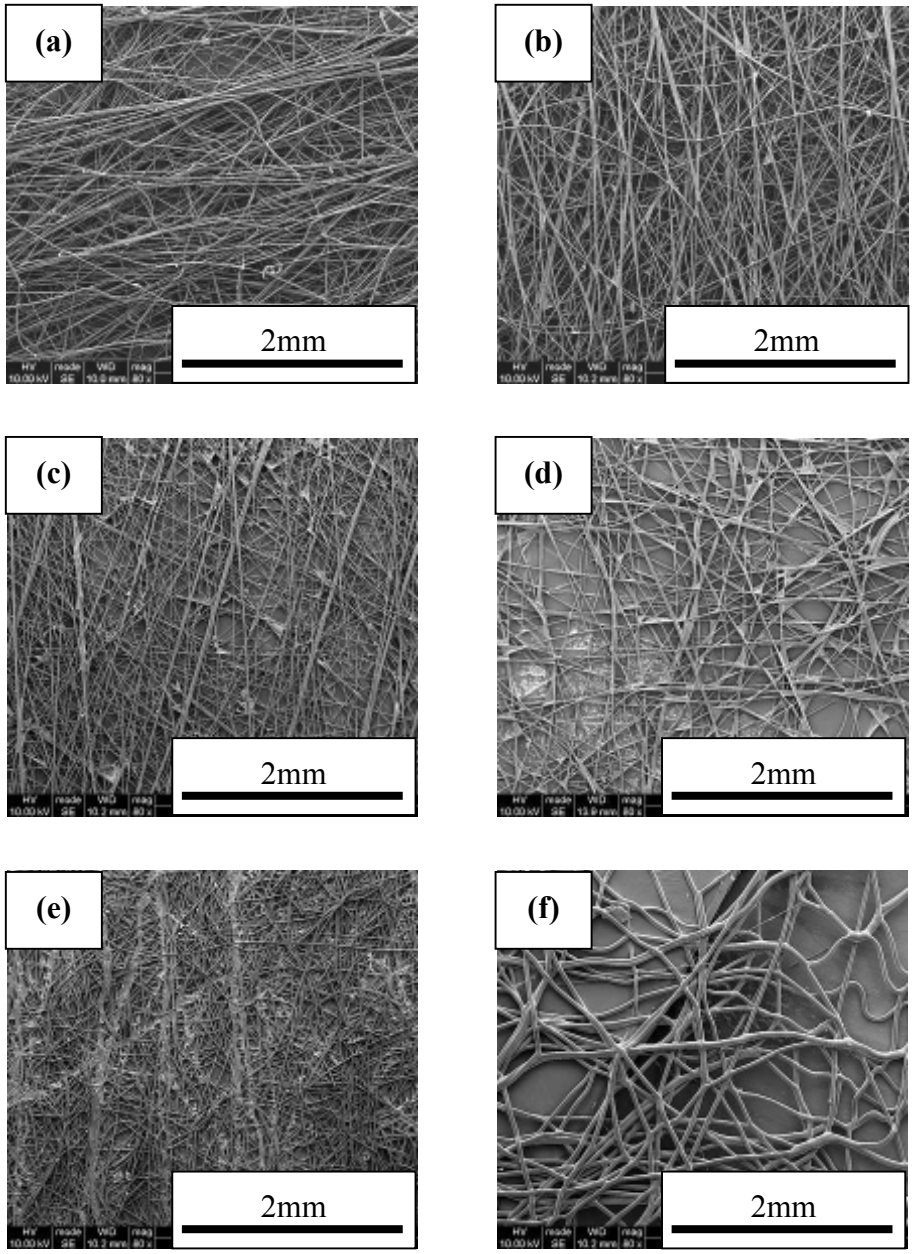

Figure 3.2 SEM pictures of non-woven interleaf veils: (a) PE/C (70:30) hybrid, (b) PE/C (80:20) hybrid, (c) Carbon, (d) Polyester (10g/m^2), (e) Polyester (20g/m^2), (f) Polyamide

3.2.2 Fabrication Methods of Composites for Mode-I Test

A schematic diagram of the moulding process is illustrated in Figure. 3.3. A steel mould was wiped with three layers of release agent to make sure that the composite panels could be removed easily from the mould. A tacky tape was placed on the surround of the mould. For specimens for interlaminar toughness testing, the fabrics and

interleaf veils were cut into 400mm (in length) x 210mm (in width) rectangles. 5-harness satin and plain weave (2-D) and unidirectional (UD) fabrics were laid in stacks of 10 plies (2-D) or 6 plies (UD) on the rigid mould, respectively. A single interleaf veil (400mm x 210mm), except for pure polyester/pure carbon (PE/C) and carbon veils, and release film (A6000, supplied by Aerovac, 470mm x 100mm) were placed at the mid layer of the stack. PE/C veils were overlapped PE1 and carbon veils before lay-up. For the carbon veil, 2 plies of interleaf veils were used, in order to provide corresponding areal weights of the interleaf materials. A purpose of the release film was to provide the starter crack for specimens cut from panels for toughness tests. The starter crack length was set at 50mm.

The laminate fabrics were covered by a peel ply, which prevents the panel adhering to the bag film. A flow media, which is a knitted thermoplastic monofilament, was put on the peel ply. The flow media is to accelerate resin flow across the dry materials. Two spring coils were connected to PVC inlet/outlet pipes at each end. These coils were put on the mould, as shown in Figure 3.3.

During infusion processing, epoxy1 (Ep1) resin and mould were pre-heated to 45^{o}C. The Ep1 was degassed for 30min using vacuum oven, thereafter the resin was infused into the mould. When impregnation was finished, the resin infused mould was put into the oven at 130^{o}C for 1h. The epoxy2 (Ep2) resin was also heated and degassed before infusion. After infusion, the mould was put in an oven where the temperature was programmed to increase from 30^{o}C to 120^{o}C ramping at 2^{o}C/min. When the temperature reached 120^{o}C, the oven was held at 120^{o}C for 4h. After curing, the infused panel was removed from mould and post-cured. The post-curing temperature was set to increase from 30^{o}C to 180^{o}C ramping at 7^{o}C/min, followed by holding at 180^{o}C for 2h.

The vinyl ester (VE) resin was mixed with 2wt% methyl ethyl ketone peroxide (MEKP) beforehand. After the VE resin had infused completely, the mould was held at ambient temperature for 24h. The composite panel was removed from mould, and post-cured for 3h in the oven at 80^{o}C.

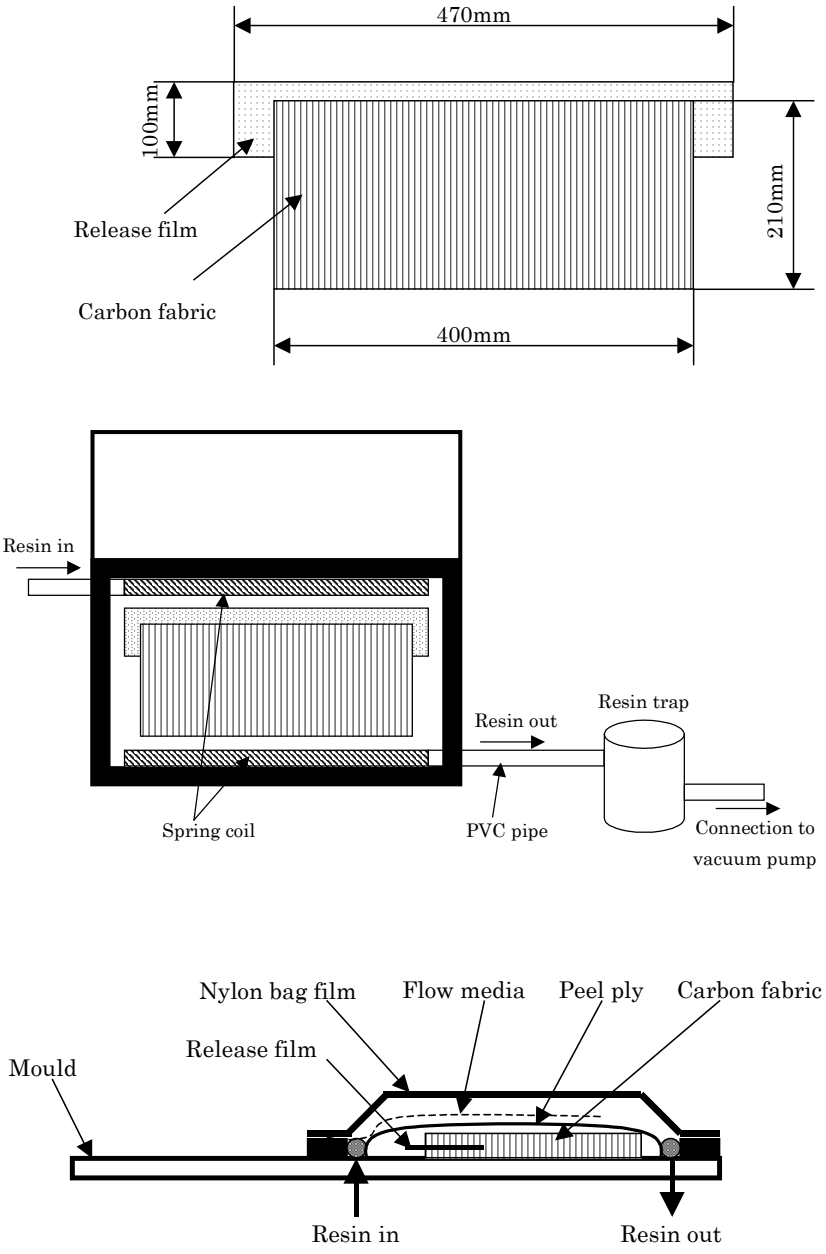

Figure 3.3 Schematic diagrams of fabrication

3.2.3 Mode-I Interlaminar Toughness Tests

The Mode-I interlaminar toughness of the composites was evaluated using the double cantilever beam (DCB) test. The dimensions and test conditions of DCB test were in accordance with ASTM D5528 and ISO 15024 [178-179]. Figure 3.4 illustrates schematically the DCB test specimen. The DCB specimens were rectangular in shape, 142mm (in length) x 20mm (in width). The side face of the specimens were polished

and painted with a white spray. One side of the specimens was marked from the insert film with vertical lines every 1mm up to 60mm. The piano hinges used to hold the specimens in the test machine fixture were made from 1mm thickness continuous hinges, and cut to 20mm lengths. The ends of the specimens and hinges were sandblasted using 320-grade grid to provide a clean and rough surface for adhesive bonding. The blasted surfaces of the specimens and hinges were wiped with acetone to remove all contaminants. The hinges were bonded to the specimens with Hysol HY932, a two-part epoxy adhesive. Bulldog clips were used to clamp the piano hinges until the resin was cured. Excess adhesion that squeezed out was removed with a spatula. Clamped specimens were put in oven at 50^{o}C for 24 hours.

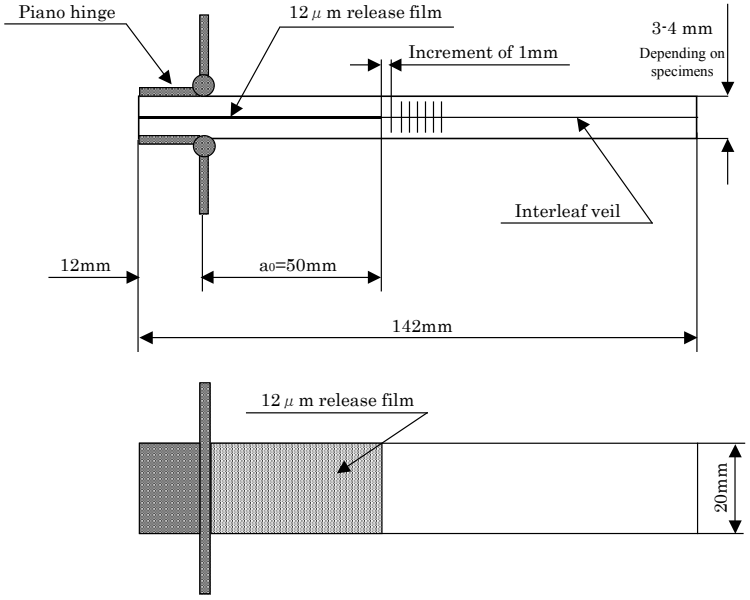

Figure 3.4 Dimensions of the DCB specimen

The DCB tests were carried out using a multipurpose test machine (Hounsfield) equipped with a 1kN load cell. The DCB specimens were clamped via the piano hinges in the fixtures. The crosshead speed was set at a constant 1mm/min. During loading, the load-displacement data were recorded, and the onset of delamination crack propagation was visually observed on the edge of specimen and the crack length noted. When the crack length grew 3 to 5mm, the specimen was unloaded at a constant crosshead speed of 10mm/min, except for 5-harness satin weave specimens. Thereafter the specimen was reloaded at the same constant crosshead speed of 1mm/min, until the final delamination crack length increment (50mm to 60mm) was reached. The 5-harness satin weave

specimens were loaded to failure directly. Figure 3.5 and 3.6 show pictures of the test machine and DCB test, respectively.

Figure 3.5 Picture of test machine, Hounsfield

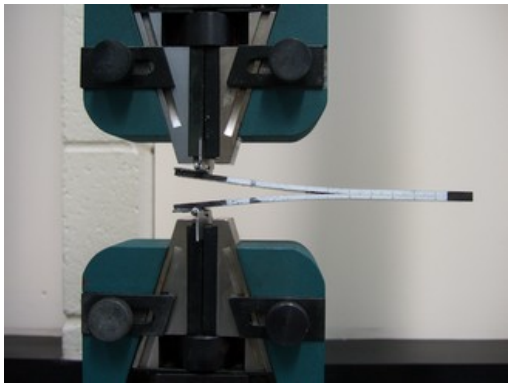

Figure 3.6 Picture of DCB test

3.2.4 Thickness and Volume Fraction of Each Laminate

Table 3.3 – 3.5 show the information of the thickness and volume fraction (V_f) for each laminate. Volume fractions of specimens were calculated using weight fraction of specimen and density of carbon fibre and resin.

Table 3.3 Summary of thickness and volume fraction (V_f) for 5-harness satin weave specimens

Fabric	Resin	Interleaf veils	Thickness [mm]	V_f (%)
5-harness satin weave	Epoxy1	Non-interleaved	4.48	57
		PE/C (70:30)	3.90	55
		PE/C (80:20)	4.05	55
		Carbon	4.03	57
		Polyester	4.06	51
		Polyamide	4.06	55
	Vinyl ester	Non-interleaved	3.65	57
		PE/C (70:30)	-*	-
		PE/C (80:20)	-	-
		Carbon	-	-
		Polyester	3.85	55
		Polyamide	3.88	56

*: Not examined

Table 3.4 Summary of thickness and volume fraction (V_f) for unidirectional fabric specimens

Fabric	Resin	Interleaf veils	Thickness [mm]	V_f (%)
Unidirectional	Epoxy1	Non-interleaved	3.44	61
		PE/C (70:30)	3.69	60
		PE/C (80:20)	3.69	58
		Carbon	3.84	63
		Polyester	3.48	62
		Polyamide	3.44	60
	Vinyl ester	Non-interleaved	3.47	51
		PE/C (70:30)	3.46	56
		PE/C (80:20)	3.49	56
		Carbon	3.44	57
		Polyester	3.46	56
		Polyamide	3.43	56

Table 3.5 Summary of thickness and volume fraction (V_f) for plain weave specimens

Fabric	Resin	Interleaf veils	Thickness [mm]	V_f (%)
Plane (LAW$^+$)	Epoxy2	Non-interleaved	3.01	56
Plain (HAW*)		Non-interleaved	3.90	57
Plane (LAW)		PE/C (100:100)	3.22	54
		PE/C (80:20)	3.32	52
		Polyester	3.23	53
		Polyamide	3.29	53
Plain (HAW)	Vinyl ester	Non-interleaved	3.87	52
		PE/C (100:100)	4.29	45
		PE/C (70:30)	3.93	53
		PE/C (80:20)	4.05	51
		Carbon	4.12	51
		Polyester	4.10	50
		Polyamide	4.07	51

+: Law areal weight, *: High areal weight

3.2.5 Data Reduction Methods for Calculation of Strain Energy Release Rate

The methods for Mode-I strain energy release rate were determined according to ASTM D5528-94 [178] which describes the derivation of interlaminar toughness of FRP. The following is from ASTM D5528-94.

3.2.5.1 Interpretation for Test Results

Two initiation energy release rate values are determined from the load-displacement plots and used along with subsequent propagation values to generate the R-curve. These initiation values are indicated on a typical R-curve shown in Figure 3.7 and described below. For each of these techniques, the initial delamination length, $\boldsymbol{a_0}$*, should be used to calculate* $\boldsymbol{G_I}$*. For this study, the initial energy release rate values at the non-linear (NL) and 5%/MAX points were defined as* $\boldsymbol{G_{IC}}$*. The energy release rate at propagation,* $\boldsymbol{G_{I\text{-}prop}}$*, was calculated using average propagation values from max* $\boldsymbol{G_I}$ *value.*

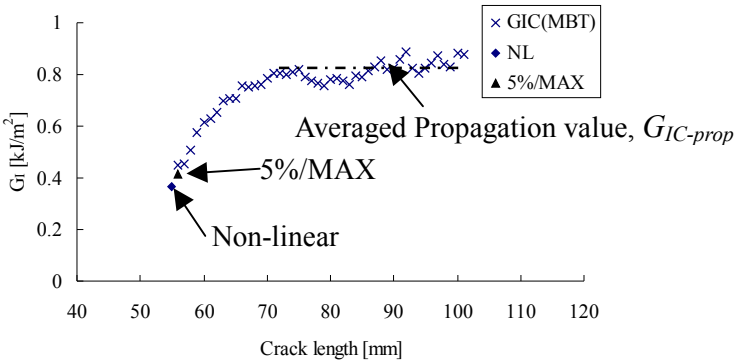

Figure 3.7 A typical crack propagation resistance curve (R-curve)

3.2.5.2 Deviation from Linearity (NL)

An initiation (or onset) value for $\boldsymbol{G_{IC}}$ *should be calculated from the load and displacement at the point of deviation from linearity, or onset of non-linearity (NL). This calculation assumes that the delamination starts to grow from the insert in the interior of the specimen at this point. The NL value represents a lower bound value for* $\boldsymbol{G_{IC}}$*. For brittle matrix composites, this is typically the same point at which the delamination is observed to grow from the insert at the specimen edge, as shown in Figure. 3.8 (a). For tough matrix composites, however, a region of nonlinear behaviour may precede the visual observation of delamination onset at the specimen edges, even if the unloading curve is linear, as shown in Figure.3.8 (b).*

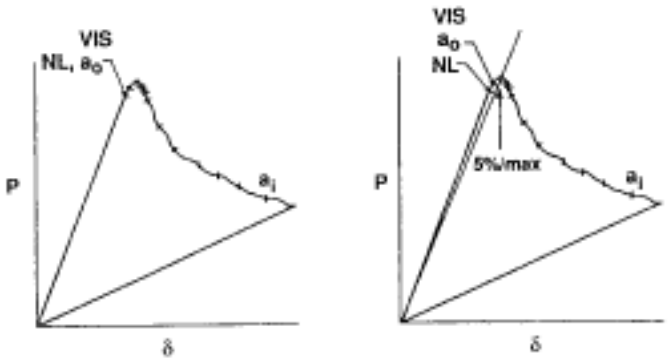

(a) brittle matrix (b) tough matrix

Figure 3.8 Load-displacement curve obtained by DCB test [178]

3.2.5.3 5% Offset/Maximum Load (5%/MAX)

A value of $\boldsymbol{G_{IC}}$ *may be calculated by determining the intersection of the load-displacement curve, once it has become nonlinear, with a line compliance from the original linear region of the load-displacement curve (Figure.3.8). If the intersection*

occurs after the maximum load point, the maximum load should be used to calculate this value.

3.2.6 Calculation of G_{IC}

Three data reduction methods for calculating G_{IC} values were used. These consisted of a Modified Beam Theory (MBT), a Compliance Calibration (CC) method and a Modified Compliance Calibration (MCC) method. The following is also from ASTM D5528-94 [178].

3.2.6.1 Modified Beam Theory (MBT) Method

The beam theory expression for the strain energy release rate of a perfectly built-in (that is, clamped at the delamination front) DCB is as follows:

$$G_I = \frac{3P\delta}{2ba} \tag{3.1}$$

where P *is the load,* δ *is the load point displacement,* b *is the specimen width, and* a *is the delamination length.*

In practice, this expression will overestimate G_I *because the beam is not perfectly built-in (that is, rotation may occur at the delamination front). One way of correcting for this rotation is to treat the DCB as if it contained a slightly longer delamination,* $a+|\Delta|$*, where* Δ *may be determined experimentally by generating a least square plot of the cube root of compliance,* $C^{1/3}$*, as a function of delamination length (Figure.3.9). The compliance,* C*, is the ratio of the load point displacement to the applied load,* δ/P*. The values used to generate this plot should be the load and displacements corresponding to the visually observed delamination onset on the edge and all the propagation values. Calculate the Mode-I interlaminar fracture as follows:*

$$G_I = \frac{3P\delta}{2b\left(a+|\Delta|\right)} \tag{3.2}$$

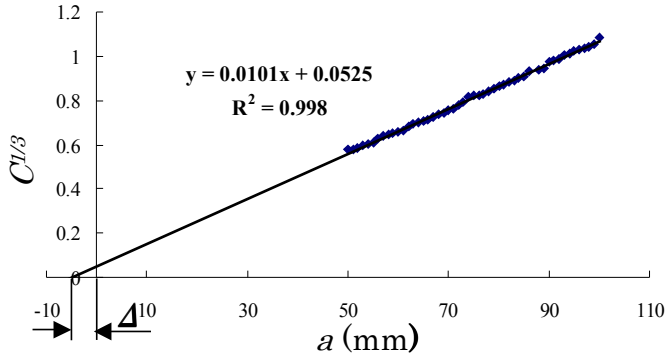

Figure 3.9 Sample $C^{1/3}$ versus displacement, a, diagram to determine crack offset for MBT method

3.2.6.2 Compliance Calibration (CC) Method

Generate a least squares plot of log(δ_i/P_i) versus log(a_i) using the visually observed delamination onset values and all the propagation values. Draw a straight line through the data which results in the best least-square fit. Calculate the exponent n from the slope of this line according to $n = \Delta y/\Delta x$*, where* Δy *and* Δx *are defined in Figure. 3.10. Calculating the Mode-I interlaminar toughness as follows:*

$$G_I = \frac{nP\delta}{2ba} \tag{3.3}$$

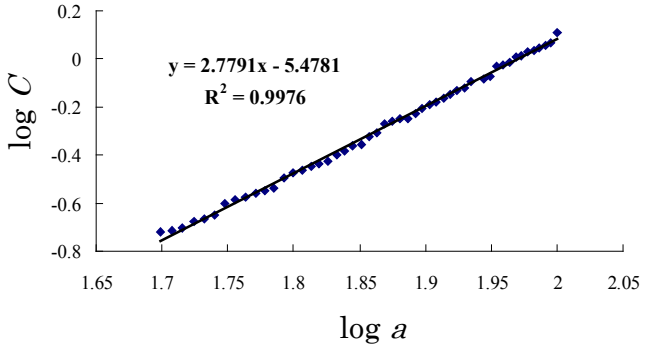

Figure 3.10 Sample log C versus *log a* diagram to determine the slope, n, for CC method

3.2.6.3 Modified Compliance Calibration (MCC) Method

Generate a least squares plot of the delamination length normalised by specimen thickness, a/h*, as a function of the cube root of compliance,* $C^{1/3}$*, as shown in Figure 3.11, using the visually observed delamination onset values and all the propagation*

values. The slope of this line is A_1*. Calculating the Mode-I interlaminar toughness as follows:*

$$G_I = \frac{3P^2C^{2/3}}{2A_1bh} \tag{3.4}$$

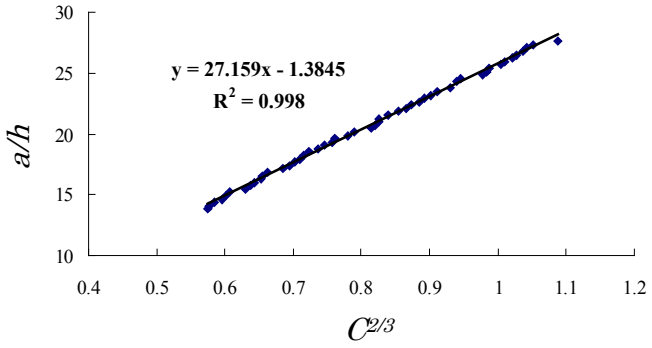

Figure 3.11 Sample $C^{2/3}$ versus *a/h* diagram to determine the slope, A_1, for MCC method

3.2.7 Observation by Microscopy

The fracture surfaces were observed using two scanning electron microscopes (SEM), the Jeol JSM-6300 or FEI Inspect F. Tested specimens were cut about 10mm in length from the crack initiation point. SEM specimens were coated with a thin layer of gold prior to observation. The acceleration voltage is 15kV (Jeol JSM-6300) or 10kV (FEI Inspect F). The SEM observation was used to evaluate the suppression behaviour of crack propagation in each interleaved specimen. All SEM pictures show regions that are near to the crack initiation point. Cross-sections of tested specimens were viewed using an optical microscope, Olympus BX60. Tested specimens were cut along the longitudinal direction and polished by abrasive papers.

3.3 Results

3.3.1 Classification of the Load-Displacement Curve

Load-displacement curves obtained by DCB tests were classified three types: (a) Jagged shape, (b) Bow shape, and (c) Triangle shape. Figure 3.12 indicates representative load-displacement curves. Figure 3.13 indicates the examples of the load-displacement curves. The Ep1 and Ep2 resin system specimens were basically jagged shape. The satin and UD with the VE system laminates were bow type. On the other hand, the plain weave with the VE system samples were triangle type. Representative results of the DCB test are shown in Appendix A.

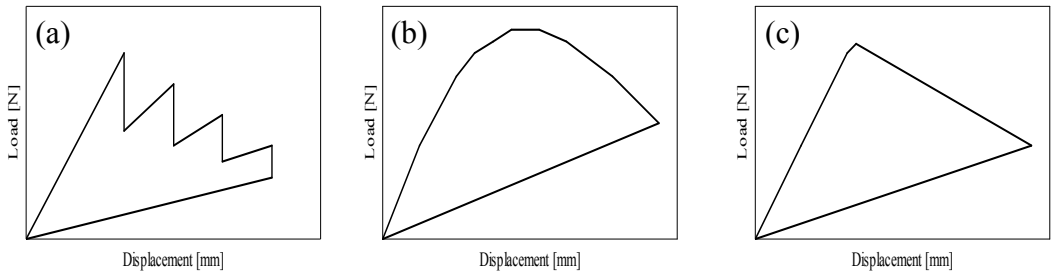

Figure 3.12 Classified load-displacement curves: (a) Jagged shape, (b) Bow shape, (c) Triangle shape

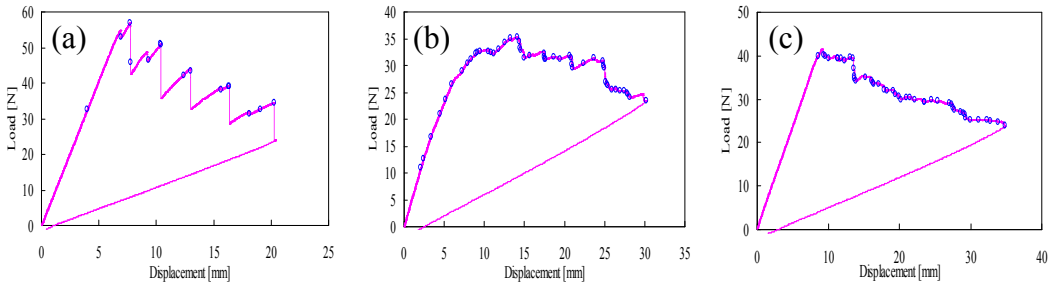

Figure 3.13 Representative examples of the load-displacement curves: (a) Jagged shape, (b) Bow shape, (c) Triangle shape

3.3.2 Resistance-Curves for Non-interleaved Specimens

In this section, the representative R-curves calculated by the MBT method for various interleaved laminates are shown. Figure 3.14 and 3.15 show typical R-curves for the non-interleaved Ep and VE resin system specimens respectively. In the Ep resin composite, the load-displacement curves were basically jagged shape, type A curve. These specimens were where the crack jumped extensively during the DCB test. For the weave specimens, while the initiation values for the each woven fabric laminate are varied, the propagation values are similar. In the UD composite, the load-displacement curve was type B shape. The crack propagation was gradual and slow, unlike the woven specimens. The propagation values of the UD specimen are the twice as high as those of the woven fabric cases.

On the other hand, the tendency of the R-curves in the VE system specimens is similar to the Ep1 system samples. In the satin weave and unidirectional fabrics, the increase of the G_{IC} values tends to be gradual. In the plain weave specimen, the propagation values appear earlier than the other fabric cases. The UD fabric laminate possesses the highest propagation values of all fabric with the VE system materials. The propagation values in the plain weave specimen are slightly higher than that of the satin weave laminates.

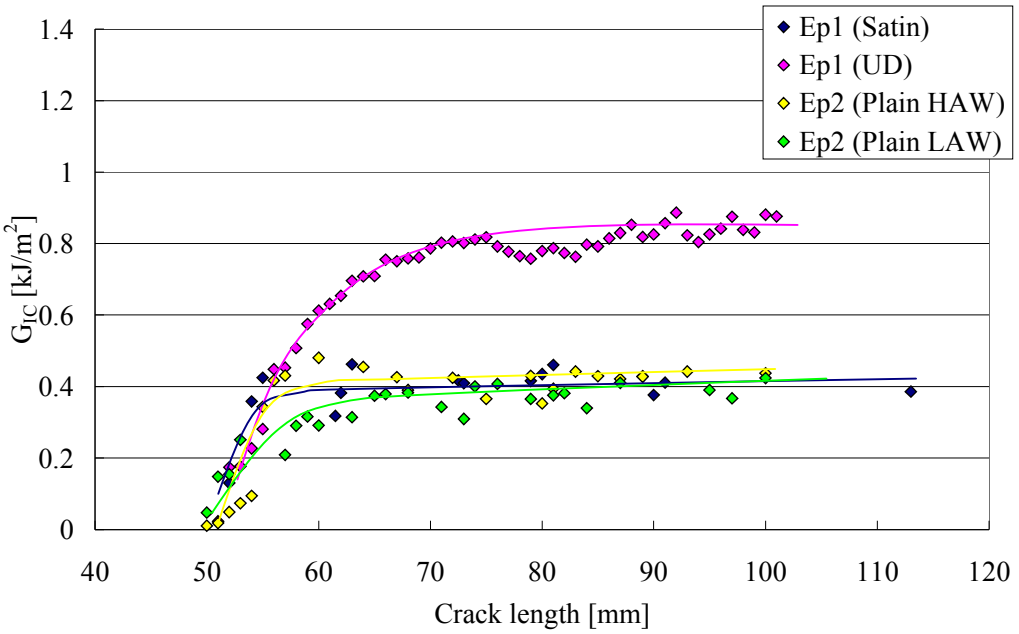

Figure 3.14 R-curves for non-interleaved epoxy system specimens – calculated by MBT method

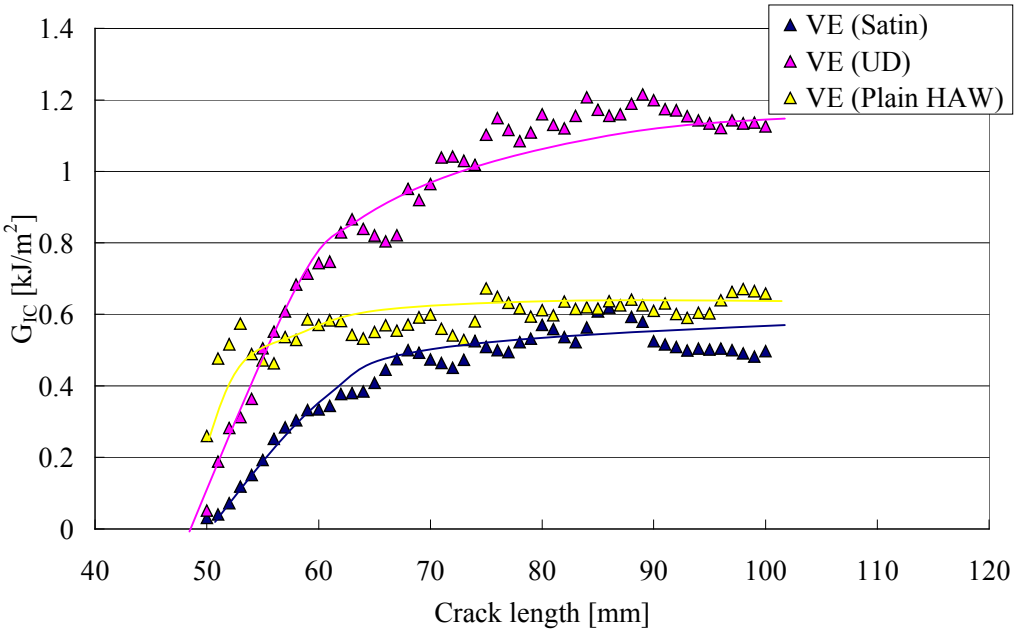

Figure 3.15 R-curves for non-interleaved vinyl ester system specimens – calculated by MBT method

3.3.3 Resistance-Curves for Interleaved Specimens

3.3.3.1 5-harness Satin Weave Fabric Specimens

Figure 3.16 and 3.17 illustrate the R-curves for the interleaved 5-harness satin weave with both resin composites. In the Ep1 system laminates, the typical load-displacement curves were basically type A (jagged) shape. The crack jumped extensively, except for the non-interleaved and PE veil interleaved laminates. In particular, carbon and PA veil interleaved laminates exhibited crack propagation that was significantly rapid and large. Therefore, the number of G_{IC} data points recorded for these interleaved specimens were limited. Both interleaved composites have significantly low G_I values, especially the PA interleaved case. The propagation values for both hybrid veil interleaved laminates are slightly lower than that for the non-interleaved case. For the PE veil interleaved laminate, the G_{IC} values are the highest of all interleaved specimens. The crack propagation was relatively slow compared to the other interleaved samples.

For the VE resin system, only the PE and PA veil interleaved specimens were examined. Both interleaved laminates show quite similar G_{IC} values, as shown in Figure 3.17. The tendency of the load-displacement curves for the VE system was type B (bow) shape. The crack propagation was quite slow and gradual. Therefore, a lot of data points could be obtained. Both veil-interleaved laminates possessed higher G_I values than the non-interleaved case. The transition of G_I values is different from the Ep1 system. The propagation values for both interleaved laminates are quite similar.

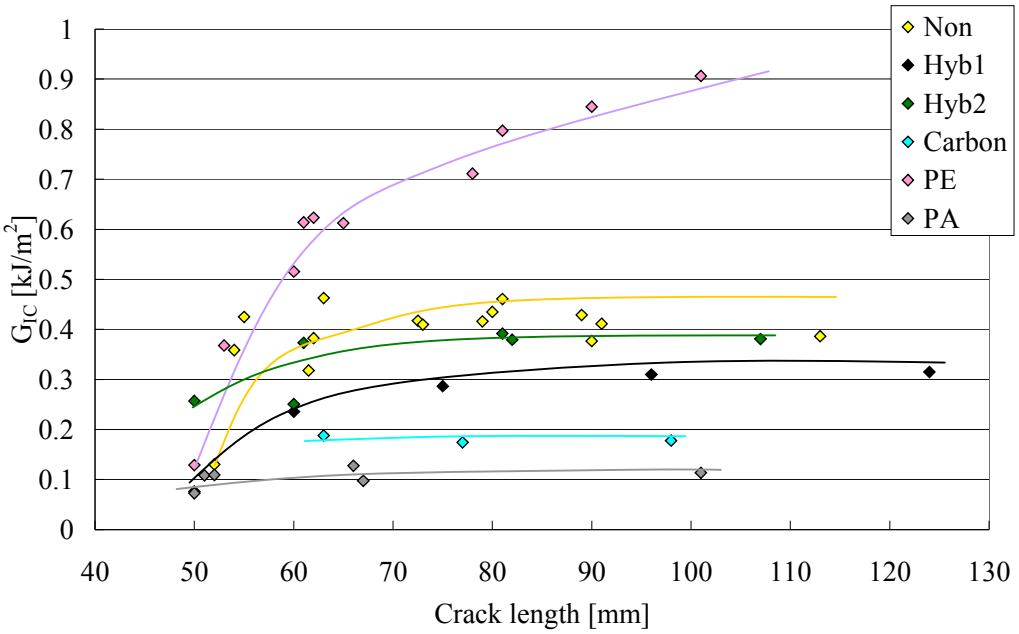

Figure 3.16 R-curves for non-interleaved and interleaved 5-harness satin weave fabric specimens with epoxy1 system – calculated by MBT method

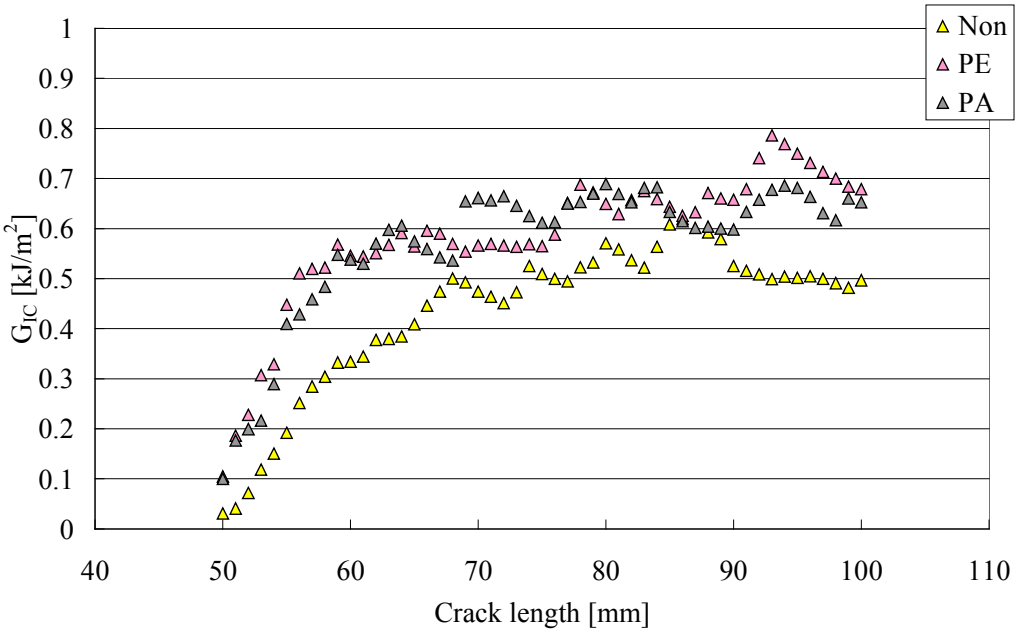

Figure 3.17 R-curves for non-interleaved and interleaved 5-harness satin weave fabric specimens with vinyl ester system – calculated by MBT method

3.3.3.2 Unidirectional Fabric Specimens

The R-curves for both resin systems interleaved composites are shown in Figure 3.18 and 3.19. The typical load-displacement curves in the Ep1 system are divided into two types. The non-interleaved, Hyb1, and PE veil interleaved laminates were type C (triangle) curve. In these specimens, the crack propagation was gradual. The propagation values for these composites are significantly higher than the satin weave cases. On the other hand, the other interleaved laminates were type A shape. The crack propagated sharply and rapidly. These interleaved specimens exhibit lower G_{IC} values than the other interleaved samples. In particular, the carbon veil interleaved composite exhibited almost the same G_I values as the satin weave specimen. Moreover, the initial and propagation values are almost the same. The PA veil interleaved specimen in the UD fabric showed a moderate improvement, compared with the satin weave laminate.

The typical load-displacement curves for the VE system were all type B shape. The behaviour of the crack propagation was significantly slow and gradual. The G_I values between all interleaved cases are quite similar, as shown in Figure 3.19. Both hybrid veil interleaved specimens are almost same G_{IC} values as the control. The PE and PA veil interleaved laminates possess higher Mode-I toughness than the other interleaved cases. However, the carbon-veil interleaved specimen has the lowest propagation values. Compared to the Ep1 system specimens, the G_{IC} values in all of the interleaved VE laminates are significantly high, including the carbon veil interleaved VE specimens.

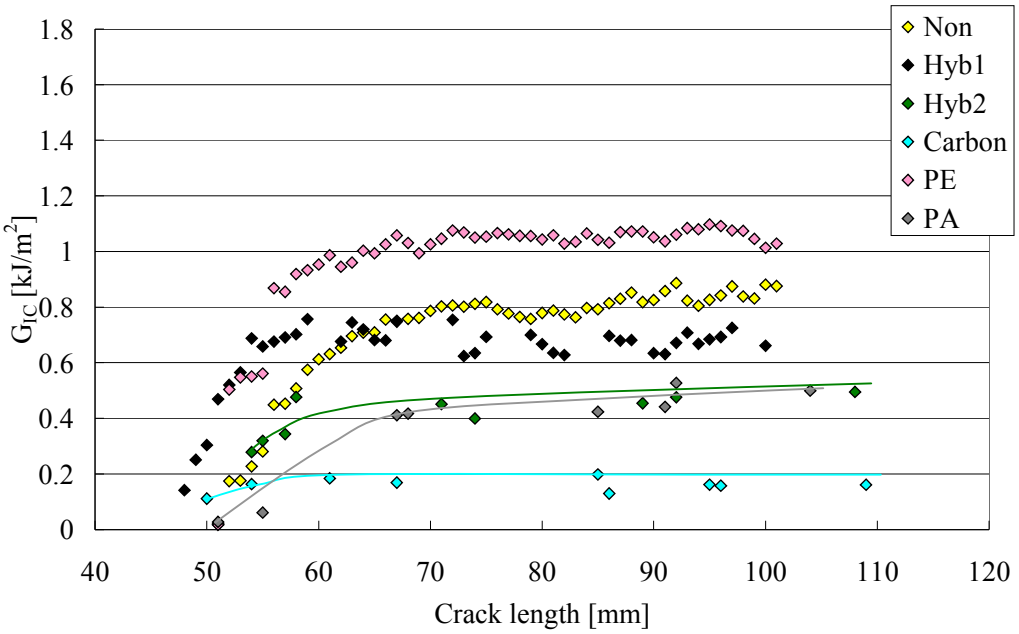

Figure 3.18 R-curves for non-interleaved and interleaved unidirectional fabric specimens with epoxy1 system – calculated by MBT method

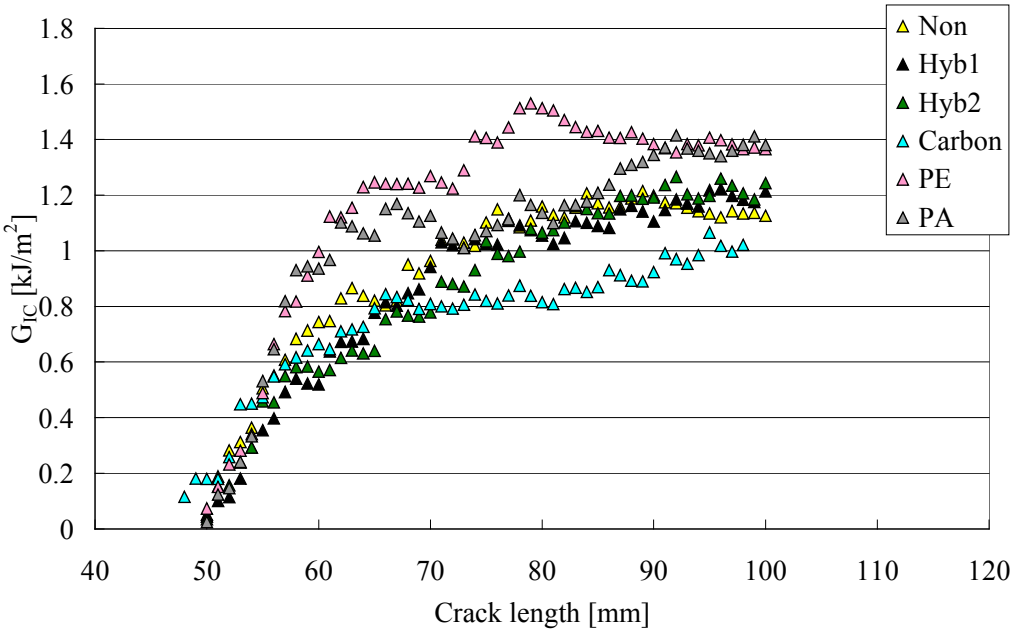

Figure 3.19 R-curves for non-interleaved and interleaved unidirectional fabric specimens with vinyl ester system – calculated by MBT method

3.3.3.3 Plain Weave Fabric Specimens

Figure 3.20 and 3.21 shows the R-curves for composites with both resin systems. In the Ep2 system composites, the LAW plain weave was used as the base material. The load-displacement curves for the Ep2 system were all type A shapes. Compared to the satin weave with the Ep1 system laminates, the crack jumps and propagation rates in the interleaved specimens were significantly smaller and slower, except for the PA veil interleaved composite. The PE/C and Hyb2 veil interleaved specimens have almost the same propagation values as the non-interleaved cases. The PE veil interleaved laminate possesses high G_{IC} values. Surprisingly, the PA veil interleaved specimen in the Ep2 system exhibits significantly high G_{IC} values, over 1.0kJ/m^2. The crack propagation was significantly large but the time that took the crack propagation was very long.

In the VE system, the typical load-displacement curves were all type C shape. The base materials for the VE resin system were HAW fabric. The crack propagation speed was faster than the Ep2 system cases. From Figure 3.21, the G_{IC} values for all interleaved specimens exhibit a similar tendency. The PE and PA veil interleaved laminates have a slightly higher propagation values than the other interleaved samples. In the VE resin system, the difference of the G_I values for all interleaved specimens was small, compared with the Ep system. The Mode-I interlaminar toughness for the plain weave laminates is almost the same as the 5-harness satin weave materials.

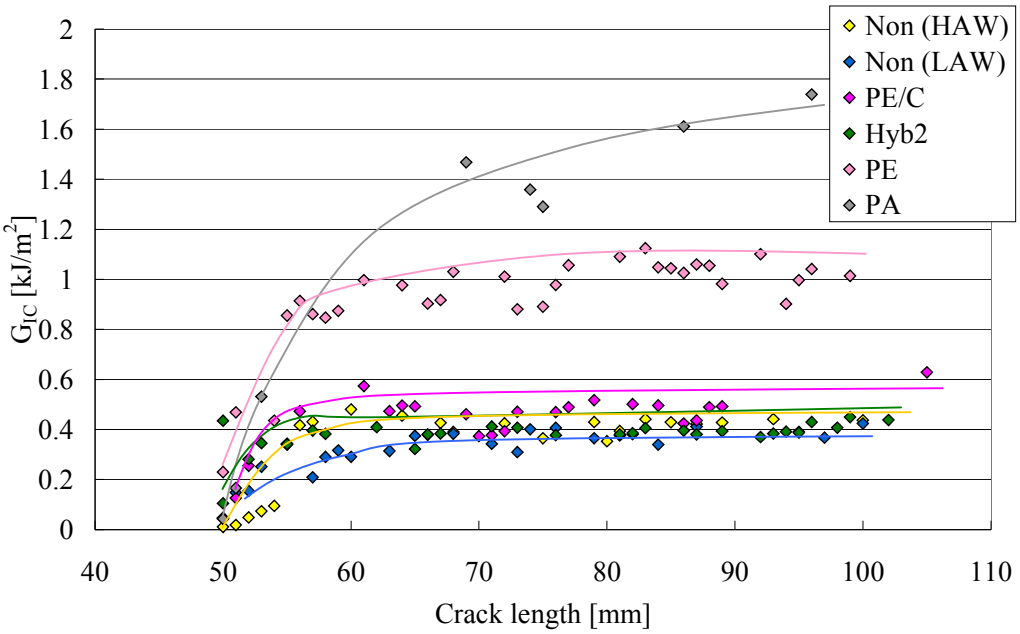

Figure 3.20 R-curves for non-interleaved and interleaved plain weave fabric specimens with epoxy2 system – calculated by MBT method

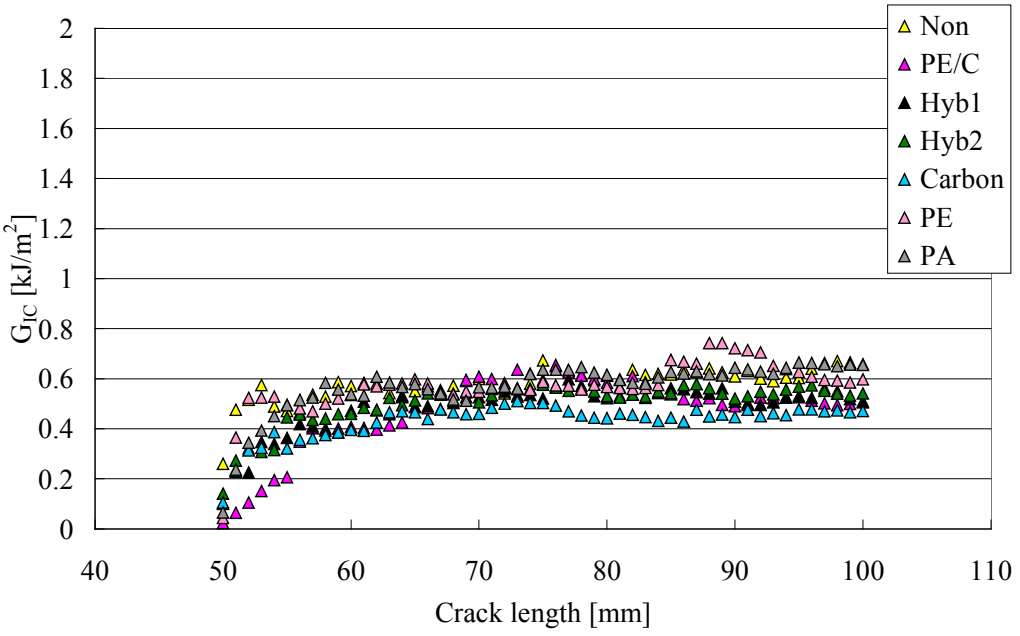

Figure 3.21 R-curves for non-interleaved and interleaved plain weave fabric specimens with vinyl ester system – calculated by MBT method

3.3.4 Mode-I Critical Energy Release Rate (G_{IC})

3.3.4.1 5-harness Satin Weave Fabric Specimen

The G_I values for 5-harness satin with the Ep1 system from the three methods are shown in Table 3.6 with the standard deviations (S.D.) and coefficient of variations (C.V.). Figure 3.22 gives diagrams of $G_{IC\text{-}NL}$, $G_{IC\text{-}5\%/MAX}$, and $G_{I\text{-}prop}$ values. The G_{IC} values of Hyb1, Hyb2, and PE veil interleaved laminates are higher than the control. The Hyb1 veil interleaved specimens are slightly improved with moderate G_{IC} values, 0.20kJ/m^2 (MBT). The G_{IC} values of the Hyb2 and PE veil interleaved specimens increased more than the Hyb1 veil interleaved case. The carbon and PA veil interleaved specimens, however, are lower than the non-interleaved samples. In particular, the PA-veil interleaved composite has the lowest Mode-I critical energy release rate, $G_{IC\text{-}NL}$=0.06kJ/m^2. Compared to the non-interleaved case, the gap between NL and 5%/MAX values for interleaved is quite small. In particularly, the Hyb1, carbon and PE veil interleaved specimens exhibit the same values.

For the $G_{I\text{-}prop}$ values, the PE veil interleaved specimen is the highest, approximately 0.77kJ/m^2. The non-interleaved laminate is the second highest $G_{I\text{-}prop}$ value, 0.42kJ/m^2. The other veil-interleaved specimens, however, are lower $G_{I\text{-}prop}$ values than the non-interleaved case. In particular, the carbon and PA veil interleaved specimens exhibit significantly lower values, about 0.16 and 0.13kJ/m^2 respectively. These interleaved samples are where the crack jumped sharply. Therefore, the G_{IC} values decrease compared to the non-interleaved laminate. The S.D. values (standard deviations) of initiation and propagation values are small.

Table 3.6 Mode-I critical strain energy release rate values of 5-harness satin weave epoxy1 system specimens with/without interleaf veils

Interleaf Veil	MBT			CC			MCC			
	G_I [kJ/m^2]	S.D.	C.V.	G_I [kJ/m^2]	S.D.	C.V.	G_I [kJ/m^2]	S.D.	C.V.	
Non-interleaved	0.16	0.047	0.305	0.17	0.059	0.340	0.17	0.052	0.306	$G_{IC\text{-}NL}$
	0.25	0.111	0.435	0.28	0.131	0.467	0.28	0.123	0.450	$G_{IC\text{-}5\%/MAX}$
	0.42	0.039	0.091	0.42	0.042	0.099	0.46	0.036	0.079	$G_{I\text{-}Prop}$
Hyb1	0.20	0.034	0.168	0.21	0.035	0.168	0.23	0.053	0.234	$G_{IC\text{-}NL}$
	0.20	0.034	0.168	0.21	0.035	0.168	0.23	0.053	0.234	$G_{IC\text{-}5\%/MAX}$
	0.29	0.030	0.104	0.27	0.028	0.105	0.31	0.038	0.123	$G_{I\text{-}Prop}$
Hyb2	0.26	0.025	0.098	0.29	0.033	0.115	0.37	0.040	0.108	$G_{IC\text{-}NL}$
	0.20	0.112	0.089	0.25	0.121	0.075	0.29	0.165	0.100	$G_{IC\text{-}5\%/MAX}$
	0.37	0.031	0.083	0.37	0.031	0.083	0.51	0.059	0.115	$G_{I\text{-}Prop}$
Carbon	0.15	0.027	0.174	0.16	0.020	0.122	0.18	0.019	0.106	$G_{IC\text{-}NL}$
	0.15	0.027	0.174	0.16	0.020	0.122	0.18	0.019	0.106	$G_{IC\text{-}5\%/MAX}$
	0.16	0.010	0.063	0.17	0.010	0.061	0.18	0.021	0.113	$G_{I\text{-}Prop}$
PE	0.31	0.042	0.134	0.35	0.032	0.090	0.34	0.038	0.112	$G_{IC\text{-}NL}$
	0.31	0.004	0.139	0.35	0.034	0.096	0.35	0.040	0.117	$G_{IC\text{-}5\%/MAX}$
	0.77	0.031	0.042	0.74	0.020	0.027	0.80	0.023	0.028	$G_{I\text{-}Prop}$
PA	0.06	0.026	0.467	0.07	0.037	0.573	0.07	0.047	0.636	$G_{IC\text{-}NL}$
	0.09	0.096	0.201	0.10	0.028	0.295	0.11	0.038	0.345	$G_{IC\text{-}5\%/MAX}$
	0.13	0.018	0.143	0.13	0.017	0.133	0.16	0.020	0.131	$G_{I\text{-}Prop}$

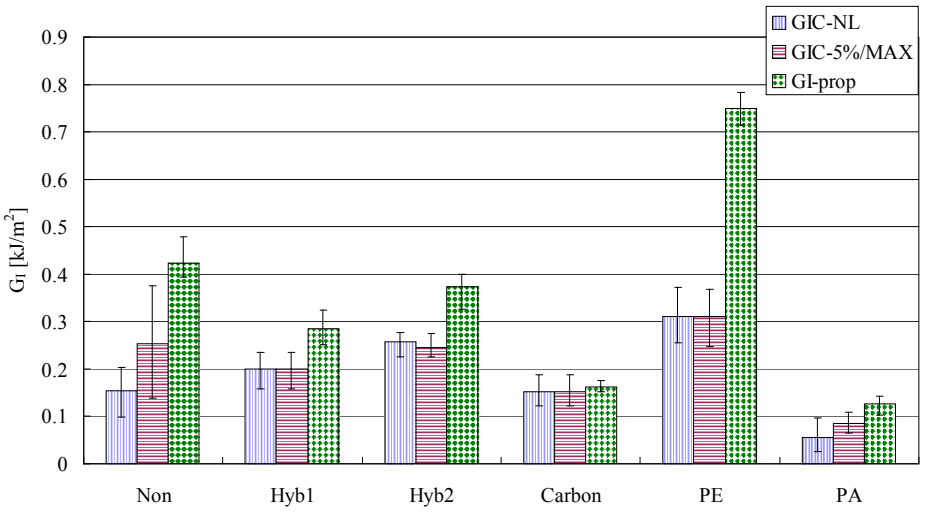

Figure 3.22 Comparison of Mode-I initiation and propagation energy release rate values (calculated by MBT) for 5-harness satin weave epoxy1 system with/without interleaf veils

The G_I values calculated by the three calculation methods are shown in Table 3.7 with the S.D. and C.V. for the VE system composites. Figure 3.23 shows a graph of Mode-I initial and propagation energy release rates. The G_{IC} values of all specimens are almost the same with $G_{IC\text{-}NL}$ values about 0.07kJ/m^2. The $G_{IC\text{-}5\%/MAX}$, are around 0.11 to 0.14kJ/m^2. The $G_{IC\text{-}5\%/MAX}$ of the PA veil interleaved laminate is slightly larger than the other specimens. Compared to the Ep1 system, the G_{IC} initial values for the VE system are smaller. The S.D. values for all samples are quite small, and these specimens have good repeatability.

For the $G_{I\text{-}prop}$ values for the VE system, the propagation values for three laminates increase significantly from the initiation values. The G_{IC} value of the non-interleaved specimen is approximately 0.52kJ/m^2. On the other hand, the $G_{I\text{-}prop}$ values for the PE and PA veil interleaved specimens are about 0.70 and 0.65kJ/m^2, respectively. The PA veil interleaved composites exhibit a significantly increased $G_{I\text{-}prop}$ value compared with the Ep1 system samples. The S.D. for propagation values is larger than that for initial values. In particular, the PA veil interleaved specimen shows the largest deviation for the propagation value, approximately 0.08.

Table 3.7 Mode-I critical strain energy release rate values of 5-harness satin weave vinyl ester system specimens with/without interleaf veils

Interleaf veil	MBT			CC			MCC			
	G_I [kJ/m^2]	S.D.	C.V.	G_I [kJ/m^2]	S.D.	C.V.	G_I [kJ/m^2]	S.D.	C.V.	
Non-interleaved	0.06	0.019	0.304	0.07	0.020	0.302	0.06	0.020	0.309	$G_{IC\text{-}NL}$
	0.11	0.014	0.137	0.11	0.015	0.143	0.10	0.014	0.138	$G_{IC\text{-}5\%/MAX}$
	0.52	0.046	0.088	0.51	0.044	0.085	0.52	0.046	0.088	$G_{I\text{-}Prop}$
PE	0.07	0.011	0.146	0.07	0.011	0.156	0.07	0.011	0.153	$G_{IC\text{-}NL}$
	0.11	0.029	0.269	0.11	0.029	0.272	0.11	0.028	0.266	$G_{IC\text{-}5\%/MAX}$
	0.70	0.046	0.066	0.70	0.048	0.068	0.71	0.046	0.066	$G_{I\text{-}Prop}$
PA	0.07	0.014	0.197	0.07	0.014	0.197	0.07	0.014	0.190	$G_{IC\text{-}NL}$
	0.14	0.018	0.132	0.14	0.019	0.134	0.14	0.017	0.123	$G_{IC\text{-}5\%/MAX}$
	0.65	0.083	0.127	0.65	0.084	0.130	0.65	0.084	0.128	$G_{I\text{-}Prop}$

*: Hyb1 and 2, and Carbon veil interleaved specimens were not examined.

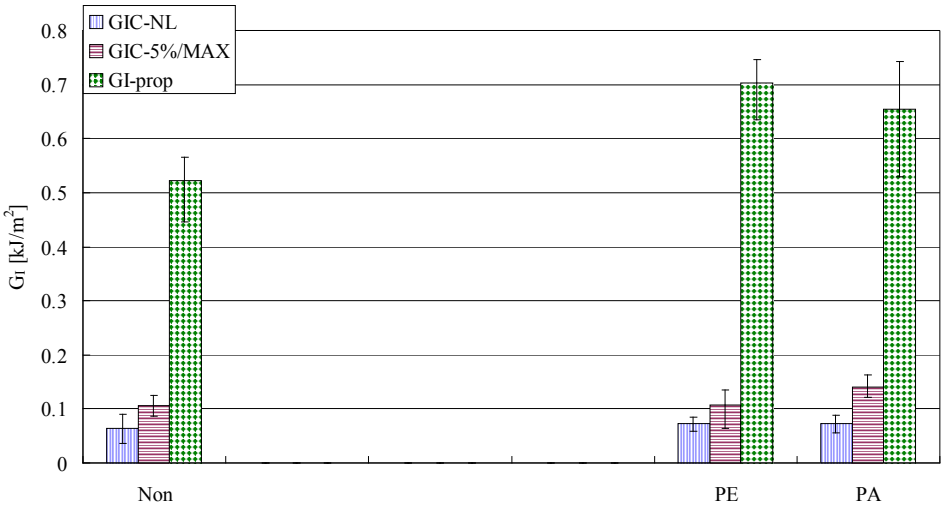

Figure 3.23 Comparison of Mode-I initiation and propagation energy release rate values (calculated by MBT) for 5-harness satin weave vinyl ester system specimens with/without interleaf veils

3.3.4.2 Unidirectional Fabric Specimens

The Mode-I energy release rate values for the Ep1 system specimens from the three calculation methods are shown in Table 3.8 together with the S.D. and C.V. values. Figure 3.24 illustrates the $G_{IC\text{-}NL}$, $G_{IC\text{-}5\%/MAX}$, and $G_{I\text{-}prop}$ values. The tendency of the G_{IC} values is similar to the satin weave with the Ep1 system composites. The non-interleaved, hybrid and PA veil interleaved laminates possess similar G_{IC}, values, range from 0.36 to 0.46kJ/m^2. The PE veil interleaved case has the highest G_{IC} value, around 0.61kJ/m^2. The carbon veil interleaved specimens, on the other hand, are significantly low G_{IC} values compared with the control, about 0.14kJ/m^2. In this fabric system, interleaving with the PA-veil moderately improved the Mode-I interlaminar toughness. The S.D. values for interleaved specimens are larger than the non-interleaved samples. Both hybrid veil interleaved laminates show quite a large deviation.

Surprisingly, the $G_{I\text{-}prop}$ value of the non-interleaved specimen is increased significantly from the initiation values. However, the $G_{I\text{-}prop}$ values of interleaved specimens, except for the PE veil interleaved case, are lower rather than the control laminate. The Hyb1, Hyb2, and PA veil interleaved samples have similar propagation values, range of 0.47 to 0.57kJ/m^2. The carbon veil interleaved specimen does not show an improvement for the propagation value, 0.14kJ/m^2. In contrast, the PE veil interleaved specimen has the highest $G_{IC\text{-}prop}$ value and good interlaminar toughness, $G_{IC\text{-}prop}$=0.99kJ/m^2. The S.D. values of the non-interleaved, carbon and PE veil interleaved specimens exhibit small values, nearly 0.04. However, the other interleaved specimens have a significantly large deviation, range from 0.09 to 0.12.

Table 3.8 Mode-I critical strain energy release rate values of unidirectional fabric epoxy1 system specimens with/without interleaf veils

Interleaf veils	MBT			CC			MCC			
	G_I [kJ/m^2]	S.D.	C.V.	G_I [kJ/m^2]	S.D.	C.V.	G_I [kJ/m^2]	S.D.	C.V.	
Non-interleaved	0.39	0.037	0.097	0.39	0.043	0.108	0.38	0.039	0.102	$G_{IC\text{-}NL}$
	0.44	0.032	0.072	0.45	0.037	0.081	0.44	0.030	0.068	$G_{IC\text{-}5\%/MAX}$
	0.86	0.032	0.037	0.85	0.036	0.042	0.86	0.034	0.040	$G_{I\text{-}Prop}$
Hyb1	0.46	0.048	0.111	0.45	0.051	0.113	0.48	0.115	0.239	$G_{IC\text{-}NL}$
	0.51	0.073	0.143	0.52	0.061	0.118	0.56	0.085	0.153	$G_{IC\text{-}5\%/MAX}$
	0.57	0.118	0.207	0.57	0.102	0.181	0.60	0.073	0.121	$G_{I\text{-}Prop}$
Hyb2	0.39	0.108	0.276	0.41	0.103	0.252	0.42	0.112	0.266	$G_{IC\text{-}NL}$
	0.40	0.099	0.248	0.42	0.100	0.238	0.46	0.158	0.342	$G_{IC\text{-}5\%/MAX}$
	0.47	0.091	0.194	0.47	0.113	0.242	0.53	0.123	0.232	$G_{I\text{-}Prop}$
Carbon	0.14	0.041	0.291	0.15	0.020	0.292	0.04	0.186	0.270	$G_{IC\text{-}NL}$
	0.16	0.055	0.350	0.46	0.054	0.341	0.21	0.099	0.474	$G_{IC\text{-}5\%/MAX}$
	0.14	0.037	0.264	0.14	0.038	0.277	0.18	0.045	0.246	$G_{I\text{-}Prop}$
PE	0.61	0.085	0.139	0.62	0.081	0.132	0.61	0.082	0.135	$G_{IC\text{-}NL}$
	0.83	0.085	0.104	0.83	0.085	0.103	0.81	0.080	0.098	$G_{IC\text{-}5\%/MAX}$
	0.99	0.049	0.050	0.99	0.050	0.051	0.99	0.050	0.050	$G_{I\text{-}Prop}$
PA	0.36	0.109	0.346	0.31	0.089	0.285	0.36	0.099	0.174	$G_{IC\text{-}NL}$
	0.39	0.138	0.358	0.38	0.111	0.292	0.46	0.142	0.310	$G_{IC\text{-}5\%/MAX}$
	0.48	0.100	0.209	0.48	0.093	0.196	0.58	0.090	0.154	$G_{I\text{-}Prop}$

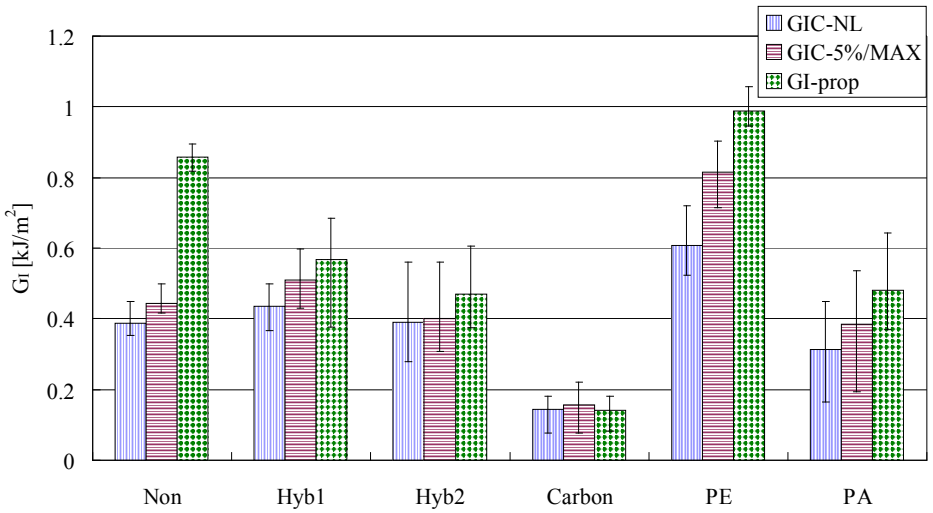

Figure 3.24 Comparison of Mode-I initiation and propagation energy release rate values (calculated by MBT) for unidirectional fabric epoxy1 system specimens with/without interleaf veils

The G_I values obtained by the three calculation methods are shown in Table 3.9 with the S.D. and C.V. values for unidirectional fabric with the VE system. Figure 3.25 illustrates diagrammatically the initial and propagation values. The Mode-I initial energy release rate values for all specimens are similar. The range of $G_{IC\text{-}NL}$ of all specimens is around 0.25 to 0.39kJ/m^2. On the other hand, the $G_{IC\text{-}5\%/MAX}$ values vary more widely than the NL values and range from 0.33 to 0.57kJ/m^2. Within the VE system specimens the difference between initial values of non-interleaved and interleaved laminate is small. The S.D. of all specimens is small.

The $G_{I\text{-}prop}$ values for all specimens are significantly increased from the G_{IC} values. The propagation value in the non-interleaved specimen is 1.17kJ/m^2. The PE veil interleaved laminate has an especially high $G_{I\text{-}prop}$ value of approximately 1.53kJ/m^2. Surprisingly, even the carbon veil interleaved specimens exhibit a value of 0.91kJ/m^2. The other interleaved samples are slightly higher than the control, approximately 1.2kJ/m^2. The S.D. values of the control, Hyb2, carbon, and PA veil interleaved samples are small, about 0.02 to 0.07. The Hyb1 and PE veil interleaved cases, on the other hand, have large S.D. values, approximately 0.13 and 0.19, respectively.

Table 3.9 Mode-I critical strain energy release rate values of unidirectional fabric vinyl ester system specimens with/without interleaf veils

Interleaf veils	MBT			CC			MCC			
	G_I [kJ/m^2]	S.D.	C.V.	G_I [kJ/m^2]	S.D.	C.V.	G_I [kJ/m^2]	S.D.	C.V.	
Non-interleaved	0.29	0.045	0.156	0.30	0.047	0.154	0.29	0.045	0.153	$G_{IC\text{-}NL}$
	0.40	0.079	0.199	0.41	0.081	0.195	0.39	0.075	0.191	$G_{IC\text{-}5\%/MAX}$
	1.17	0.031	0.027	1.13	0.033	0.029	1.17	0.031	0.027	$G_{I\text{-}Prop}$
Hyb1	0.25	0.034	0.137	0.26	0.036	0.141	0.25	0.035	0.140	$G_{IC\text{-}NL}$
	0.33	0.040	0.119	0.35	0.038	0.111	0.33	0.035	0.105	$G_{IC\text{-}5\%/MAX}$
	1.24	0.126	0.102	1.21	0.132	0.109	1.24	0.125	0.101	$G_{I\text{-}Prop}$
Hyb2	0.34	0.036	0.104	0.36	0.036	0.101	0.34	0.036	0.105	$G_{IC\text{-}NL}$
	0.43	0.047	0.109	0.45	0.046	0.103	0.43	0.049	0.114	$G_{IC\text{-}5\%/MAX}$
	1.21	0.018	0.015	1.17	0.021	0.018	1.21	0.018	0.015	$G_{I\text{-}Prop}$
Carbon	0.29	0.066	0.231	0.29	0.071	0.243	0.28	0.068	0.241	$G_{IC\text{-}NL}$
	0.40	0.065	0.163	0.41	0.067	0.166	0.39	0.060	0.154	$G_{IC\text{-}5\%/MAX}$
	0.91	0.050	0.055	0.90	0.050	0.055	0.91	0.050	0.055	$G_{I\text{-}Prop}$
PE	0.35	0.032	0.091	0.36	0.031	0.088	0.34	0.030	0.086	$G_{IC\text{-}NL}$
	0.57	0.087	0.152	0.58	0.084	0.144	0.56	0.085	0.151	$G_{IC\text{-}5\%/MAX}$
	1.53	0.190	0.124	1.53	0.187	0.123	1.54	0.190	0.124	$G_{I\text{-}Prop}$
PA	0.39	0.074	0.190	0.40	0.074	0.185	0.39	0.072	0.186	$G_{IC\text{-}NL}$
	0.54	0.083	0.156	0.55	0.084	0.153	0.53	0.080	0.15	$G_{IC\text{-}5\%/MAX}$
	1.25	0.070	0.056	1.23	0.074	0.061	1.25	0.069	0.055	$G_{I\text{-}Prop}$

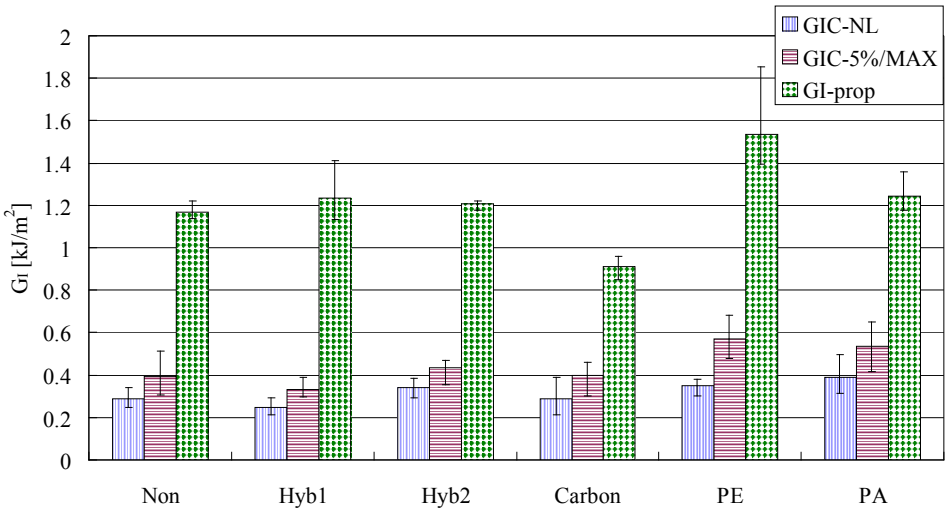

Figure 3.25 Comparison of Mode-I initiation and propagation energy release rate values (calculated by MBT) for unidirectional fabric vinyl ester system specimens with/without interleaf veils

3.3.4.3 Plain Weave Fabric Specimens

The Mode-I energy release rate values from the three calculation methods are shown in Table 3.10 with the S.D. and C.V. values for the Ep2 system. Figure 3.26 is a graph of $G_{IC\text{-}inii}$ and $G_{I\text{-}prop}$ values. For this resin system, most testing was performed on LAW plain weave specimens, except for the non-interleaved specimen. The non-interleaved specimens used for tests consisted of both of HAW and LAW plain weave fabrics.

In the non-interleaved laminates, the $G_{IC\text{-}NL}$ values of both woven specimens are around 0.45 and 0.30kJ/m^2, respectively. Although the load-displacement curves show different load behaviour, the HAW specimens have only a slightly higher $G_{IC\text{-}NL}$ value than the LAW specimens (see in Figure 3.14). Basically the G_{IC} of HAW specimen is higher than that of LAW specimen. The PE/C and Hyb2 veil interleaved laminates show similar G_{IC} values to the non-interleaved sample, as indicated in Table 3.10 and Figure 3.26. The PE/C and Hyb2 veil interleaved specimens are almost same G_{IC} values, about 0.41 to 0.44kJ/m^2 respectively. On the other hand, the PE and PA veil interleaved composites exhibit quite different properties from the other interleaved cases. The G_{IC} value of the PE veil interleaved specimen is approximately 0.81kJ/m^2. The PA veil interleaved laminate has the highest G_{IC} value, over 1.09kJ/m^2. Surprisingly, this

interleaved sample has a significantly improved toughness unlike the Ep1 system case. The S.D. values of all specimens are small. The deviation range is from 0.07 to 0.09, except for $G_{IC\text{-}5\%/MAX}$ of the PA veil interleaved case. The PA veil interleaved laminates have the highest S.D. value in all specimens, range of 0.17 (MBT) to 0.30 (MCC).

For the $G_{I\text{-}Prop}$ values, the propagation value for the control increases only slightly from the initial value. The $G_{I\text{-}prop}$ values of the PE/C and Hyb2 veil interleaved specimens are slightly increased compared with the initial values, 0.53kJ/m^2 and 0.48kJ/m^2. Those of the PE and PA veil interleaved specimens, on the other hand, are significantly increased. The $G_{I\text{-}prop}$ values of the PE and PA veil interleaved laminates are about 1.10 and 1.52kJ/m^2, respectively. The S.D. values of the control, and interleaved laminates, except for the PE veil interleaved sample, are approximately 0.02 to 0.07. The data of these specimens have low scatter. On the other hand, that of the PE veil interleaved cases has higher than the other specimens, about 0.11.

Table 3.10 Mode-I critical strain energy release rate values of plain weave epoxy2 system specimens with/without interleaf veils

Interleaf veils	MBT			CC			MCC			
	G_I [kJ/m^2]	S.D.	C.V.	G_I [kJ/m^2]	S.D.	C.V.	G_I [kJ/m^2]	S.D.	C.V.	
Non-interleaved (HAW)	0.45	0.090	0.239	0.46	0.091	0.239	0.46	0.094	0.250	$G_{IC\text{-}NL}$
	0.38	0.082	0.217	0.38	0.082	0.215	0.38	0.086	0.229	$G_{IC\text{-}5\%/MAX}$
	0.41	0.026	0.063	0.41	0.029	0.070	0.42	0.027	0.064	$G_{I\text{-}Prop}$
Non-Interleaved (LAW)	0.30	0.033	0.109	0.30	0.035	0.114	0.30	0.032	0.108	$G_{IC\text{-}NL}$
	0.31	0.020	0.064	0.31	0.021	0.068	0.31	0.020	0.067	$G_{IC\text{-}5\%/MAX}$
	0.40	0.022	0.056	0.40	0.022	0.057	0.40	0.023	0.057	$G_{I\text{-}Prop}$
PE/C	0.41	0.072	0.176	0.42	0.069	0.163	0.44	0.052	0.119	$G_{IC\text{-}NL}$
	0.45	0.046	0.102	0.46	0.047	0.102	0.48	0.053	0.109	$G_{IC\text{-}5\%/MAX}$
	0.53	0.065	0.121	0.53	0.061	0.115	0.57	0.081	0.142	$G_{I\text{-}Prop}$
Hyb2	0.44	0.072	0.164	0.45	0.073	0.162	0.44	0.073	0.165	$G_{IC\text{-}NL}$
	0.46	0.075	0.163	0.47	0.078	0.167	0.46	0.071	0.154	$G_{IC\text{-}5\%/MAX}$
	0.48	0.045	0.094	0.48	0.047	0.098	0.49	0.043	0.087	$G_{I\text{-}Prop}$
PE	0.81	0.082	0.102	0.83	0.079	0.095	0.81	0.075	0.092	$G_{IC\text{-}NL}$
	0.87	0.096	0.111	0.87	0.092	0.103	0.87	0.087	0.100	$G_{IC\text{-}5\%/MAX}$
	1.10	0.113	0.102	1.10	0.113	0.103	1.12	0.114	0.102	$G_{I\text{-}Prop}$
PA	1.09	0.084	0.077	1.11	0.077	0.069	1.11	0.068	0.061	$G_{IC\text{-}NL}$
	1.21	0.169	0.139	1.24	0.189	0.152	1.35	0.295	0.219	$G_{IC\text{-}5\%/MAX}$
	1.52	0.022	0.014	1.56	0.054	0.035	1.65	0.071	0.043	$G_{I\text{-}Prop}$

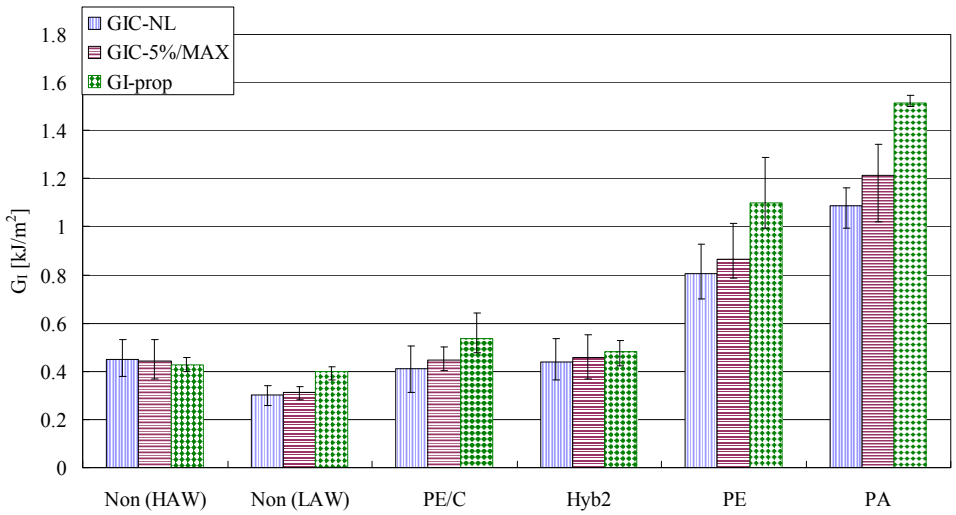

Figure 3.26 Comparison of Mode-I initiation and propagation energy release rate values (calculated by MBT) for plain weave epoxy2 system specimens with/without interleaf veils

Table 3.11 shows G_I values obtained by the three calculation methods with the S.D. and C.V. values for the VE system composites. Figure 3.27 gives a diagram of $G_{IC\text{-}NL}$, $G_{IC\text{-}5\%/MAX}$, and $G_{IC\text{-}prop}$ values. Compared to the satin weave with the VE system specimens, the G_{IC} values of the control, PE, and PA veil interleaved laminates are significantly higher. The non-interleaved and both hybrid veil interleaved cases have almost the same G_{IC} values, around 0.38J/m^2. The $G_{IC\text{-}NL}$ values of the PE/C and carbon veil interleaved specimens, on the other hand, are slightly smaller than that of the non-interleaved case, nearly 0.3kJ/m^2. The energy release rate values of the PE and PA veil interleaved specimens have higher than the other laminates, approximately 0.45kJ/m^2. The S.D. values for all specimens are not so large. However, the PE and PA veil interleaved laminates show a slightly larger deviation than the other interleaved samples.

For the propagation values, the non-interleaved sample is nearly $G_{I\text{-}prop}$ of 0.61kJ/m^2. Both hybrids and carbon veil interleaved specimens are around 0.47 to 0.53kJ/m^2. The PE/C veil interleaved sample is almost the same $G_{I\text{-}prop}$ values as the control. Values for both hybrid and carbon veil-interleaved laminates, however, are slightly lower than the non-interleaved case. The PE and PA veil interleaved specimens possess higher values, approximately 0.70kJ/m^2. The propagation values of the PE and

PA veil interleaved materials are similar to that of the satin weave samples (see in Table 3.7). The difference of G_{IC} values between interleaved materials is smaller than the Ep2 system cases. The S.D. of the propagation values is larger than that of the initial values. The S.D. of the PE interleaved is the highest value, approximately 0.08.

Table 3.11 Mode-I critical strain energy release rate values of plain weave vinyl ester system specimens with/without interleaf veils

Interleaf veils	MBT			CC			MCC			
	G_I [kJ/m^2]	S.D.	C.V.	G_I [kJ/m^2]	S.D.	C.V.	G_I [kJ/m^2]	S.D.	C.V.	
Non-interleaved (HAW)	0.40	0.042	0.105	0.40	0.044	0.111	0.40	0.042	0.105	$G_{IC\text{-}NL}$
	0.48	0.050	0.104	0.48	0.049	0.103	0.48	0.047	0.097	$G_{IC\text{-}5\%/MAX}$
	0.61	0.052	0.086	0.62	0.052	0.084	0.61	0.053	0.086	$G_{I\text{-}Prop}$
PE/C	0.32	0.036	0.112	0.32	0.035	0.112	0.32	0.037	0.113	$G_{IC\text{-}NL}$
	0.38	0.051	0.134	0.37	0.049	0.132	0.38	0.049	0.130	$G_{IC\text{-}5\%/MAX}$
	0.57	0.039	0.069	0.58	0.039	0.067	0.57	0.040	0.070	$G_{I\text{-}Prop}$
Hyb1	0.39	0.037	0.097	0.38	0.038	0.100	0.38	0.036	0.094	$G_{IC\text{-}NL}$
	0.43	0.010	0.023	0.42	0.006	0.014	0.43	0.011	0.025	$G_{IC\text{-}5\%/MAX}$
	0.53	0.046	0.088	0.53	0.058	0.090	0.53	0.047	0.088	$G_{I\text{-}Prop}$
Hyb2	0.37	0.028	0.076	0.36	0.026	0.072	0.37	0.027	0.074	$G_{IC\text{-}NL}$
	0.41	0.032	0.078	0.40	0.029	0.072	0.41	0.030	0.073	$G_{IC\text{-}5\%/MAX}$
	0.51	0.036	0.070	0.52	0.035	0.069	0.51	0.035	0.068	$G_{I\text{-}Prop}$
Carbon	0.31	0.039	0.126	0.31	0.035	0.112	0.31	0.036	0.115	$G_{IC\text{-}NL}$
	0.36	0.041	0.114	0.36	0.035	0.099	0.36	0.036	0.102	$G_{IC\text{-}5\%/MAX}$
	0.47	0.027	0.058	0.47	0.028	0.060	0.47	0.027	0.059	$G_{I\text{-}Prop}$
PE	0.46	0.056	0.122	0.46	0.058	0.127	0.46	0.056	0.120	$G_{IC\text{-}NL}$
	0.58	0.089	0.153	0.58	0.086	0.148	0.59	0.088	0.150	$G_{IC\text{-}5\%/MAX}$
	0.69	0.084	0.121	0.70	0.083	0.119	0.70	0.084	0.121	$G_{I\text{-}Prop}$
PA	0.44	0.041	0.094	0.44	0.044	0.100	0.44	0.046	0.105	$G_{IC\text{-}NL}$
	0.51	0.045	0.087	0.51	0.048	0.094	0.52	0.047	0.091	$G_{IC\text{-}5\%/MAX}$
	0.69	0.069	0.085	0.70	0.060	0.086	0.70	0.060	0.086	$G_{I\text{-}Prop}$

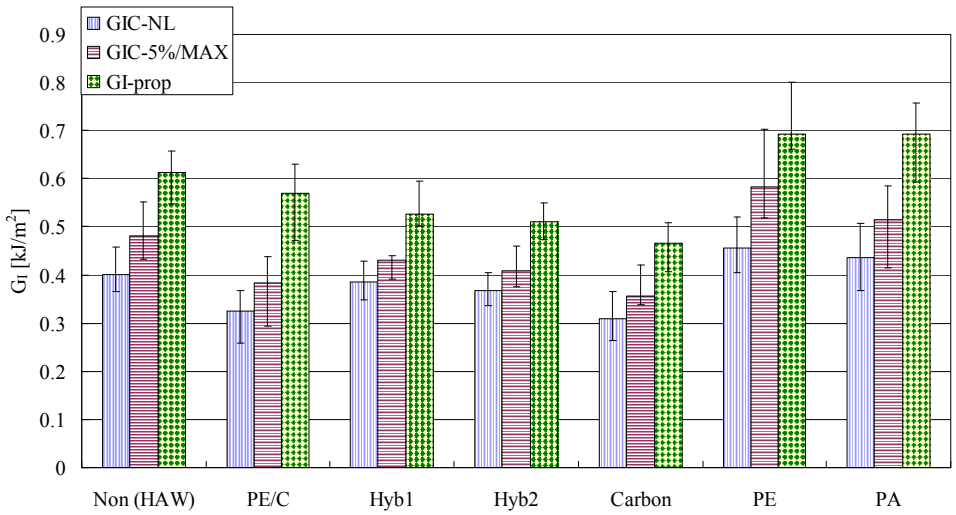

Figure 3.27 Comparison of Mode-I initiation and propagation energy release rate values (calculated by MBT) for plain weave vinyl ester system specimens with/without interleaf veils

In this section, the Mode-I energy release rates for the non-woven interleaved specimens have been evaluated. For the 5-harness satin weave with Ep1 system laminates, the PE veil interleaved specimen has the highest G_I values. In contrast, the carbon and PA veil interleaved samples exhibit poor toughness properties. The PE and PA veil interleaved VE system specimens do not show much difference in the Mode-I energy release rates.

The tendency of the unidirectional fabric with the Ep1 system is almost the same as the 5-harness satin composites. While the carbon veil interleaved sample exhibits significantly low G_{IC} values, the PA veil interleaved case has a moderate toughness with lower G_{IC} values than the control. For the VE system, the general trend is similar to the Ep1 system laminates. The propagation values are significantly increased for all specimens.

The plain weave specimens with the Ep2 system exhibit different toughness behaviour compared with the other fabric systems. Surprisingly, the PA veil interleaved laminate has a significantly increased G_{IC} value. The PE veil interleaved specimen has the second highest G_{IC} value. The PE/C and Hyb2 veil interleaved samples, however, do not improve toughness enough. For the VE system, the influence of the interleaf veil on

the Mode-I toughness is smaller than the Ep2 system.

Figure 3.28 shows the relationship between the Mode-I initial energy release rate with the fabric and resin system. The G_{IC} values are influenced slightly by both factors of fabric and resin. The satin weave specimens have the lowest G_{IC} values of all fabrics. The plain weave laminates have higher initiation values compared with the other fabric samples. Compared with areal weight of fabric, the HAW specimen has a slightly higher initial value than the LAW sample. It is thought that surface of the HAW plain weave specimen is coarser than the other woven fabric. Therefore, crack initiation was delayed and G_{IC} values increased. As far as resin systems are concerned, the Ep resin laminates are higher than the VE cases.

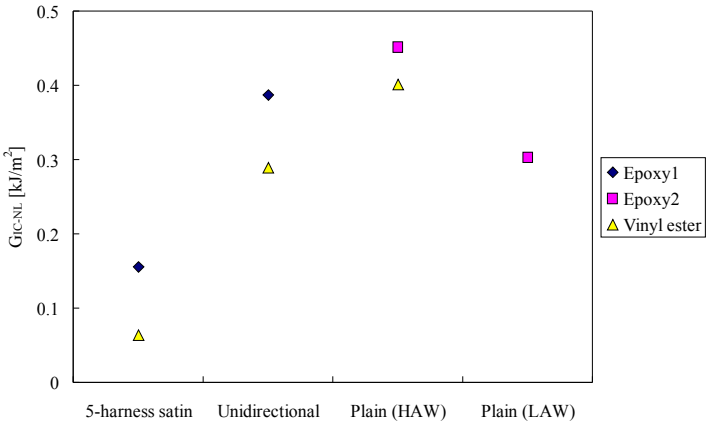

Figure 3.28 Relationship of Mode-I initial energy release rate between fabric and resin system for non-interleaved specimens

3.4 Discussion

3.4.1 Mechanisms of Mode-I Interlaminar Toughness for Non-interleaved Specimens

Figure 3.29 shows fracture surface pictures taken by SEM. In the satin and plain weave with the Ep-system specimens, it can be seen that the fracture surface is covered with the matrix, as shown in Figure 3.29 (a) and (c). The fracture surface in the satin weave specimen is smooth overall. It can be found that the crack propagated in the matrix region from SEM pictures. This suggests that the adhesion between carbon woven fibre and epoxy matrix is good [241], and the crack propagated in the weakest area, which is resin rich zone between layers. This is confirmed by the observation that both sides of the fracture surfaces are covered with the matrix resin. The Ep2 resin for

the plain weave specimen is also adhered to both fracture side surfaces. The plain weave fibres are not pulled out from fracture surface, therefore the carbon woven fibres cannot provide a bridging reinforcement. The fracture surface of the UD specimen shows the matrix and carbon fibres are exposed on the surface, as shown in Figure 3.29 (b). Although a few exposed fibres are pulled out, most carbon fibres are not unravelled on the fracture surface. However, these pulled out fibres would be responsible for some bridging. Therefore, the G_I values would increase.

On the other hand, the fracture surfaces for the VE system reveal that the carbon fabrics are exposed. These fibres are unravelled on the fracture surface, as illustrated in Figure 3.29 (d) – (f). For the VE system, the crack propagation behaviour was different from the Ep1 system. It is thought that the crack propagated between the woven fabric and the matrix. In the UD laminates, it can be seen that many carbon fibres are pulled out and unravelled, as shown in Figure 3.29 (e). The extent of the fibre-bridging region spread, and the $G_{I\text{-}prop}$ values were increased [162, 164]. The crack of the non-interleaved specimen went through the lower side or upper side of the woven surface. The fracture surface in the plain weave composite reveals almost the same tendency for the crack growth as the satin weave sample. The fracture surface contains the woven fabric that is exposed, as shown in Figure 3.29 (f). The adhesion between carbon fibre and matrix would be poorer in the VE resin system than the Ep resin. Therefore, some carbon fibres are pulled out and provide a fibre-bridging effect. It is thought that this effect would contribute to moderately improving G_{IC} values.

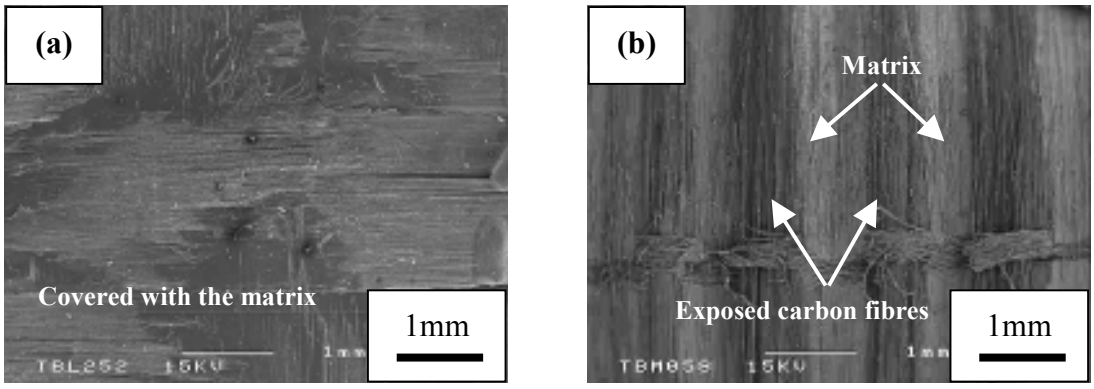

Figure 3.29 Micrographs of fracture surface taken by SEM for non-interleaved specimens: (a) Satin weave Ep1 system, (b) UD fabric Ep1 system, (c) Plain weave Ep2 system, (d) Satin weave VE system, (e) UD fabric VE system, (f) Plain weave VE system

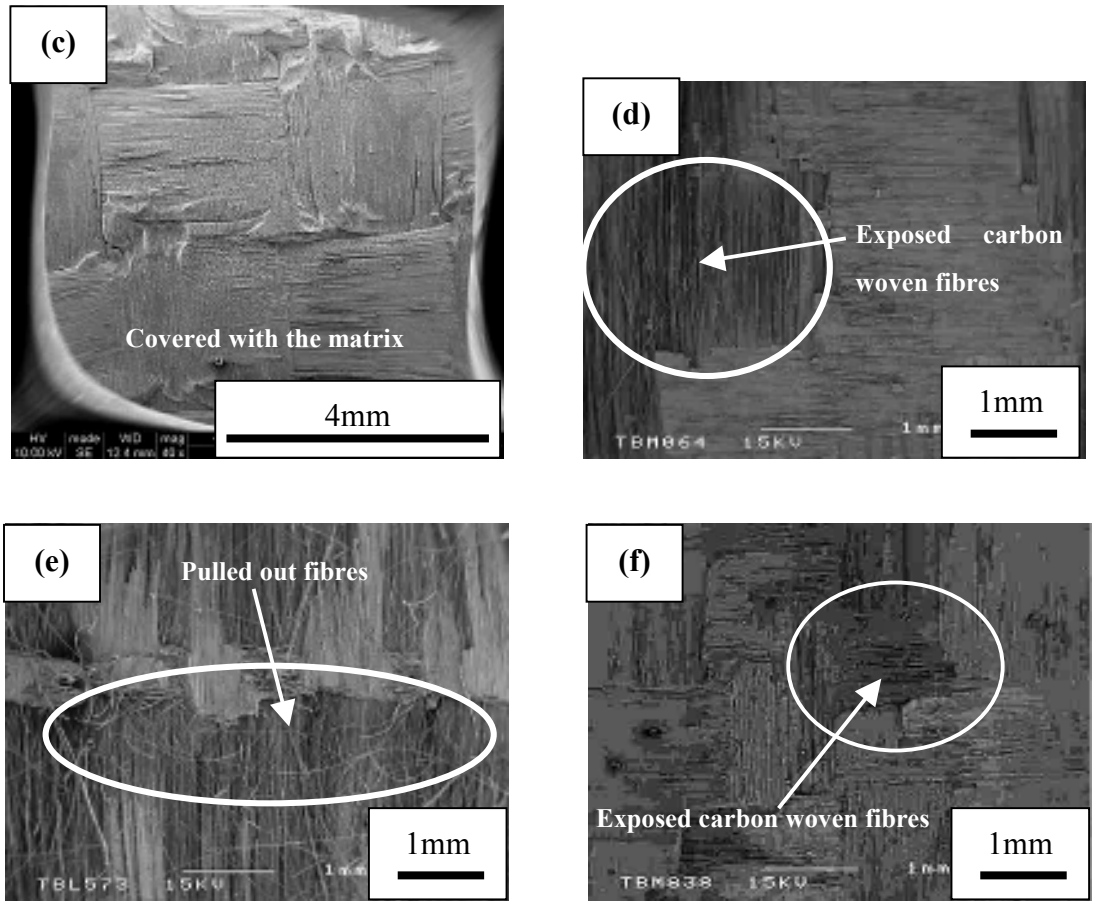

Figure 3.29 (*Continued*)

Figure 3.30 illustrates cross-section images observed by optical microscope for the non-interleaved laminates. For the satin weave and UD fabric specimens, the interlaminar crack is straight for both resin systems, as shown in Figure 3.30 (a) – (b) and (d) – (e). For the plain weave with the Ep2 system, it can be seen that some bundles of woven fibres are broken, as shown in Figure 3.30 (c). The G_{IC} values of plain specimens values are larger than that of 5-harness satin samples. The plain weave has a coarser surface and crack propagation would start later than in the satin specimen. Therefore, it is thought that the G_{IC} initial values are somewhat higher. However, the $G_{I\text{-}prop}$ values are similar to those of 5-harness satin laminates. Although this surface condition affects the initiation values, the propagation values are not influenced. For the UD specimen, both the initial and propagation values are higher than the satin and plain weave cases. Some carbon fibres are exposed and unravelled on the surface, as illustrated in Figure 3.29 (c). It is thought that these unravelled fibres would contribute

to increase the Mode-I energy release rate.

The crack paths of the VE system specimens are similar to those of the Ep1 system laminates. It can be seen that the carbon fibres are unravelled on the fracture surface, as shown in Figure 3.30 (d) – (f). When the crack went though woven surface, woven fibres were unravelled and worked as fibre-bridging. As a result, the crack propagation was more stable than the Ep resin system samples. Moreover, these unravelled fibres contribute to improve delamination resistance during the DCB test. Consequently, the propagation values for the VE system laminates can be increased significantly.

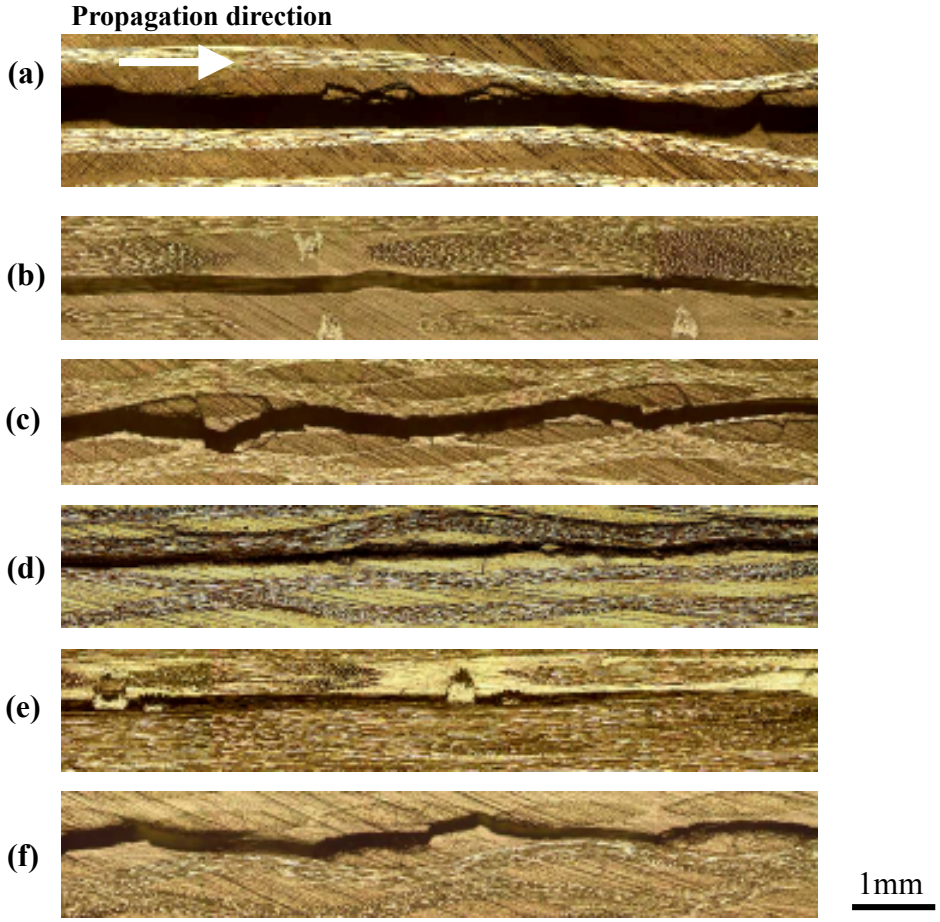

Figure 3.30 Micrographs of cross-section taken by optical microscope for non-interleaved specimens: (a) Satin weave Ep1 system, (b) UD fabric Ep1 system, (c) Plain weave Ep2 system, (d) Satin weave VE system, (e) UD fabric VE system, (f) Plain weave VE system

3.4.2 Mechanisms of Mode-I Interlaminar Toughness for Interleaved Specimens

3.4.2.1 5-harness Satin Weave Fabric Specimens

Figure 3.31 shows SEM pictures of the fracture surface for the Ep1 system specimens. The fracture surface was selected at a place near the crack initiation point. The condition of the fracture surface is divided into two types. The veil fibres are either pulled out from the matrix or embedded in the matrix. The hybrid and PE veil interleaved laminates are classified into the former. On the other hand, the carbon and PA veil interleaved laminates are categorised by the latter. For the Hyb1 veil interleaved specimens, the interleaf veil fibres are mainly embedded in the matrix. However, it can be found that a few veil fibres are pulled out from the matrix, as shown in Figure 3.31 (a). The fracture behaviour in the Hyb2 veil interleaved composite is similar to the Hyb1 veil interleaved case. Pulled out Hyb2 veil fibres from the matrix are much than the Hyb1 veil fibres. The fracture surface for the PE veil interleaved laminate is covered with many pulled out veil fibres, as shown in Figure 3.31 (b). These pulled out veil fibres would work for bridging when the crack propagated in the interlaminar region. The Mode-I interlaminar toughness is therefore improved. However, hybrid veil cannot considerably improve the delamination resistance, because many veil fibres are embedded in the matrix. The initiation values of both hybrid veil interleaved specimens are relatively higher than the non-interleaved specimens (see in section 3.3.2.1). Nevertheless, the difference in the propagation values between the non-interleaved and hybrid veil interleaved samples is small. If the crack propagates rapidly, the bridging effect of veil fibres may not contribute to the suppression of crack growth. Compared to both hybrid veils, the extent of fibre pull-out with the PE veils is considerable. As a result, the PE veil interleaved laminate possesses high G_{IC} values.

The fracture surface in the carbon-veil interleaved specimen is completely covered with the matrix. Although a few veil fibres are pulled out from the matrix, most remain embedded in the matrix, as shown in Figure 4.31 (c). From the SEM picture, it is seen that the carbon veil fibres exhibit brittle fracture. When the crack propagated in the interlaminar area, the veil fibres would not be working effectively bridging for crack suppression. The carbon veil fibres, therefore, would not contribute to the delamination resistance. Both fracture sides in the PA veil interleaved composite are also covered with the matrix, as illustrated in Figure 3.31 (d). The PA veil fibres are not clearly found on the fracture surface. The veil fibres may be embedded in the matrix and this aspect of the fracture surface differs from the carbon veil interleaved specimen.

Figure 3.32 shows cross-section images taken by optical microscope for the PE and PA veil interleaved specimens. From Figure 3.32 (a), the crack goes through in the interleaf veil region. The PE veil fibres formed bridging during the crack growth. This bridging effect can contribute to the improvement of the initiation and propagation values. The hybrid veils are similar in behaviour to the PE veil. On the other hand, it can be seen that the crack propagates in the PA veil fibres, as shown in Figure 3.32 (b). The PA veil fibres are adhered to the matrix, not pulled out from the matrix completely. The surface of the PA veil fibres appears on the fracture surface (see in Figure 3.31 (d)).

The hybrid and PE veil fibres would be expected to exhibit poor adhesion to the matrix. As a result, these veil fibres are pulled out from matrix, and contribute to stable crack propagation via bridging effects. Consequently, the toughness can be improved significantly. In contrast, the carbon veil fibres would possess good adhesion to the epoxy resin, and the interleaf veils would not pull out from the matrix. Moreover, the interleaf veil reduces the interlaminar region and would prevent the formation of a plastic zone. The crack propagation, therefore, was significantly rapid and jumped. The adhesion between the Ep1 matrix and the PA veil fibres may not be good. Therefore, the veil fibres cannot improve delamination resistance.

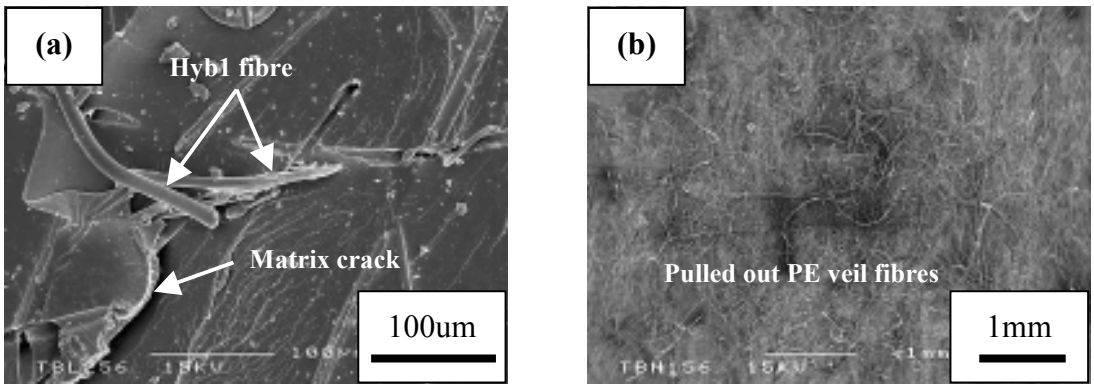

Figure 3.31 Micrographs of fracture surface taken by SEM for 5-harness satin weave epoxy1 system specimens: (a) Hyb1 veil interleaved, (b) PE veil interleaved, (c) Carbon veil interleaved, (d) PA veil interleaved

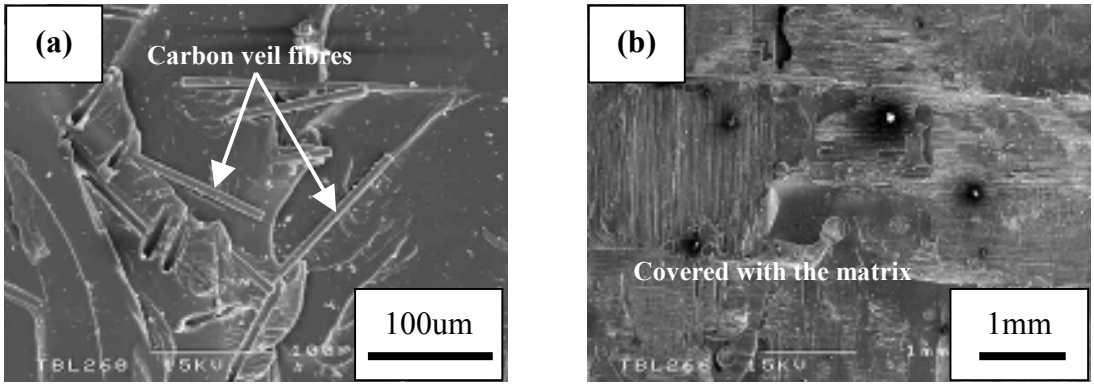

Figure 3.31 (*Continued*)

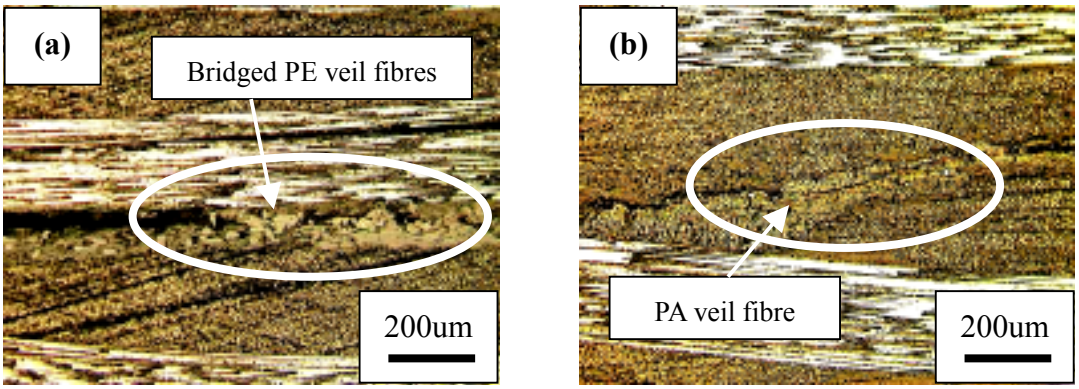

Figure 3.32 Micrographs of cross-section taken by optical microscope for 5-harness satin weave epoxy1 system specimens: (a) PE veil interleaved, (b) PA veil interleaved

The fracture surfaces of the interleaved VE system laminates are shown in Figure 3.33. The fracture surfaces for the PE and PA veil interleaved composites are a combination of the exposed woven fabric and the matrix, the same as the non-interleaved specimen (see in Figure 3.29 (d)). The PE veil fibres are pulled out in selected areas only, unlike the Ep1 system specimens. Moreover, the carbon woven fibres are unravelled, as illustrated in Figure 3.33 (a). The PA veil fibres are exposed from matrix, however the fibres are adhered to the matrix, as shown in Figure 3.33 (b). It can be seen that the tip of PA veil fibre is extended. The veil fibres were deformed, when the crack propagated in the interleaf veil region.

In the VE system, the carbon woven fibres are unravelled and would provide a bridging effect. Therefore, the crack growth in this resin system was made stable. It is thought that the adhesion between the carbon woven and the VE resin is poorer than the

Ep1 resin. In VE system specimens, only a limited number of veil fibres are pulled out from the fracture surface and this improved the Mode-I interlaminar toughness marginally.

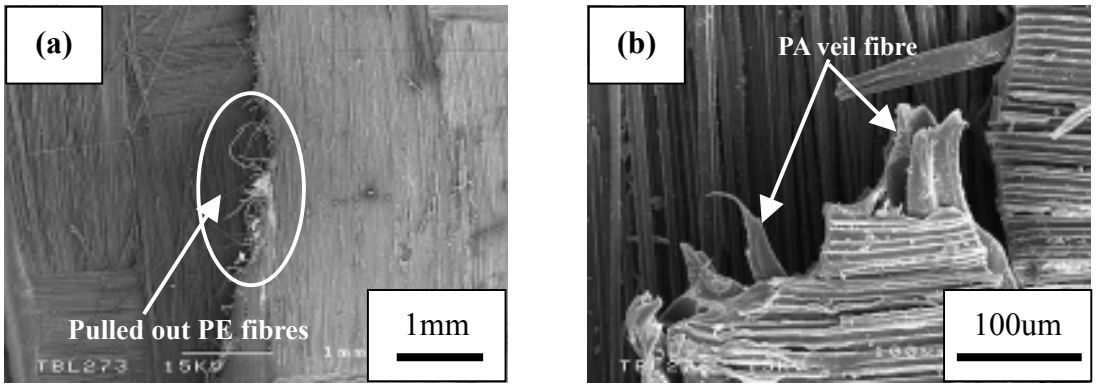

Figure 3.33 Micrographs of fracture surface take by SEM for 5-harness satin weave vinyl ester system specimens: (a) PE veil interleaved, (b) PA veil interleaved

3.4.2.2 Unidirectional Fabric Specimens

Figure 3.34 shows micrographs of the fracture surfaces taken by SEM for the Ep1 system specimens. The fracture surface is basically a similar condition to the satin weave cases. The Hyb1 veil fibres are pulled out in a partial area, as shown in Figure 3.34 (a). The fracture surfaces for the Hyb2 veil interleaved laminates also showed a few pulled out fibres, as shown in Figure 3.34 (b). However, the G_{IC} values in the both hybrid veil interleaved samples are not increased (see in section 3.3.4.2). It is thought that pulled out fibres are not many. Hence, the delamination resistance cannot improve much. The fracture surface of the PE veil interleaved specimen reveals many veil fibres pulled out from the matrix, as shown in Figure 3.34 (c). These fibres would provide crack bridging and improve the Mode-I initial energy release rate significantly. Moreover, the pulled out PE veil fibres are much than the hybrid veil fibres. Therefore, the Mode-I interlaminar toughness can be increased considerably.

In the carbon and PA veil interleaved laminates, the fracture surface is almost the same as in the satin weave specimen. The carbon veil fibres are embedded in the matrix, as shown in Figure 3.34 (d). It is thought that the adhesion between the carbon veil fibres and the Ep1 resin is good. Therefore, the interleaf veil fibres would not pull out and provide a bridging effect. Consequently, the Mode-I toughness is significantly poor. The surface for the PA veil interleaved specimen is completely covered with the

matrix, as shown in Figure 3.34 (e). The fracture surface is similar to that of the satin specimens (see in Figure 3.31 (d)). Although the interleaf veil fibres are not seen on the fracture surface clearly, a smooth area appears on some parts of the surface. It is thought that this would be the PA veil fibres.

Figure 3.35 shows cross-section pictures for the PE and PA veil interleaved specimens. In the PE veil interleaved sample, the crack goes through in the interleaf veil region, as shown in Figure 3.35 (a). The extensive pull-out of veil fibres has improved the Mode-I toughness. On the other hand, the crack for the PA veil interleaved laminate passes through the surface of the interleaf veil. In the UD fabric specimens, the behaviour of the veil fibres is almost same as the satin weave cases.

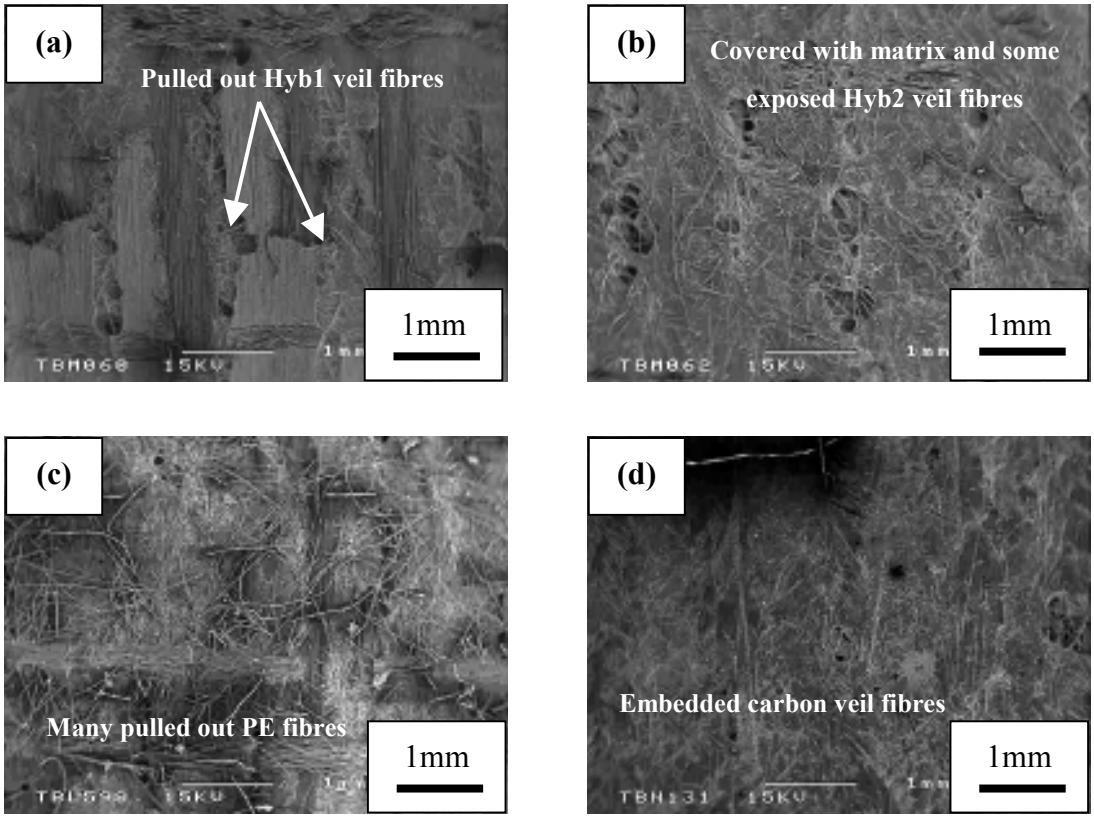

Figure 3.34 Micrographs of fracture surface take by SEM for unidirectional fabric epoxy1 system specimens: (a) Hyb1 veil interleaved, (b) Hyb2 veil interleaved. (c) PE veil interleaved, (d) Carbon veil interleaved, (e) PA veil interleaved

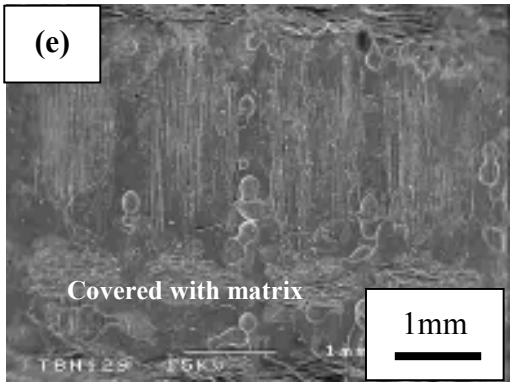

Figure 3.34 (*Continued*)

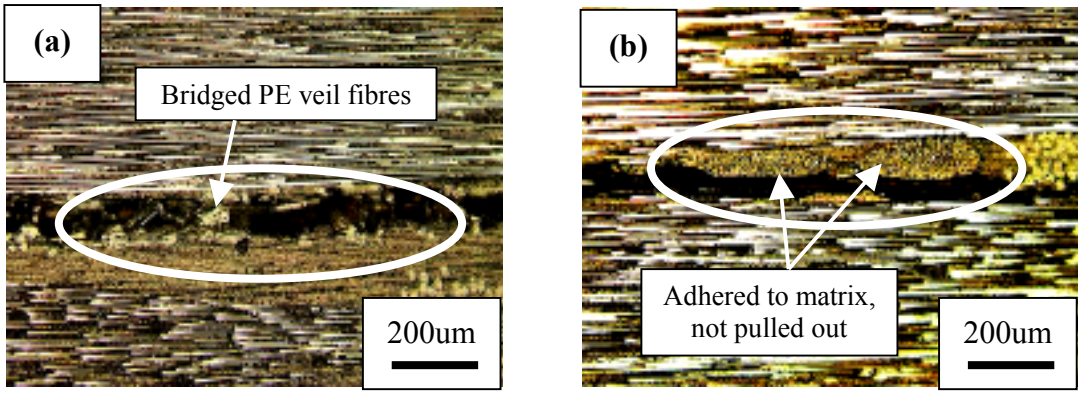

Figure 3.35 Micrographs of cross-section taken by optical microscope for unidirectional fabric epoxy1 system specimens (a) PE veil interleaved, (b) PA veil interleaved

The SEM pictures of the fracture surface for the VE system laminates are illustrated in Figure 3.36. The fracture behaviour for the UD specimens is different from the satin weave cases. In the hybrid and carbon veil interleaved composites, while one surface side is covered with the matrix, another side shows that the UD fibres are exposed and unravelled, as shown in Figure 3.36 (a) and (b). From SEM images, the crack would pass through between the fabric surface (lower side) and matrix (upper side). However, the interleaf veil fibres cannot be recognised on the surface. The veil fibres are completely embedded in the matrix. The interleaf veil fibres, therefore, could not work for crack resistance and contribute to an improvement of Mode-I interlaminar toughness. Nevertheless, the G_{IC} values are increased in all interleaved samples, even in the carbon-veil interleaved materials. It is thought that these unravelled carbon fibres provide bridging and contribute to the improvement of delamination resistance. For the

PE and PA veil interleaved laminates, the fracture surfaces are the same as the satin weave specimens. The surface in the PE veil interleaved composite reveals exposed woven fabric and matrix surface. Moreover, many PE veil fibres are pulled out from the matrix and some UD fabrics are also unravelled, as shown in Figure 3.36 (c). The PE veil and carbon fabric would lead to a considerable improvement of delamination resistance. Consequently, the G_{IC} values can significantly increase. The fracture surface in the PA veil interleaved specimen is almost the same as the PE veil interleaved case. From Figure 3.36 (d), although the PA veil fibres are also pulled out from the matrix, the pull-out fibre length is smaller than for the PE veil fibres.

Figure 3.37 shows cross-sections of the Hyb1, PE, and PA veil interleaved laminates, It can be seen that the Hyb1 veil fibres are embedded in the matrix, as shown in Figure 3.37 (a). The crack behaviour for the Hyb2 and carbon veil interleaved specimens is almost the same as the Hyb1 veil interleaved sample. These veil fibres are completely embedded in the matrix. Moreover, the UD carbon fibres are unravelled on one fracture side. The unravelled fibres would work to provide a bridging effect. These would contribute to increase the Mode-I interlaminar toughness moderately, even in the carbon veil interleaved material. For the PE veil, some PE veil fibres are pulled out from the matrix, as shown in Figure 3.37 (a). Although the PA veil fibres are adhered to the matrix, it seems that the veil fibres are elongated. These veil fibres and unravelled carbon fibres can improve the Mode-I interlaminar toughness compared with the other interleaved cases.

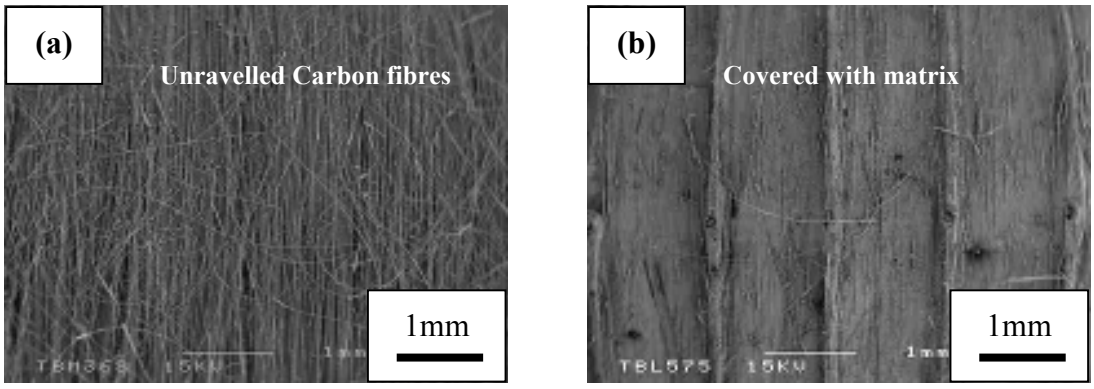

Figure 3.36 Micrographs of fracture surface taken by SEM for unidirectional fabric vinyl ester system specimens: (a) Hyb1 veil interleaved on lower side, (b) Hyb1 veil interleaved on upper side, (c) PE veil interleaved, (d) PA veil interleaved

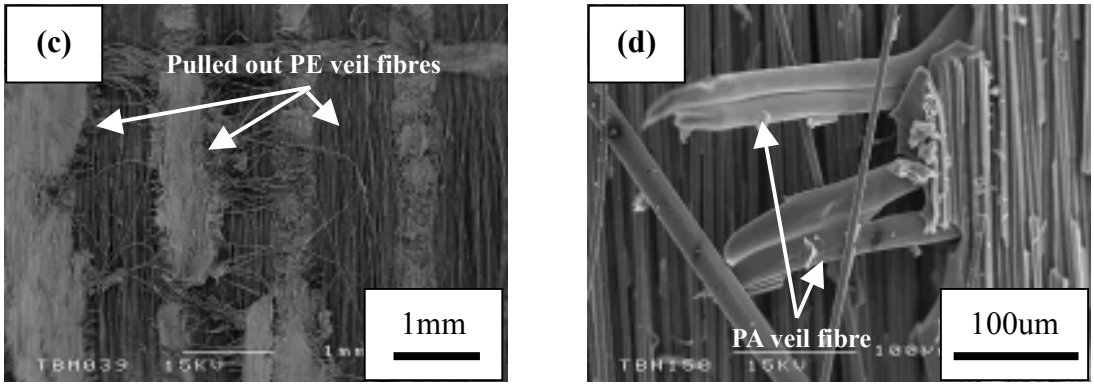

Figure 3.36 (*Continued*)

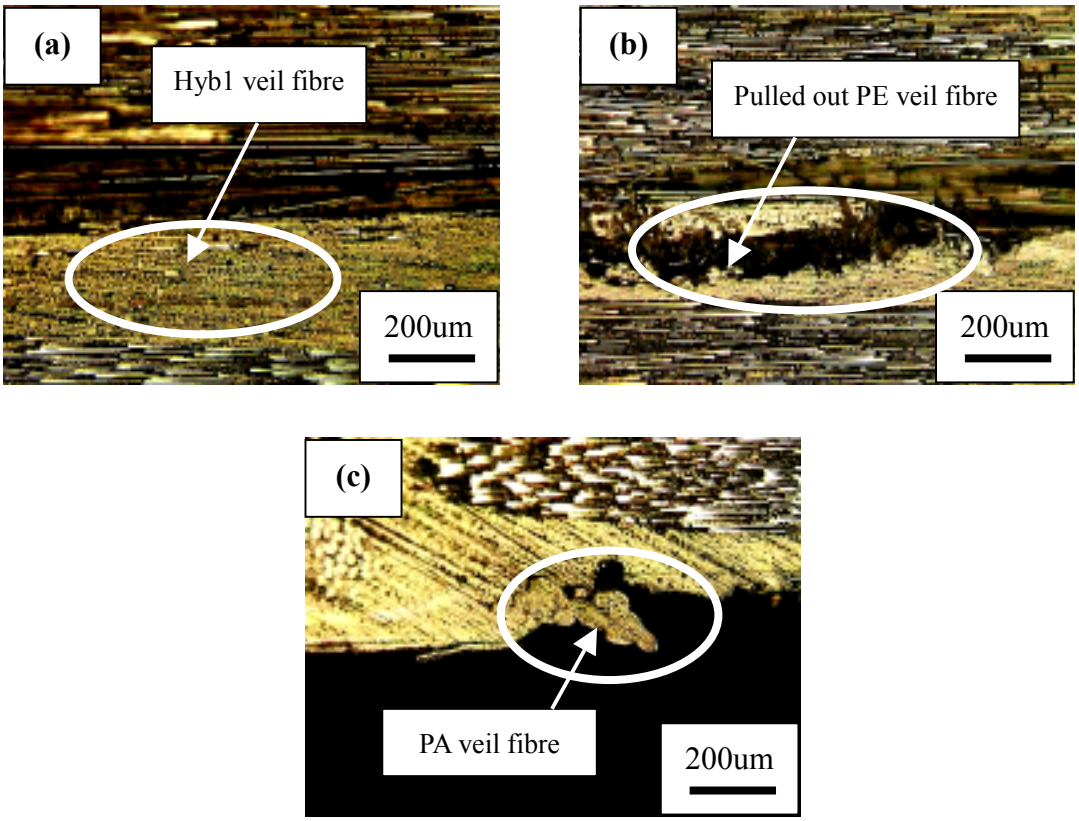

Figure 3.37 Micrographs of cross-section taken by optical microscope for unidirectional fabric vinyl ester system specimens: (a) Hyb1 veil interleaved, (b) PE veil interleaved, (c) PA veil interleaved

3.4.2.3 Plain Weave Fabric Specimens

Figure 3.38 shows the fracture surface photographs taken by SEM for the Ep2 system specimens. For the PE/C veil interleaved laminate, it can be seen that the

interleaf veil fibres are pulled out in a small area, as shown in Figure 3.38 (a). The pulled out fibres are bent and curved. It seems that these fibres are the PE veil fibre. The carbon veil fibres cannot be found on the fracture surface. These pulled out PE veil fibres would be responsible for bridging and suppress crack propagation during the DCB test. The fracture surface in the Hyb2 veil interleaved specimen is almost the same as the PE/C veil interleaved sample. A few veil fibres are pulled out from the matrix and appeared only in a partial area. The pulled out Hyb2 veil fibres are less compared with the PE/C veils fibres. It is thought that many Hyb2 veil fibres would be embedded in the matrix. Hence, the crack suppression effect by the interleaf veil is not considerably improved. Consequently, the Mode-I interlaminar toughness can barely improve. For the PE veil interleaved laminates, the fracture surface is similar to the satin and UD fabric Ep1 system specimens. Many PE veil fibres are pulled out on the fracture surface, as shown in Figure 3.38 (c). These pulled out veil fibres would work as crack-bridging fibres and suppress crack propagation. The fracture surface for the PA veil interleaved composite is covered with the matrix, as shown in Figure 3.38 (d). The PA veil fibres cannot be clearly found on the fracture surface, same as the satin and UD cases. Although the fracture behaivour is almost the same as the other fabric specimens, the fracture surface seems slightly different from the Ep1 system specimens. Practically, the surface for the Ep2 system specimen is coarser than that for the Ep1 system specimens.

The cross-section pictures taken by the optical microscope for the PE and PA veil interleaved composites are shown in Figure 3.39. In the PE veil, it can be seen that many veil fibres are pulled out from the matrix, as shown in Figure 3.39 (a). These pulled out fibres can significantly improve the Mode-I interlaminar toughness. On the other hand, the PA veil fibres are adhered to the matrix, as illustrated in Figure 3.39 (b). However, the delamination resistance is completely different from the Ep1 system specimens. In the Ep2 system, the G_{IC} values are significantly higher than the Ep1 system specimens (see in section 3.3.3.1 and 3.3.3.3). It is thought that the epoxy type in the PA veil interleaved specimens may strongly affect the Mode-I interlaminar toughness. The Ep2 resin would have superior adhesion to the Ep1 resin in the PA veil. Therefore, the G_{IC} values can be increased considerably.

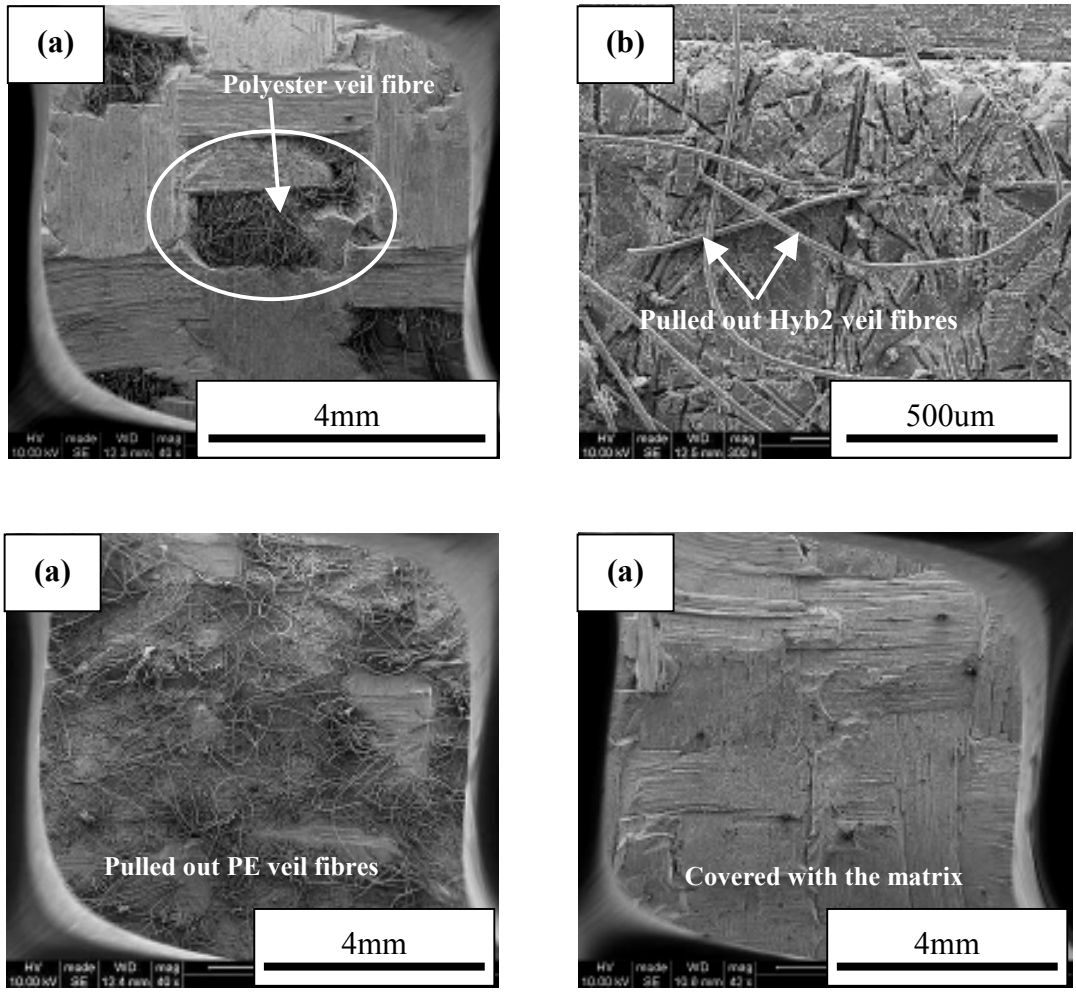

Figure 3.38 Micrographs of fracture surface taken by SEM for plain weave epoxy2 system specimens: (a) PE/C (100:100) veil interleaved, (b) Hyb2 veil interleaved, (c) PE veil interleaved, (d) PA veil interleaved

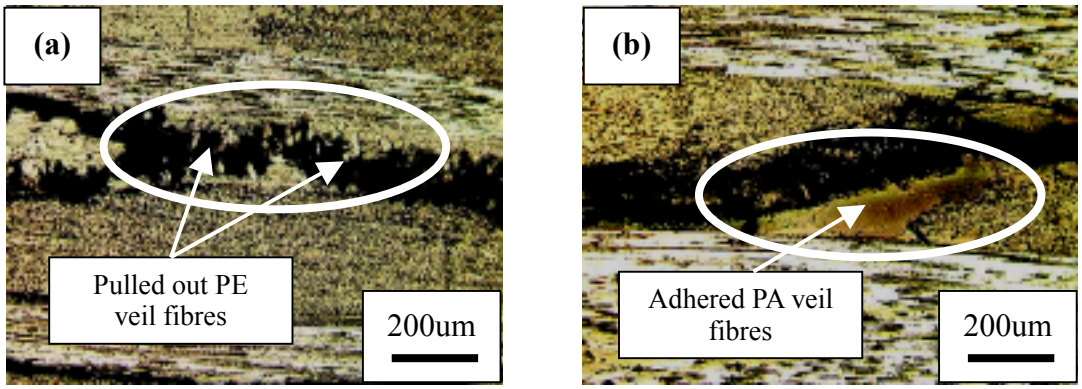

Figure 3.39 Micrograph of cross-section taken by optical microscope for plain weave epoxy2 system specimens: (a) PE veil interleaved, (b) PA veil interleaved

Figure 3.40 illustrates the fracture surface photographs taken by the SEM for the VE resin composites. The fracture surface in the PE/C veil interleaved specimen shows the exposed woven fibres and matrix. The interleaf veil fibres, however, cannot be found on the surface, as shown in Figure 3.40 (a). It is thought that both PE and carbon veil fibres would be embedded in the matrix. The crack passed through between matrix and woven surface. For the Hyb1 and carbon veil interleaved laminate, the fracture surface is almost the same as the PE/C veil interleaved sample. The surface is covered with the matrix, and the interleaf veil fibres do not appear on the matrix. These veil fibres are completely embedded in the matrix. Hence, the delamination resistance cannot be improved. The fracture surface in the Hyb2 veil interleaved material, on the other hand, is a mixture of the exposed woven fabric and matrix, as shown in Figure 3.40 (b). It can be seen that some Hyb2 veil fibres are pulled out in a small area. Many Hyb2 veil fibres, however, are still embedded in the matrix. Therefore, the G_{IC} values could not increase considerably. In all resin systems, the carbon veil fibres are embedded in the matrix. It is thought that the adhesion between the carbon veil and matrix is too good and the veil fibres cannot pull out. Moreover, the interleaf veil would reduce the plastic zone in the interlaminar region. Consequently, the carbon veils may not be improved and contribute to the Mode-I interlaminar toughness. The fracture surfaces in the PE and PA veil interleaved laminates are similar to the Hyb2 veil interleaved case. The PE veil fibres are pulled out from part of the fracture region, as illustrated in Figure 3.40 (c). Some of pulled out veil fibres and unravelled fabric would improve the toughness. The fracture surface in the PA veil interleaved sample is that some PA veil fibres are pulled out from the matrix, as shown in Figure 3.40 (d). The PA veil fibres in the VE resin system provide a bridging effect for the suppression of crack

propagation. Compared to the PE veil fibres, the pulled out PA veil fibres are fewer and adhered to the matrix. It is thought that the PA veil fibres may possess better adhesion to the VE matrix than the PE veil fibres. On the other hand, the adhesion between the PA veil and matrix in the VE system would be poorer than the Ep2 system. Therefore, some veil fibres are pulled out from the matrix.

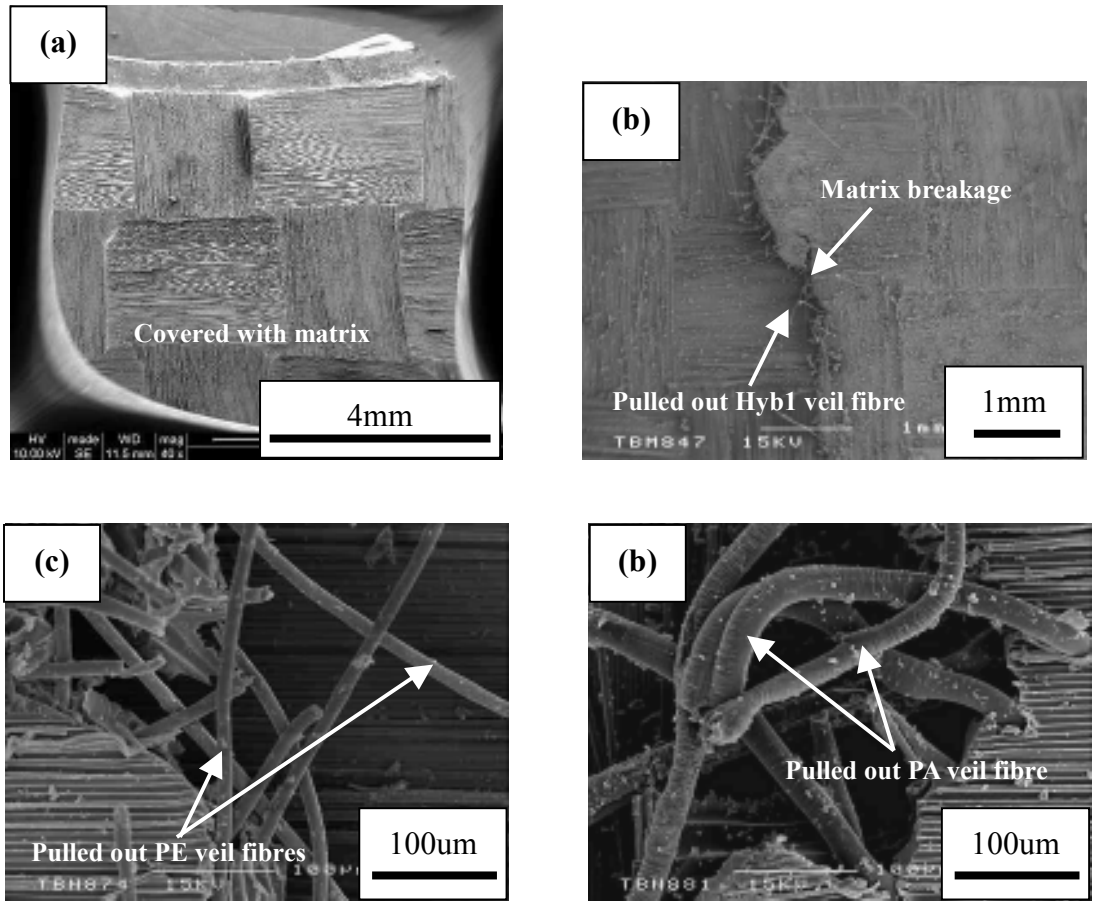

Figure 3.40 Micrographs of fracture surface taken by SEM for plain weave vinyl ester system specimens: (a) PE/C (100:100) veil interleaved, (b) Hyb1 veil interleaved, (c) PE veil interleaved, (d) PA veil interleaved

3.5. Conclusion

Evaluating the study for the Mode-I interlaminar toughness of non-woven interleaved CFRP fabricated VaRTM method, the following conclusions are drawn:

(1) From SEM pictures the Ep resins provide stronger adhesion to the carbon fabrics than to the VE resin. The fracture surfaces for Ep system samples are covered with

the resin. For the VE resin samples, the crack mainly has propagated between the matrix and woven surface. Also the carbon fibres are unravelled.

(2) For the 5-harness satin weave with the Ep1 system specimens, the PE veil interleaved case had the highest Mode-I interlaminar toughness. Many PE veil fibres were pulled out on the fracture surface. These pulled out fibres seem to work as bridging and suppress crack propagation. The G_{IC} value, therefore, was significantly increased. The fibres of both hybrid veils were also pulled out from the matrix, but less than the PE veil fibres. In the Ep1 resin system, the G_{IC} values of the hybrid veil interleaved laminates were same or slightly lower than the non-interleaved case. In contrast, the carbon and PA veil interleaved composites had a significantly lower value of G_{IC} than the other samples. Both veil fibres were not completely pulled out on the surface. The carbon veil fibres were embedded in the matrix and could not be worked as bridging. The PA veil fibres behaved differently. The PA veil fibres were exposed on the fracture surface, but adhered to the matrix. The crack passed on the surface of PA veil fibres. The adhesion property could not contribute to the improvement of Mode-I interlaminar toughness. For the VE system, the crack propagated between the carbon fabric and the matrix. The carbon fabric was exposed and unravelled over a partial area. Moreover, the PE and PA veil fibres were exposed at part of the matrix region. These exposed veil fibres would work as bridging and suppress crack growth.

(3) For the UD fabric with the Ep1 system laminates, the toughening behaviour of the interleaf veil was similar to the satin samples. The PE veil interleaved specimen had the highest G_I value. Both hybrid veil interleaved composites had a slightly higher value than the control. The carbon veil interleaved specimen had the poorest Mode-I interlaminar toughness in all interleaved cases. The PA veil interleaved laminate, on the other hand, had higher value of the G_{IC} compared with the satin weave specimen. For the VE system, all of the specimens had similar G_{IC} values. The $G_{I\text{-}prop}$ values of specimens, on the other hand, were significantly increased even in the carbon veil interleaved case. It is thought that the UD fabres are unravelled and worked to provide bridging. These unravelled fibres would improve the delamination resistance including the carbon veil interleaved materials.

(4) For the plain weave with the Ep2 system laminates, the Mode-I interlaminar toughness of the PA veil interleaved specimen was significantly changed compared

with the Ep1 system samples. The PA veil interleaved case was enormously improved for G_{IC} values. The PE veil interleaved laminate had the second highest Mode-I interlaminar toughness. The toughness for the PE/C and Hyb2 veil interleaved composites, on the other hand, was only slightly increased compared with the non-interleaved case. For the VE system, the difference of the G_{IC} values between each specimen was not so much compared with the Ep2 system materials. The G_{IC} values of the plain weave specimens were quite higher than that of the 5-harness satin weave samples. The surface of the plain weave is coarse, and crack initiation would be more difficult than with the satin weave. On the other hand, both woven specimens had similar $G_{I\text{-}prop}$ values, in particular the PE and PA veil interleaved specimens. Once the crack propagates, weave types would not affect the propagation values.

(5) The Ep resin system specimens showed clear difference of the G_{IC} values between each veil interleaved laminate, whereas the G_{IC} values between each interleaved VE resin system composite were similar. For the VE system laminates, when the crack propagated in the interlaminar region, the woven fibres were unravelled and caused fibre-bridging. Consequently, it is thought that a low interlaminar toughness specimen such as the carbon veil interleaved specimen even has moderate G_{IC} values. On the other hand, in the Ep system specimens fibre-bridging by the woven fibres did not occur. Therefore, the interlaminar toughness was directly influenced only by properties of interleaf veil.

Chapter 4

Toughening Mechanisms of Mode-II Interlaminar Fracture using Non-woven Veils as Interleaf Materials

4.1 Introduction

In this chapter, the main objective is to investigate the mechanisms of Mode-II interlaminar toughness for the interleaved composites. Several types of the non-woven veils were chosen as interleaf materials. The four-point end notched flexure (4ENF) tests were carried out for evaluating the Mode-II interlaminar toughness properties. The mechanisms of the inerlaminar toughness and the contribution to the toughness by the non-woven veils were examined and discussed using the test results and microscopy.

4.2 Materials and Experiment Methods

4.2.1 Materials Information

The materials using this study are the same as in chapter 3. These are described in section 3.2.1.

4.2.2 Fabrication Methods of Composites for Mode-II Test

The fabrication of the specimens is the same as chapter 3. The details of moulding are explained in section 3.2.2.

4.2.3 Mode-II Interlaminar Toughness Tests

The Mode-II interlaminar toughness properties of the composites were evaluated using the 4ENF test. The 4ENF test specimens were rectangular in shape, 140mm (in length) x 20mm (in width), as shown in Figure 4.1. The side faces of the specimens were polished and painted using a white spray. The specimens were marked from the edge of the insert film with vertical lines every 1mm up to 40mm

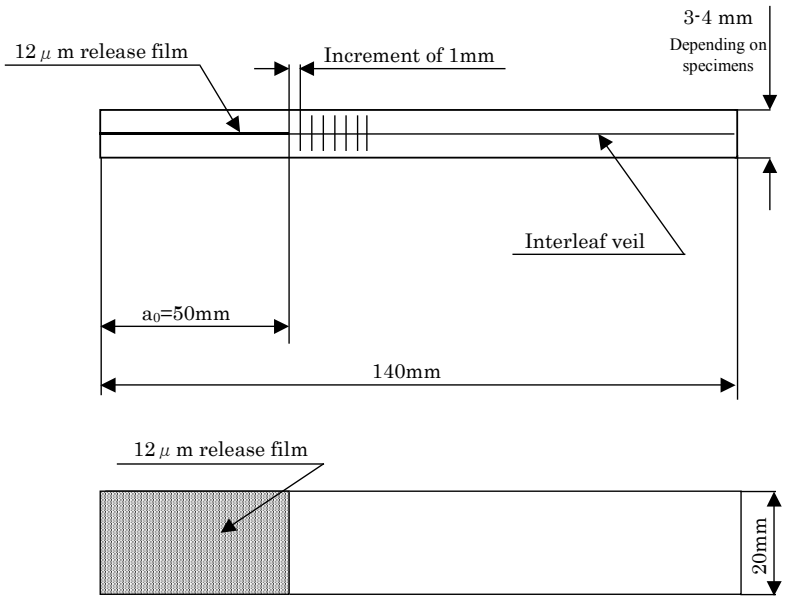

Figure 4.1 Dimensions of the 4ENF specimen

For the 4ENF test fixtures, the spans of the support rollers and the loading rollers are 100mm and 60mm, respectively. The 4ENF specimens were loaded in a Hounsfield testing machine with a 25kN load cell. The Mode-II pre-cracking was performed as follows. The specimen was loaded at a constant crosshead speed of 0.5mm/min. The load and displacement, at which the delamination crack moved from the insert film, were recorded up to crack propagation of 4mm. The specimen was then unloaded at a constant crosshead speed of 10mm/min. Thereafter the specimen was reloaded at the same constant crosshead speed of 0.5mm/min without stopping and the crack length was recorded until the final crack length increment. The load and displacement were recorded for every 1mm mark if possible. If bending fracture started, the crack would not grow and the test was stopped. Finally, the specimen was unloaded at a crosshead speed of 10mm/min until the displacement reached the start point. Mode-II energy release rate (G_{II}) was calculated using compliance data reduction method (see in section 2.7.3.4). Figure 4.2 and 4.3 show schematic of 4ENF test and picture of 4ENF fixture.

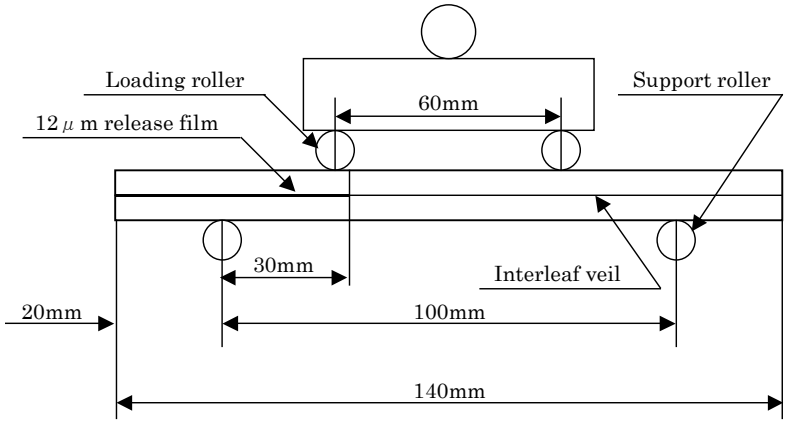

Figure 4.2 Schematic of the 4ENF test

Figure 4.3 Picture of 4ENF rig

4.2.4 The Thickness and Volume Fraction of Each Laminate

The details of specimen thickness and volume fraction (V_f) used 4ENF tests are same as the DCB specimens and are summarised in section 3.2.4.

4.2.5 Calculation of G_{IIC}

For the calibration of the Mode-II energy release rate, the adjusted compliance versus the delamination length is plotted and a curve-fitting routine was used to fit a straight line to the data of the second loading test (see in Figure 4.4) [94, 192]. The gradient of this line, m, is then used to calculate the G_{II} by the following equation:

$$G_{II} = \frac{P^2 m}{2B} \tag{4.1}$$

where P is the load, m is the gradient from CC curve, and B is the width of specimen.

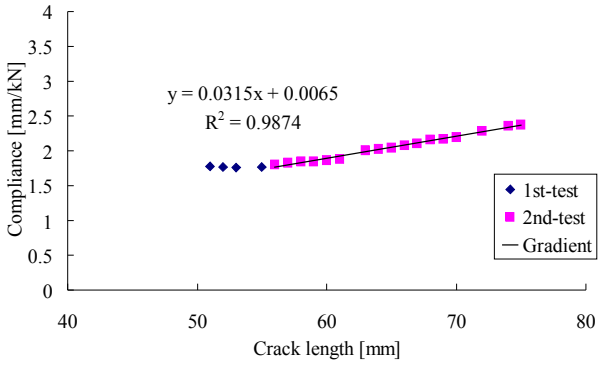

Figure 4.4 Typical 4ENF compliance calibration diagram

The R-curve (resistance curve) can then be plotted and the propagation values of the G_{II} are obtained as shown in Figure 4.5. The Mode-II initial energy release rate used values at non-linear (NL) and 5%/MAX points. The definition of NL and 5%/MAX values is mentioned in the section 2.7.1. The energy release rate at propagation region, $G_{II\text{-}prop}$, is calculated as the average of propagation values from the maximum G_{II} value (see in Figure 4.5).

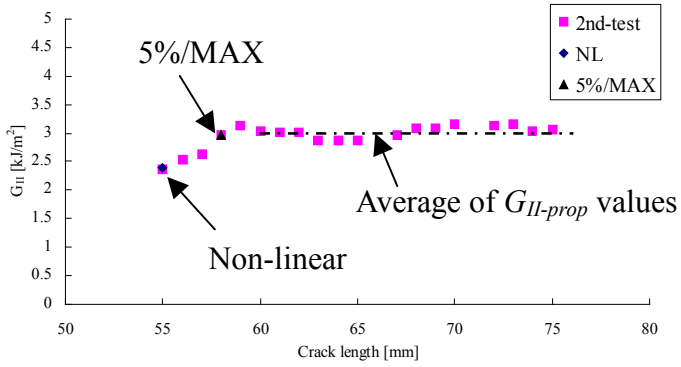

Figure 4.5 Typical Mode-II crack propagation resistance curve (R-curve)

4.2.6 Observation by Microscopy

Tested specimens were observed using SEM and optical microscopy. Details of the preparation method are indicated in section 3.2.7.

4.3 Results

4.3.1 Resistance-Curves for Non-Interleaved Specimens

In this section, the representative R-curves for various interleaved laminates are shown. Figure 4.6 shows the typical R-curves obtained by 4ENF tests for the non-interleaved Ep resin system laminates. The G_{IIC} values for each fabric type appear to give different results, as shown in the diagram. The propagation values in the satin weave laminate are the highest in all non-interleaved cases. The G_{IIC} values in the UD specimen has the second highest. On the other hand, two different areal weight plain weave laminates show different behaviour. The HAW specimen possesses higher propagation values than the LAW case. The areal weight of the base materials affects the Mode-II interlaminar toughness, unlike the Mode-I interlaminar toughness which is unaffected (see in Figure 3.14).

Figure 4.7 illustrates the R-curves for the non-interleaved VE system composites. The results are opposite to the Ep-system specimens. The satin weave laminate has the lowest G_{II} value in all VE system samples. The propagation values in the UD specimen increase to over 2kJ/m^2. On the other hand, the propagation values for the plain weave laminate rises to over 1.5kJ/m^2, but then G_{II} value drops suddenly, as bending fracture starts during 4ENF test. Once bending fracture occurred, the crack propagated no longer.

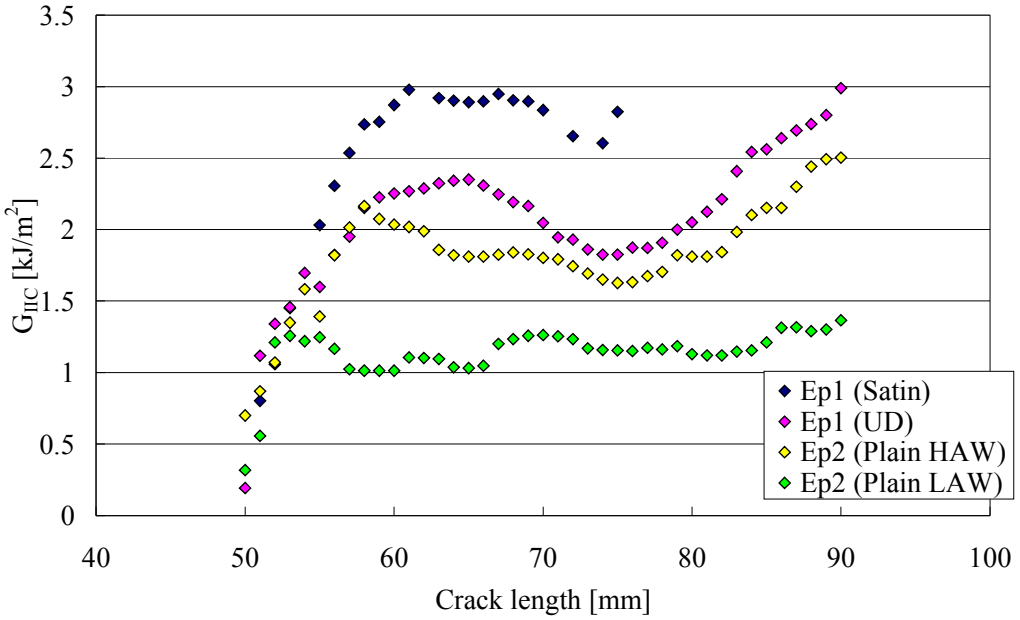

Figure 4.6 R-curves for the non-interleaved epoxy system specimens

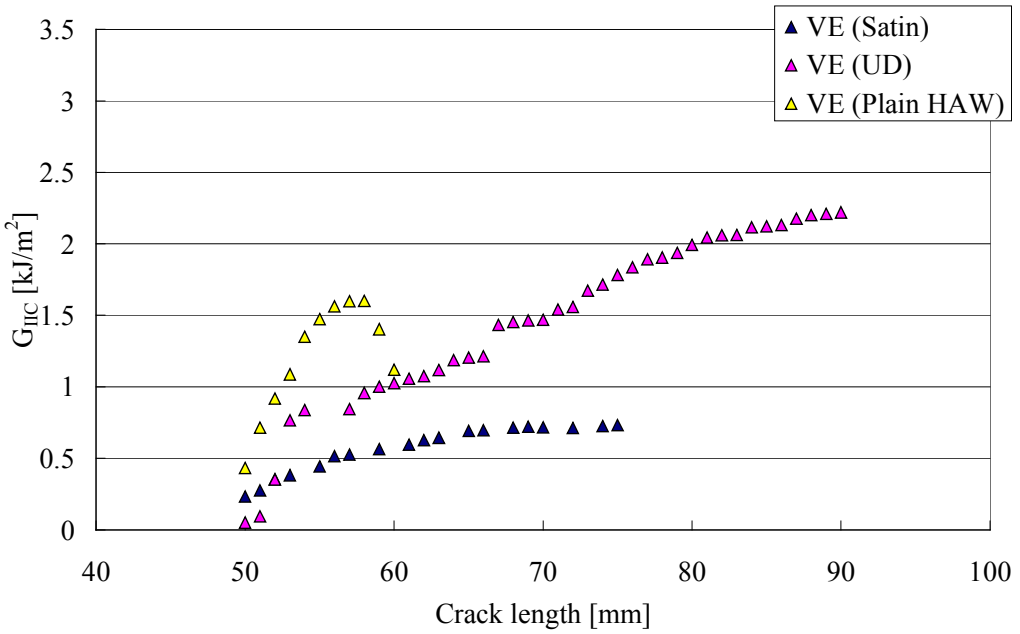

Figure 4.7 R-curves for the non-interleaved vinyl ester system specimens

4.3.2 Resistance-Curves for Interleaved Specimens

4.3.2.1 5-harness Satin Weave Fabric Specimens

Figure 4.8 illustrates the typical R-curves for control and interleaved Ep1 system laminates. The tendency of the G_{II} values is different from the Mode-I interlaminar toughness (see in Figure 3.16). The Hyb2 and PE veil interleaved specimens possess quite high G_{II} values. In particular, the Hyb2 veil interleaved case is over 5kJ/m^2. On the other hand, the Hyb1 veil interleaved composite is moderately higher G_{IIC} value than the non-interleaved sample. The carbon veil interleaved laminate has the lowest propagation value of all interleaved specimens. The PA veil interleaved composite also exhibits low G_{II} values. However, the propagation values increase until the end of the test. Ultimately, $G_{II\text{-}prop}$ values for the PA veil interleaved sample exceed 3kJ/m^2.

The R-curves obtained by the 4ENF tests for the VE system are shown in Figure 4.9. In the VE system, only the PE and PA veil interleaved specimens were examined. Both interleaved laminates have higher G_{II} values than the non-interleaved case. The propagation values in both interleaved samples are similar. The PE veil interleaved laminate shows slightly lower G_{II} values than the Ep1 laminates. On the other hand, the PA veil interleaved samples possess higher propagation values than the Ep1 system case.

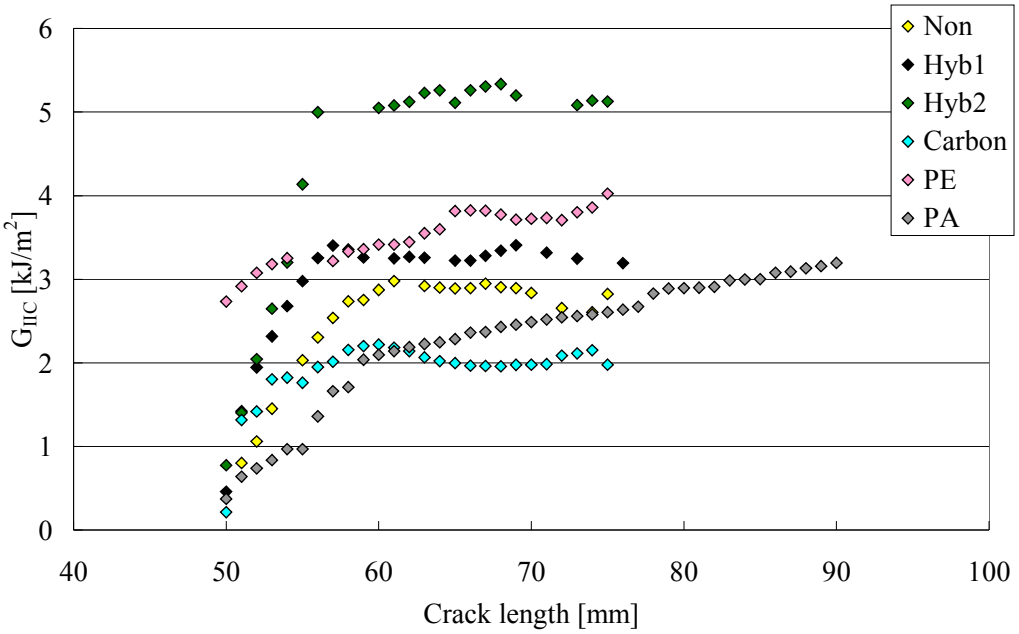

Figure 4.8 R-curves for non-interleaved and interleaved 5-harness satin weave fabric specimens with epoxy1 system

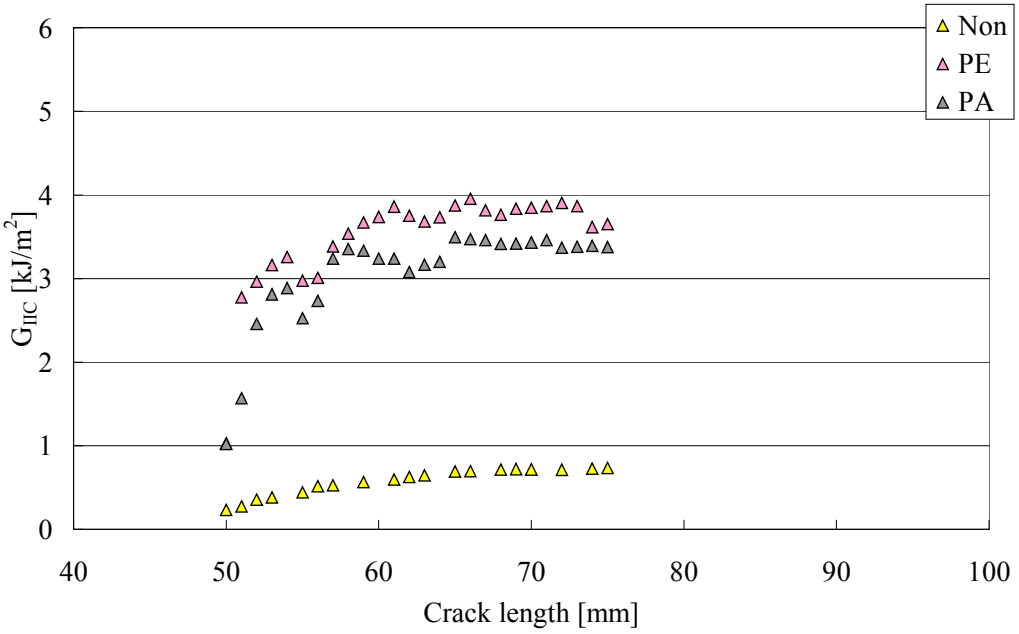

Figure 4.9 R-curves for non-interleaved and interleaved 5-harness satin weave fabric specimens with vinyl ester system

4.3.2.2 Unidirectional Fabric Specimens

Figure 4.10 shows the R-curves for the control and interleaved Ep1 system composites. The general trend in the G_{II} values is similar to the satin specimens. The Hyb2 veil interleaved specimen has the highest G_{II} values, over 5kJ/m^2. The Hyb1 and PE veil interleaved cases have almost the same propagation values. In the PA veil interleaved sample, the G_{II} values are same as the Hyb1 and PE veil interleaved cases until a crack length of 70mm. Thereafter, the propagation values are increased and over 5kJ/m^2. Surprisingly, the carbon veil interleaved specimen has slightly higher G_{II} values than the control.

Figure 4.11 shows the typical R-curves obtained by the 4ENF tests for the VE system composites. The R-curves for all specimens show quite similar behaviour, unlike the Ep1 system samples. The PA veil interleaved laminate performs well after 80mm crack length. The PE and PA veil interleaved samples possess slightly higher G_{II} values than the other interleaved cases. Compared to the satin weave VE system composite, the UD samples exhibit low G_{II} values. In Mode-I interlaminar toughness, the UD fabric VE resin composites possess excellent G_I values compared with the Ep1 system cases. However, the Mode-II interlaminar toughness does not appear to be improved by fibre-bridging effect.

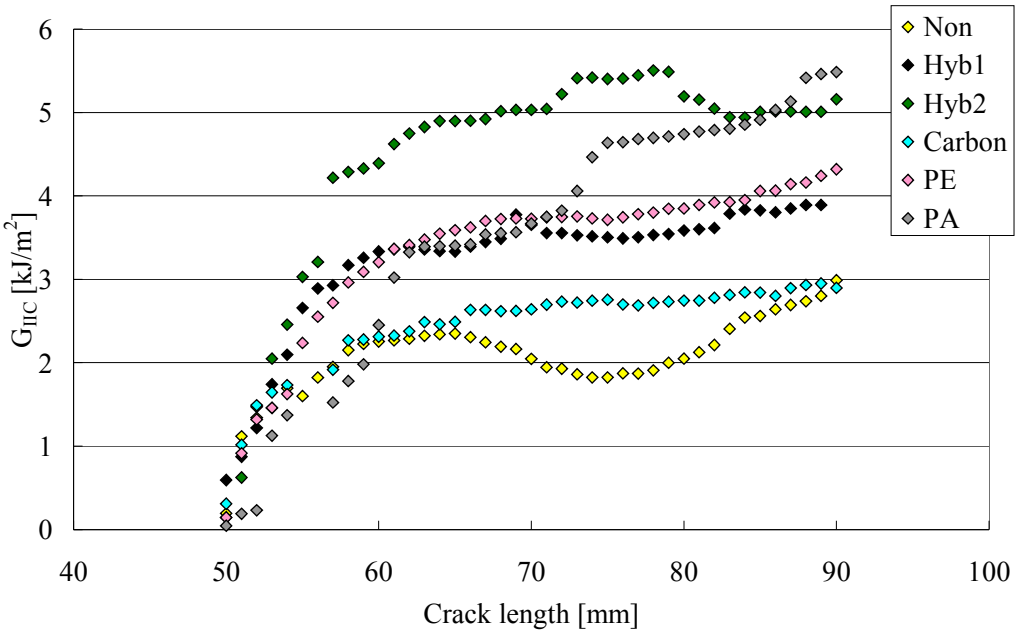

Figure 4.10 R-curves for non-interleaved and interleaved unidirectional fabric specimens with epoxy1 system

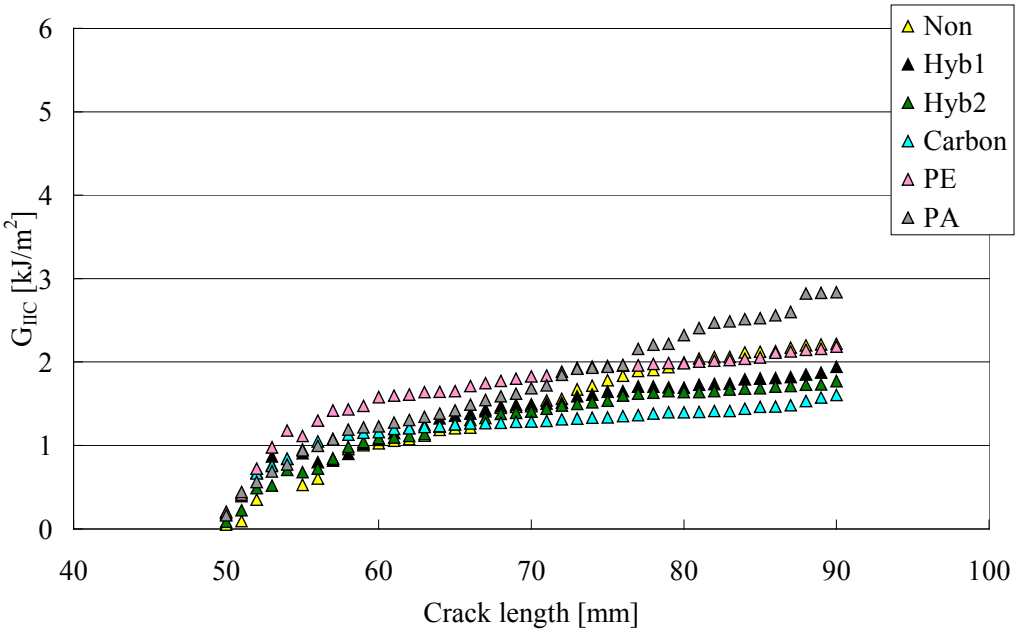

Figure 4.11 R-curves for non-interleaved and interleaved unidirectional fabric specimens with vinyl ester system

4.3.2.3 Plain Weave Fabric Specimens

Figure 4.12 shows the representative R-curves for the Ep2 system composites. From the graph, the G_{II} values in all interleaved laminates are increased relative to the control. The PE/C veil interleaved sample possesses only a slightly higher G_{IIC} value than the non-interleaved case. For the Hyb2 veil interleaved specimen, it can be seen that the G_{II} values are increased. However, the improvement of the Mode-II interlaminar toughness is less than the other fabrics with the Ep1 system. The toughness of the PE and PA veil interleaved composites is increased significantly. However, in these interleaved laminates bending fracture occurred at an early stage. Therefore, data points are less than the other interleaved materials.

The diagram of the typical R-curves for the VE system composites is shown in Figure 4.13. The general trend is similar to the Ep2 system specimens. The PE/C, Hyb1, and carbon veil interleaved laminates have almost the same propagation values. In contrast, the Hyb2 veil interleaved case possesses the lowest G_{IIC} values. The PE and PA veil interleaved composites have higher propagation values than the other interleaved samples. Basically, the G_{IIC} values in the VE system interleaved specimens are overall lower than the Ep system interleaved cases.

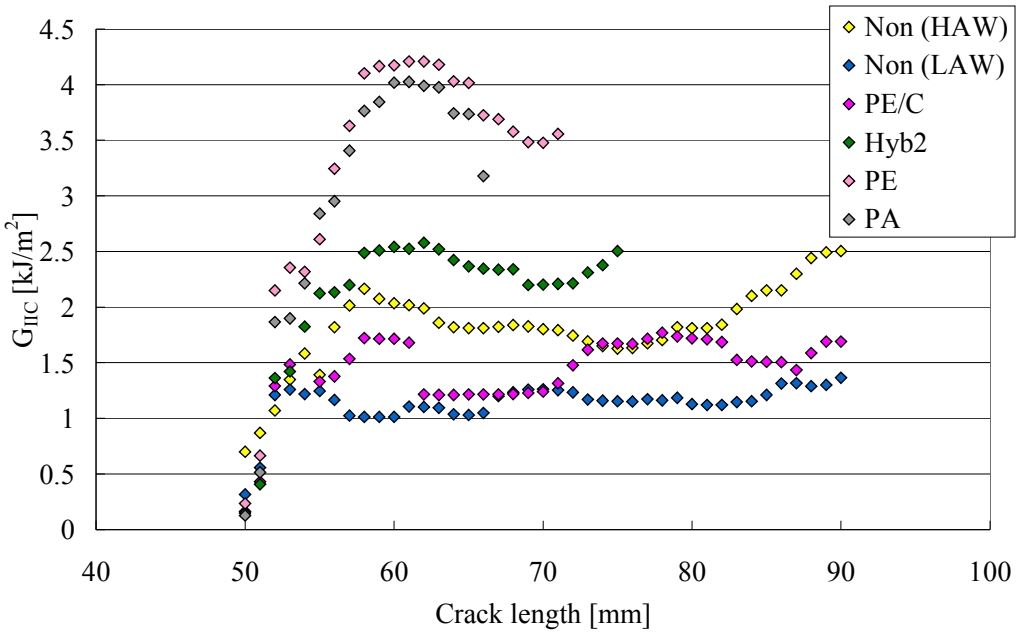

Figure 4.12 R-curves for non-interleaved and interleaved plain weave fabric specimens with epoxy2 system

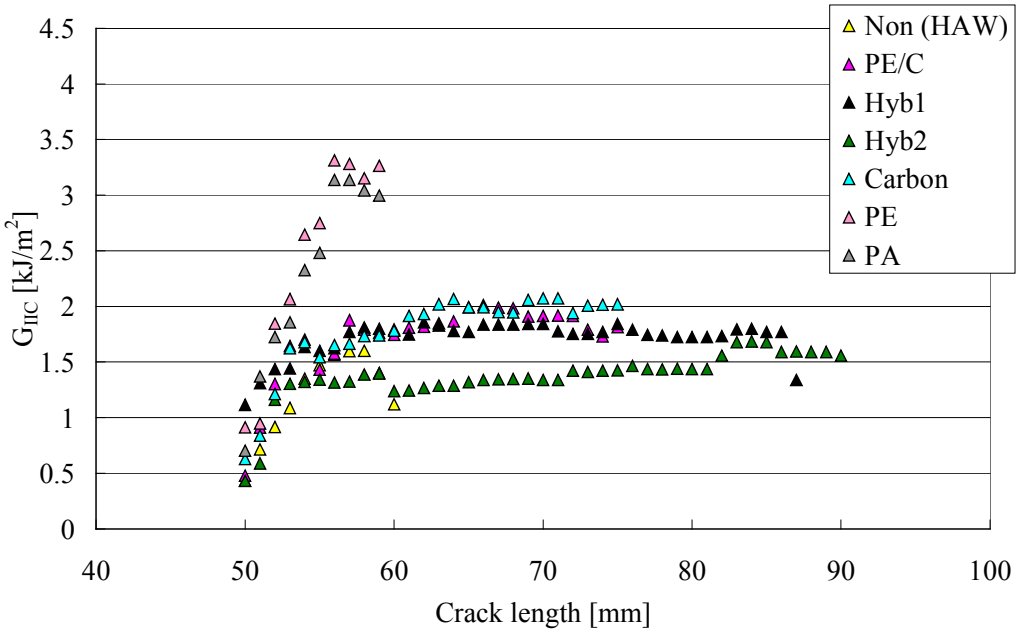

Figure 4.13 R-curves for non-interleaved and interleaved plain weave fabric specimens with vinyl ester system

4.3.3 Mode-II Critical Energy Release Rate (G_{IIC})

4.3.3.1 5-harness Satin Weave Fabric Specimens

The G_{II} initiation and propagation values for the satin weave Ep1 system specimens are summarised in Table 4.1 with the standard deviations (S.D.) and coefficient of variations (C.V.). Figure 4.14 plots diagram of $G_{IIC\text{-}NL}$, $G_{IIC\text{-}5\%/MAX}$, and $G_{II\text{-}prop}$ values. The tendency of the G_{II} initial values is similar to the Mode-I critical energy release rate (see in Figure 3.22). The Hyb2 and PE interleaved specimens show significantly high initiation values. In particular, the $G_{IC\text{-}5\%/MAX}$ value of the Hyb2 veil interleaved case is significantly large, about 4.87kJ/m^2. However, the carbon and PA veil interleaved laminates show lower G_{II} values than the non-interleaved specimen in the same way as the DCB results. The S.D., except for the Hyb2 and PE veil interleaved sample, is around 0.11 to 0.25. The S.D. in the Hyb2 and PE veil interleaved material have approximately 0.36 and 0.65, respectively.

The $G_{II\text{-}prop}$ values exhibit a similar tendency to the initial values, except for the PA interleaved specimen. The Hyb2 and PE veil interleaved specimens show significantly higher $G_{II\text{-}prop}$ values, 5.27 and 4.76kJ/m^2 respectively. The propagation value for the carbon veil interleaved laminate is still lower than the control, nearly 2.04kJ/m^2. The PA veil interleaved specimen has almost the same value as the non-interleaved sample, approximately 2.76kJ/m^2. The S.D. for the control, Hyb1, carbon, and PA veil interleaved materials is moderate with values ranging from 0.14 to 0.26. The Hyb2 and PE interleaved specimens, however, have quite large values, approximately 0.39 and 0.69 respectively.

Table 4.1 Mode-II critical strain energy release rate values of 5-harness satin weave epoxy1 system specimens with/without interleaf veils

Interleaf	G_{II} [kJ/m^2]	S.D.	C.V.	
Non-interleaved	2.43	0.153	0.063	$G_{IIC\text{-}NL}$
	2.74	0.175	0.060	$G_{IIC\text{-}5\%/MAX}$
	2.75	0.138	0.050	$G_{II\text{-}Prop}$
Hyb1	2.74	0.246	0.090	$G_{IIC\text{-}NL}$
	3.24	0.219	0.070	$G_{IIC\text{-}5\%/MAX}$
	3.19	0.165	0.052	$G_{II\text{-}Prop}$
Hyb2	3.14	0.360	0.114	$G_{IIC\text{-}NL}$
	4.87	0.420	0.090	$G_{IIC\text{-}5\%/MAX}$
	5.27	0.393	0.075	$G_{II\text{-}Prop}$
Carbon	1.93	0.241	0.125	$G_{IIC\text{-}NL}$
	2.18	0.241	0.110	$G_{IIC\text{-}5\%/MAX}$
	2.04	0.183	0.089	$G_{II\text{-}Prop}$
PE	3.60	0.653	0.181	$G_{IIC\text{-}NL}$
	4.31	0.632	0.150	$G_{IIC\text{-}5\%/MAX}$
	4.76	0.694	0.146	$G_{II\text{-}Prop}$
PA	1.41	0.107	0.076	$G_{IIC\text{-}NL}$
	1.95	0.191	0.100	$G_{IIC\text{-}5\%/MAX}$
	2.76	0.256	0.093	$G_{II\text{-}Prop}$

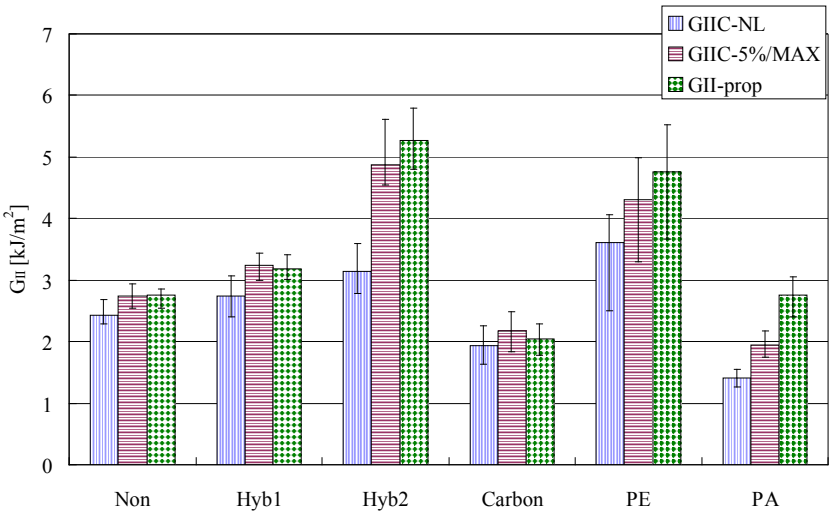

Figure 4.14 Comparison of Mode-II initiation and propagation energy release rate values for 5-harness satin weave epoxy1 system specimens with/without interleaf veils

The G_{IIC} initiation values for the VE system specimens are shown in Table 4.2 with S.D. and C.V. values. Figure 4.15 is a diagram of initiation and propagation values. The G_{II} initial value for the non-interleaved laminate is quite low, about 0.45kJ/m^2. On the other hand, the G_{II} initial values of the PE and PA veil interleaved specimens are about 3.11 and 2.53kJ/m^2, respectively. Both interleaved samples have higher S.D. values than the control. In particular, the PE veil interleaved laminates are approximately 0.46 for the initial value.

For the propagation value, the non-interleaved specimen still has a low $G_{II\text{-}prop}$ value, approximately 0.7kJ/m^2. The $G_{II\text{-}prop}$ of the PE and PA veil interleaved laminates increases slightly from the G_{II} initial values, 3.76 and 3.20kJ/m^2 respectively. Compared to the control, the PE and PA veil interleaved cases have significantly high G_{II} values. However, the Mode-II interlaminar toughness values for the VE system are lower than the Ep1 system. The S.D. value of the non-interleaved specimen is quite small and test results have good repeatability. On the other hand, the S.D. of both interleaved samples are moderate, approximately 0.28 (PE) and 0.19 (PA) respectively.

Table 4.2 Mode-II critical strain energy release rate values of 5-harness satin weave vinyl ester system specimens with/without interleaf veils

Interleaf	G_{II} [kJ/m^2]	S.D.	C.V.	
Non-interleaved	0.45	0.034	0.076	$G_{IIC\text{-}NL}$
	0.61	0.040	0.066	$G_{IIC\text{-}5\%/MAX}$
	0.73	0.034	0.047	$G_{II\text{-}Prop}$
PE	3.11	0.459	0.148	$G_{IIC\text{-}NL}$
	3.49	0.464	0.124	$G_{IIC\text{-}5\%/MAX}$
	3.76	0.280	0.074	$G_{II\text{-}Prop}$
PA	2.53	0.256	0.101	$G_{IIC\text{-}NL}$
	2.84	0.264	0.093	$G_{IIC\text{-}5\%/MAX}$
	3.20	0.186	0.058	$G_{II\text{-}Prop}$

*: Hyb1 and 2, and carbon veil interleaved specimens were not examined.

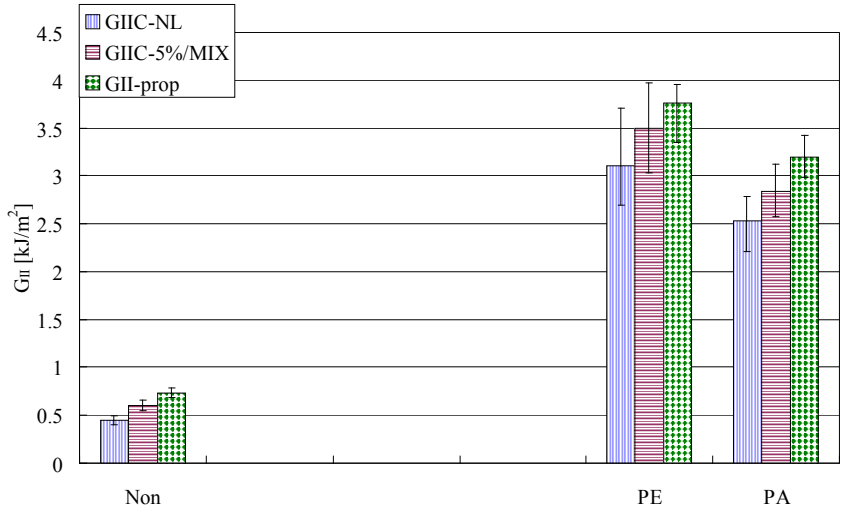

Figure 4.15 Comparison of Mode-II initiation and propagation energy release rate values for 5-harness satin weave vinyl ester system specimens with/without interleaf veils

4.3.3.2 Unidirectional Fabric Specimens

Table 4.3 shows the G_{II} initiation and propagation values with the S.D. and C.V. values for unidirectional fabric Ep1 system. Figure 4.16 illustrates diagram of $G_{IIC\text{-}NL}$, $G_{IIC\text{-}5\%/MAX}$, and $G_{II\text{-}prop}$ values. The G_{II} initial values for all specimens are similar tendency to the satin weave Ep1 system laminates. The Hyb2 interleaved specimen has the highest $G_{II\text{-}NL}$ initial values, approximately 3.06kJ/m^2. The Hyb1 and PE veil interleaved composites have moderately high $G_{IIC\text{-}NL}$ values, approximately 1.97 and 2.29kJ/m^2 respectively. The carbon and PA veil interleaved specimens are slightly higher than the control, approximately 1.9kJ/m^2. The tendency of the $G_{IC\text{-}5\%/MAX}$ values is similar to that of the $G_{IIC\text{-}NL}$ values. The S.D. values of the non-interleaved, Hyb1, carbon, and PA veil interleaved specimens are not large, ranging from 0.09 to 0.18. Those of the Hyb2 and PE veil interleaved specimens, however, are higher than the other specimens. In particular, that of the Hyb2 interleaved sample is quite high, nearly 0.59.

The $G_{II\text{-}prop}$ values of the Hyb2 veil interleaved specimen are increased significantly, about 5.78kJ/m^2. Surprisingly, the PA veil interleaved laminate has a significantly high $G_{II\text{-}prop}$ value, approximately 4.73kJ/m^2. The Hyb1 and PE veil interleaved materials have almost the same value, 3.79 and 3.74kJ/m^2 respectively. Even the carbon veil interleaved specimen is slightly higher than the non-interleaved case, about 2.74kJ/m^2. In the UD composites, the Mode-II interlaminar toughness is improved for all interleaved samples, unlike the satin weave cases. The S.D. values of both hybrid veil interleaved samples are quite larger than the other specimens, approximately 0.42 (Hyb1) and 0.56 (Hyb2). The carbon, PE and PA veil interleaved specimens are moderate S.D. values, around 0.16 to 0.28.

Table 4.3 Mode-II critical strain energy release rate values of unidirectional fabric epoxy1 system specimens with/without interleaf veils

Interleaf	G_{II} [kJ/m^2]	S.D.	C.V.	
Non-interleaved	1.47	0.155	0.106	$G_{IIC\text{-}NL}$
	1.80	0.332	0.185	$G_{IIC\text{-}5\%/MAX}$
	2.53	0.206	0.081	$G_{II\text{-}Prop}$
Hyb1	1.97	0.155	0.079	$G_{IIC\text{-}NL}$
	2.81	0.324	0.115	$G_{IIC\text{-}5\%/MAX}$
	3.79	0.420	0.111	$G_{II\text{-}Prop}$
Hyb2	3.06	0.592	0.193	$G_{IIC\text{-}NL}$
	4.45	0.453	0.102	$G_{IIC\text{-}5\%/MAX}$
	5.78	0.561	0.097	$G_{II\text{-}Prop}$
Carbon	1.90	0.179	0.094	$G_{IIC\text{-}NL}$
	2.23	0.250	0.112	$G_{IIC\text{-}5\%/MAX}$
	2.74	0.174	0.063	$G_{II\text{-}Prop}$
PE	2.29	0.269	0.117	$G_{IIC\text{-}NL}$
	2.93	0.236	0.080	$G_{IIC\text{-}5\%/MAX}$
	3.74	0.162	0.043	$G_{II\text{-}Prop}$
PA	1.85	0.086	0.046	$G_{IIC\text{-}NL}$
	2.95	0.247	0.084	$G_{IIC\text{-}5\%/MAX}$
	4.73	0.282	0.060	$G_{II\text{-}Prop}$

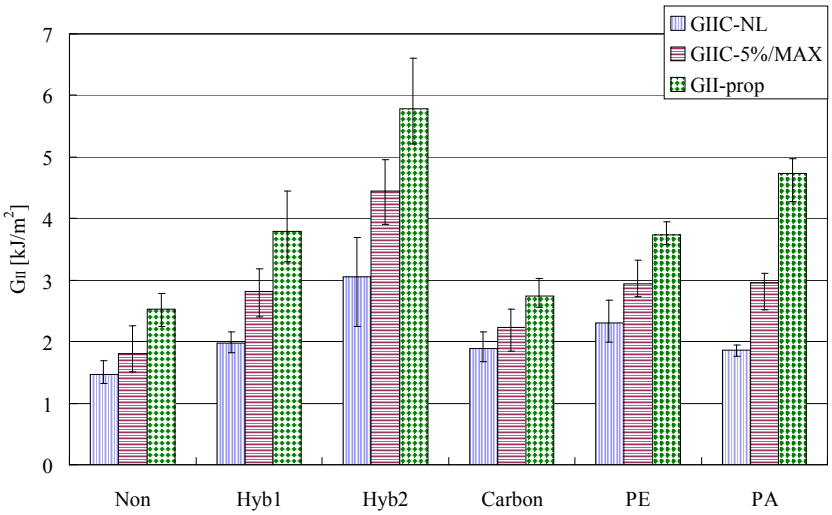

Figure 4.16 Comparison of Mode-II initiation and propagation energy release rate values for unidirectional fabric epoxy1 system specimens with/without interleaf veils

The G_{IIC} initiation and propagation values for the UD fabric VE system specimens are indicated in Table 4.4 and Figure 4.17 with the S.D. and C.V. values. The G_{II} initial values for all specimens are overall lower than the Ep1 system samples. The differences in the initial values between each interleaved specimen are quite small. The range of the $G_{IIC\text{-}NL}$ values for all specimens is 0.74 to 1.03kJ/m^2. The $G_{IIC\text{-}5\%/MAX}$ values, on the other hand, varied more widely than the $G_{IIC\text{-}NL}$ values, in a range from 0.88 to 1.42kJ/m^2. The S.D. values of all specimens are quite lower than the Ep1 system, and these specimens have good repeatability.

The propagation values for all specimens show a similar tendency to the initial values. The $G_{II\text{-}prop}$ value of the non-interleaved laminate is approximately 1.36kJ/m^2. Both hybrid and carbon veil interleaved specimens have similar $G_{II\text{-}prop}$ values, about 1.54kJ/m^2 (Hyb1), 1.53kJ/m^2 (Hyb2), and 1.43kJ/m^2 (carbon) respectively. The PE and PA veil interleaved specimens have higher $G_{II\text{-}prop}$ values than the other interleaved cases, approximately 1.98 and 2.14kJ/m^2, respectively. The Mode-II propagation energy release rates are also lower than the Ep1 system. The S.D. for all specimens is quite small. Hence these results seem to be reliable.

Table 4.4 Mode-II critical strain energy release rate values of unidirectional fabric vinyl ester system specimens with/without interleaf veils

Interleaf	G_{II} [kJ/m^2]	S.D.	C.V.	
Non-interleaved	0.74	0.090	0.122	$G_{IIC\text{-}NL}$
	0.88	0.101	0.115	$G_{IIC\text{-}5\%/MAX}$
	1.36	0.216	0.159	$G_{II\text{-}Prop}$
Hyb1	0.93	0.081	0.087	$G_{IIC\text{-}NL}$
	1.13	0.085	0.075	$G_{IIC\text{-}5\%/MAX}$
	1.54	0.035	0.023	$G_{II\text{-}Prop}$
Hyb2	0.83	0.016	0.020	$G_{IIC\text{-}NL}$
	1.08	0.058	0.054	$G_{IIC\text{-}5\%/MAX}$
	1.53	0.055	0.036	$G_{II\text{-}Prop}$
Carbon	0.92	0.051	0.055	$G_{IIC\text{-}NL}$
	1.12	0.089	0.079	$G_{IIC\text{-}5\%/MAX}$
	1.43	0.065	0.046	$G_{II\text{-}Prop}$
PE	1.03	0.111	0.108	$G_{IIC\text{-}NL}$
	1.42	0.055	0.039	$G_{IIC\text{-}5\%/MAX}$
	1.98	0.138	0.070	$G_{II\text{-}Prop}$
PA	0.84	0.091	0.108	$G_{IIC\text{-}NL}$
	1.23	0.103	0.084	$G_{IIC\text{-}5\%/MAX}$
	2.14	0.276	0.129	$G_{II\text{-}Prop}$

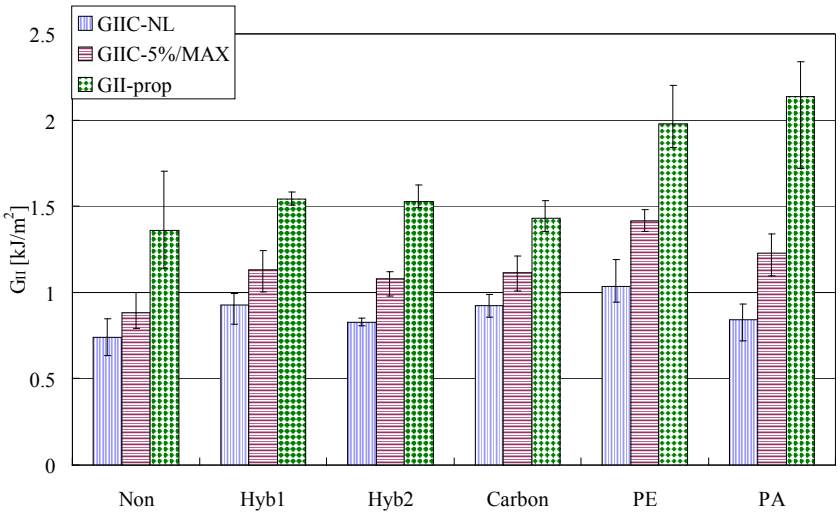

Figure 4.17 Comparison of Mode-II initiation and propagation energy release rate values for unidirectional fabric vinyl ester system specimens with/without interleaf veils

4.3.3.3 Plain Weave Fabric Specimens

Table 4.5 and Figure 4.18 show the G_{II} initiation and propagation values with the S.D. and C.V. values for the Ep2 system specimens. For the non-interleaved samples, the $G_{IIC\text{-}NL}$ values of the HAW and LAW laminates are about 1.66 and 1.54kJ/m^2, respectively. The HAW specimen has slightly higher G_{IC} value than the LAW case. The PE/C veil interleaved laminates have slightly lower $G_{IIC\text{-}NL}$ values than the control, around 1.51kJ/m^2. The $G_{IIC\text{-}NL}$ value in the Hyb2 veil interleaved composite, on the other hand, is slightly higher than the non-interleaved case, nearly 1.72kJ/m^2. The PE and PA veil interleaved specimens have higher G_{II} initial values than the other interleaved samples, 2.18 and 2.78kJ/m^2 respectively. In particular, the Mode-II initial property for the PA veil interleaved laminate has the highest G_{IIC} value. The S.D. values for all specimens, except for the Hyb2 veil interleaved sample, are large. In particular, the S.D. values of the PE and PA veil interleaved composites are around 0.5.

The $G_{II\text{-}prop}$ values exhibit almost the same trends as the G_{II} initial values. The non-interleaved and PE/C veil interleaved specimens are the same values, about 1.61kJ/m^2. The Hyb2 veil interleaved specimen is slightly higher than the control and PE/C veil interleaved cases around 2.15kJ/m^2. The $G_{II\text{-}prop}$ value of the PE veil interleaved laminate is nearly 3.05kJ/m^2. The PA veil interleaved specimen has the highest propagation value, approximately 3.71kJ/m^2. The $G_{II\text{-}prop}$ values of interleaved

specimens are substantially increased from the initial values, except for the PE/C veil interleaved sample. For the S.D. values, all specimens have deviations between 0.25 and 0.30, except for the PE veil interleaved material. The S.D. value of the PE veil interleaved composite is the largest, around 0.70.

Table 4.5 Mode-II critical strain energy release rate values of plain weave epoxy2 system specimens with/without interleaf veils

Interleaf	G_{II} [kJ/m^2]	S.D.	C.V.	
Non-interleaved (HAW)	1.66	0.214	0.129	$G_{IIC\text{-}NL}$
	1.91	0.235	0.123	$G_{IIC\text{-}5\%/MAX}$
	1.66	0.339	0.204	$G_{II\text{-}Prop}$
Non-interleaved (LAW)	1.54	0.223	0.144	$G_{IIC\text{-}NL}$
	4.59	0.475	0.299	$G_{IIC\text{-}5\%/MAX}$
	1.56	0.199	0.128	$G_{II\text{-}Prop}$
PE/C	1.51	0.376	0.249	$G_{IIC\text{-}NL}$
	1.81	0.366	0.202	$G_{IIC\text{-}5\%/MAX}$
	1.61	0.262	0.163	$G_{II\text{-}Prop}$
Hyb2	1.72	0.101	0.059	$G_{IIC\text{-}NL}$
	2.27	0.161	0.071	$G_{IIC\text{-}5\%/MAX}$
	2.15	0.302	0.141	$G_{II\text{-}Prop}$
PE	2.18	0.505	0.212	$G_{IIC\text{-}NL}$
	3.12	0.615	0.197	$G_{IIC\text{-}5\%/MAX}$
	3.05	0.698	0.229	$G_{II\text{-}Prop}$
PA	2.78	0.526	0.189	$G_{IIC\text{-}NL}$
	3.48	0.100	0.029	$G_{IIC\text{-}5\%/MAX}$
	3.71	0.254	0.068	$G_{II\text{-}Prop}$

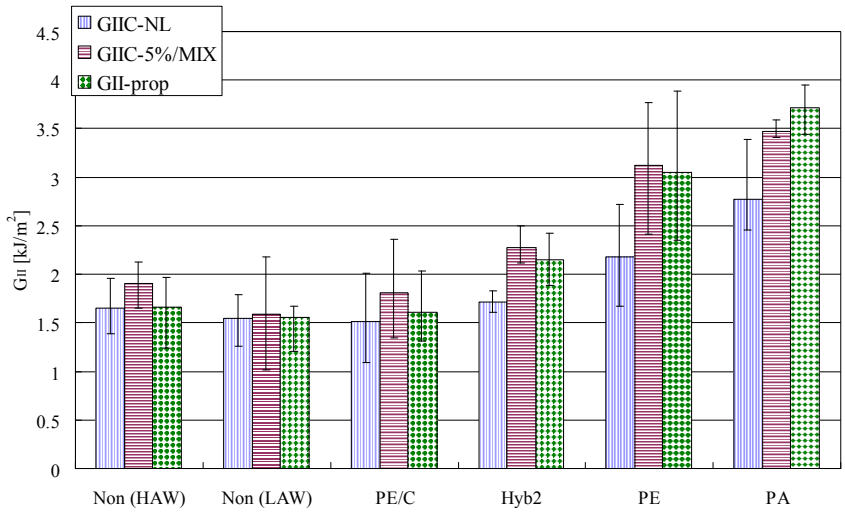

Figure 4.18 Comparison of Mode-II initiation and propagation energy release rate values for plain weave epoxy2 system specimens with/without interleaf veils

The G_{IIC} initiation and propagation values for the VE system composites are shown in Table 4.6 with the S.D. and C.V. values. Figure 4.19 plots $G_{IIC\text{-}NL}$, $G_{IIC\text{-}5\%/MAX}$, and $G_{II\text{-}prop}$ values. The G_{II} initial values of the non-interleaved, PE/C, hybrid, and carbon veil interleaved specimens are similar values, range from 1.47 to 1.78kJ/m^2. The PE and PA veil interleaved laminates have quite higher G_{II} initial values than the other interleaved cases, 2.48 and 2.69kJ/m^2 respectively. Some of these specimens exhibited bending fracture when 4ENF tests were carried out. Some data was of a too large a value and therefore omitted. The S.D. values for the non-interleaved, PE/C, hybrid, and carbon veil interleaved specimens are not such a large value. On the other hand, the other two interleaved composites have significantly large S.D. values. For these specimens, the crack growth rate was quite slow and bending failure occurred at an early stage. Consequently, some results would not be reliable.

The $G_{II\text{-}prop}$ values for all specimens are slightly increased only. The reason for this seems to be that the gap between $G_{IIC\text{-}NL}$ and $G_{II\text{-}prop}$ values are quite small. The propagation value of the non-interleaved specimen is 2.11kJ/m^2. Both hybrid veil interleaved laminates have slightly lower $G_{II\text{-}prop}$ values than the control, about 1.7kJ/m^2. The PE/C and carbon veil interleaved samples have marginally higher propagation value than the non-interleaved case, nearly 2.03 to 2.30kJ/m^2. The $G_{II\text{-}prop}$ values of the PE and PA veil interleaved composites are approximately 3.38 and 3.63kJ/m^2,

respectively. The $G_{II\text{-}prop}$ values for the VE system interleaved composites are similar to the Ep2 system cases, except for the PE veil interleaved sample. The PE interleaved samples have slightly higher $G_{II\text{-}prop}$ values than the Ep2 system cases. The tendency of the S.D. is similar to the initial results. The Hyb1 veil interleaved laminate has the smallest S.D. value, 0.12. The control and other interleaved specimens, except for the PA veil interleaved case, have similar S.D. values, range from 0.26 to 0.31. The deviation in the PA veil interleaved sample is the highest, approximately 0.51.

Table 4.6 Mode-II critical strain energy release rate values of plain weave vinyl ester system specimens with/without interleaf veils

Interleaf	G_{II} [kJ/m^2]	S.D.	C.V.	
Non-interleaved (HAW)	1.78	0.326	0.183	$G_{IIC\text{-}NL}$
	2.07	0.388	0.188	$G_{IIC\text{-}5\%/MAX}$
	2.11	0.310	0.147	$G_{II\text{-}Prop}$
PE/C	1.66	0.257	0.155	$G_{IIC\text{-}NL}$
	1.92	0.308	0.161	$G_{IIC\text{-}5\%/MAX}$
	2.03	0.270	0.133	$G_{II\text{-}Prop}$
Hyb1	1.57	0.117	0.074	$G_{IIC\text{-}NL}$
	1.72	0.142	0.083	$G_{IIC\text{-}5\%/MAX}$
	1.70	0.122	0.072	$G_{II\text{-}Prop}$
Hyb2	1.47	0.285	0.194	$G_{IIC\text{-}NL}$
	1.56	0.343	0.219	$G_{IIC\text{-}5\%/MAX}$
	1.66	0.275	0.165	$G_{II\text{-}Prop}$
Carbon	1.61	0.131	0.081	$G_{IIC\text{-}NL}$
	1.85	0.200	0.108	$G_{IIC\text{-}5\%/MAX}$
	2.30	0.258	0.112	$G_{II\text{-}Prop}$
PE	2.48	0.298	0.120	$G_{IIC\text{-}NL}$
	2.97	0.211	0.071	$G_{IIC\text{-}5\%/MAX}$
	3.38	0.283	0.084	$G_{II\text{-}Prop}$
PA	2.69	0.568	0.212	$G_{IIC\text{-}NL}$
	2.93	0.904	0.308	$G_{IIC\text{-}5\%/MAX}$
	3.63	0.507	0.140	$G_{II\text{-}Prop}$

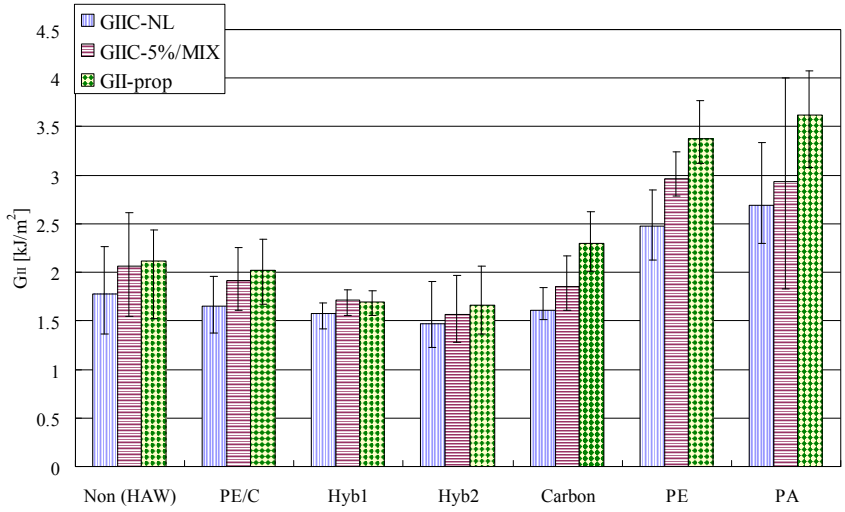

Figure 4.19 Comparison of Mode-II initiation and propagation energy release rate values for plain weave vinyl ester system specimens with/without interleaf veils

In this section, the Mode-II energy release rates for the non-woven veil interleaved specimens are mentioned. The general trend of 5-harness satin Ep1 system is similar to that of the Mode-I interlaminar toughness. The Hyb2 and PE veil interleaved specimens show a good improvement of the Mode-II interlaminar toughness, in particular propagation values. In contrast, the carbon and PA veil interleaved laminates are degraded in Mode-II interlaminar toughness in the same way as the Mode-I interlaminar toughness. For the VE system, both the PE and PA veil interleaved cases show significantly increased toughness compared with the control.

The UD fabric Ep1 system specimens are that the interleaved are improved by the interleaf veils, even the carbon veil interleaved case. On the other hand, the Mode-II interlaminar toughness for the VE system is a small overall. Moreover, the difference in the G_{II} values between each interleaved specimen is quite small.

In the plain weave Ep2 system, the G_{II} values for all specimens are lower than the Ep1 system cases. Whilst the Mode-II interlaminar toughness in the PE and PA veils is greatly improved, those in the PE/C and Hyb2 veils are only slightly increased. The tendency of the G_{II} values in the VE system is similar to the Ep2 system composites. The tendency of the Mode-II interlaminar toughness in the UD fabric VE system is

completely different from that of the Mode-I interlaminar toughness.

Figure 4.20 illustrates the relationship of the Mode-II initial energy release rate with the fabric and resin system. The G_{IIC} values in the control are affected strongly by both factors, fabric and resin. The satin weave Ep1 system laminate has the highest G_{IIC} value in all fabric and resin systems. In contrast, the satin weave VE system specimen has the lowest Mode-II initial toughness. For the unidirectional fabric composite, the G_{IIC} value in the Ep1 system is the lowest of all Ep system cases. The VE system specimen also has a low G_{IIC} value. It is thought that surface of the UD fabric is smooth, and the crack can propagate more easily than in the woven fabrics. In the plain weave fabric system, the fabric surface is coarser than the other fabric. The initial value, therefore, is moderately high. Moreover, the areal weight of the fabric in the Ep2 system affects slightly the initial value. In the plain weave specimens, some test samples suffered bending fracture during 4ENF test. Therefore, some samples did not give adequate data.

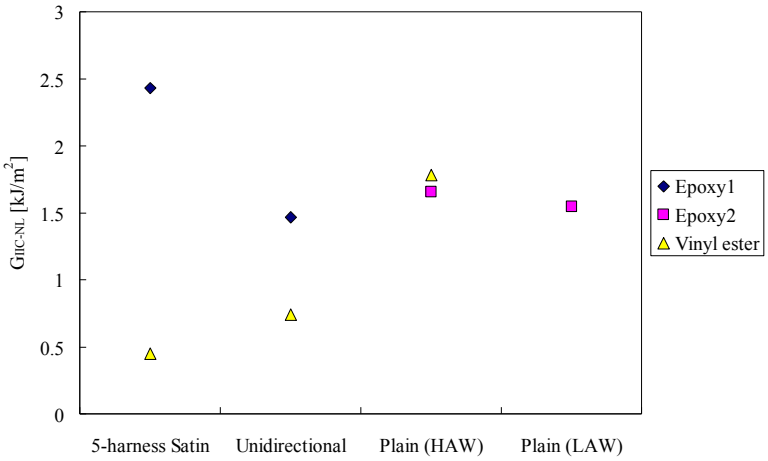

Figure 4.20 Relationship of Mode-II initial energy release rate between fabric and resin system for non-interleaved specimens

4.4 Discussion

4.4.1 Mechanisms of Mode-II Interlaminar Toughness for Non-Interleaved Specimens

Figure 4.21 shows SEM pictures of fracture surface for the non-interleaved specimens. For the satin weave Ep1 system laminate, the fracture surface is covered with the matrix on the both fracture surfaces. It is found that there are many hackles on

the surface, as illustrated in Figure 4.21 (a). These hackles would contribute to improving the Mode-II initial value [19]. The crack propagation tends to pass through the matrix region, same as the Mode-I fracture behaviour. It is thought that the adhesion between woven fabric and matrix is good. The crack, therefore, can propagate only in the matrix area. In the VE system composite, the matrix and exposed woven fibres appear on the fracture surface, as illustrated in Figure 4.21 (b). The exposed woven fibres are unravelled. The hackles are not seen on the surface. The adhesion between the carbon woven fabric and VE resin may not be as good as the Ep1 resin system. Consequently, the woven fibres are unravelled on the surface. This poor adhesion of the VE resin would lead to the crack propagating easily. Therefore, the initial values are significantly smaller than the Ep1 case.

The fracture surface in the UD fabric Ep1 system laminate is similar to the satin weave Ep1 system specimens. Both fracture surfaces are covered with the matrix. Although the fracture surface reveals trace of the UD fibres, they are not unravelled on the surface, as shown in Figure 4.21 (c). It can be seen that the hackles appear on the fracture surface. It seems that these hackles are less than the satin weave samples. Hence, the Mode-II interlaminar toughness may be low, compared with the satin weave case. The fracture surface in the VE system is similar to the satin with VE system. The UD carbon fibres are exposed and unravelled (see in Figure 4.21 (d)). However, these frayed fabrics would not work as fibre-bridging reinforcements significantly. In the UD fabric VE system laminate, the poor adhesion and flat surface would lead to be poor G_{IIC} values, compared with the satin weave materials. Therefore, the Mode-II interlaminar toughness could not improve considerably.

In the plain weave Ep2 system laminate, the fracture surface is covered with the matrix, as shown in Figure 4.21 (e). The woven fibres are not unravelled completely. In Ep2 system, the hackles also appear on the fracture surface. Moreover, the fracture surface seems to be coarser than samples made with the other fabrics. On the other hand, the fracture surface for the VE system is the same as the 5-harness satin weave cases. Some of woven fibres are frayed over a partial area, as shown in Figure 4.21 (f). These fibres would work for bridging during crack propagation.

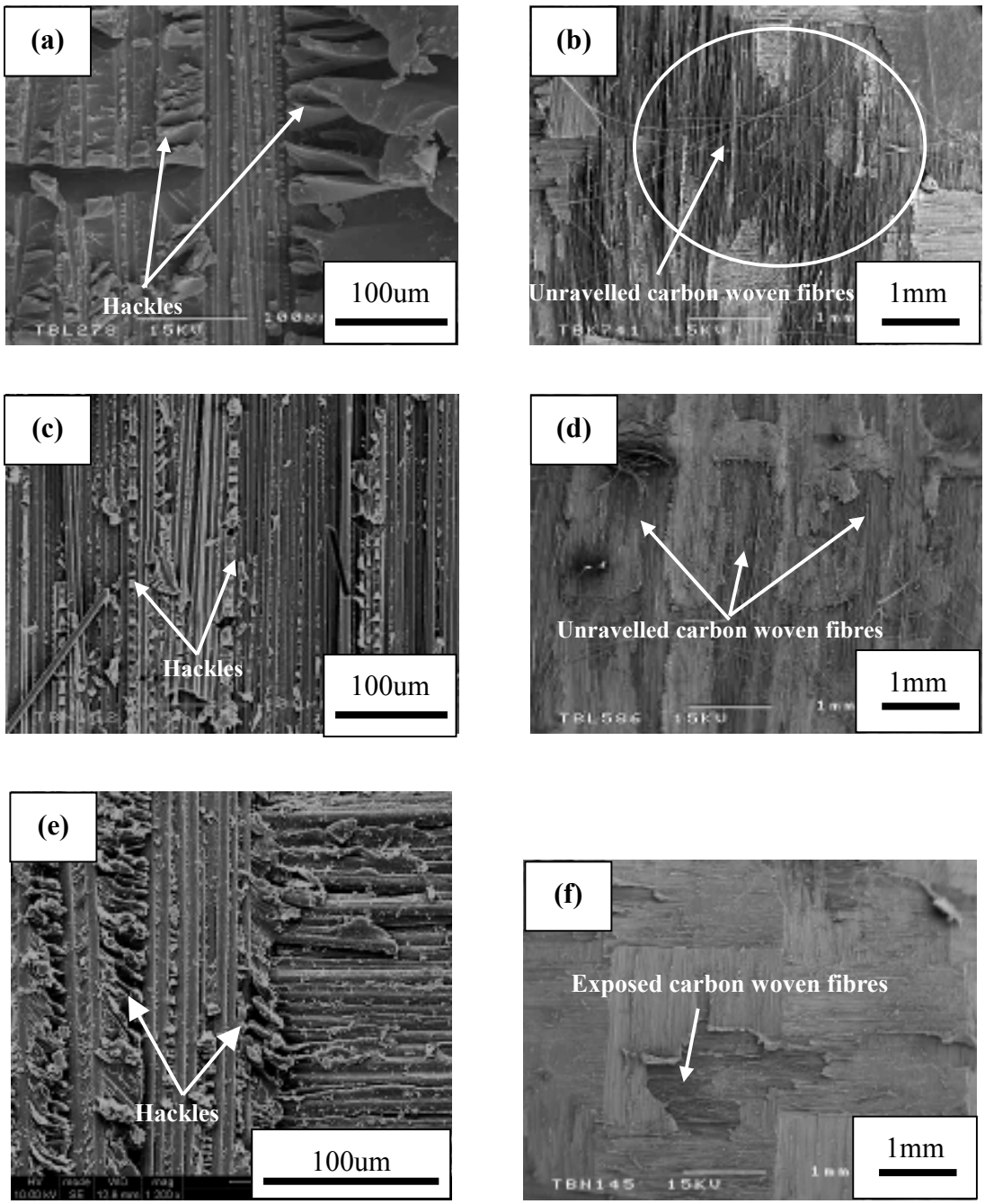

Figure 4.21 Micrographs of fracture surface taken by SEM for non-interleaved specimens: (a) Satin weave Ep1 system, (b) Satin weave VE system, (c) UD fabric Ep1 system, (d) UD fabric VE system, (e) Plain weave Ep2 system, (f) Plain weave VE system

The cross-sections taken by the optical microscope are illustrated in Figure 4.22. From Figure 4.22 (a), it can be seen that the crack path is not straight, unlike the DCB

tested specimen (see in Figure 3.30 (a)). The crack propagates in the matrix region. For the VE system, the crack would propagate along one side weave surface and then some of the carbon woven fibres seem to work as fibre-bridging. The fracture surface is almost the same as the Mode-I fracture surface (see in Figure 3.29(b)). It can be seen that the woven fibres are unravelled, as shown in Figure 4.22 (b). The crack paths in UD specimens with both resin systems are straight, as shown in Figure 4.22 (c) and (d). Therefore, it is thought that the crack growth would be easier than the satin weave case. The crack paths in the plain weave with both composites of either resin are not straight in the interlaminar region, as shown in Figure 4.22 (e) and (f). This is because the surface of the plain weave is rougher than that of the 5-harness satin weave and UD fabric samples. The fibre-bridging does not contribute to the improvement of the Mode-II interlaminar toughness unlike the Mode-I interlaminar toughness. The behaviour of the crack propagation in the Ep2 system laminate is almost the same as the satin weave Ep1 system case. Compared to the areal weight of the fabrics, the HAW specimen has higher G_{IIC} values than the LAW sample. In the Mode-II interlaminar toughness, surface of the fabric would influence crack growth strongly. The non-interleaved specimen in the VE system has a crack path that is a mixture of intralaminar and interlaminar regions. The crack propagation in the plain weave VE system laminate was significantly slow. Therefore, bending fracture was initiated at an early stage. It is thought that the roughness of the fabric surface is a cause.

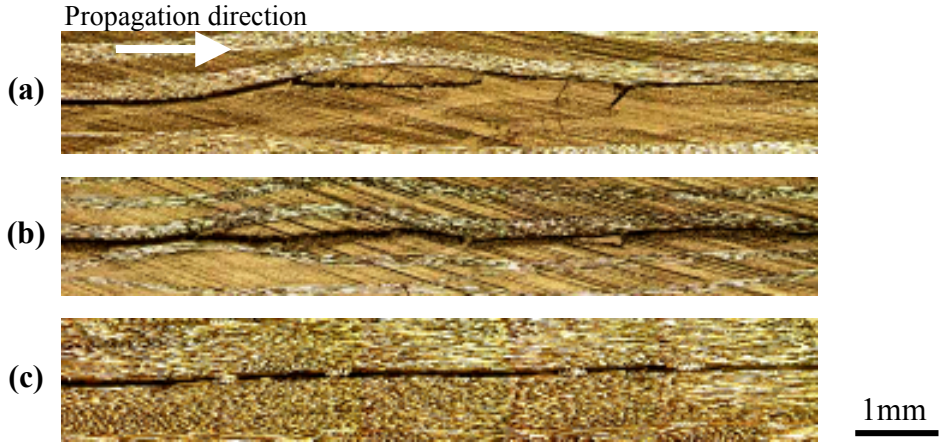

Figure 4.22 Micrographs of cross-section taken by optical microscope for non-interleaved specimens: (a) Satin weave Ep1 system, (b) Satin weave VE system, (c) UD fabric Ep1 system, (d) UD fabric VE system, (e) Plain weave Ep2 system, (f) Plain weave VE system

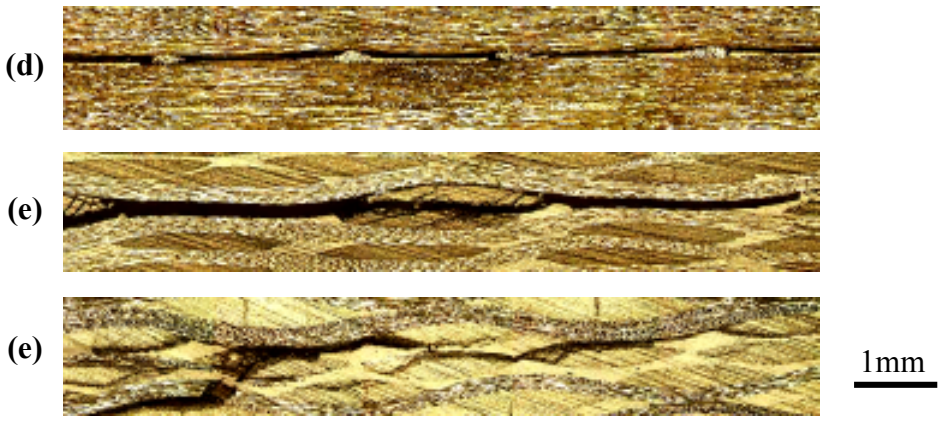

Figure 4.22 (*Continued*)

4.4.2 Mechanisms of Mode-II Interlaminar Toughness for Interleaved Specimens

4.4.2.1 5-harness Satin Weave Fabric Specimens

Figure 4.23 shows SEM pictures for the interleaved Ep1 system specimens examined after 4ENF tests. The veil fibres in the Hyb1 veil interleaved laminate are found on the fracture surface and pulled out (see in Figure 4.23 (a)). The satin weave fibres, however, are barely unravelled, and the surface condition is similar to the non-interleaved sample. These pulled out Hyb1 veil fibres may contribute to the suppression of the crack propagation. The Hyb2 veil fibres adhere widely on the fracture surface, as shown in Figure 4.23 (b). When the crack propagated, the Hyb2 veil fibres would be pulled out from matrix and work to provide fibre-bridge in the same way as the Hyb1 veil fibres. The Hyb2 veil fibres, on the other hand, are pulled out more than the Hyb1 veil fibres. The Hyb2 veil interleaved laminate, therefore, possesses better Mode-II interlaminar toughness than the Hyb1 veil interleaved case. In the carbon veil interleaved composite, it can be found that there are many scratches on the surface, as shown in Figure 4.23 (c). The carbon veil fibres, however, cannot be found on the fracture surface. It is thought that the carbon veil fibres are embedded in the matrix completely. The fracture surface with the PE veil interleaved specimens are covered with the matrix, as illustrated in Figure 4.23 (d). Moreover, the PE veil fibres are found to pull out from the matrix. The pulled out veil fibres are significantly more numerous than from both hybrid veils. When the crack grew during the 4ENF test, the PE veil fibres pulled out from the matrix and would have worked to provide fibre-bridging. The fracture surface in the PA veil interleaved laminate is covered with the matrix resin, as shown in Figure 4.23 (e). It can be seen that the PA veil fibres are adhered to the matrix. It seems that the crack propagates in the 4ENF test in the PA veil region, unlike the

DCB tested specimens.

Figure 4.24 shows micrographs of the cross-section taken by the optical microscope for the interleaved composites. Both hybrid veils show similar behaviour. Some veil fibres are pulled out on the surface, as shown in Figure 4.24 (a). However, many veil fibres are embedded in the matrix. Compared to the Hyb1 veil interleaved sample, there seem to be many Hyb2 veil fibres pulled out from the matrix. Therefore the Hyb2 veil fibres can contribute to a significant improvement of the Mode-II interlaminar toughness. For the carbon veil interleaved case, it can be seen that the veil fibres are embedded in the matrix completely, as shown in Figure 4.24 (b). Therefore, the carbon veil cannot contribute to improvement of the Mode-II interlaminar toughness, same as the Mode-I interlaminar toughness. Moreover, the existence of the carbon veils may reduce the resin rich region and growing plastic zone. Consequently, the toughness is less than that of the non-interleaved material. Many PE veil fibres are pulled out on the fracture surface widely, as shown in Figure 4.24 (c). The PE veil interleaved specimens can realise significant improvement of the Mode-II interlaminar toughness, compared with the hybrid veil interleaved laminates. Because pulled out veil fibres are much more numerous and these fibres could contribute to high G_{IIC} values. For the PA veil, it can be found that the crack goes through in the veil fibre, as shown in Figure 4.24 (d). It is thought that the crack propagation would be suppressed by deformation or elongation of the PA veil fibres.

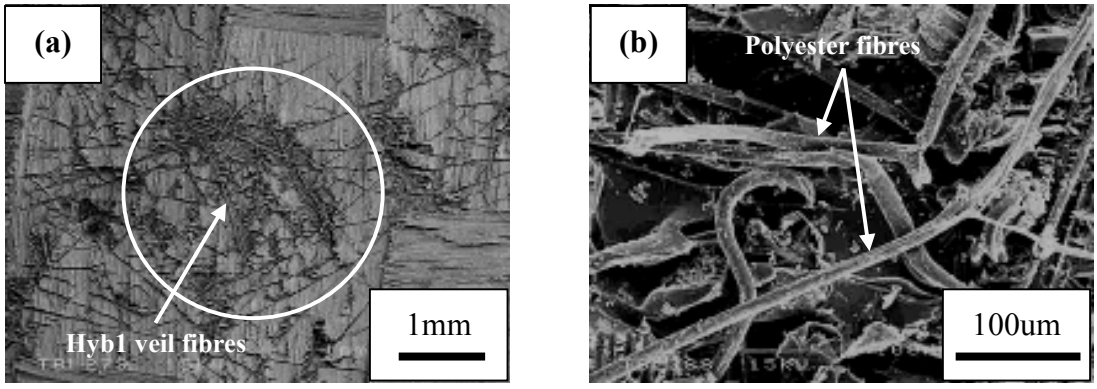

Figure 4.23 Micrographs of fracture surface taken by SEM for 5-harness satin weave epoxy1 system specimens: (a) Hyb1 veil interleaved, (b) Hyb2 veil interleaved, (c) Carbon veil interleaved, (d) PE veil interleaved, (e) PA veil interleaved

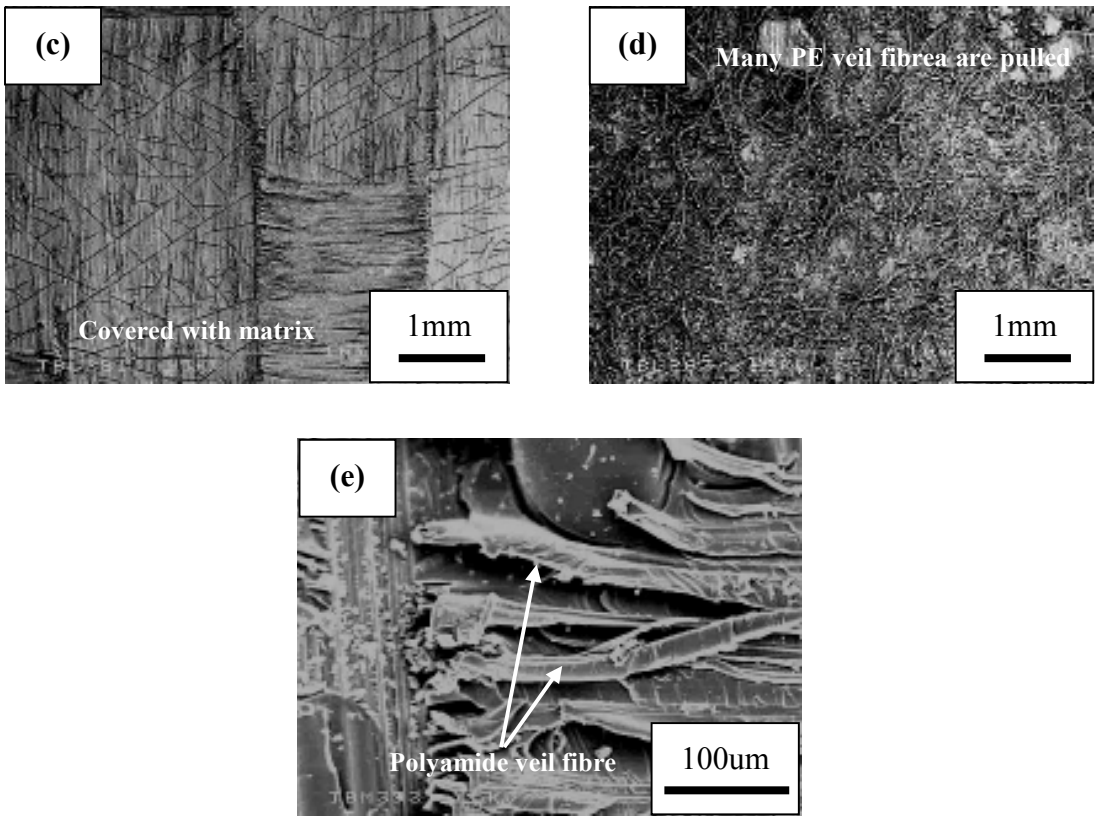

Figure 4.23 (*Continued*)

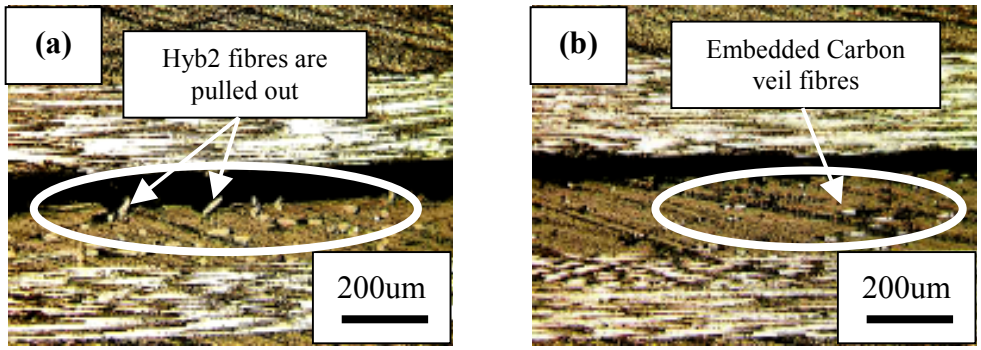

Figure 4.24 Micrographs of cross-section taken by optical microscope for 5-harness satin weave epoxy1 system specimens: (a) Hyb2 veil interleaved, (b) Carbon veil interleaved, (c) PE veil interleaved, (d) PA veil interleaved

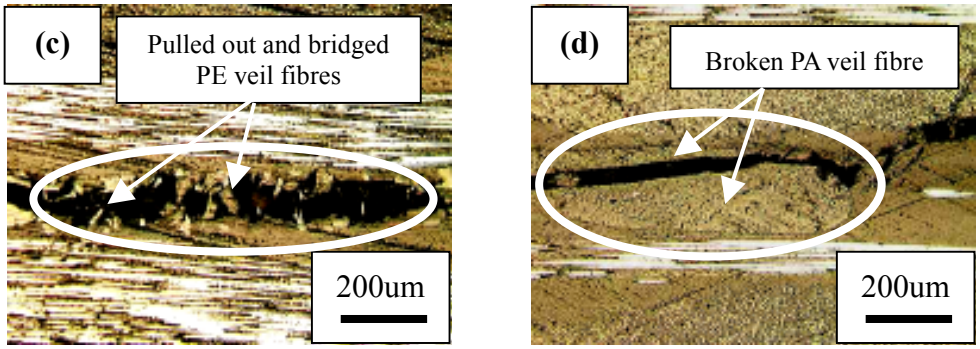

Figure 4.24 (*Continued*)

Fracture surface photographs taken by SEM for the VE system specimens are illustrated in Figure 4.25. The crack passes through between the woven fabric surface and the matrix. It can be seen that the PE veil fibres are pulled out locally, as shown in Figure 4.25 (a). The pulled out PE veil fibres in the VE system specimen are fewer compared with the Ep1 system laminate. It is thought that the crack suppression by veil fibres cannot work adequately. The G_{IIC} value, therefore, is lower than the Ep1 system case. The fracture surface in the PA veil interleaved composite is similar to the PE veil interleaved sample. The PA veil fibres are adhered to the matrix, not pulled out from the matrix, as seen in Figure 4.25 (b). The PA veil fibres are also partially exposed, same as the PE veil interleaved case.

Figure 4.26 shows cross-sections of tested specimens. From Figure 4.26 (a), the pulled out fibres in the PE veil are not many compared with the Ep1 system sample (see in Figure 4.24 (a)). Many interleaf veil fibres would be embedded in the matrix. On the other hand, the PA veil fibres are different in behaviour from the PE fibres. The PA veil fibres would be deformed and elongated, as shown in Figure 4.26 (b). When the crack propagated in the interlaminar region, the PA veil fibres were deformed. This may contribute to improving the Mode-II interlaminar toughness.

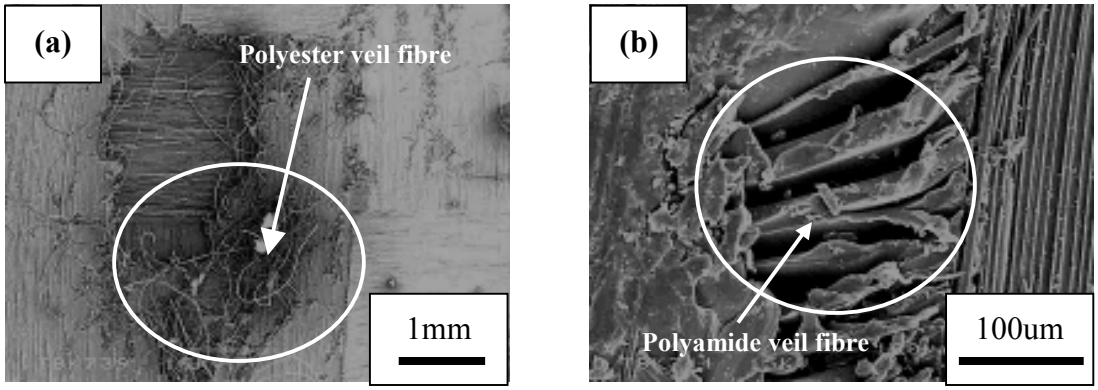

Figure 4.25 Micrographs of fracture surface taken by SEM for 5-harness satin weave vinyl ester system specimens: (a) PE veil interleaved, (b) PA veil interleaved

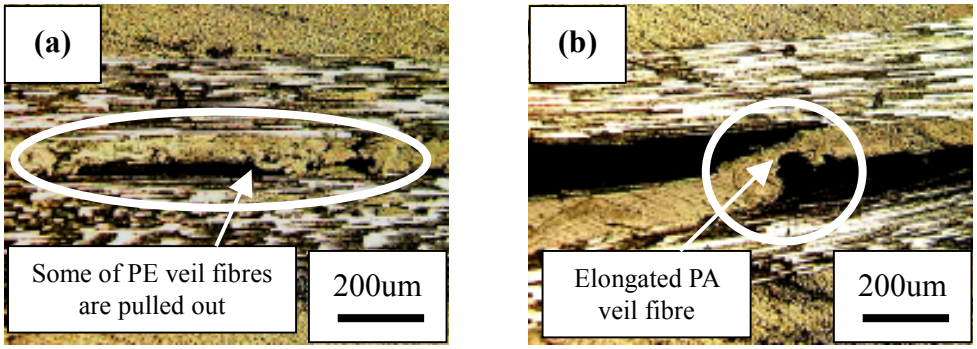

Figure 4.26 Micrographs of cross-section taken by optical microscope for 5-harness satin weave vinyl ester system specimens: (a) PE veil interleaved, (b) PA veil interleaved

4.4.2.2 Unidirectional Fabric Specimens

The images of the fracture surface in the Ep1 system taken by SEM are shown in Figure 4.27. The fracture surface in the Hyb1 interleaved laminate is similar to the satin weave case. The fracture surface is covered with the matrix and some Hyb1 veil fibres are pulled out, as shown in Figure 4.27 (a). The fracture surface in the Hyb2 veil interleaved laminate is almost the same as the Hyb1 veil interleaved sample. However, there are more fibres pulled out as compared with the Hyb1 veil. For the carbon veil interleaved composite, both fracture surface sides are covered with the matrix. The surface is similar to the non-interleaved sample (see in Figure 4.23 (c)). The interleaf veil fibres do not appear on the surface. The veil fibres would be embedded in the matrix. The fracture surface in the PE veil interleaved specimen is similar to the satin

weave Ep1 system case. Both fracture surface sides are covered with the matrix and the PE veil fibres are pulled out, as shown in Figure 4.27 (c). The pulled out PE veil fibres appear widely on the fracture surface. The fracture surface in the PA veil interleaved material is covered with the matrix. A few PA veil fibres appear on the surface, as shown in Figure 4.27 (d). From the picture, it can be seen that the PA veil fibres are deformed on the surface. It is thought that the veil fibres would work to suppress the crack propagation.

Figure 4.28 shows the cross-section pictures taken by the optical microscope. It can be seen from Figure 4.28 (a) that a few Hyb1 veil fibres are pulled out. However, many veil fibres are embedded in the matrix. The G_{IIC} values, therefore, can increase only moderately. The Hyb2 veil interleaved specimen has more pulled out fibres than the Hyb1 interleaved case. In contrast, the carbon veil fibres are embedded in the matrix, as shown in Figure 4.28 (b). The carbon veils in the Ep1 system cannot improve G_{IIC} values for satin weave and UD fabrics specimens. Moreover, the existence of the carbon veils may prevent the extension of the plastic zone. This would tend to degrade the interlaminar toughness. It can be seen that the PE veil fibres are pulled out from the matrix, as illustrated in Figure 4.28 (c). These PE veil fibres seem to cause suppression of crack propagation by a fibre-bridging effect. For the PA veil fibres, it can be seen that the crack goes through the surface of the veil fibre, as illustrated in Figure 4.28 (d). From SEM and optical micrographs, the interleaf veil fibres are not pulled out from the matrix completely. It is though that the adhesion of the PA veil would contribute to the improvement of the Mode-II interlaminar toughness.

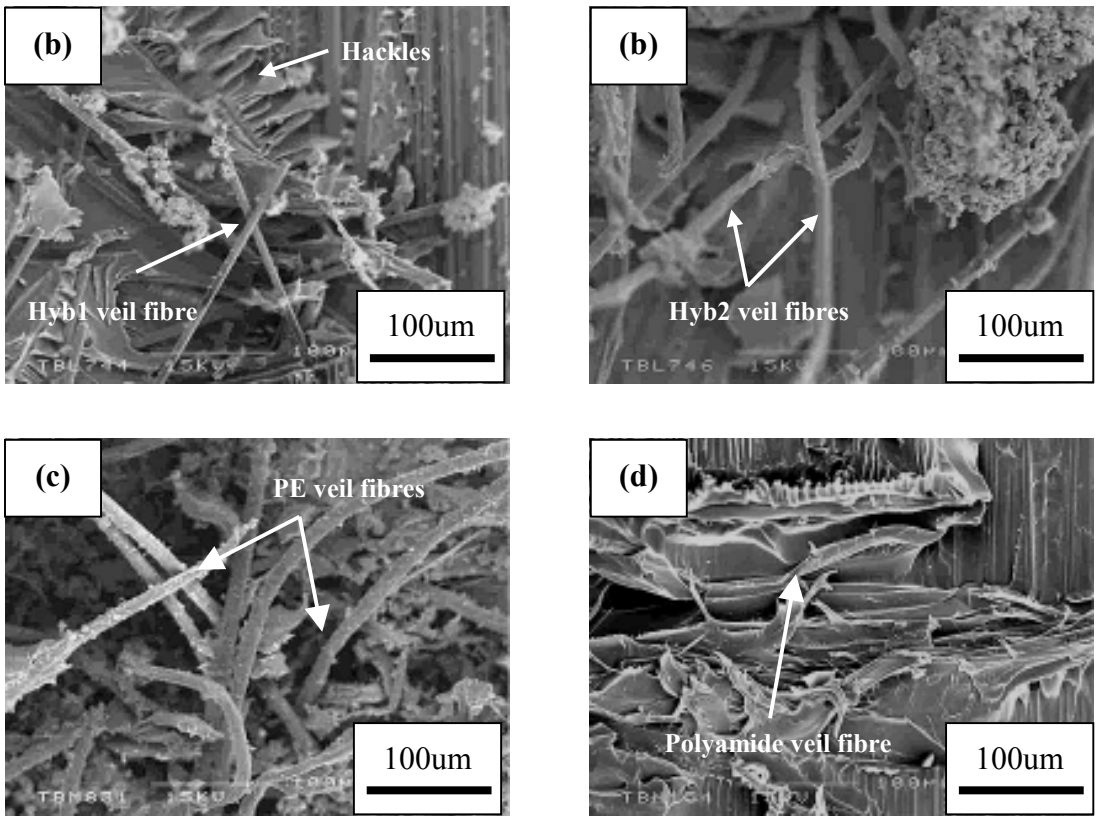

Figure 4.27 Micrographs of fracture surface taken by SEM for unidirectional fabric epoxy1 system specimens: (a) Hyb1 veil interleaved, (b) Hyb2 veil interleaved, (c) PE veil interleaved, (d) PA veil interleaved

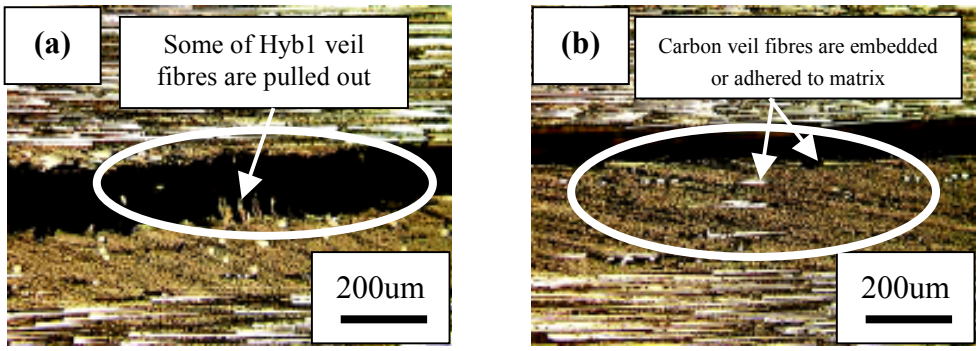

Figure 4.28 Micrographs of cross-section taken by optical microscope for unidirectional fabric epoxy1 system specimens: (a) Hyb1 veil interleaved, (b) Carbon veil interleaved, (c) PE veil interleaved, (d) PA veil interleaved

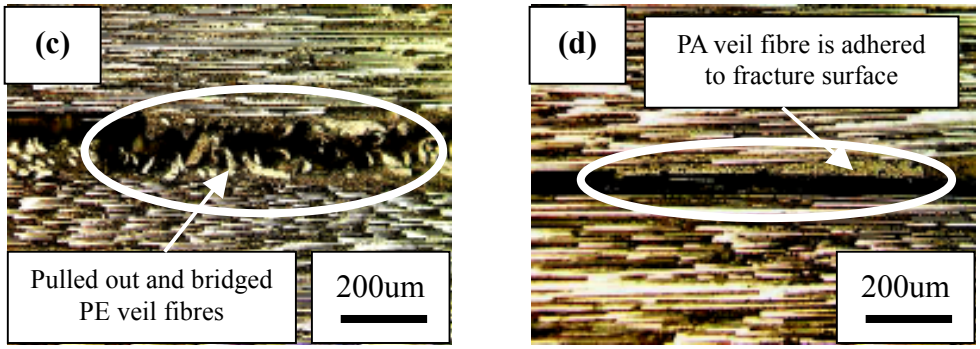

Figure 4.28 (*Continued*)

Figure 4.29 illustrates SEM pictures of the fracture surface for the VE system laminates. The hybrid and carbon veil interleaved specimens have the same type of fracture surface. Whereas one side of the fracture surface is covered with the matrix, the UD carbon fibres on the other fracture side are exposed and unravelled, as illustrated in Figure 4.29 (a) and (b). The crack seems to propagate between the surface of the fabric material and the matrix. However, the interleaf veil does not appear on the surface. It is thought that these veils would be embedded in the matrix. In the PE veil interleaved sample, many pulled out veil fibres appear on the fracture surface, as shown in Figure 4.29 (c). Compared to the Ep1 system specimens, the VE resin case has less pulled out veil fibres. The fracture surface in the PA veil interleaved laminate is a combination of covered with the matrix and exposed UD carbon fibres. It can be found that the PA veil fibres are exposed on the matrix resin, as shown in Figure 4.29 (d). These exposed fibres in the PE and PA interleaved cases would contribute to improving the Mode-II interlaminar toughness.

Micrographs of cross-sections of VE resin laminate are shown in Figure 4.30. From Figure 4.30 (a), it can be seen that the Hyb1 veil fibres are completely embedded in the matrix. The Hyb2 and carbon veil fibres show the same behaviour as the Hyb1 veil. The interleaf veil cannot contribute to improvement of the Mode-II interlaminar toughness considerably. On the other hand, the PE and PA veil fibres are pulled out or exposed on the surface, unlike the other interleaved cases. However, it can be seen that many PE veil fibres are embedded in the matrix, as illustrated in Figure 4.30 (b). Therefore, the G_{IIC} values can increase only moderately. The PA veil fibres are also embedded in the matrix, same as the PE veil. Moreover, the veil fibres are not pulled out much, but adhered to the matrix. It is thought that the adhesion of the PA veil would be

good in the VE resin system. When the crack propagated, the PA veil fibres would be deformed or elongated, but not pulled out. This behaviour would contribute to improvement of the Mode-II interlaminar toughness. In the UD fabric VE system, the fibre-bridging of carbon fabric does not considerably improve the Mode-II interlaminar toughness. It is thought that the bridging effect would not contribute to the improvement of the Mode-II interlaminar toughness. Moreover, the G_{IIC} values would not increase significantly, because the crack can propagate easily by poor adhesion between the VE matrix and UD fabric or smooth surface of fabric.

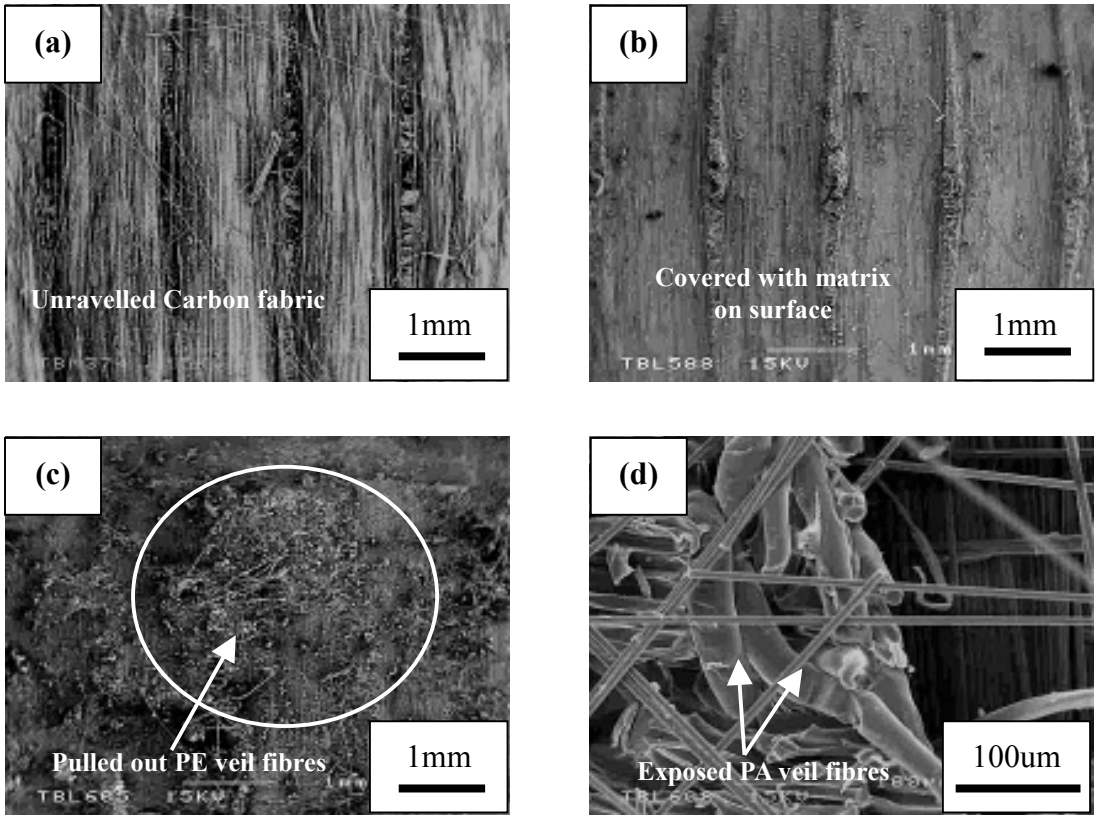

Figure 4.29 Micrographs of fracture surface taken by SEM for unidirectional fabric vinyl ester system specimens: (a) Hyb1 veil interleaved on lower side, (b) Hyb1 veil interleaved on upper side, (c) PE veil interleaved, (d) PA veil Interleaved

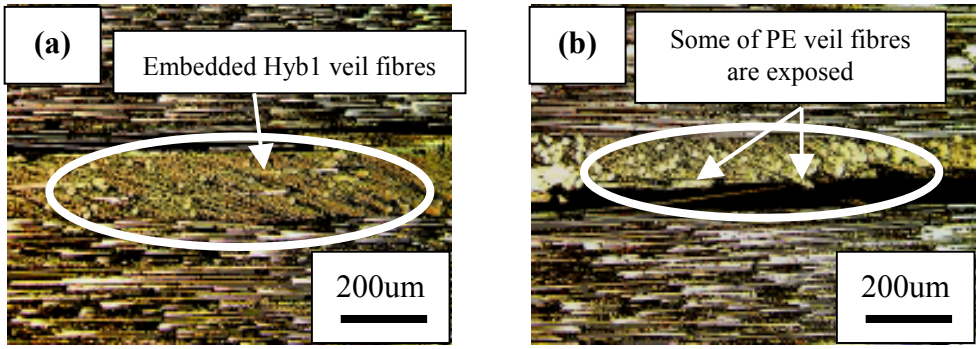

Figure 4.30 Micrographs of cross-section taken by optical microscope for unidirectional fabric vinyl ester system specimens: (a) Hyb1 veil interleaved, (b) PE veil interleaved

4.4.2.3 Plain Weave Fabric Specimens

Figure 4.31 illustrates the fracture surface images taken by SEM for the Ep2 system specimens. The fracture surfaces in the PE/C veil interleaved laminate are covered with the matrix. On the other hand, it can be seen that some veil fibres are pulled out on the fracture surface, as shown in Figure 4.31 (a). These pulled out fibres seem to be PE veil fibres, because the carbon veil fibres are stiff and predominantly straight but the pulled out fibres are curled. The carbon veil fibres, therefore, would be embedded in the matrix. When the crack passed through, some pulled out veil fibres would cause fibre-bridging. The fracture surface in the Hyb2 veil interleaved sample is almost the same as the PE/C veil interleaved case. A few pulled out veil fibres could be found on the surface. However, many veil fibres seem to be embedded in the matrix. In the PE veil interleaved composite, the fracture surface are covered with the matrix and appeared many pulled out PE veil fibres, as shown in Figure 4.31 (b). When the crack passed through in interlaminar region, the veil fibres were pulled out and would be worked for bridging. This effect leads to contribute to improvement of the Mode-II interlaminar toughness significantly. In the PA veil interleaved laminate, the fracture surface is basically covered with the matrix. A few PA veil fibres are found at partial area, as shown in Figure 4.31 (c). It can be found that resin are adhered to the PA veil fibres. This adhesion between the resin and veil fibres would contribute to improvement of the Mode-II crack resistance.

The cross-section pictures of specimen examined by 4ENF test are shown in Figure 4.32. Unfortunately, both veil fibres in the PE/C interleaved laminate are

embedded in the matrix, as shown in Figure 4.32 (a). In this interleaved specimen, the interleaf veils would not work suppression of the crack propagation considerably. Because, many veil fibres are embedded in the matrix. In the Hyb2 veil, the interleaf fibres are also embedded in the matrix, same as the PE/C veils. In this fabric and resin system, the Hyb2 veil worked little suppression of Mode-II interlaminar fracture, unlike the satin and UD fabric Ep1 system specimen. For the PE veil interleaved sample, it can be seen that the veil fibres are pulled out from the matrix, as shown in Figure 4.32 (b). The pulled out fibres are longer than the PE/C veils. As a result, the G_{II} values can increase significantly. In the PA veil, the interleaf veil fibres are adhered to the matrix, as illustrated in Figure 4.32 (c). For the Mode-II fracture behaviour, some of PA veil fibres are found on the surface unlike the Mode-I tested cases. From Figure 4.32 (c), the crack would mainly propagate in the veil region. Consequently, the interleaf veil can improve the G_{IIC} values due to deform or elongate veil fibres.

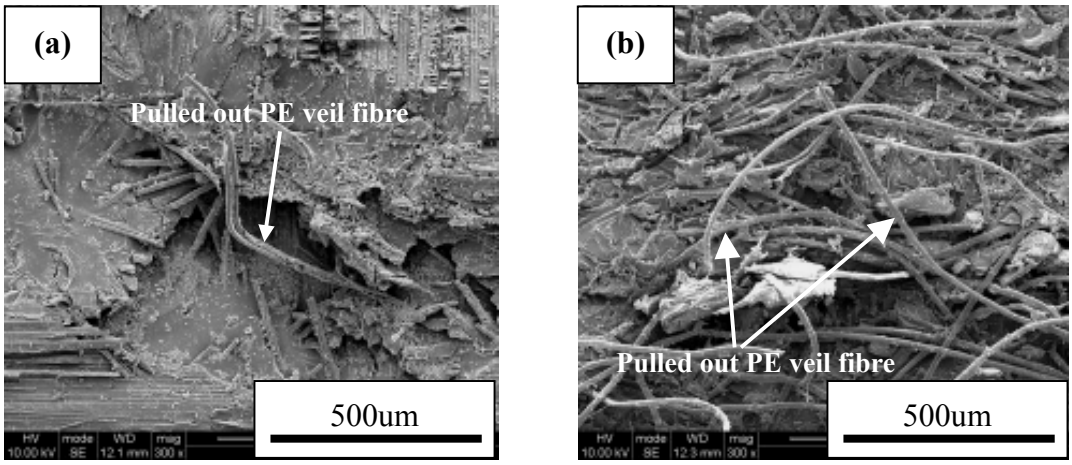

Figure 4.31 Micrographs of fracture surface taken by SEM for plain weave epoxy2 system specimens: (a) PE/C (100:100) veil interleaved, (b) PE veil interleaved, (c) PA veil interleaved

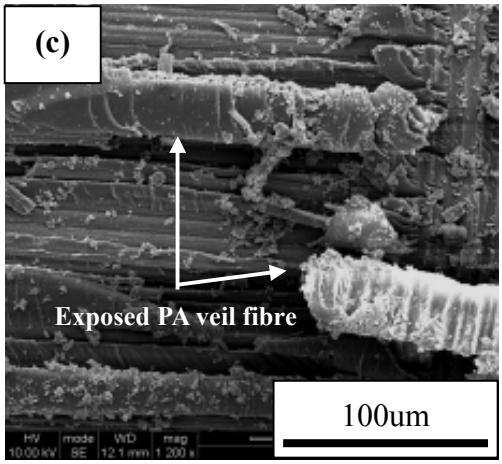

Figure 4.31 (*Continued*)

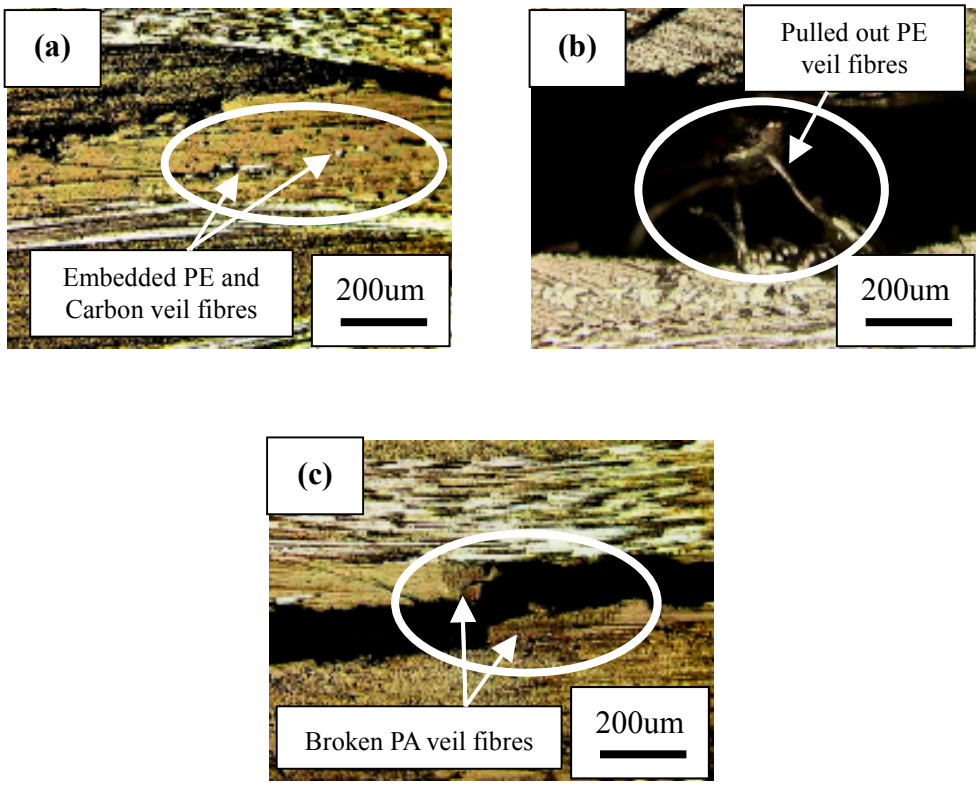

Figure 4.32 Micrographs of cross-section taken by optical microscope for plain weave epoxy2 system specimens: (a) PE/C (100:100) veil interleaved, (b) PE veil interleaved, (c) PA veil interleaved

Fracture surfaces for the VE system laminates are shown in Figure 4.33. For the PE/C veil interleaved specimen, it can be found that the fracture surface is covered with the matrix, as shown in Figure 4.33 (a). A few PE veil fibres appear on the surface. The carbon veil fibre, however, cannot be recognised on the surface. Almost all veil fibres would be embedded in the matrix. For the hybrid and carbon veil interleaved samples, the fracture surface is similar. The woven fibres in the plain weave are barely unravelled on the fracture surface. The interleaf veil fibres also do not appear on the surface. The veil fibres seem to be embedded in the matrix. The PE and PA veil interleaved specimens have fracture surfaces that are similar to the satin and UD fabric VE system cases (see in Figure 4.25 and 4.29). The crack path for the plain weave specimen is between the matrix and surface of the woven fabric. The PE veil fibres in plain weave laminate are not pulled out but adhered to the matrix, as shown in Figure 4.33 (c). During 4ENF testing, the flexure failure began at an early stage. Therefore, it is thought that the veil fibre could not pull out enough. On the other hand, the fracture surface in the PA veil interleaved sample is that some PA veil fibres are pulled out from a partial region, as shown in Figure 4.33 (d). These interleaf veil fibres and woven fibres would work as fibre-bridging effect and contribute to improvement of the Mode-II interlaminar toughness.

Figure 4.34 shows cross-section of the PE/C veil interleaved specimen. The crack behaviour in all interleaved specimens is similar. Basically, the interleaf veil is embedded in the matrix. From Figure 4.34, it can be seen that the PE/C veil fibres are embedded in the matrix. Consequently, the interleaf veils, except for the PE and PA veils, cannot contribute to improvement of the Mode-II interlaminar toughness considerably. In the case of the PE and PA veils, some veil fibres appear on the fracture surface. These veil fibres can moderately increase the G_{IIC} values. In the plain weave specimens, the crack propagation was significantly slow. Therefore, some specimens were undergone bending failure before the crack propagated enough. It is thought that the surface of plain weave is coarse. Hence, the crack growth would be difficult. In particular, in the PE and PA veil interleaved samples crack propagation was significantly slower than the other interleaved cases. As a result, data points for these interleaved specimens are less than the other interleaved materials (see in Appendix B).

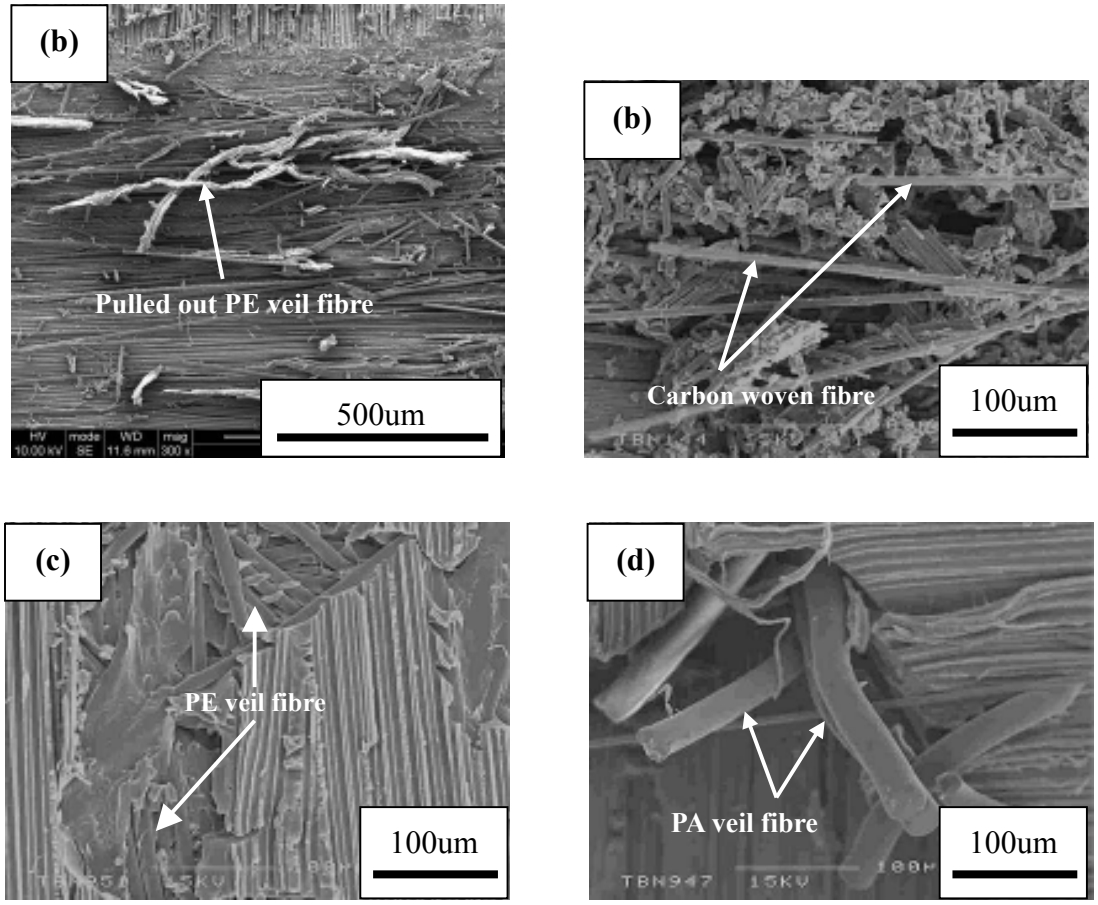

Figure 4.33 Micrographs of fracture surface taken by SEM for plain weave vinyl ester system specimens: (a) PE/C (100:100) veil interleaved, (b) Hyb1 veil interleaved, (c) PE veil interleaved, (d) PA veil interleaved

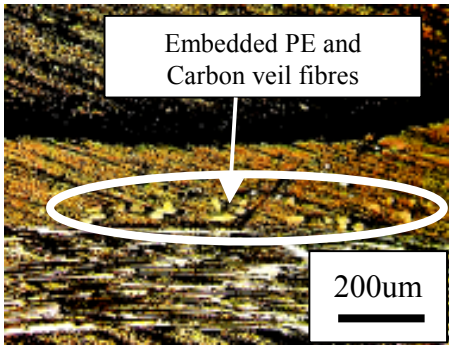

Figure 4.34 Micrographs of cross-section taken by optical microscope for plain weave PE/C (100:100) veil interleaved vinyl ester system specimen

4.5 Conclusion

As a result of evaluating the study for the Mode-II interlaminar toughness of non-woven interleaved CFRP, the following conclusions are drawn:

(1) The many hackles in the Ep1 system composites appeared on the fracture surface. These hackles would work to improve the Mode-II interlaminar toughness. Moreover, the hackles in the Ep2 system laminate were also seen. On the other hand, the hackles in the VE system specimens did not appear. In this resin system, the crack propagated in between the fabric and matrix, the same as the Mode-I interlaminar fracture. It is thought that the hackle would be affected by the type of the resin.

(2) For the 5-harness satin weave Ep1 system composites, the Hyb2 and PE veil interleaved specimens had a considerably higher Mode-II initial critical energy release rate. The Hyb1 veil interleaved laminate improved slightly the toughness. For the carbon and PA veil interleaved composites, the G_{IIC} values were lower than the non-interleaved sample. The $G_{II\text{-}prop}$ value of the PA veil interleaved laminate, on the other hand, was almost the same as the control. The carbon veil interleaved specimen, however, still had lower toughness than the other interleaved cases. The tendency of the Mode-II interlaminar toughness for interleaved samples was similar to the Mode-I interlaminar toughness.

(3) For the UD fabric Ep1 system, the Hyb2 veil interleaved laminate had the highest G_{IIC} value in all materials. The PE veil interleaved specimen had the second highest Mode-II initial toughness. The other veil interleaved composites had a moderate improvement in the Mode-II crack resistance behaviour. The $G_{II\text{-}prop}$ values of the interleaved samples were significantly increased, except for the carbon veil interleaved case. The hybrid and PE veil fibres were pulled out from the fracture surface. These pulled out fibres would work as bridging for the crack suppression. The PA veil fibres, on the other hand, were not pulled out completely. The PA veil fibres, however, seemed to improve crack propagation resistance by deformation or elongation of the veil fibres. For the VE system, the difference of the G_{IIC} between each interleaved case was quite small. The crack propagated between the carbon fabric and the matrix. Moreover, the interleaf veil fibres, except for the PE and PA veil, were embedded in the matrix. These interleaved specimens, therefore, would not improve the Mode-II interlaminar toughness considerably. In the UD fabric VE

system, the fibre-bridging by UD carbon fabric could not contribute to the improvement of the Mode-II interlaminar toughness.

(4) For the plain weave Ep2 system composites, the PA veil interleaved specimen had the highest G_{IIC} value of all interleaved cases in the same way as the Mode-I interlaminar toughness. The PE veil interleaved laminate had the second highest Mode-II interlaminar toughness. The PE/C and Hyb2 veil interleaved specimens, however, had almost the same G_{IIC} values as the non-interleaved sample. For the VE system, the tendency of the G_{II} value was almost the same as the Ep2 system cases. The PE and PA veil interleaved specimens had superior Mode-II interlaminar toughness compared with the other interleaved cases. Some 4ENF test specimens underwent bending fracture during the 4ENF test. It is thought that crack propagation by coarse surface may be more difficult than the other fabric composites. When the specimen starts to undergo bending fracture before crack growth, a toughness measurement is impossible [183].

(5) In all fabric and resin system, the PE veils are superior interleaf materials for Mode-I and Mode-II interlaminar toughness. The hybrid veils give a modest improvement of both modes of fracture toughness for the Ep system. However, these veils do not contribute to the interlaminar toughness for the VE system. Although the PA veils had significantly poor interlaminar toughness for the Ep1 system, they improved the interlaminar toughness for the Ep2 system. On the other hand, the PA veils for the VE system contributed to the moderate improvement of both modes of the fracture toughness. As a result, the PA veils are strongly affected by the resin system. The carbon veils had the poorest toughness for both fracture modes, and all fabric and resin systems.

Chapter 5

Mechanisms of Impact and CAI Resistance Behaviour using Non-Woven veils as Interleaf Materials

5.1 Introduction

In this chapter, the main objectives are to evaluate the damage resistance provided by the non-woven interleaf veils under impact and post-impact compression loading. The low-energy impacted composite materials were inspected using ultrasonic C-scanning and observed in cross-section by microscopy. In this work, the plain weave fabrics with epoxy2 and vinyl ester resin matrices, and five different interleaf veils were selected for evaluation of the impact and the CAI resistance. Low-impact energies were applied to the laminated specimens using a drop weight testing machine. Afterwards, non-impacted and impacted laminates were tested in compression. The effects of the impact damage and CAI resistance were evaluated experimentally.

5.2 Materials and Experiment Methods

5.2.1 Materials Information

Information on the materials is given in section 3.2.1. In this study, only the plain weave fabric was selected as the base material, with epoxy2 and vinyl ester resins.

5.2.2 Fabrication Methods of Composites for Impact and CAI Tests

The method of fabrication of the CAI specimens was the same as the DCB/4ENF test specimens. Details of the moulding method have been given in section 3.2.2. For the CAI laminates, the fabrics and interleaf veils were cut into 480mm (in length) x 370mm (in width) rectangles. The plain weave fabrics were laminated with 6 plies onto the rigid mould. The HAW weave fabric was chosen in both resin system specimens. For the VE system, the non-interleaved and the PA veils interleaved samples used the LAW fabrics for comparison to the HAW materials. The interleaf veils were prepared with 5 plies of each placed between the carbon weave layers. The PE/C veils

were overlapped before laminating, and inserted between the carbon woven fabric layers. Figure 5.1 illustrates model of stacking diagrams of impact and CAI specimens.

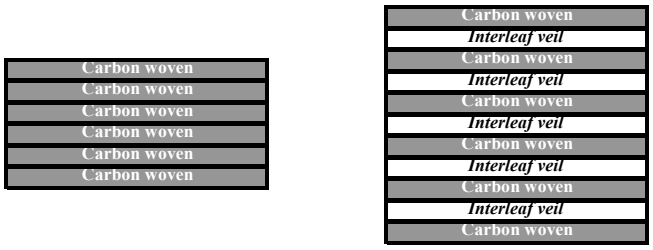

Figure 5.1 Stacking diagrams of (a) Non-interleaved specimen and (b) Interleaved specimen

5.2.3 Impact Test

In the CAI test, non-penetrating low-energy impact tests were performed on a rectangular shape coupon of 89 x 55mm, using an instrumented drop-weight machine. Figure 5.2 illustrates the impact/CAI specimen. The impact tests were carried out using two machines, CEAST "Dartvis" (at Queen Mary, University of London) and "Fractovis Plus" (at Brunel University). The impact machine pictures are shown in Figure 5.3. For the Dartvis, as shown in Figure 5.3 (a) and (b), the striker shape and mass are a hemisphere of 20mm diameter and 0.78kg respectively. The specimen was clamped between two plates each with a circular (40mm diameter) opening window and held together by compressed air pressure. The incident impact energy of the striker during impact test was varied by adjusting the drop height of striker and adding weight. For the Fractovis Plus, as illustrated in Figure 5.3 (c) and (d), the striker shape was the same as Dartvis (20mm of diameter and hemisphere), and the striker mass was 5.045kg. The laminates were not clamped, but just placed on the fixture. The incident impact energy was varied by changing drop height. The input energies of all specimens were set 4, 8, and 12J.

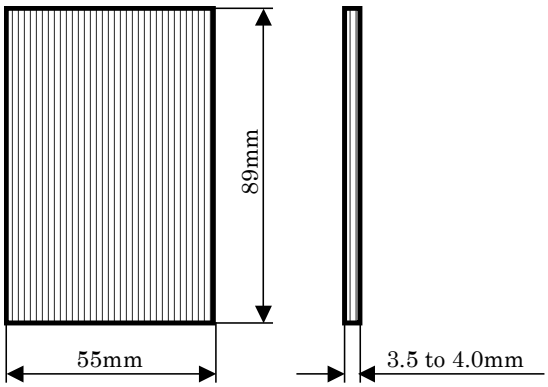

Figure 5.2 Schematic of impact and CAI test specimen

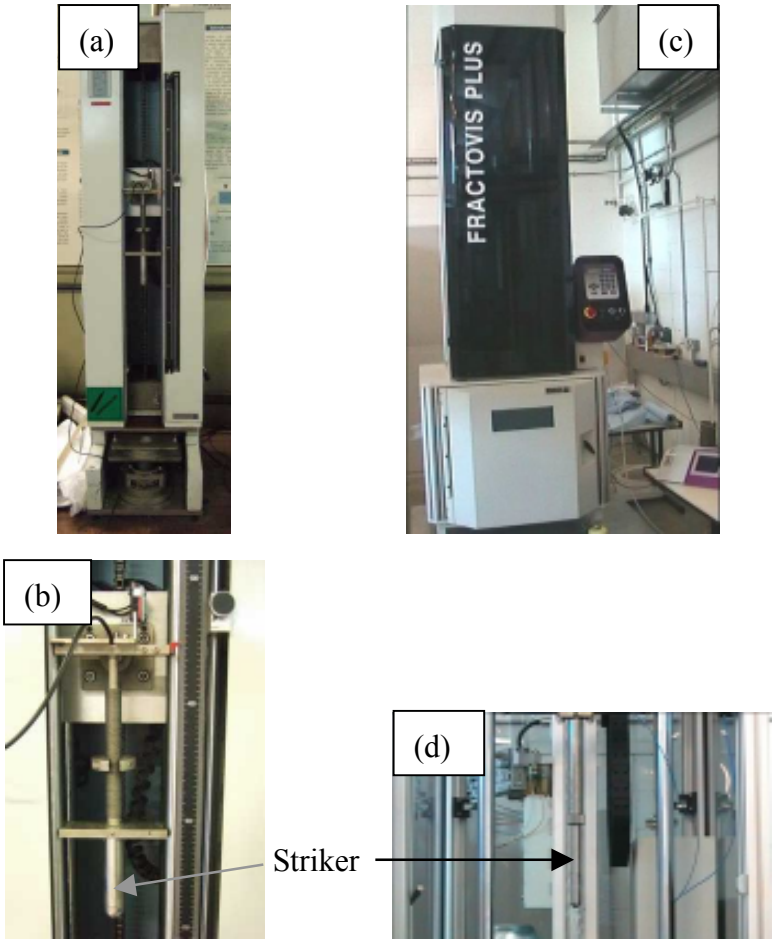

Figure 5.3 Pictures of Impact machine: (a) CEAST "Dartvis", (b) Striker (CEAST "Dartvis") (c) Fractovis Plus, (d) Striker (Fractovis Plus)

5.2.4 Compression After Impact (CAI) Test

The CAI tests were employed to evaluate the impact damage resistance of the composites. The CAI test was carried out using an anti-buckling fixture, as shown in Figure 5.4. The detail of the geometry for the rig is also illustrated in Figure 5.5. The CAI specimen was not supported completely by the anti-buckling fixture, and there was short unsupported length. The CAI specimens were put into a slot at the bottom of the fixture and supported by knife edge side anti-buckling guides. The fixture can prevent out-of-plane buckling of the specimens during the compression test. This CAI fixture can accommodate variable specimen thicknesses.

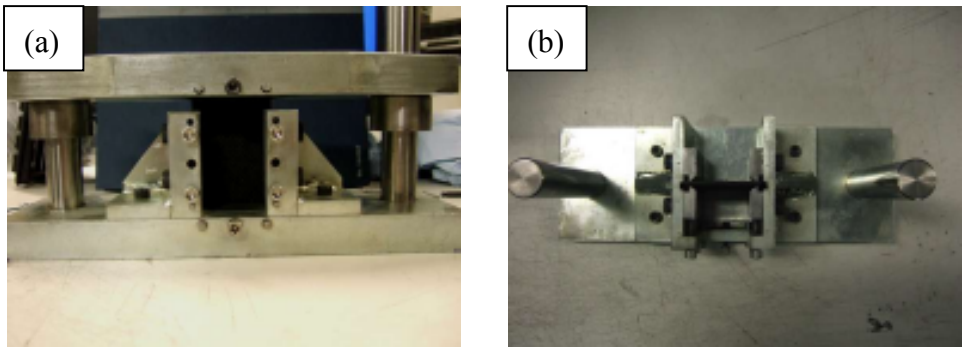

Figure 5.4 Anti-backling rig: (a) Front view, (b) Top view

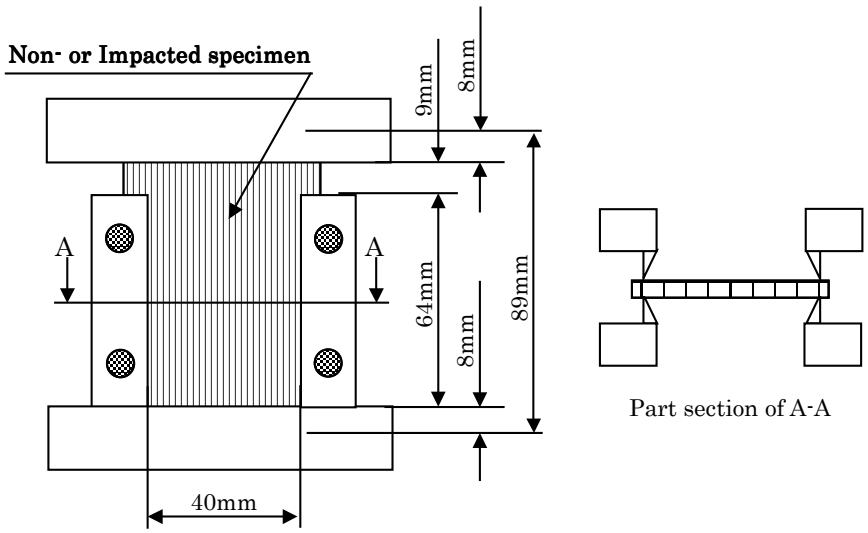

Figure 5.5 Schematic of CAI rig

The CAI tests were conducted using a screw driven mechanical testing machine, Instron 6025, at a constant crosshead rate of 0.5mm/min at room temperature. The load and displacement were logged using a computer. During the compression test, the anti-buckling guide was used to support the laminate. The compression strengths of the non-impacted specimens were also measured. Figure 5.6 shows compression test machine, Instron 6025.

Figure 5.6 Picture of Instron 6025 for compression test

5.2.5 Damage assessment

Ultrasonic C-scan was used to assess the impact damage. Figure 5.7 shows the Physical Acoustics C-scan machine. The specimens were placed in the air, as shown in Figure 5.7 (b) and (c), and then scanned. The Physical Acoustics unit has 5MHz flat probes which act as the transmitter and receiver. The transmitter and receiver were connected to Pulser/Receiver module DIO 2000 BP LF, as shown in Figure 5.7 (a). Figure 5.8 is a schematic of C-scanning. This information was passed to a computer storage device which built up the images on a 1 mm spaced grid. In the assessment of damage resistance, the damage width, obtained by measuring the end of delamination perpendicular to load direction from the C-scan [171], was used.

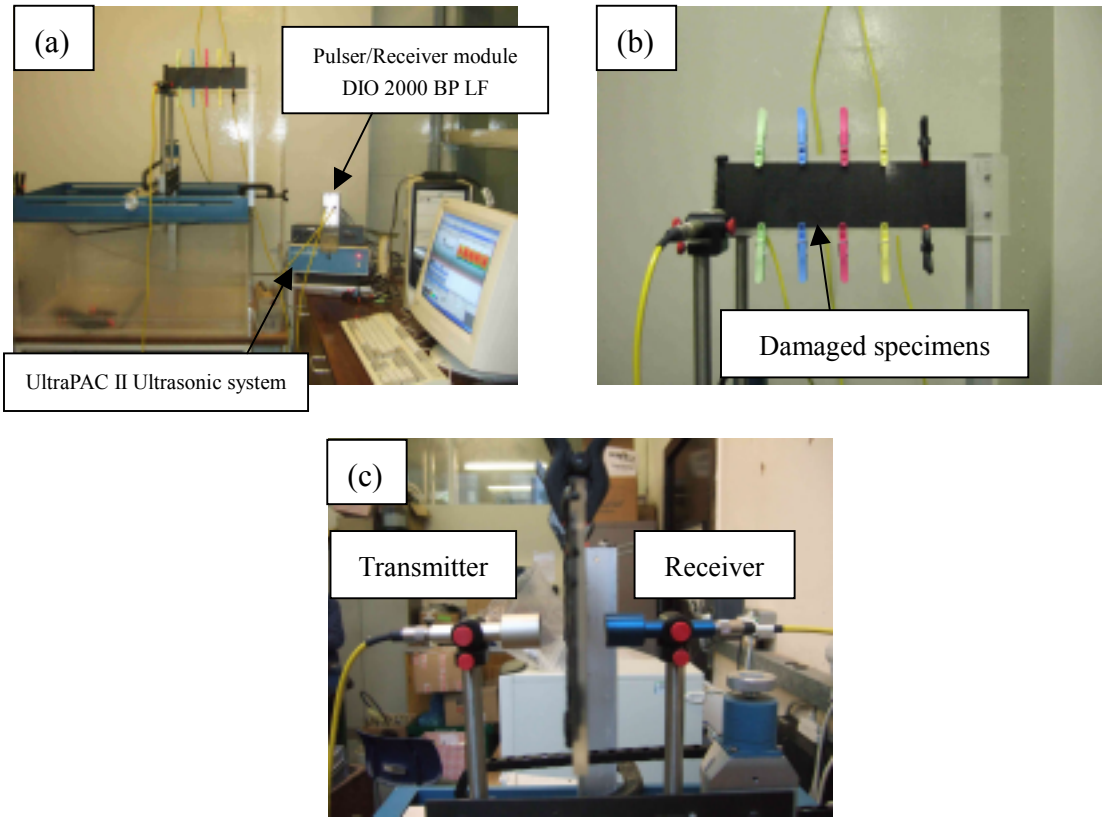

Figure 5.7 Pictures of C-scanning: (a) Configuration of C-scan, (b) Front view of C-scanning (c) Side view of C-scanning

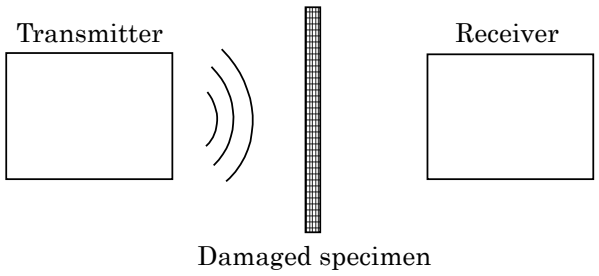

Figure 5.8 Schematic of ultrasonic C-scanning

5.2.6 Thickness and Volume Fraction of Each Laminates

Table 5.1 gives information of the thickness and volume fraction (V_f) for each laminate. Volume fractuions of specimens were calculated using weight fraction of specimen and density of carbon fibre and resin.

Table 5.1 Summary of thickness and volume fraction (V_f) for impact and CAI specimens

Fabric	Resin	Interleaf veils	Thickness [mm]	V_f (%)
Plain weave (HAW*)	Epoxy2	Non-interleaved	2.85	36
		PE/C (100:100)	3.10	42
		PE/C (80:20)	3.10	42
		Polyester	2.71	48
		Polyamide	2.53	52
Plain weave (HAW)	Vinyl ester	Non-interleaved	2.33	54
Plain weave (LAW**)		Non-interleaved	1.95	51
Plain weave (HAW)		PE/C (100:100)	3.32	36
		PE/C (70:30)	2.92	43
		PE/C (80:20)	3.07	40
		Polyester	2.82	44
		Polyamide	2.81	41
Plain weave (LAW)		Polyamide	2.42	41

*: High areal weight, **: Low areal weight

5.2.7 Observation by Microscopy

Cross-sections of impacted specimens were viewed using an Olympus BX60 optical microscope. Tested specimens were cut along the longitudinal direction and the cross-section was polished by abrasive papers. The CAI tested specimens were also observed by the optical microscope. These specimens were cut in the transverse direction and polished. Cross-sections of the CAI tested specimens were observed using a scanning electron microscope, FEI Inspect F. The specimens were cut along the width direction and polished using abrasive papers. The SEM specimens were coated with a thin layer of gold prior to observation. The acceleration voltage was 10kV. The SEM observations were used to evaluate the suppression behaviour of the crack propagation in each interleaved specimen. All SEM pictures show regions that are near to the impact point.

5.3 Results

5.3.1 Impact Damage Width

The damage width caused by impact test is plotted in Figure 5.9 as a function of impact energy normalised by specimen thickness for the Ep2 system laminates. For all impact energies, the non-interleaved samples have the largest damage width, as shown in Figure 5.9. The damage width at the lowest energy (4J) is approximately 22mm in the control. Afterwards, the increase in the width is gradual. For the interleaved laminates, the general trend of the damage extension is the same as the non-interleaved samples, but the impact damage resistance is improved by the veils. At the lowest impact energy, the damage width for all interleaved laminates is almost the same. The interleaved specimens, except for the PA veil interleaved case, are similar in behaviour for all substantial impact energies. The PE/C, Hyb2, and PE veils contribute to damage resistance slightly. For the PA veil interleaved composite, however, the increase in damage width is small compared with the other interleaved samples. The PA veils possess the greatest damage resistance of all interleaf veils. Table 5.3 indicates the summary of the damage width for all specimens as a function of incident impact energy.

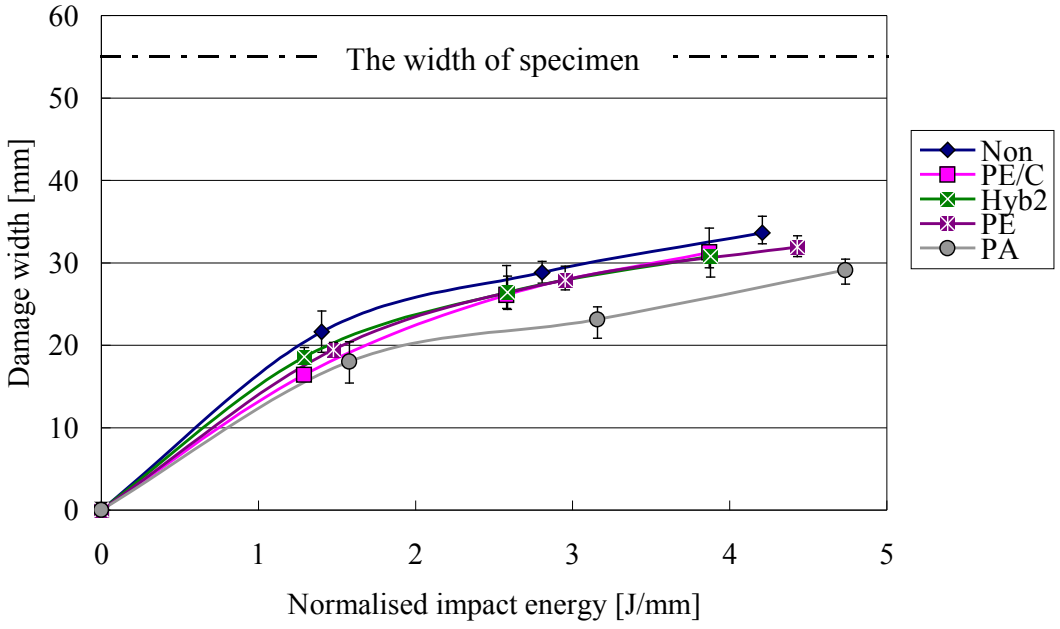

Figure 5.9 Damage width obtained by impact test as a function of normalised impact energy for epoxy2 system specimens with/without non-woven interleaf veils

Table 5.2 Summary of damage width by each incident impact energy for epoxy2 system specimens with/without non-woven interleaf veils

	Incident impact energy [J]					
	4		8		12	
Interleaf veil	**Damage width [mm]**	**S. D.**	**Damage width [mm]**	**S. D.**	**Damage width [mm]**	**S. D.**
Non-interleaved	21.6	2.111	28.8	1.161	33.7	1.220
PE/C	16.4	0.892	26.1	2.053	31.3	2.036
Hyb2	18.6	1.646	26.4	1.538	30.8	1.451
PE	19.4	0.719	27.9	1.086	31.9	1.031
PA	18.0	1.930	23.1	1.702	29.1	1.170

Figure 5.10 is a diagram of damage width for the VE system specimens as a function of the impact energy normalised by the specimen thickness. The damage width for the VE composites is overall much larger than that of the Ep2 samples. Compared to the Ep2 resin specimens, the damage resistance by the veils show a different behaviour. In the lowest impact energy (4J), the damage width of the Hyb2 veil interleaved specimen is the smallest of all interleaved materials. However, the damage width at 8 and 12J of impact energy is not the smallest. The PE/C and PA veil interleaved laminates possess superior damage resistance at high impact energies. On the other had, the Hyb1 and PE veil interleaved cases have similar damage widths for all impact energies. The PA veils contribute to the impact damage resistance in both resin systems. Table 5.43 gives a summary of the damage width for all VE resin specimens. In previous researches, the Hyb2 and PA veils interleaved with the VE resin composites possessed good impact damage resistance [129, 152]. However, the results for the Hyb2 veils are different from previous studies. The impact damage would be influenced by the difference of the fabric areal weight. For the PA veil interleaved laminates, the damage width of the HAW fabric samples has larger than that of the LAW fabric cases.

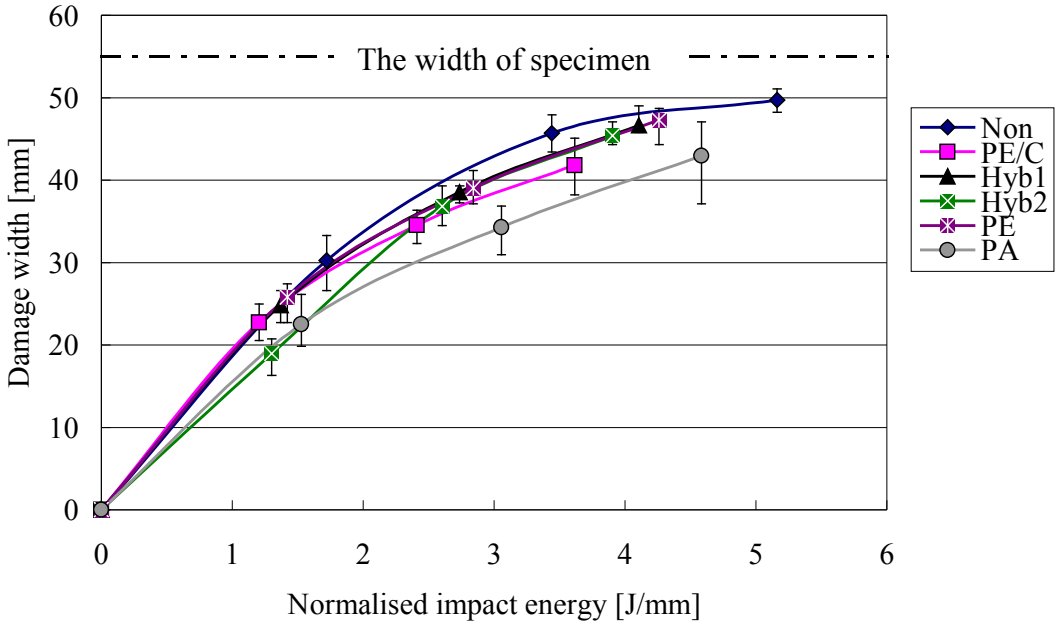

Figure 5.10 Damage width obtained by impact test as a function of normalised impact energy for vinyl ester system specimens with/without non-woven interleaf veils

Table 5.3 Summary of damage width by each incident impact energy for vinyl ester system specimens with/without non-woven interleaf veils

	Incident impact energy [J]					
	4		8		12	
Interleaf veil	**Damage width [mm]**	**S. D.**	**Damage width [mm]**	**S. D.**	**Damage width [mm]**	**S. D.**
Non-interleaved	30.3	2.853	45.7	1.643	49.7	1.209
PE/C	22.7	1.739	34.5	1.451	41.8	2.859
Hyb1	24.8	1.494	38.5	0.956	46.7	1.352
Hyb2	19.0	1.703	36.8	2.222	45.4	1.171
PE	25.8	1.857	39.0	1.500	47.3	1.764
PA (HAW)*	22.1	2.504	35.1	1.293	45.1	1.606
PA (LAW)**	23.6	0.587	32.1	1.606	37.5	0.587

*: used HAW plain weave fabric, **: used LAW plain weave fabric

The PA veil interleaved both resin systems specimens possess excellent damage resistance. In particular, significant suppression of the impact damage can be realised in the Ep2 system. The PE/C and hybrid veils have moderately improved damage resistance for both resin systems. However, the PE veil interleaved specimens exhibit relatively poor impact resistance compared with the other interleaved samples.

5.3.2 Compression After Impact Test

5.3.2.1 Non-Interleaved Specimens

Representative results of compression tests for the non-impacted and impacted specimens with both resin systems are illustrated in Figure 5.11. In the Ep2 system laminates, the fracture behaviour for all non-impacted and impacted cases is the same. The collapse after the compression load is clear, as shown in figure 5.11. Although the maximum compression load and extension in the non-impacted case are about 42kN and 1.65mm, those in the impacted specimens drop significantly even for 4J-impacted specimen. The maximum load values for the impacted specimens are approximately 24kN (4J), 20kN (8J), and 19kN (12J) respectively.

For the VE system composites, both the maximum compressive load and extension are significantly smaller than the Ep2 system cases. Cracking was audible quite early. The compressive collapse behaviour for 0 and 4J impacted specimens was similar to the Ep2 system samples. However, those of 8 and 12J impacted specimens were different. For these specimens, the compressive collapse was gradual and slow. Moreover, the drop of compression load was small. The maximum load values for the non-impacted and impacted laminates are 14kJ (0J), 11kN (4J), 6kN (8J), and 5kN (12J) respectively.

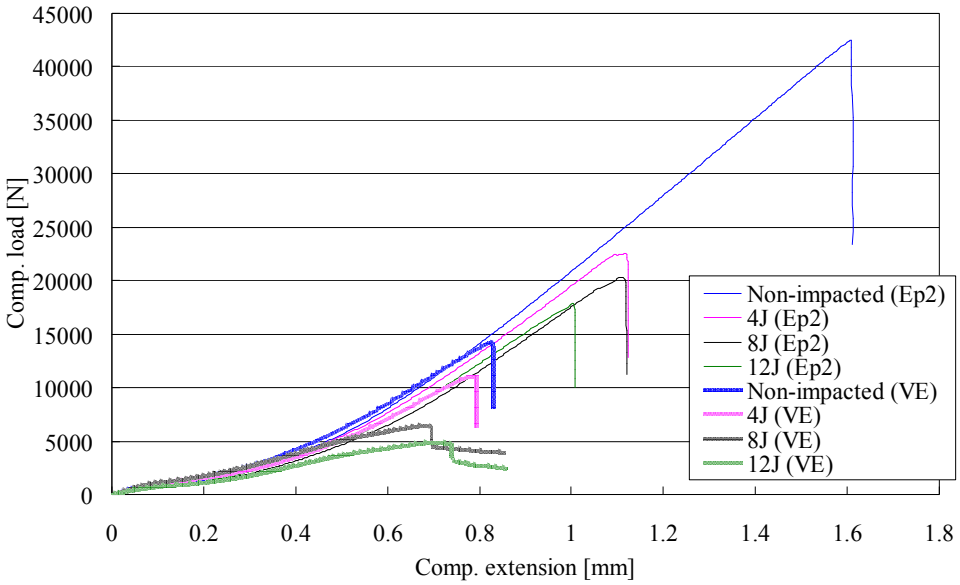

Figure 5.11 Representative CAI test results of non-impacted and impacted specimens for non-interleaved both resin systems

5.3.2.2 Polyester/Carbon Veil Interleaved Specimens

Results of the CAI tests for both resin systems are shown in Figure 5.12. Compared to the non-interleaved Ep2 resin specimens, both the compression load and extension in the PE/C veil interleaved laminates have almost the same values. Moreover, the fracture behaviour by compression load is the same as the control. The maximum loads for all laminates are about 42kN (0J), 27kN (4J), 23kN (8J), and 19kN (12J) respectively.

Compared with the Ep2 system specimens, the maximum load values for the VE system laminates are again much smaller. The maximum load for the non-impacted specimen is about 20kN. The maximum compressive loads for each impacted case are about 17kN (4J), 14kN (8J), and 12kN (12J) respectively. The maximum load values of the PE/C veil interleaved laminates have higher than those of the non-interleaved samples. In PE/C veil interleaved laminates, the compressive collapse behaviour tended to be sudden and be sharp, unlike the non-interleaved specimens.

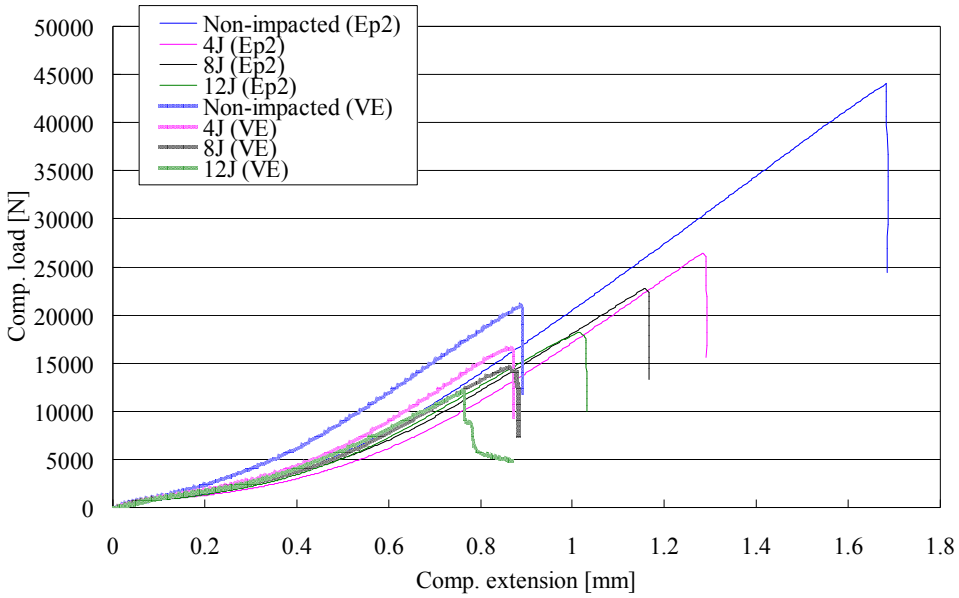

Figure 5.12 Representative CAI test results of non-impacted and impacted specimens for PE/C (100:100) veil interleaved both resin systems

5.3.2.3 Polyester/Carbon (70:30) Hybrid Veil Interleaved Specimens

Figure 5.13 illustrates typical results of the CAI tests for composites. In the Hyb1 veil interleaved laminates, only the VE resin system specimens were tested, not the Ep2 system specimens. For the non-damaged specimens, the maximum load was 19kN. The fracture started early stage, around 3 to 7kN. The maximum loads for all impacted laminates are about 15kN (4J), 12kN (8J), and 7kN (12J) respectively. The maximum compressive extensions for all specimens are almost the same as the non-interleaved samples. It can be seen that the Hyb1 veils do improve the CAI resistance slightly (compare to Figure 5.11 and 5.13).

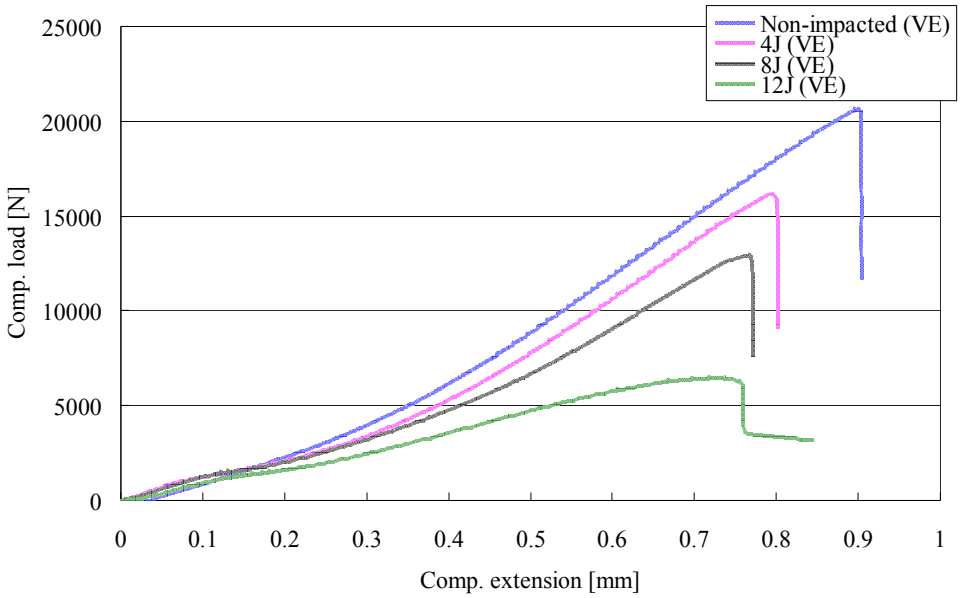

Figure 5.13 Representative CAI test results of non-impacted and impacted specimens for PE/C (70:30) hybrid veil interleaved vinyl ester system

5.3.2.4 Polyester/Carbon (80:20) Hybrid Veil Interleaved Specimens

Figure 5.14 shows a diagram of the CAI test results for both resin systems. The maximum load for the non-damaged specimens is approximately 43kN. The compressive fracture progressed quite slowly, afterwards the collapse occurred suddenly. The maximum loads for all impacted laminates are approximately 26kN (4J), 22kN (8J), and 20kN (12J) respectively. The maximum compression load values are almost the same as the PE/C veil interleaved cases.

For the non-damaged VE system specimens, the maximum load is about 18kN. The fracture started around 3 to 7kN of compression load. The maximum compressive loads for all impacted specimens are about 16kN (4J), 12kN (8J), and 8kN (12J) respectively. The maximum load values are almost the same as the Hyb1 veil interleaved samples. The compressive fracture was also the same in behaviour as the Hyb1 veil interleaved laminates.

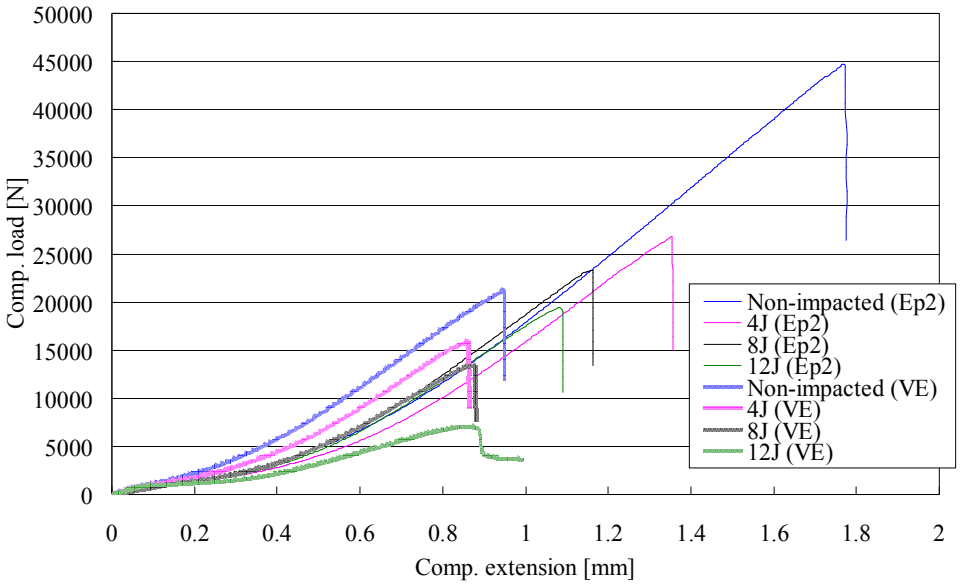

Figure 5.14 Representative CAI test results of non-impacted and impacted specimens for PE/C (80:20) hybrid veil interleaved both resin systems

5.3.2.5 Polyester Veil Interleaved Specimens

Figure 5.15 shows typical CAI test results for both resin systems. The average maximum load values for the non-impacted specimens is approximately 34kN. Compared to the PE/C and Hyb2 veil interleaved cases, the maximum compressive load in the non-impacted material has smaller values. The maximum load values for all impacted samples are about 28kN, (4J), 25kN (8J), and 23kN (12J) respectively. The maximum compression loads in the impacted cases are slightly higher than the PE/C and Hyb2 veil interleaved laminates. Moreover, the reduction of the compression load for impacted specimens is relatively small, compared with the other interleaved composites.

For the VE resin system, the maximum load of the non-damaged specimen is about 20kN. The maximum compressive loads for all impacted laminates are approximately 16kN (4J), 13kN (8J), and 8kN (12J) respectively. The maximum load values are slightly higher than the non-interleaved samples and almost the same as the other interleaved cases.

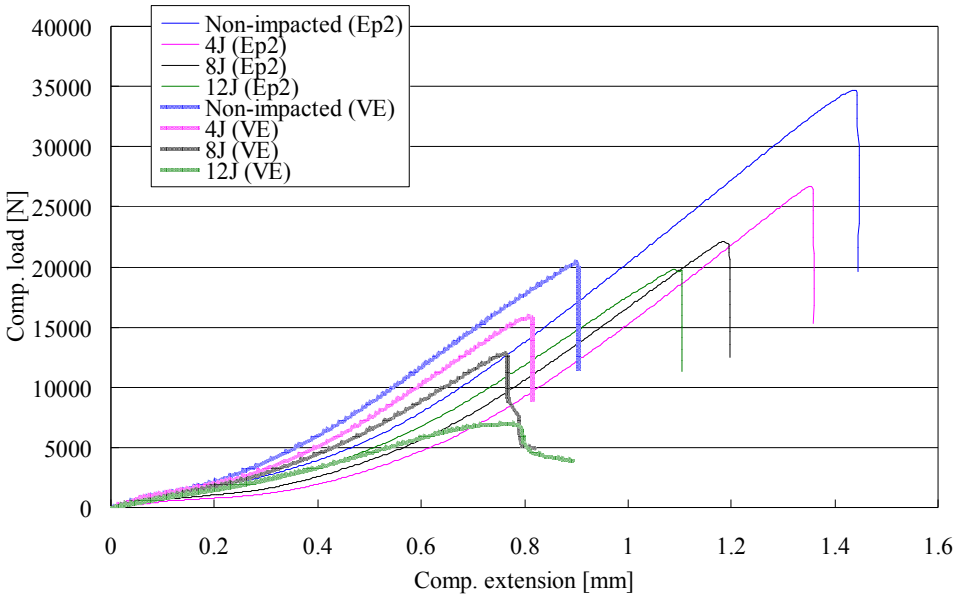

Figure 5.15 Representative CAI test results of non-impacted and impacted specimens for PE veil interleaved both resin systems

5.3.2.6 Polyamide Veil Interleaved specimens

Representative results of the CAI tests are plotted in Figure 5.16 for both resin systems. The maximum load value of the non-damaged specimens is approximately 35kN. The fracture initiation was significantly later than the other veil interleaved cases. The maximum compressive load values for all impacted specimens are about 28kN (4J), 25kN (8J), and 23kN (12J) respectively. Compared to the other interleaved laminates, the reduction of the maximum load for impacted samples is significantly small. It is thought that the PA veil interleaved specimens would possess good compressive fracture resistance.

In the VE system, the maximum compression load for the non-impacted laminate is approximately 17kN. The maximum load values for all impacted specimens are approximately 16kN (4J), 13kN (8J), and 8kN (12J) respectively. While the Ep2 system laminates improve compression resistance, the VE resin composites are almost the same as the other interleaved cases.

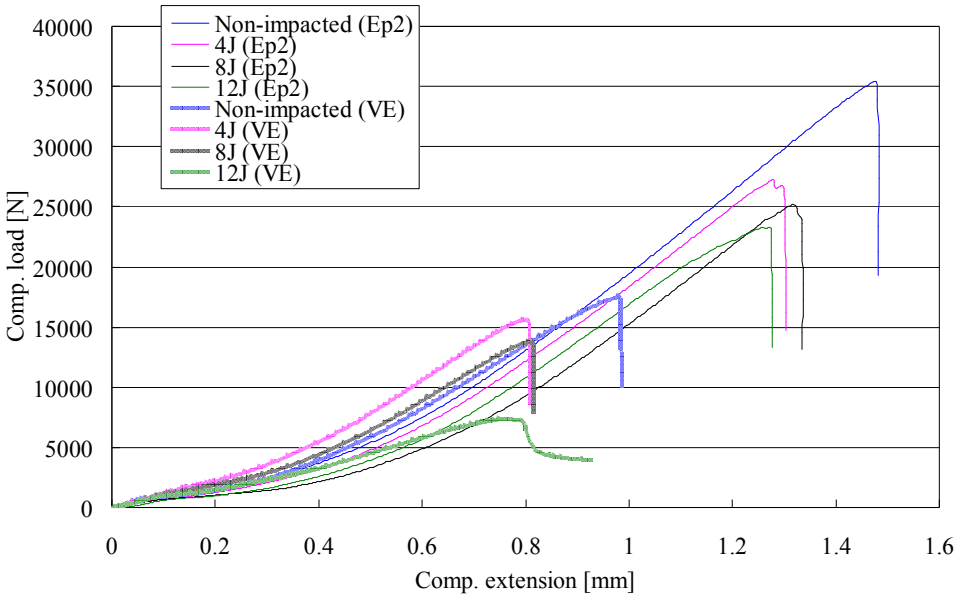

Figure 5.16 Representative CAI test results of non-impacted and impacted specimens for PA veil interleaved both resin systems

Compressive fracture behaviour would be influenced by the resin system. The Ep2 system specimens undergo a sudden compression collapse and the compressive load dropped substantially. For the Ep2 system specimens, the crack initiation was significantly delayed compared to the VE system specimens. Moreover, time from the crack initiation to the collapse was short compared with the VE system cases. On the other hand, the VE system specimens exhibited slow and gradual collapse progression. The crack initiation for the VE resin specimens occurred relatively earlier than the Ep2 system laminates. Crack propagation started at quite an early stage and grew gradually during compression test.

5.3.3 Compression After Impact Strength

Figure 5.17 shows a diagram of CAI strength against impact energies normalised by specimen thickness for the Ep2 system composites. The compression strength values for all non-impacted specimens are approximately 250MPa. For the PE/C and Hyb2 veil interleaved cases, the CAI strength is almost the same values as the non-interleaved samples. The CAI strength values for these specimens are range from 150 to 155MPa at 4J of impact energy. The reduction of the CAI strength from non-impact is approximately 40%. The compression strength for the PE veils interleaved laminates has higher value than the PE/C and Hyb2 veil interleaved specimens, about 178MPa.

For the PA veils interleaved specimens, the CAI strength has the highest value of all interleaved laminates, approximately 207MPa. The reduction of compression strength from undamaged specimen was the smallest, a decrease of only 18%. While the reduction of CAI strength from 0J to 4J impacted specimens, except for the PA veil interleaved composites, is large, that of the compression strength from 4J to 8J and 8J to 12J reveals quite a small drop. The PE/C and Hyb2 veil interleaved laminates have almost the same CAI strength at each impact energy as the non-interleaved sample. These interleaf veils would not contribute to the improvement of the CAI strength for the CFRP. Nevertheless the impact damage resistance for the PE veil interleaved composites shows a poor improvement, the CAI strength is the second highest value. The PA veil interleaved specimens are significantly improved for the CAI resistance, even if the maximum compression load is lower than the other interleaved samples. The reduction of CAI strength with increasing impact energy is small for all specimens. The deviations of the CAI strength for all impact energies are quite small. Table 5.4 summarises the CAI strengths and standard deviations for all specimens.

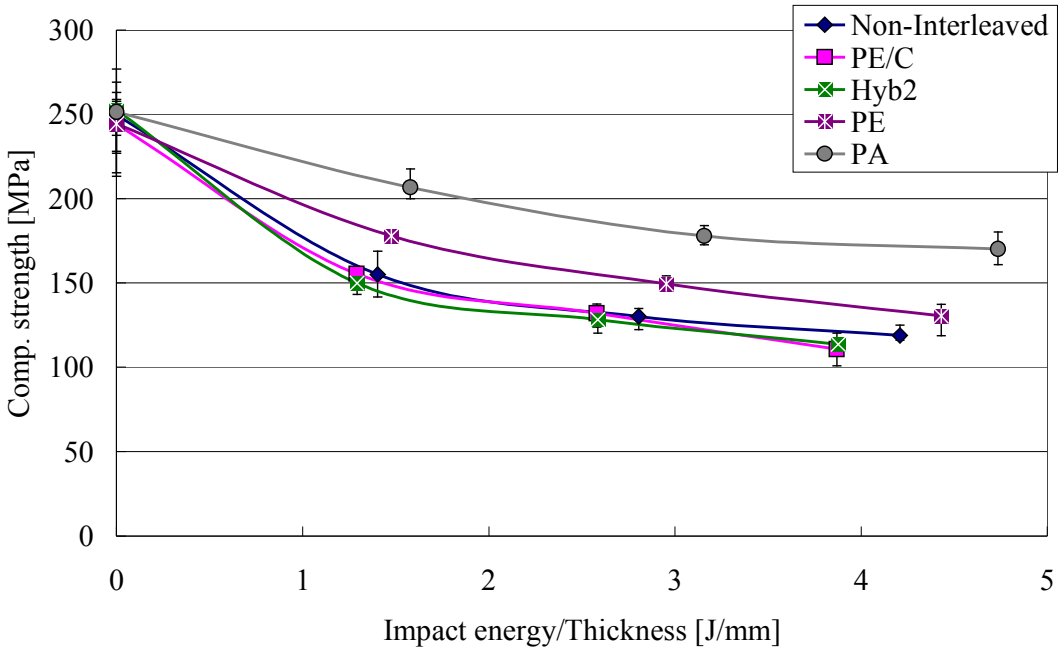

Figure 5.17 CAI strength against incident impact energy normalized by thickness for epoxy2 system specimens with/without non-woven interleaf veils

Table 5.4 Summary of CAI strengths and standard deviations for epoxy2 system specimens with/without non-woven interleaf veils

	Impact energy [J]							
	0		4		8		12	
Interleaf	**CAI [MPa]**	**S.D.**	**CAI [MPa]**	**S.D.**	**CAI [MPa]**	**S.D.**	**CAI [MPa]**	**S.D.**
Non-Interleaved	249.70	13.75	155.05	10.89	130.13	5.06	118.92	3.64
PE/C	244.13	14.94	155.45	2.28	132.00	5.06	110.72	7.89
Hyb2	252.46	26.84	149.93	4.84	128.28	7.36	113.61	3.82
PE	244.26	9.83	177.86	1.61	149.38	3.05	130.40	7.05
PA	251.34	21.52	206.64	7.45	177.84	4.93	170.09	6.97

In the VE resin composites, the CAI strengths as a function of normalised impact energies are shown in Figure 5.18. Compared to the Ep2 resin composites, the CAI strength of the VE system specimens is overall lower. For the non-interleaved case, the CAI strength of non-impacted specimens is approximately 123MPa. The CAI strength from 4J to 8J impact energy decreases at a faster rate. For interleaved specimens, the reduction in CAI strength is gradual. In this resin system, the improvement of the CAI resistance by the interleaf veils is moderate. Previous literature mentioned that the PE/C (80:20) hybrid veil interleaved specimens had higher CAI strength than PE veil interleaved [129]. In this research, the Hyb2 veil cannot be obtained the highest CAI strength of all interleaved samples. The difference between each veil interleaved is quite small. The PA veil interleaved specimens show relatively higher CAI strengths than the other veil interleaved cases. The HAW and LAW fabrics were compared to the CAI properties using the PA veils interleaved specimens. As a result, the LAW specimens are slightly smaller CAI strength than the HAW cases, except for 12J impacted specimens. The influence by areal weight of fabric seems small. Table 5.6 summarises the results of the CAI test with standard deviations.

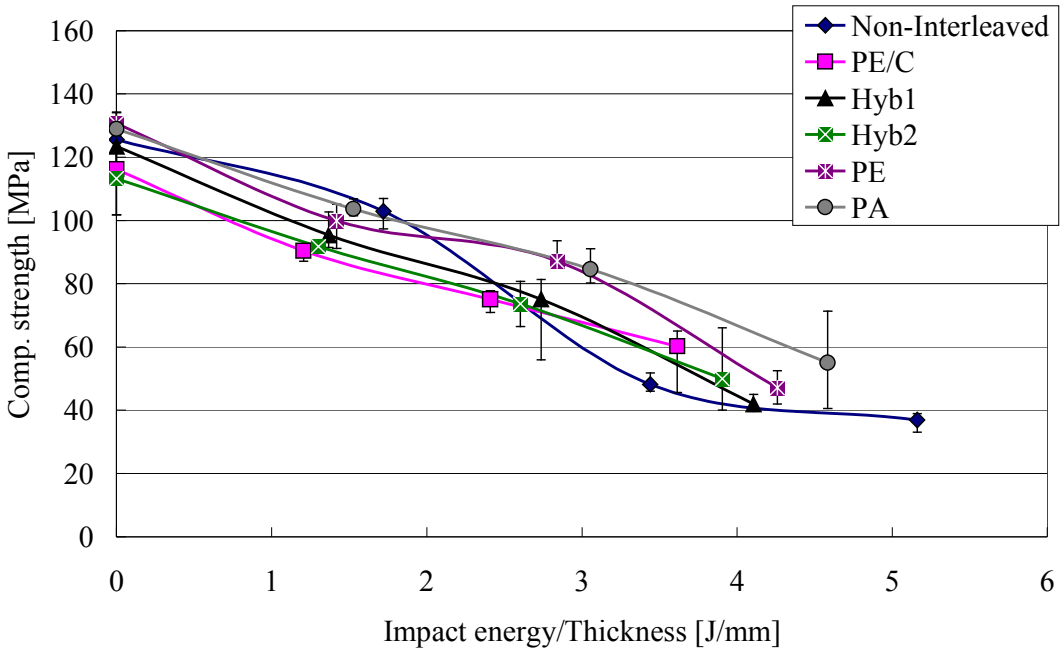

Figure 5.18 CAI strength against incident impact energy normalised by thickness for the vinyl ester system specimens with/without non-woven interleaf veils

Table 5.5 Summary of CAI strengths and standard deviations for vinyl ester system specimens with/without non-woven interleaf veils

	Impact energy [J]							
	0		4		8		12	
Interleaf	**CAI [MPa]**	**S.D.**	**CAI [MPa]**	**S.D.**	**CAI [MPa]**	**S.D.**	**CAI [MPa]**	**S.D.**
Non-Interleaved	125.53	5.46	102.91	3.82	48.15	3.19	36.90	2.24
PE/C	116.18	11.96	90.36	2.26	75.01	3.07	60.22	8.29
Hyb1	123.45	6.49	95.36	4.68	75.10	10.83	41.95	2.59
Hyb2	113.19	12.59	91.74	1.40	73.58	6.25	49.92	11.84
PE	130.69	2.96	99.84	5.32	87.16	3.59	47.08	3.98
PA (HAW)	128.92	5.14	103.64	2.29	85.92	3.00	49.17	11.82
PA (LAW)	-*	-	97.14	9.81	81.17	1.44	69.66	2.38

*: Not examined

For the Ep2 system specimens, the trend of the CAI resistance for interleaved composites differs from that of impact resistance. Specifically, although the PE/C and Hyb2 veil interleaved specimens possess good impact resistance, these veils do not contribute to the CAI resistance properties. In contrast, the PE veil interleaved laminates improve the CAI resistance but not impact resistance. The PA veil interleaved specimens have excellent both impact and CAI resistance properties. The tendency of the CAI strength for the VE system composites is similar to that of impact resistance. The CAI strengths for the VE resin specimens are overall lower than the Ep2 system samples.

5.4 Discussion

5.4.1 Impact Resistance

5.4.1.1 Non-interleaved Specimens

Figure 5.19 shows C-scans of the impacted specimens for the Ep2 system. The increase of damage width from 4J to 8J is spread along the transverse direction, as illustrated in Figure 5.19 (a) and (b). The spread from 8J to 12J is slightly increased, as shown in Figure 5.19 (b) and (c). Figure 5.20 is a micrograph of the cross-section of a 12J impacted specimen. From Figure 5.20, it can be seen that the fracture is localised around the impact point consisting of matrix fracture and fibre breakage. In flexible specimens, the impact damage tends to initiate in the lowest ply due to flexural fracture [242]. When the laminated composites receive impact loads, one or more failure modes such as matrix cracking, surface micro-buckling, delamination, ply shear-out and fibre breakage can become dominant [116, 220]. In this resin system, matrix cracking, delamination, and fibre breakage seem to be main failure modes. The length of transverse cracking is not great. It seems that the impact energy passed in the through-thickness direction. It is thought that the impact energy could not be dissipated sufficiently through the interlaminar region due to strong adhesion between the matrix and the carbon fabric.

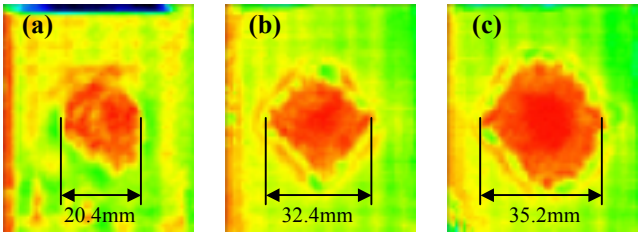

Figure 5.19 C-scan images of non-interleaved specimens for epoxy2 system with measured damage width: (a) 4J, (b) 8J, (c) 12J impacted

Figure 5.20 Cross-section image of 12J impacted specimen for non-interleaved epoxy2 system (Broad arrow indicates impact point)

Figure 5.21 shows C-scan images of the impact damaged specimens for the VE system. Compared to the Ep2 system laminates, spread of the damage width is larger. In particular, the fracture by impact for 12J-damaged specimen reaches the edge of the specimen, as shown in Figure 5.21 (c). The crack behaviour of 12J impact damaged specimen is illustrated in Figure 5.22. The impacted specimen is deformed over a wider area than the Ep2 system cases (see in Figure 5.20). The length of the crack propagation is also longer than for the Ep2 resin laminates. In this resin system, the damage modes would be dominated mainly by the delamination. In chapter 3 and 4, the adhesion properties between the VE resin and carbon fabrics are revealed to be poor by microscopy observations. The transverse cracks, therefore, can pass through the interlaminar region easily. Moreover, the impact energy seems to pass through the transverse direction and the crack can propagate at the interlaminar region.

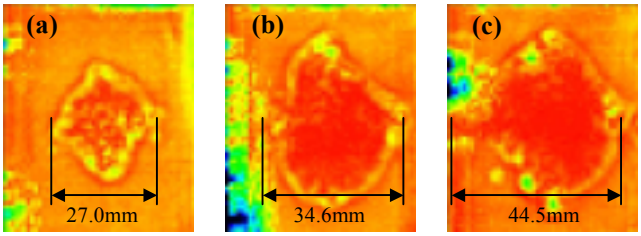

Figure 5.21 C-scan images of non-interleaved specimens for vinyl ester system with measured damage width: (a) 4J, (b) 8J, (c) 12J impacted

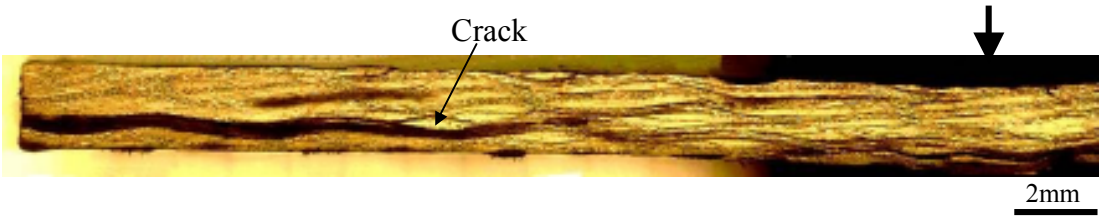

Figure 5.22 Cross-section image of 12J impacted specimen for non-interleaved vinyl ester system (Broad arrow indicates impact point)

5.4.1.2 Polyester/Carbon Veil Interleaved Specimens

C-scanning images for the Ep2 system specimens are shown in Figure 5.23. The damage width for the 4J impacted specimen is approximately 17mm. For 8J impact energy, the damage width is spread widely, about 24mm. The increase of damage from 8J to 12J impact energy, on the other hand, is not so much. Figure 5.24 shows micrographs of the cross-section of a 12J impact damaged specimen. Compared to the non-interleaved laminates, the PE/C veil interleaved specimen does not fracture at the impact point. However, some short cracks are spread in the interlaminar area, as shown in Figure 5.24. For this resin system, it is thought that transverse cracking is the dominant damage mode. The PE veil would work to provide modest toughening for impact resistance.

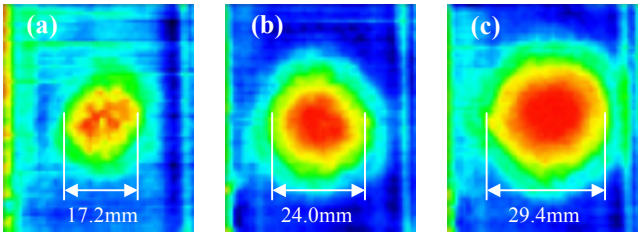

Figure 5.23 C-scan images of PE/C (100:100) veil interleaved specimens for epoxy2 system with measured damage width: (a) 4J, (b) 8J, (c) 12J impacted

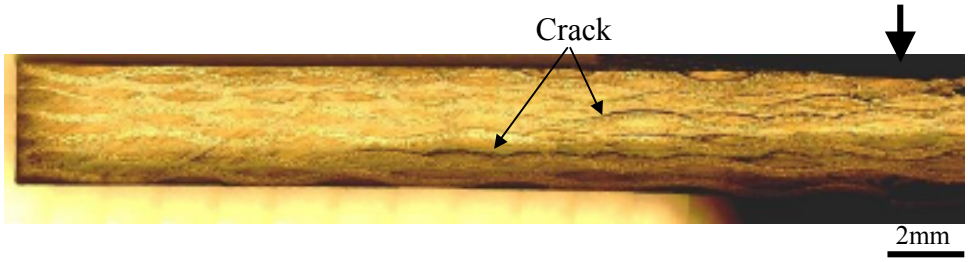

Figure 5.24 Cross-section image of 12J impacted specimen for PE/C (100:100) veil interleaved epoxy2 system (Broad arrow indicates impact point)

The images of damaged area taken by C-scan for the VE resin composites are shown in Figure 5.25. The damage width increases greatly with increasing impact energy. In particular, in the 12J impacted specimen the damage spread is significantly large, as shown in Figure 5.25 (c). The impact damage of the PE/C veil interleaved laminates is smaller than that of the non-interleaved cases. Hence the interleaf veils would contribute to the suppression of crack propagation during the damage spread. Figure 5.26 shows a cross-section image of a 12J impacted specimen. It can be seen that there are many small cracks in the interlaminar region. Compared to the Ep2 system samples, the cracks are widely distributed. The interleaf veils could suppress long crack propagation. However, the growth of short cracks could not be controlled.

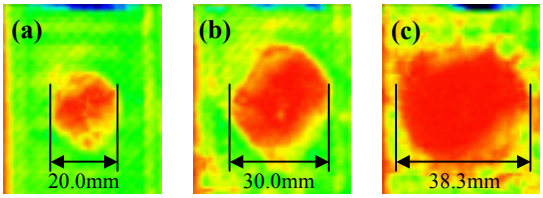

Figure 5.25 C-scan images of PE/C (100:100) veil interleaved specimens for vinyl ester system with measured damage width: (a) 4J, (b) 8J, (c) 12J impacted

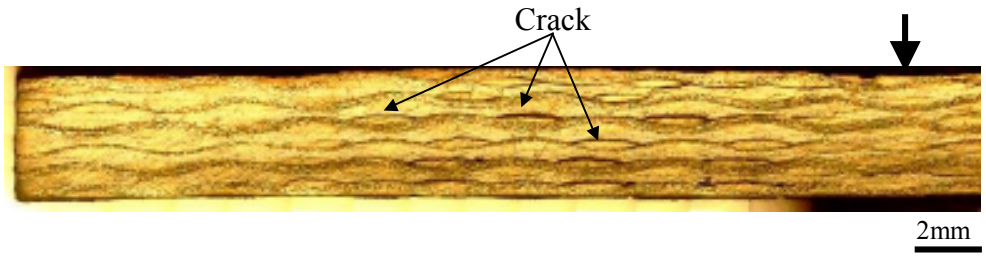

Figure 5.26 Cross-section image of 12J impacted specimen for PE/C (100:100) veil interleaved vinyl ester system (Broad arrow indicates impact point)

5.4.1.3 Polyester/Carbon (70:30) Hybrid Veil Interleaved Specimens

The C-scans of the VE system specimens are shown in Figure 5.27. The trend of increase in the damage width is similar to the PE/C veil interleaved VE system cases (see in Figure 5.25). For the 12J impacted specimen, impact damage reaches the edge of the specimen. A micrograph of the cross-section of a 12J impact damaged specimen is shown in Figure 5.28. The crack propagated over a long range in the interlaminar region. The interleaf veils seem not to work to provide crack resistance.

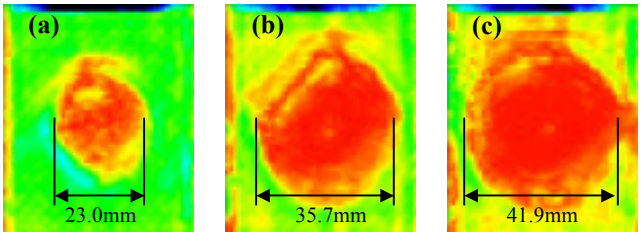

Figure 5.27 C-scan images of PE/C (70:30) hybrid veil interleaved specimens for vinyl ester system with measured damage width: (a) 4J, (b) 8J, (c) 12J impacted

Figure 5.28 Cross-section image of 12J impacted specimen for PE/C (70:30) hybrid veil interleaved vinyl ester system (Broad arrow indicates impact point)

5.4.1.4 Polyester/Carbon (80:20) Hybrid Veil Interleaved Specimens

Figure 5.29 shows C-scan images for the Ep2 system specimens with damage width indicated. The damage spread is similar in tendency to the PE/C veil interleaved Ep2 system samples. The crack distribution is also similar to the PE/C veil interleaved case. The damage width increases significantly from 4J to 8J impact energy. The impact damage width from 8J to 12J, however, increases only slightly. A micrograph of the cross-section for a 12J impact damaged specimen is shown in Figure 5.30. The impact damage is a combination of intralaminar and interlaminar fractures, as shown in Figure 5.30. The damage behaviour is similar to the PE/C veil interleaved case. Some small delaminations are distributed in the interlaminar region. Moreover, the specimen is fractured under the impact point, unlike the PE/C veil interleaved cases.

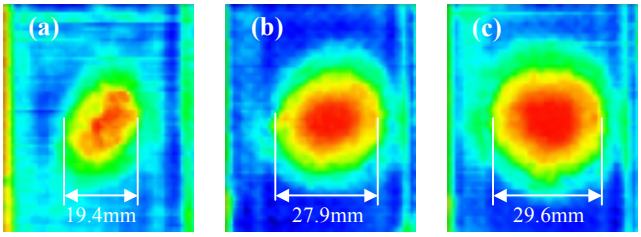

Figure 5.29 C-scan images of PE/C (80:20) hybrid veil interleaved specimens for epoxy2 system with measured damage width: (a) 4J, (b) 8J, (c) 12J impacted

Figure 5.30 Cross-section image of 12J impacted specimen for PE/C (80:20) hybrid veil interleaved epoxy2 system (Broad arrow indicates impact point)

C-scan images for the VE system specimens are shown in Figure 5.31. Compared to the Hyb1 veil interleaved laminates, the damage width is smaller. Figure 5.32 is a micrograph of cross-section for a 12J impacted specimen. The cracks are spread over a wide range. The fracture, on the other hand, cannot be recognised around the impact point. In the VE system specimen some short cracks propagated in the interlaminar region. The crack distribution is over a narrower range than the Hyb1 veil interleaved cases. Moreover, the suppression of the crack propagation is also better than the Hyb1 veil interleaved samples.

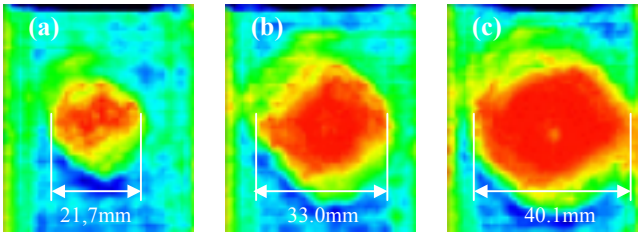

Figure 5.31 C-scan images of PE/C (80:20) hybrid veil interleaved specimens for vinyl ester system with measured damage width: (a) 4J, (b) 8J, (c) 12J impacted

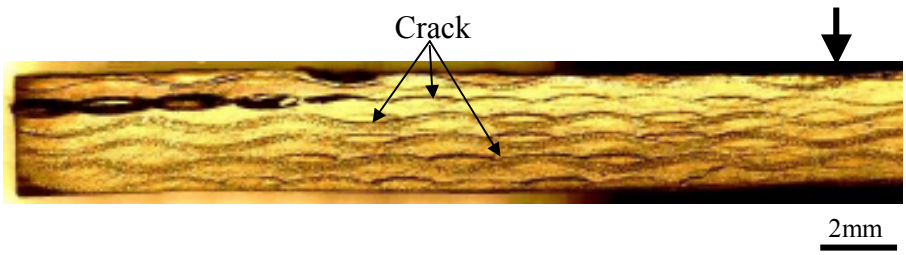

Figure 5.32 Cross-section image of 12J impacted specimen for PE/C (80:20) hybrid veil interleaved vinyl ester system (Broad arrow indicates impact point)

5.4.1.5 Polyester Veil Interleaved Specimens

Figure 5.33 shows C-scan images of the impact damage for the Ep2 system specimens. The damage width is slightly larger than the other veil interleaved laminates. Figure 5.34 shows a cross-section of a 12J impacted specimen for the Ep2 system. Although the cracks appear widespread, the crack propagation length is not long. In the Mode-I and Mode-II interlaminar toughness, the PE veil possesses superior toughening properties in all interleaf veils. The impact resistance, nevertheless, is not improved significantly. It is thought that the impact damage would grow rapidly. Consequently, to the suppression of the crack the interleaf veils could not contribute considerably.

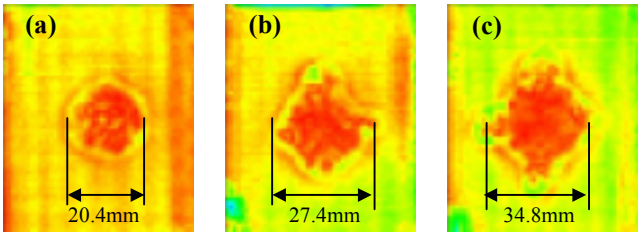

Figure 5.33 C-scan images of PE veil interleaved specimens for epoxy2 system with measured damage width: (a) 4J, (b) 8J, (c) 12J impacted

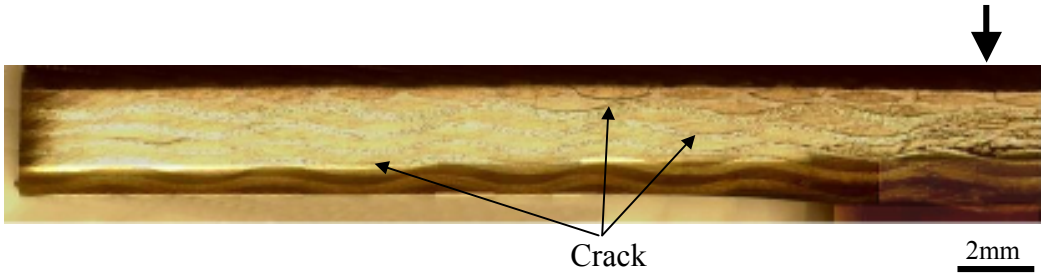

Figure 5.34 Cross-section image of 12J impacted specimen for PE veil interleaved epoxy2 system (Broad arrow indicates impact point)

C-scans of the VE system specimens are shown in Figure 5.35. The increase in damage width from 4J to 8J impact energy is larger than PE/C and Hyb2 veil interleaved composites. For 8J to 12J impact energy, the trend of the increase in damage width is similar to the other interleaved cases. Figure 5.36 indicates micrograph of the cross-section for a 12J impact damaged specimen. The crack length is longer than the Ep2 system samples, in particular at higher impact energies. Compared to the PE/C and hybrid veil interleaved specimens, the crack length seems short. However, the crack distribution is almost the same as the PE/C and hybrid veil interleaved samples.

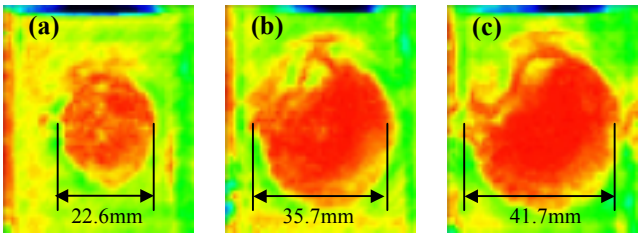

Figure 5.35 C-scan images of PE veil interleaved specimens for vinyl ester system with measured damage width: (a) 4J, (b) 8J, (c) 12J impacted

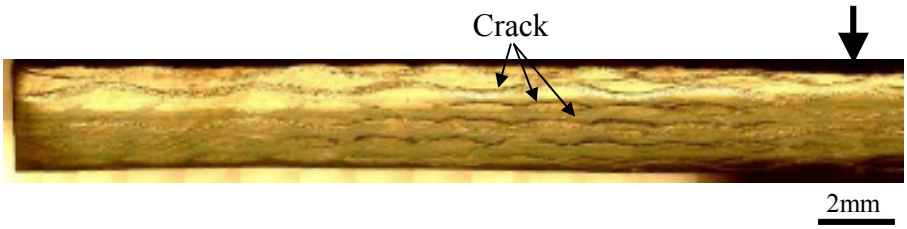

Figure 5.36 Cross-section image of 12J impacted specimen for PE veil interleaved vinyl ester system (Broad arrow indicates impact point)

5.4.1.6 Polyamide Veil Interleaved Specimens

Figure 5.37 shows C-scan images for the Ep2 system specimens. The damage width is quite smaller than the other interleaved cases. Moreover, it seems that the damage distribution is quite discontinuous. This phenomenon may contribute to the decreased impact damage by the PA veil. A microscope picture of the cross-section for a 12J impacted specimen is illustrated in Figure 5.38. From the image, the crack can barely be found in the interlaminar region. The fracture is also significantly smaller than the other interleaved samples. It is thought that the impact resistance can be improved considerably by the PA veils.

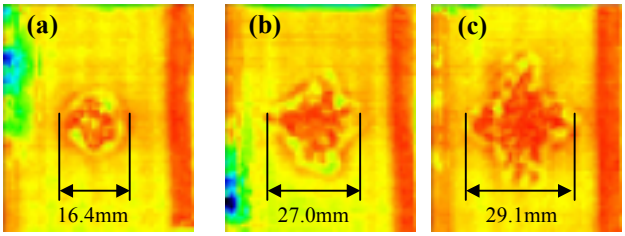

Figure 5.37 C-scan images of PA veil interleaved specimens for epoxy2 system with measured damage width: (a) 4J, (b) 8J, (c) 12J impacted

Figure 5.38 Cross-section image of 12J impacted specimen for PA veil interleaved epoxy2 system (Broad arrow indicates impact point)

Figure 5.39 shows C-scans of the VE system composites. The impact damage distribution is smaller than the other interleaved samples. The increase of the damage width is relatively moderate, compared to the other interleaved samples. Figure 5.40 is a micrograph of a cross-section of a 12J impact damaged specimen. The crack propagation length is significantly short. On the other hand, the specimen is fractured at the opposite side of impact point. It is thought that the PA veil can improve impact resistance in both resin systems.

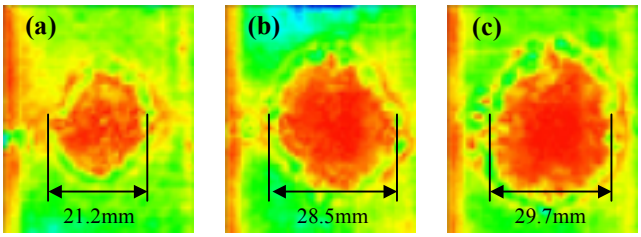

Figure 5.39 C-scan images of PA veil interleaved specimens for vinyl ester system with measured damage width: (a) 4J, (b) 8J, (c) 12J impacted

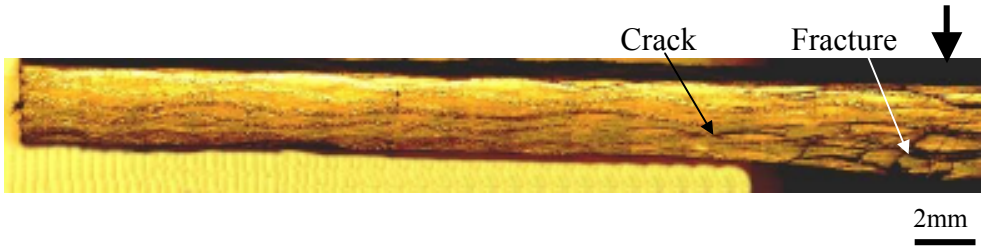

Figure 5.40 Cross-section image of 12J impacted specimen for PA veil interleaved vinyl ester system (Broad arrow indicates impact point)

For the Ep2 system specimens, growth of the damage width is quite small with increasing impact energy. The fracture modes are mainly two types, interlaminar delamination and intralaminar fracture under the impact point. The delaminations are not global but local in area. The damage resistance effects using the interleaf veils appear clearly. In particular, the PA veils provide an excellent contribution to the suppression of the impact damage spread. The delamination of the PA veil interleaved laminates is distributed unevenly. For the VE resin system specimens, the impact damage is dominated by delamination. Compared to the Ep2 system laminates, intralaminar fracture did not occur under impact point, except for the PA veil interleaved case. The difference of the damage width between each interleaved sample is not so much compared with the Ep2 system composites. However, the interleaf veils can improve impact damage moderately. In this resin system, the PE/C and PA veils contribute to the improvement of the impact damage resistance.

5.4.2 Compression After Impact Resistance

5.4.2.1 Non-Interleaved Specimens

Figure 5.41 shows micrographs of cross-sections of the CAI tested specimens. For the Ep2 system specimen, the compressive fracture is dominated mainly by interlaminar delmination and intralaminar breakage around the impact point, as shown in Figure 5.41 (a). The crack propagation speed at the interlaminar region was slow during CAI test, because the adhesion strength between the resin and carbon fabrics is strong. Hence it is thought that the impacted specimen was suddenly broken and fractured extensively. The crack behaviour for the VE system, on the other hand, is different from the Ep2 system. The fractured zone is narrower than the Ep2 resin cases, however the interlaminar crack length is longer as shown in Figure 5.41 (b). The catastrophic fracture of the VE system specimen did not occur so that the crack propagated gradually and constantly during the compression test. As a result, the CAI strength could not increase considerably.

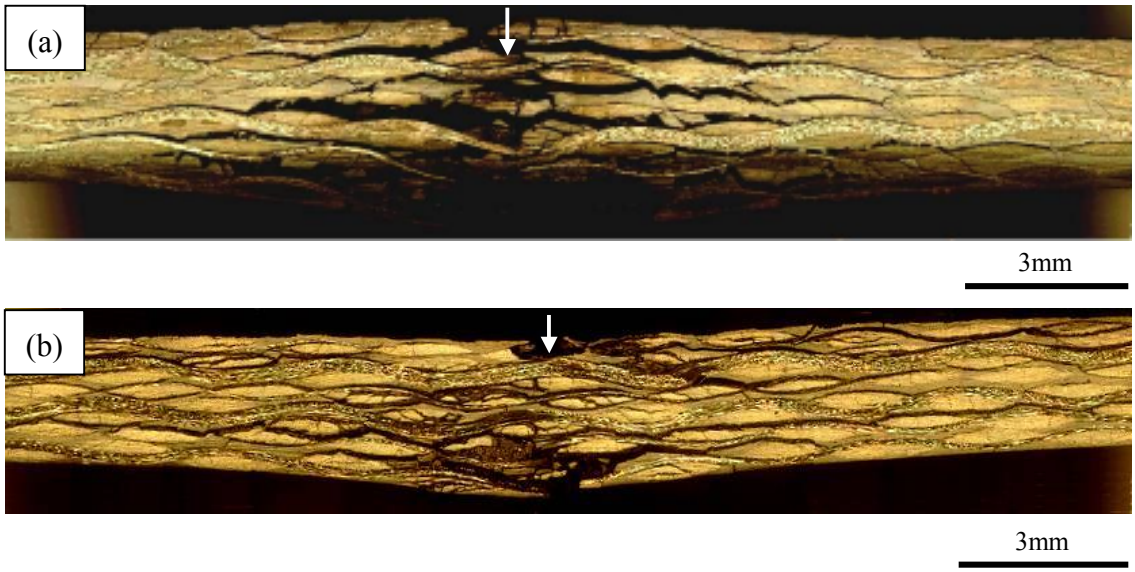

Figure 5.41 Cross-section images of CAI tested specimens for non-interleaved: (a) Epoxy2 system, (b) Vinyl ester system (White arrow indicates impact point)

5.4.2.2 Polyester/Carbon Veil Interleaved Specimens

Cross-section pictures of the CAI tested specimens are shown in Figure 5.42. For the Ep2 system, the tested specimen possesses a combination of the fracture and the crack propagation, as shown in Figure 5.42 (a). In particular, a large delamination is exhibited around the impact point. However, the fracture area is significantly smaller than the non-interleaved laminate. It is thought that the fracture could not grow largely because the crack propagation was gradual during the CAI test. On the other hand, the VE system specimen is not fractured at the surface, but the crack propagates in the interlaminar regions, as illustrated in Figure 5.42 (b). Compared to the non-interleaved VE system specimens, the crack distribution is not wide ranging. The interleaf veils would contribute to limiting the crack growth. The crack behaviour for both resin systems is similar. The crack propagated in the interlaminar region. SEM pictures of the cross-section are illustrated in Figure 5.43. From Figure 5.43 (a), it can be seen that some PE veil fibres are pulled out from the fracture surface. These pulled out fibres would work as bridging for crack suppression. For the VE system, pulled out veil fibres like the fibres that pulled out of the Ep2 system specimen are not seen in Figure 5.43 (b). The carbon woven fibres, on the other hand, are unravelled from the matrix. These unravelled fibres may suppress the crack propagation to some degree.

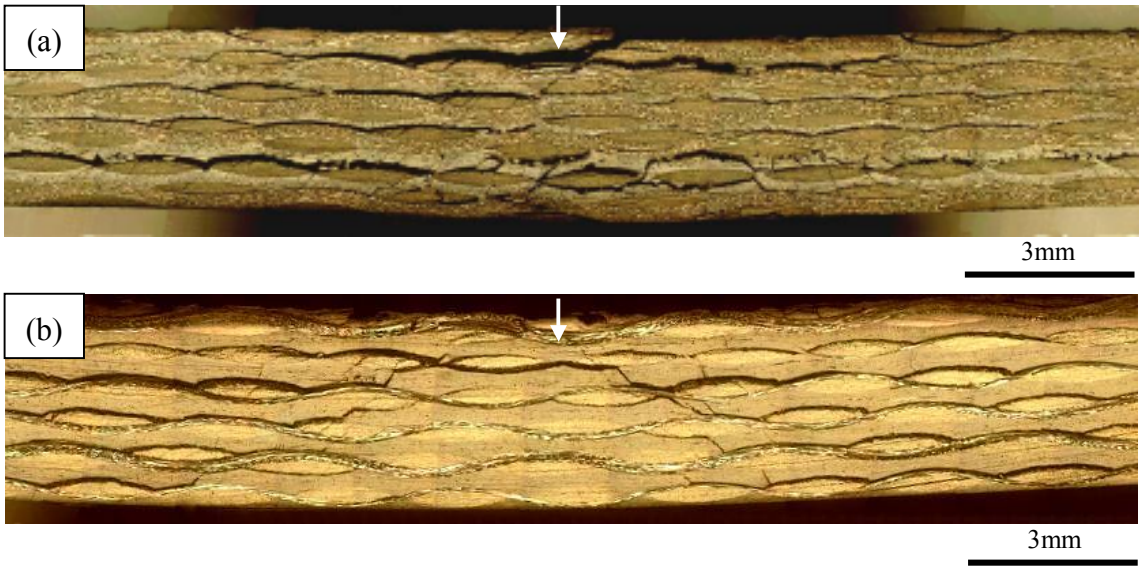

Figure 5.42 Cross-section images of CAI tested specimens for PE/C (100:100) veil interleaved: (a) Epoxy2 system, (b) Vinyl ester system (White arrow indicates impact point)

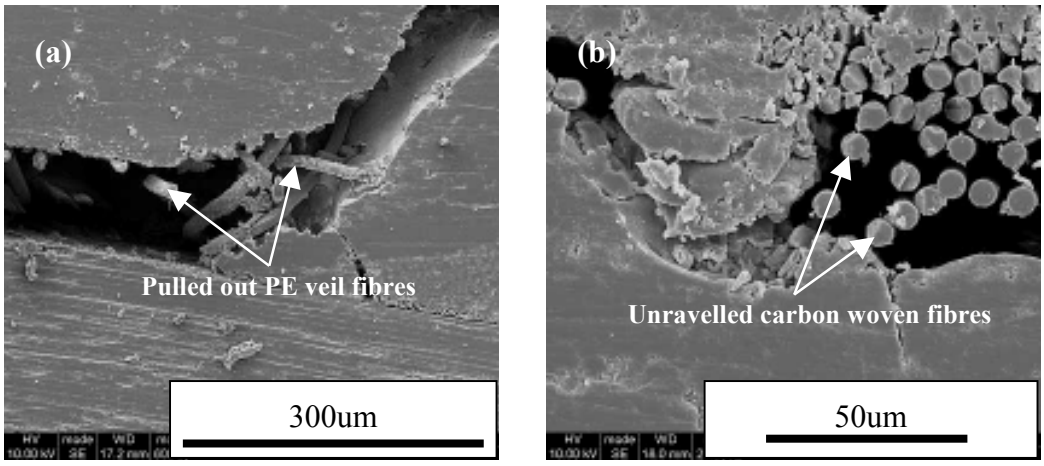

Figure 5.43 SEM pictures of CAI tested cross-section by 12J impact energy for PE/C (100:100) veil interleaved specimens: (a) Epoxy2 system, (b) Vinyl ester system

5.4.2.3 Polyester/Carbon (70:30) Hybrid Veil Interleaved Specimens

Figure 5.44 shows a micrograph of the cross-section for the CAI tested specimen. As seen in Figure 5.44, the specimen is not completely fractured, but many cracks have propagated at the interlaminar region. It seems that the interleaf veils could not suppress crack propagation at the interlaminar region. The CAI strength for 12J impact energy,

however, is slightly higher than the non-interleaved case (see in Figure 5.18 and Table 5.5). The Hyb1 veils, therefore, provide a partial suppression of the compression fracture. Figure 5.45 shows a SEM photograph of the cross-section of a 12J impacted laminate. It can be seen that some Hyb1 veil fibres are pulled out. However, many Hyb1 veil fibres may be embedded in the matrix and seem not to contribute considerably to the suppression of the crack propagation.

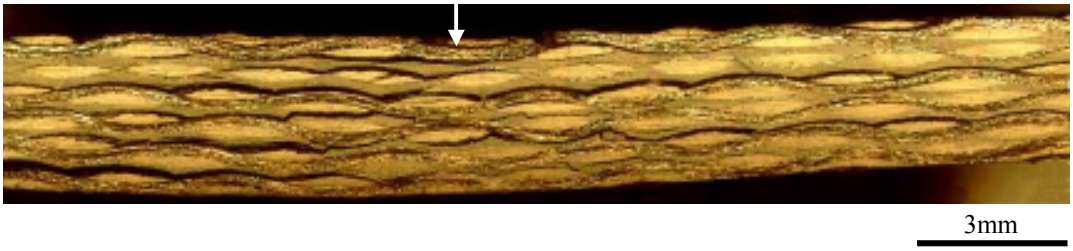

Figure 5.44 Cross-section image of CAI tested specimens with for PE/C (70:30) hybrid veil interleaved vinyl ester system (White arrow indicates impact point)

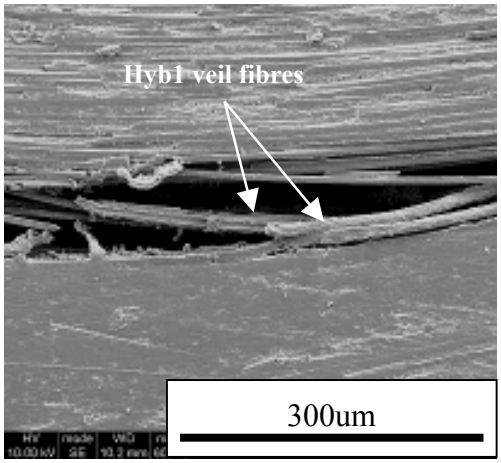

Figure 5.45 SEM picture of CAI tested cross-section by 12J impact energy for PE/C (70:30) hybrid veil interleaved vinyl ester system specimen

5.4.2.4 Polyester/Carbon (80:20) Hybrid Veil Interleaved Specimens

The cross-section pictures of the CAI tested specimens are shown in Figure 5.46. The fracture situations in both resin systems are almost the same. Many cracks pass through the interlaminar region. For the Ep2 system specimen, the crack distribution extends by going to the bottom of the sample, as illustrated in Figure 5.46 (a). When the CAI test was carried out, the compressive fracture of the specimen seemed to progress

gradually. The specimen, therefore, did not fracture sharply. On the other hand, the crack for the VE system specimen propagated through every layer, as shown in Figure 5.46 (b). The crack behaviour is similar to the Hyb1 veil interleaved laminates. The Hyb2 veils contribute slightly to the crack suppression. SEM micrographs of the cross-section for 12J-impacted specimens are shown in Figure 5.47. For the Ep2 system, it can be seen that some Hyb2 veil fibres are pulled out from the matrix, as shown in Figure 5.47 (a). When the crack passed through interlaminar areas, some pulled out veil fibres would work as bridging. Nevertheless, the CAI strength is only slightly improved. It is thought that the fracture resistance by the interleaf veils could not appear, because pulled fibres were not many. Many veil fibres would be embedded in the matrix. On the other hand, pulled out veil fibres for the VE system are not seen in the cross-section, as illustrated in Figure 5.47 (b). The Hyb2 veils seem to be embedded in the matrix. However, the unravelled carbon fabric and a few pulled out veil fibres in the VE resin work to provide marginally suppression of the crack progress.

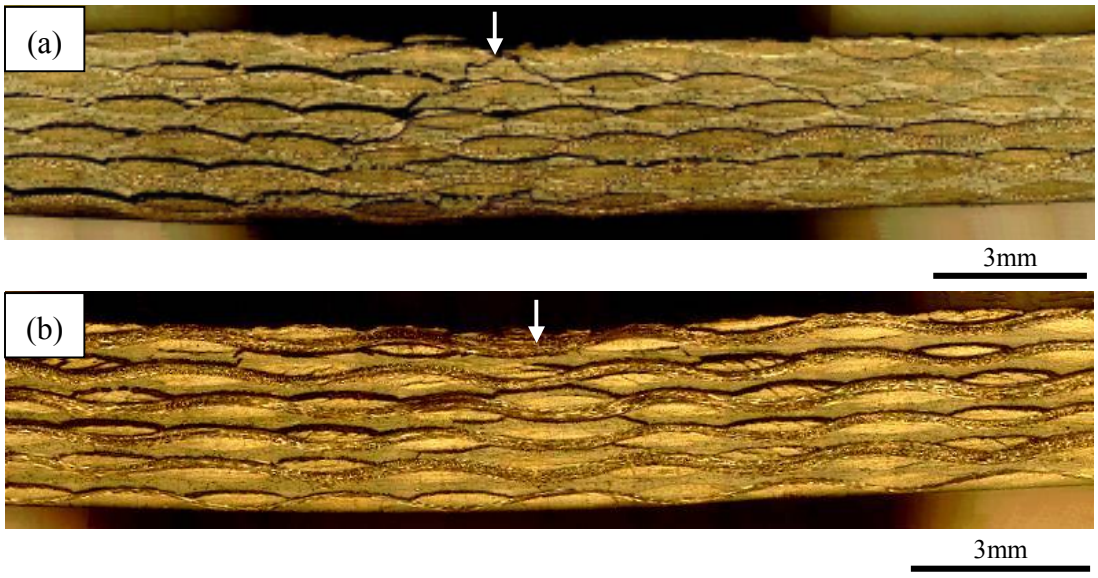

Figure 5.46 Cross-section images of CAI tested specimens for PE/C (80:20) hybrid veil interleaved: (a) Epoxy2 system, (b) Vinyl ester system (White arrow indicates impact point)

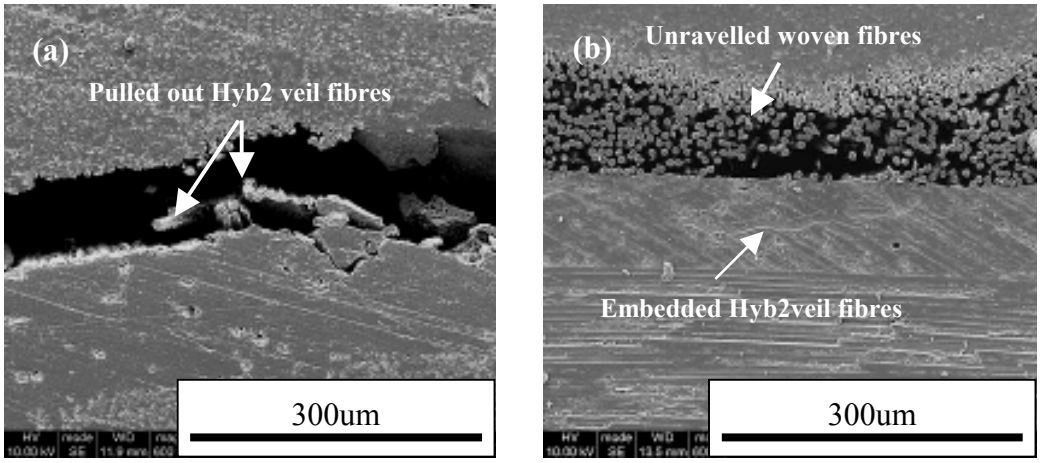

Figure 5.47 SEM pictures of CAI tested cross-section by 12J impact energy for PE/C (80:20) hybrid veil interleaved specimens: (a) Epoxy2 system, (b) Vinyl ester system

5.4.2.5 Polyester Veil Interleaved Specimens

Figure 5.48 shows cross-section images of the CAI tested specimens. The specimen in the Ep2 system is fractured around the impacted point, as shown in Figure 5.48 (a). The crack length in the interlaminar area is significantly short, as compared with the PE/C and Hyb2 veil interleaved cases. It has been mentioned that the PE veils interleaved specimens possess high Mode-I and Mode-II energy release rates in Chapter 3 and 4. The PE veils could suppress crack propagation during compressive fracture. The specimen, therefore, was catastrophically broken at the impacted point, because crack propagation was significantly slow. The VE system specimen is not fractured around the impact point, as illustrated in Figure 5.48 (b). Some long cracks can be seen in the interlaminar region. The cracks are distributed through some layers, but not every layer. Figure 5.49 shows SEM pictures of the cross-section of 12J impacted laminates. From Figure 5.49 (a), many PE veil fibres are pulled out from the fracture area compared with the other interleaved specimens. The PE veil would contribute significantly to the improvement of the CAI resistance because many pulled out veil fibres will provide fibre-bridging and suppress fracture progress. The CAI fracture is a static fracture progress. It is thought that the pulled out veil fibres can work for the static fracture mode, not dynamic fracture mode. Therefore, the interleaf veils can contribute to the improvement of the CAI resistance property, unlike the impact damage. For the VE system, the PE veil fibres adhered to matrix, not pulled out, as shown in Figure 5.49 (b). Therefore the CAI strength is improved moderately only.

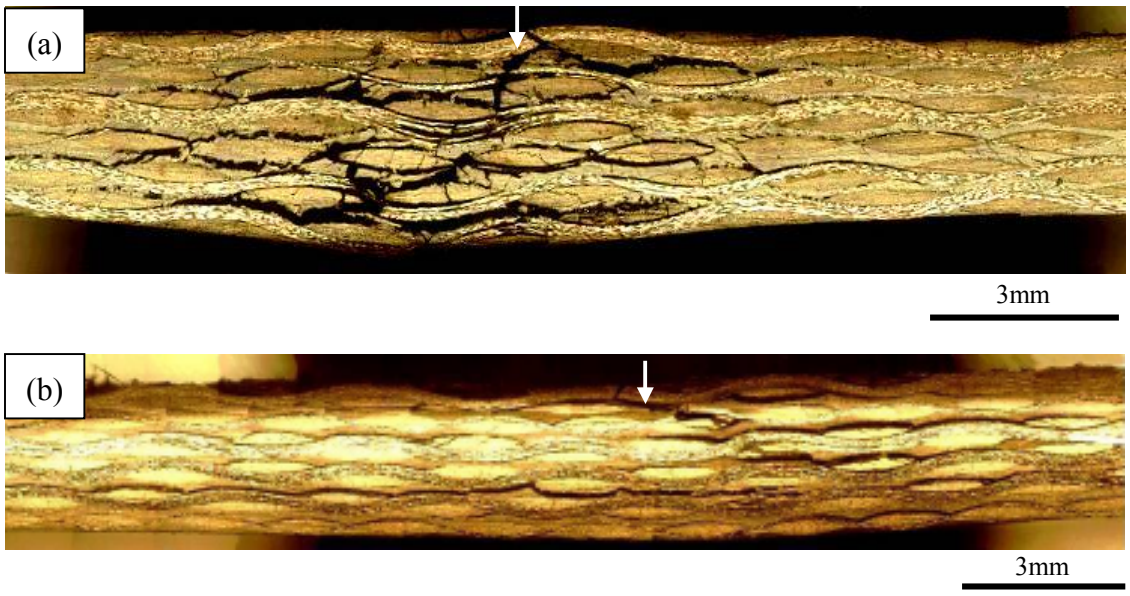

Figure 5.48 Cross-section images of CAI tested specimens for PE veil interleaved: (a) Epoxy2 system, (b) Vinyl ester system (White arrow indicates impact point)

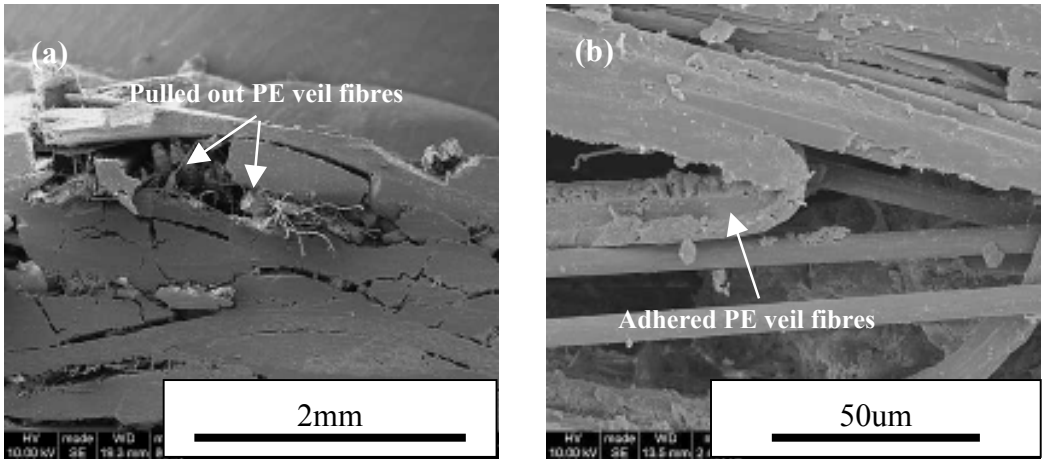

Figure 5.49 SEM pictures of CAI tested cross-section by 12J impact energy for PE veil interleaved specimens: (a) Epoxy2 system, (b) Vinyl ester system

5.4.2.6 Polyamide Veil Interleaved Specimens

Figure 5.50 shows micrographs of the cross-section for of CAI tested specimens with both resin systems. Some black points in the cross-section images, as shown in Figure 5.50 (a), indicate the PA veils. The specimen was fractured catastrophically and locally. A few cracks propagated in intralaminar region. However the cracks in the interlaminar area barely propagated. It is thought that the crack hardly propagated

during compressive collapse because the adhesion between the PA veils and the Ep2 resin is quite strong. The PA veils interleaved specimens, therefore, seem to be catastrophically collapsed over a critical compressive strength, even if the crack hardly progressed. For the VE system, the specimen has many cracks in the interlaminar region, as shown in Figure 5.50 (b). The crack length is shorter than the other interleaved samples. The PA veils can improve the crack propagation resistance in the interlaminar zone. SEM photographs of the cross-section for 12J impacted laminates are illustrated in Figure 5.51. The compressive fracture in the Ep2 system specimen appears at the intralaminar region, as shown in Figure 5.51 (a). On the other hand, the interlaminar crack would hardly grow due to the PA veils. The fracture mode in the Ep2 system specimen is dominated by fibre breakage and intralaminar fracture. Consequently, the compression collapse would be catastrophic and the CAI strength can increase considerably up to a critical point. From both Figure 5.50 (a) and 5.51 (a), The PA veil fibres in the Ep2 system are seen not to pull out completely. On the other hand, some PA veil fibres for the VE system are seen to pull out, as illustrated in Figure 5.51 (b). In this resin system, the PA veil fibres would contribute to the improvement of the CAI by pulled out fibres.

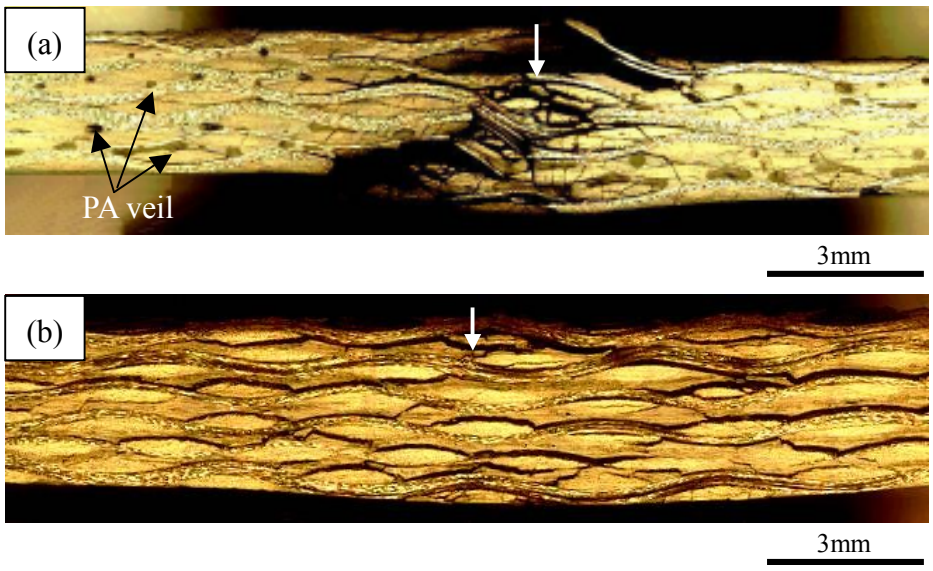

Figure 5.50 Cross-section images of CAI tested specimens for PA veil interleaved: (a) Epoxy2 system, (b) Vinyl ester system (White arrow indicates impact point)

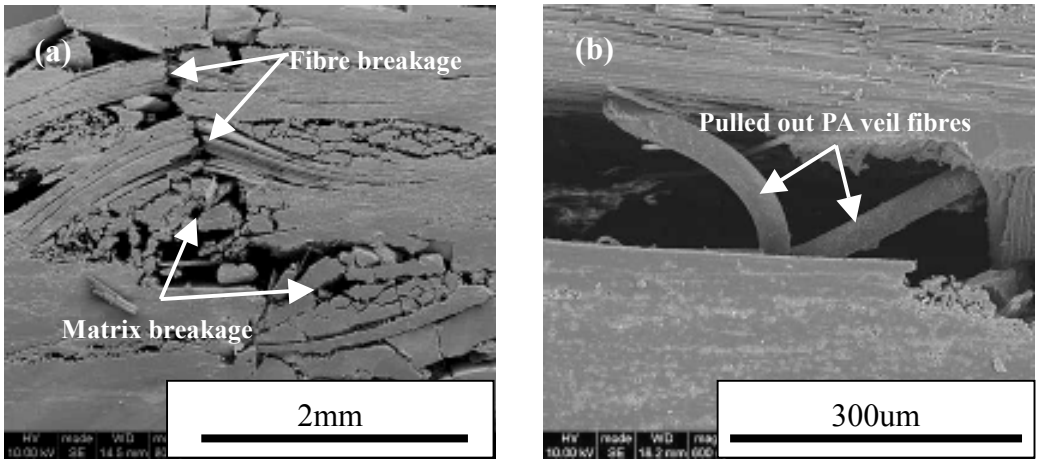

Figure 5.51 SEM pictures of CAI tested cross-section by 12J impact energy for PA veil interleaved specimens: (a) Epoxy2 system, (b) Vinyl ester system

The crack propagation in the interlaminar region is significantly small in the Ep2 system specimens. These specimens tend to be fractured around the impacted point. From observation of cross-section of the tested samples, the adhesion between the matrix and carbon woven fabrics is quite strong. Therefore, it is thought that the crack hardly propagates at the interlaminar region, and the specimen would collapse catastrophically over the critical point. The PE/C and Hyb2 veils contribute to the CAI strength only slightly. The CAI property in the PE veil interleaved laminate is improved considerably. In these veil interleaved specimens, pulled out veil fibres would work for crack suppression. Surprisingly, the PA interleaved veils possess excellent post-impact compression resistance, even if the veil fibres are not pulled out. In this veil, the adhesion between the matrix and veil fibres seems to contribute to the suppression of the fracture progress. For the VE system, the CAI strength values between each interleaved laminate are quite similar (see in section 5.3.3). The fracture resistance by interleaf veils would be improved slightly by some pulled out veil fibres. Moreover, the carbon woven fabric was also pulled out and unravelled from the matrix. The unravelled carbon fabrics and pulled out veil fibres worked marginally to provide a bridging effect for crack suppression. Consequently, the difference of the CAI strength between interleaved specimens is not so much.

Previous work mentioned that the CAI property is affected by resin [216]. The Ep2 system specimens are dominated by a combination of intralaminar and interlaminar fracture modes. The VE system specimens, on the other hand, are mainly interlaminar

delamination. It is thought that the adhesion between the matrix and fabric may influence the fracture mode.

5.5 Conclusions

As a result of evaluating the study for impact and CAI resistances by non-woven veil interleaved CFRP, the following conclusions are drawn:

(1) For impact damage tolerance by interleaf veils with the Ep2 system, the PA veil interleaved specimens exhibited an excellent improvement for all impact energies. The PE/C veil interleaved laminates showed the second smallest damage area after impact at 4J impact energy. However, the damage width for higher impact energies is similar value to the Hyb2 and PE veil interleaved cases. The PE veil interleaved samples did not show a considerable increase in impact damage resistance, unlike their improvement in Mode-I and Mode-II interlaminar toughness.

(2) The impact damage widths of all VE system were overall larger than those of the Ep2 system laminates. In this resin system, the tendency of the damage resistance by the interleaf veils was almost the same as the Ep2 system, except for the PE/C veil interleaved case. The PE/C and PA veils in this resin system contributed to the improvement of the impact resistance considerably.

(3) The CAI strengths for the PE/C and Hyb2 veil interleaved specimens are almost the same values as the non-interleaved samples, nevertheless the impact resistance is good. In contrast, the PE veils interleaved specimens have the second highest CAI strength, even if the impact resistance is poorer than the other veil interleaved cases. The crack suppression by pulled out veil fibres would be effective only in static fracture. Therefore, the interleaf veils could not contribute to the suppression of impact damage which is a dynamic fracture. The PA veil interleaved laminates significantly improve the CAI resistance. The adhesion between the PA veil fibres and matrix resin would play an important role in improving impact and CAI resistance.

(4) The CAI strengths in the VE resin system composites are quite lower than that in the Ep2 system cases. Compared to the Ep2 system specimens, the CAI behaviour for the VE system laminates showed a different tendency. For the non-interleaved specimens, the CAI strength reduced at a faster rate after 4J impact energy. On the

other hand, the reduction of CAI strength for the interleaved specimens was gradual. In this resin system, the PE/C and PA veil interleaved specimens are superior in CAI strength to the other interleaved samples, in particular after a high impact energy. The fracture in the VE system would initiate at an early stage because of poor adhesion between the matrix and carbon fabric.

Chapter 6

Correlation between Mode-I & Mode-II Interlaminar Toughness, Impact, and CAI Properties

6.1 Introduction

Each property (Mode-I and Mode-II energy release rate, G_I and G_{II}, impact damage width, and CAI strength) of the non-woven veil interleaved CFRP has been evaluated and discussed in previous chapters. In this chapter, the correlation between each property obtained by each fracture tests is evaluated and discussed. Moreover, the results of this research are compared with previous literatures.

6.2 Materials and Experiments Information

The details of materials and specimens are mentioned in previous chapters. Tables 6.1 and 6.2 show lists of specimens for four tests, DCB, 4ENF, impact, and CAI tests. For the Mode-I and Mode-II tests, the Ep1 and the VE resins were chosen for the 5-harness satin weave and the unidirectional fabrics. The Ep2 and the VE resins, on the other hand, were selected for the plain weave fabric. 6 types of the interleaf veils were used. For the impact and CAI tests, the base material was the plain weave fabric only, and the resins were Ep2 and VE matrices.

Table 6.1 List of specimens for Mode-I and Mode-II interlaminar toughness tests (The circle mean experimented specimen)

	5-harness satin			Unidirectional			Plain (HAW¥)			Plain (LAW¥¥)		
Interleaf	Ep1*	Ep2**	VE+	Ep1	Ep2	VE	Ep1	Ep2	VE	Ep1	Ep2	VE
Non	○		○	○		○		○	○		○	
PE/C#						○			○		○	
Hyb1$	○			○		○			○			
Hyb2$$	○			○		○			○		○	
Carbon	○			○		○						
PE	○		○	○		○			○		○	
PA	○		○	○		○			○		○	

¥: High areal weight, ¥¥: Low areal weight, *: CYCOM 823R, **: MVR444, +: DION9102-500, #: Polyester/Carbon (100:100) veils, $: Polyester/Carbon (70:30) hybrid veil, $$: Polyester/Carbon (80:20) hybrid veil

Table 6.2 List of specimens for impact and CAI tests

	Plain (HAW)		Plain (LAW)	
Interleaf	Ep2	VE	Ep2	VE
Non	○	○		○
PE/C	○	○		
Hyb1		○		
Hyb2	○	○		
PE	○	○		
PA	○	○		○

6.3 Correlation between Mode-I and Mode-II Interlaminar Toughness Properties

6.3.1 5-harness Satin Weave Fabric Specimens

Figure 6.1 plots the Mode-II initial energy release rate as a function of the Mode-I initial energy release rate for the 5-harness satin weave specimens. The $G_{IC\text{-}NL}$ data used in this chart are the MBT (modified beam theory) values. In the diagram, blue line means the fitted line for the Ep resin specimens. Blue chain line indicates the fitted line for the VE system laminates. For the Ep1 system, there can be seen a good correlation between the $G_{IC\text{-}NL}$ and $G_{IIC\text{-}NL}$ values. The general trend is that the $G_{IC\text{-}NL}$ values increase with an increase in the $G_{IIC\text{-}NL}$ values. A correlation for the VE system is also good, but with a flat relationship. The $G_{IC\text{-}NL}$ values for all VE specimens are almost the same. The Mode-II initial energy release rate for the VE system is influenced relatively more than the Ep1 system samples. In contrast, the Mode-I initial energy release rate is not affected by interleaf veils. The difference of the matrix types would affect the relationship between the G_{IC} and G_{IIC} values.

Figure 6.2 shows the correlation between the $G_{I\text{-}prop}$ and $G_{II\text{-}prop}$ values. Compared to the initiation values for both fracture modes, the correlation for the Ep1 system specimens is quite poor. In particular, the Hyb2 interleaved case has an outlier in the $G_{II\text{-}prop}$ value. The propagation values for the Ep1 system do not show a clear correlation, unlike the initial values. The improvement of the Mode-I energy release rate values by the interleaf veil is less than that of the Mode-II interlaminar toughness. In other words, the interleaf veils contribute more to the improvement of shear mode than to the delamination mode. On the other hand, it can be seen that the correlation in the VE system materials is better than the Ep1 system cases. As compared with the initial value, both $G_{I\text{-}prop}$ and $G_{II\text{-}prop}$ values are widely spread. The interleaf veils in the VE system bring about an effect to the shear fracture resistance rather than the delamination fracture resistance. In the Ep1 system interleaved specimens, except for the PE veil interleaved laminates, crack propagation was unstable and jumped. This behaviour would affect a correlation between $G_{I\text{-}prop}$ and $G_{II\text{-}prop}$ values. In the VE resin composites the cracks propagated in a stable and gradual manner. Therefore, a correlation between both modes propagation values would appear clear.

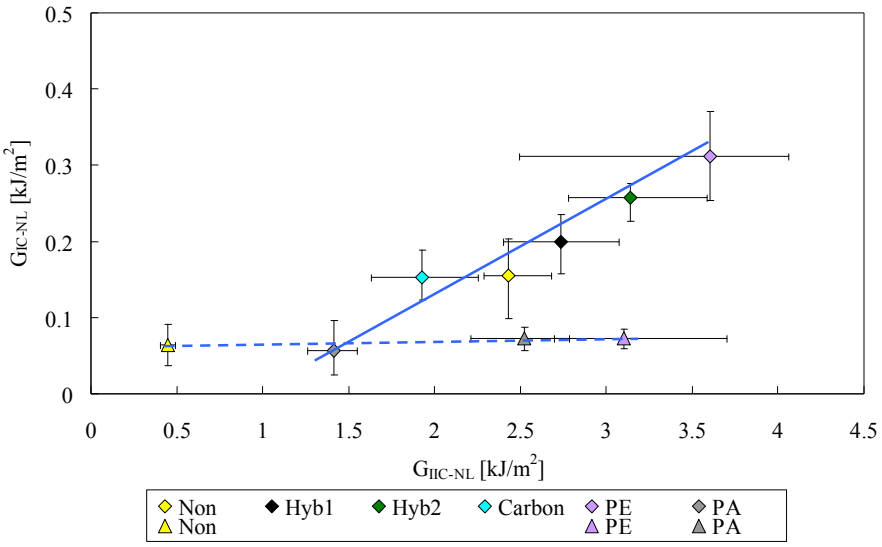

Figure 6.1 Relationship between $G_{IC\text{-}NL}$ and $G_{IIC\text{-}NL}$ for 5-harness satin weave fabric both resin system specimens (Diamond is Ep1 system and Triangle is VE system)

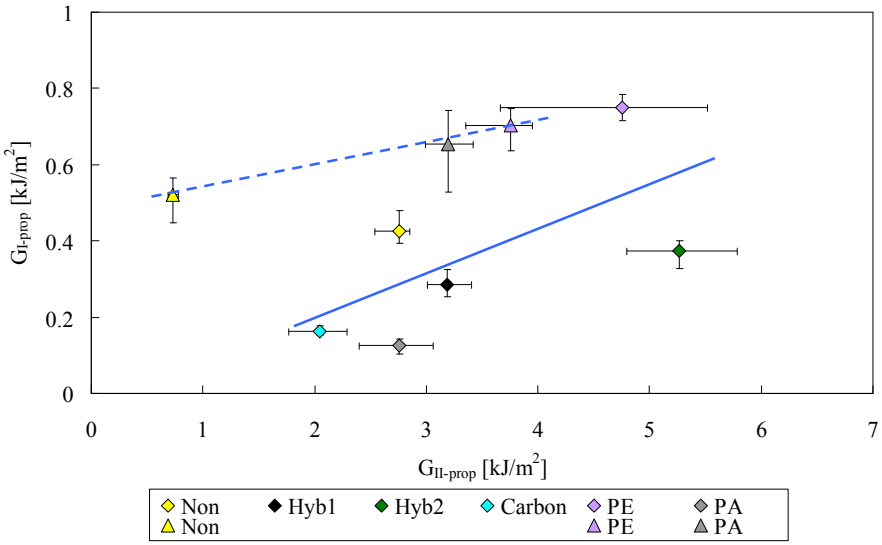

Figure 6.2 Relationship between $G_{I\text{-}prop}$ and $G_{II\text{-}prop}$ for 5-harness satin weave fabric both resin system specimens (Diamond is Ep1 system and Triangle is VE system)

6.3.2 Unidirectional Fabric Specimens

Correlations between the Mode-I and Mode-II initial energy release rate values for the unidirectional fabric composites are shown in Figure 6.3. For the Ep1 system, the correlation is not seen clearly, unlike the satin weave specimens. While the G_{IIC} values in the Ep1 system seem to be strongly influenced by interleaf veil, the difference in the G_{IC} values between each interleaved sample is small. However, data variation for the Ep1 resin system is larger than the VE system specimens. In particular, the Hyb2 veil interleaved specimens have wide error bars. For the VE system, the data spread of the both $G_{IC\text{-}NL}$ and $G_{IIC\text{-}NL}$ is significantly smaller than the Ep1 system cases.

The correlation between the propagation values of both fracture modes is illustrated in Figure 6.4. In the case of the Ep1 system, there is no clear relationship between the $G_{I\text{-}prop}$ and $G_{II\text{-}prop}$. The increase of the propagation values from the initiation values is moderate, except for the carbon veil interleaved specimen which does not show any improvement. For the VE system, the trend is similar to the relationship for the initial properties. While the $G_{I\text{-}prop}$ values are increased significantly by the type of the interleaf veil, the increase of the $G_{II\text{-}prop}$ values is small. Compared to the 5-harness satin weave laminates, the UD samples with the VE system did not exhibit a large improvement in the Mode-II interlaminar toughness. In this resin and fabric system, the UD carbon fabrics occurred fibre-bridging during crack propagation. This effect leaded to the high G_{IC} value. However, it did not contribute to the G_{IIC} values. In section 6.3.1, it is mentioned that the resin system affects both fracture mode energy release rates. In this section, it is suggested that the type of the fabric used as the basis for the material also has an influence on the correlation between the interlaminar toughness properties in each mode.

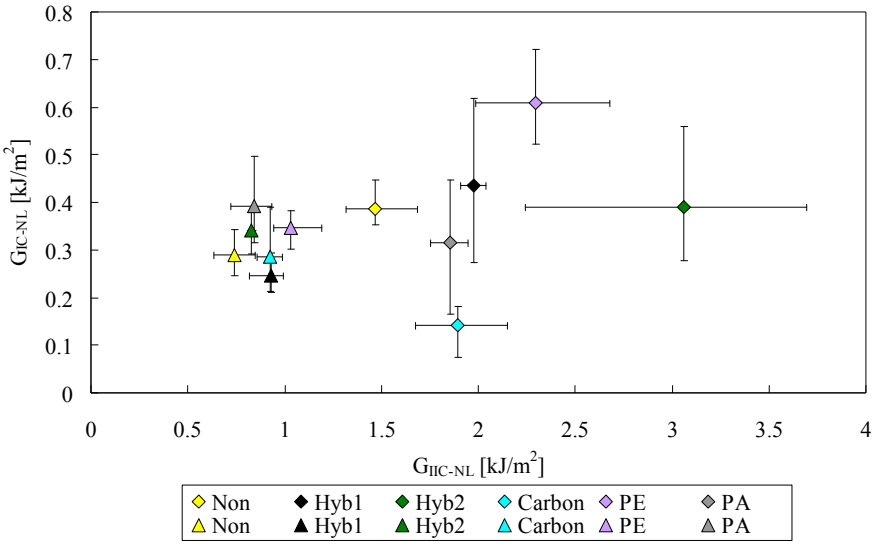

Figure 6.3 Relationship between $G_{IC\text{-}NL}$ and $G_{IIC\text{-}NL}$ for unidirectional fabric both resin system specimens (Diamond is Ep1 system and Triangle is VE system)

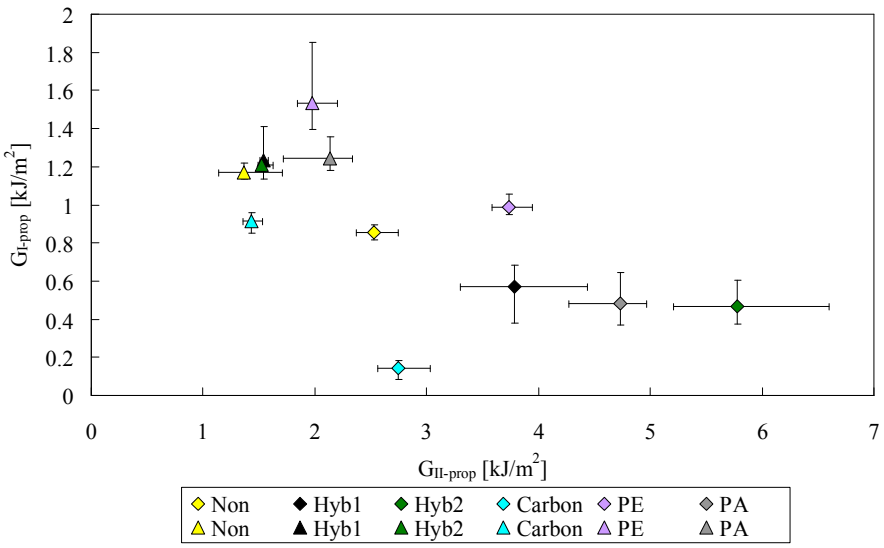

Figure 6.4 Relationship between $G_{I\text{-}prop}$ and $G_{II\text{-}prop}$ for unidirectional fabric both resin system specimens (Diamond is Ep1 system and Triangle is VE system)

6.3.3 Plain Weave Fabric Specimens

Figure 6.5 shows a diagram of the $G_{IIC\text{-}NL}$ against $G_{IC\text{-}NL}$ values. The correlation between Mode-I and Mode-II interlaminar toughness in both resin systems has a similar tendency to the results of the 5-harness satin weave materials. The relationship between the initial values is linear for the Ep2 system, but flat for the VE system. The PE and PA veil interleaved specimens exhibit excellent interlaminar toughness properties. In particular, the PA veil interleaved specimen has high G_{IC} for Ep2 system and G_{IIC} values for both resin systems. However, the PE/C and Hyb2 veil interleaved laminates do not show the improvements of the interlaminar toughness. For the VE system, the results are similar to the satin weave data. While spread of the $G_{IC\text{-}NL}$ values is quite narrow, the $G_{IIC\text{-}NL}$ values are extended over a wide range.

The relationship of the propagation values in both modes is plotted in Figure 6.6. For both resin systems, the relationships between the Mode-I and Mode-II propagation values show almost the same trend as the initial values. In both resin systems, the PE and PA veil interleaved composites possess superior initial and propagation values compared with the other interleaved systems. For the VE system, the gradient of the line linking Mode-I and Mode-II propagation values is slightly steeper than that linking the initiation values, which is a very flat relationship.

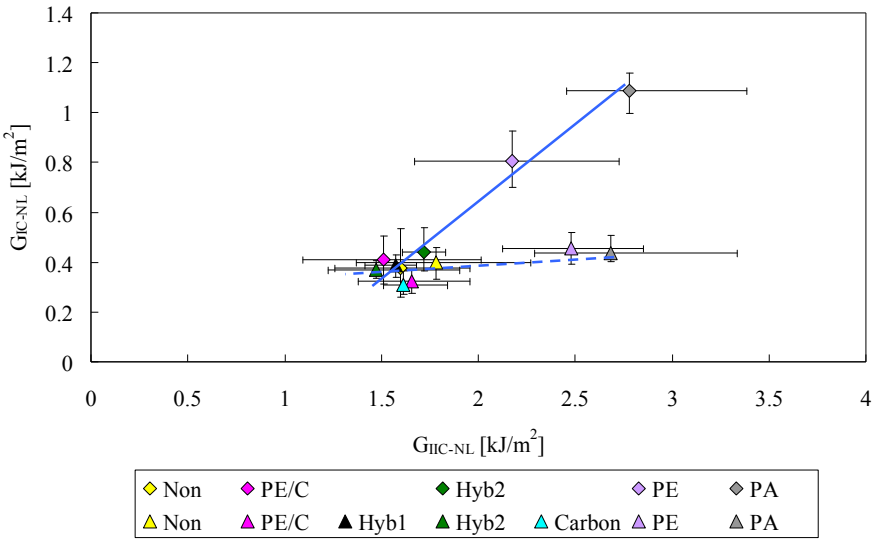

Figure 6.5 Relationship between $G_{IC\text{-}NL}$ and $G_{IIC\text{-}NL}$ for plain weave fabric both resin system specimens (Diamond is Ep2 system and Triangle is VE system)

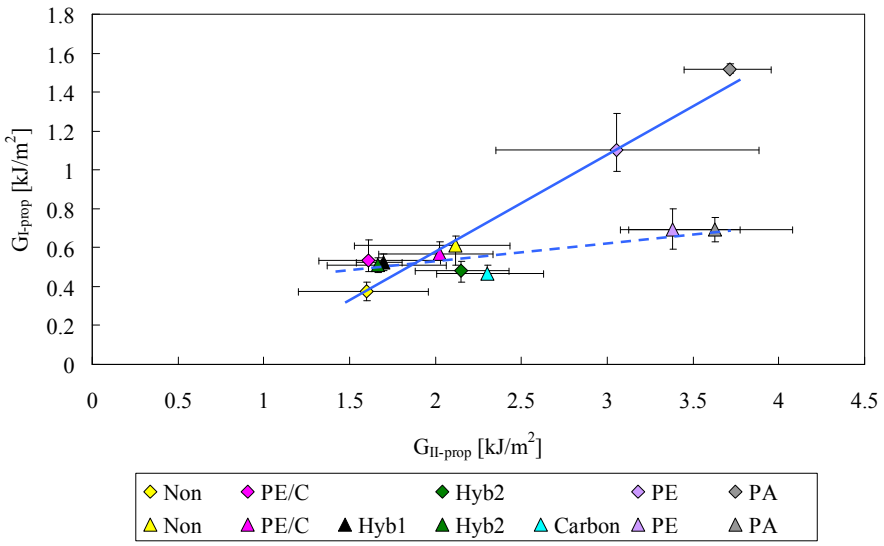

Figure 6.6 Relationship between $G_{I\text{-}prop}$ and $G_{II\text{-}prop}$ for plain weave fabric both resin system specimens (Diamond is Ep2 system and Triangle is VE system)

In this section, the correlation between the Mode-I and Mode-II interlaminar toughness is discussed. Firstly, the difference of the resin system is considered with respect to its influence on interlaminar toughness properties in both modes. For the Ep system, the spread of the G_{IC} values is larger than for the VE system specimens. It is thought that the Mode-I energy release rate would be affected strongly by resin system. On the other hand, the difference between energy release rate values in both modes in the VE system is small. Secondly, the type of the fabric also affects the correlation between Mode-I and Mode-II interlaminar toughness. Although the woven specimens exhibit a linear relationship between G_{IC} and G_{IIC} values, the UD specimens do not show any clear correlation. The VE system composites show only a small variation between each interleaved system. For UD fabric and VE system, the interleaf veils do not contribute significantly to the Mode-II interlaminar toughness. The carbon fabrics are unravelled and the interleaf veils are embedded in the matrix.

6.4 Correlation between Mode-I and Mode-II Interlaminar Toughness, and Impact Damage Width

The correlation between the Mode-I energy release rate and the damage width is shown in Figures 6.7 and 6.8. The damage width data is that resulting from a 4J impact energy. The difference of the correlation within each resin system is clear. For the Ep2 system, the variation of the damage width is small even for wide variations in $G_{IC\text{-}NL}$ values. It can be seen that the relationship is flat. On the other hand, the damage width in the VE system laminates is distributed widely compared with the Ep2 system laminates. In contrast, the $G_{IC\text{-}NL}$ values are in a narrow range. For the propagation values and damage width, the tendency is similar to the initial values. For Mode-I energy release rate and damage width, correlation for the Ep2 system specimens appears flat. However, there is no clear correlation for the VE system laminates.

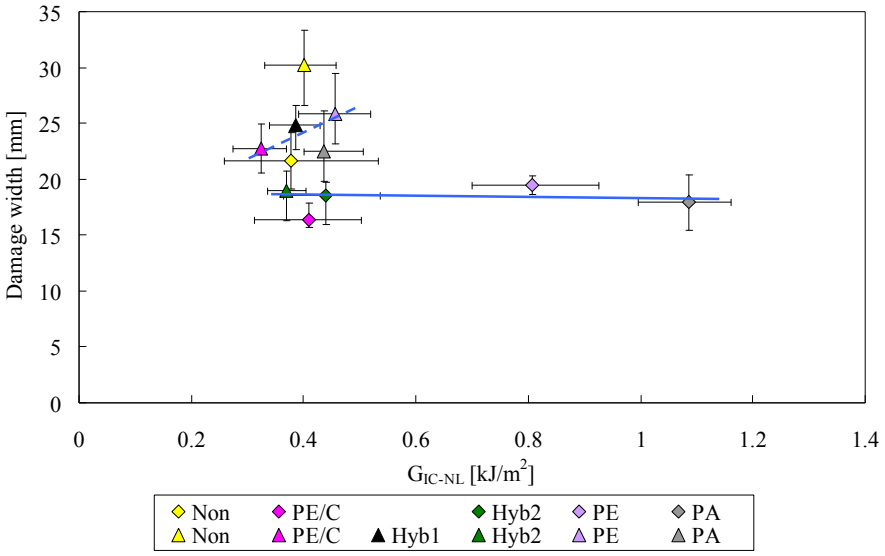

Figure 6.7 Relationship between $G_{IC\text{-}NL}$ versus damage width (4J of impact energy) for both resin system specimens with error bars (Diamond is Ep2 system and Triangle is VE system)

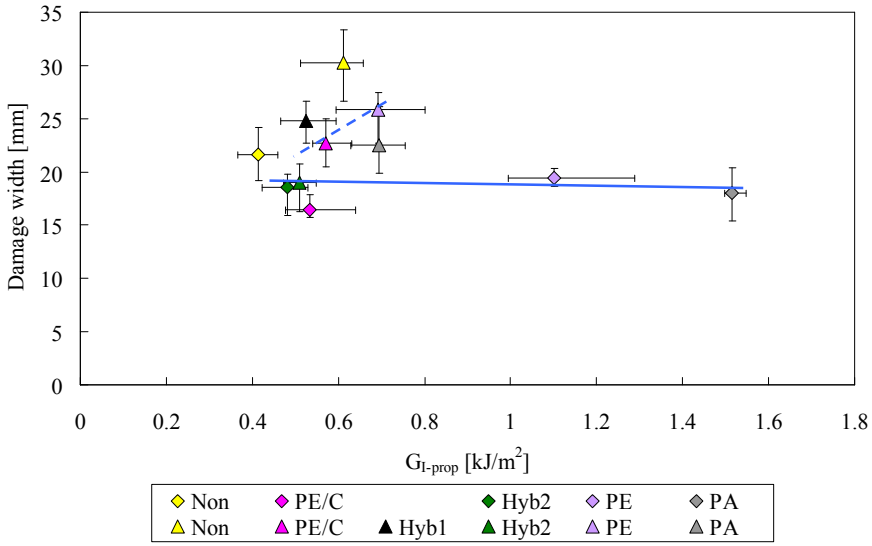

Figure 6.8 Relationship between $G_{I\text{-}prop}$ versus damage width (4J of impact energy) for both resin system specimens with error bars (Diamond is Ep2 system and Triangle is VE system)

Figures 6.9 and 6.10 show the comparison of the relationship of the Mode-II initial and propagation values with the damage width for both resin system. In the Ep2 system, the correlation between the Mode-II initial values and the damage width is similar in behaviour to the Mode-I initial values. In the VE system, the relationship between initiation values and damage width is different behaviour from the Mode-I interlaminar toughness as shown in Figure 6.7 and 6.9. The $G_{IIC\text{-}NL}$ values for the VE system distribute over a wide range. The correlation between $G_{II\text{-}prop}$ and damage width is the same trend as that between $G_{IIC\text{-}NL}$ values and damage width. In the Mode-II energy release rate, a clear correlation does not appear in the same way as the Mode-I energy release rate. The DCB and 4ENF tests are static fracture. However, the impact damage progresses dynamical. Therefore the clear correlation would not appear to be due to the different behaviour between the Mode-I and Mode-II fracture, and the impact damage

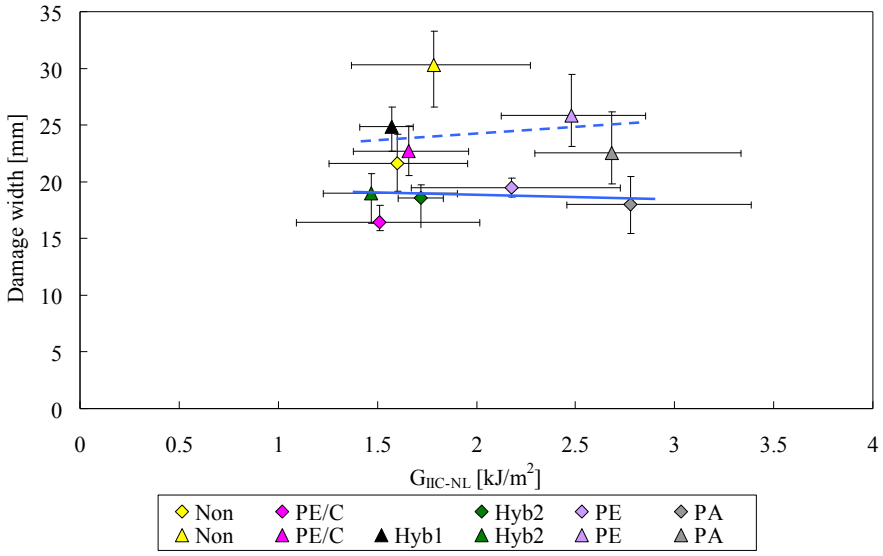

Figure 6.9 Relationship between $G_{IIC\text{-}NL}$ versus damage width (4J of impact energy) for both resin system specimens with error bars (Diamond is Ep2 system and Triangle is VE system)

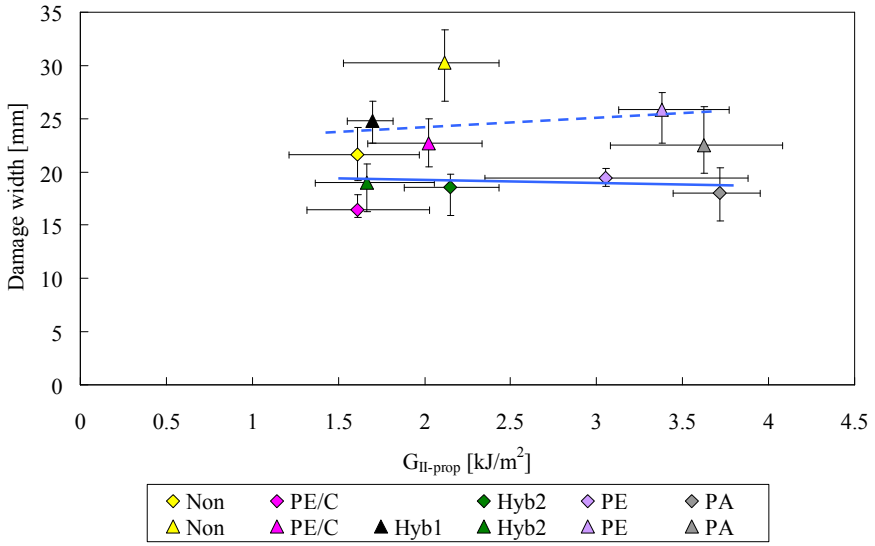

Figure 6.10 Relationship between $G_{II\text{-}prop}$ versus damage width (4J of impact energy) for both resin system specimens with error bars (Diamond is the Ep2 system and Triangle is the VE system)

6.5 Correlation between Mode-I and Mode-II Interlaminar Toughness, and CAI Strength

Figure 6.11 plots the Mode-I initial energy release rate against CAI strength for both resin systems. The tendency of increasing CAI strength with increasing G_{IC} is observed. Masters mentioned that the G_{IC} did not produce a good correlation to residual compressive strength [143-144]. However, a linear relation between the $G_{IC\text{-}NL}$ and the CAI strength is seen in this research. The correlation between the Mode-I energy release rate and CAI strength would appear to be linked to the base material, i.e. the fabric and resin system. For the VE system, both data for $G_{IC\text{-}NL}$ and CAI occur in a narrow range, and the difference of the toughness due to the interleaf veils is quite small. The Mode-I initial energy release rates in this resin system are only moderately improved. Moreover, the CAI resistances are also barely improved.

The Mode-I propagation properties and CAI strength are also compared as shown in Figure 6.12. The general trend of the correlation is quite similar to the initiation values. For the Ep2 system, the PA and PE veils interleaved specimens are significantly improved in the Mode-I propagation values and the CAI resistance properties. On the other hand, the toughness is not improved by the PE/C and Hyb2 veils. In this resin system, the Mode-I toughness seems to affect the CAI resistance via the interleaf veils interaction. The propagation values for the VE system also has a clear relationship, similar to that of initiation toughness. The spread of data, however, is quite narrow. In the VE system, the improvement of G_{IC} value by the interleaf veils seems small. This result leads to the conclusion that the CAI strength improves only slightly.

The relationship between the Mode-I interlaminar toughness and the post-impact compression resistance would be influenced by the resin system. In this research, it can be seen that the Ep2 system specimens possess a good correlation. The VE system specimens, on the other hand, provide results in a range that is quite narrow. The improvement of the Mode-I interlaminar toughness and CAI resistance by interleaf veils is smaller than the Ep2 system specimens. The adhesion between the VE resin and the carbon fabric would be weaker than the Ep2 system. It is thought that the improvement effect by interleaf veils may reduce because fibre-bridging by the base material is the main toughening mechanism. As a result, it may mean that the difference between the G_{IC} and the CAI values is hardly seen.

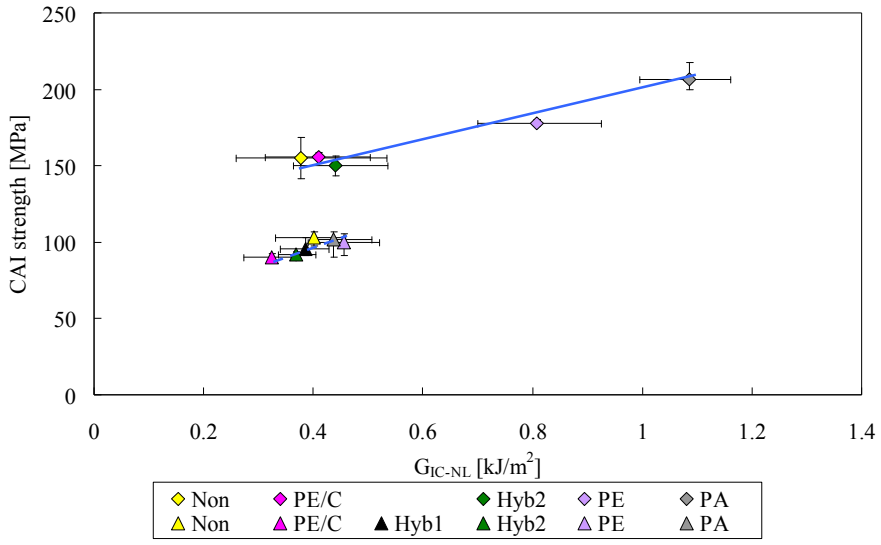

Figure 6.11 Relationship between $G_{IC\text{-}NL}$ versus CAI strength (4J of impact energy) for both resin system specimens with error bars (Diamond is Ep2 system and Triangle is VE system)

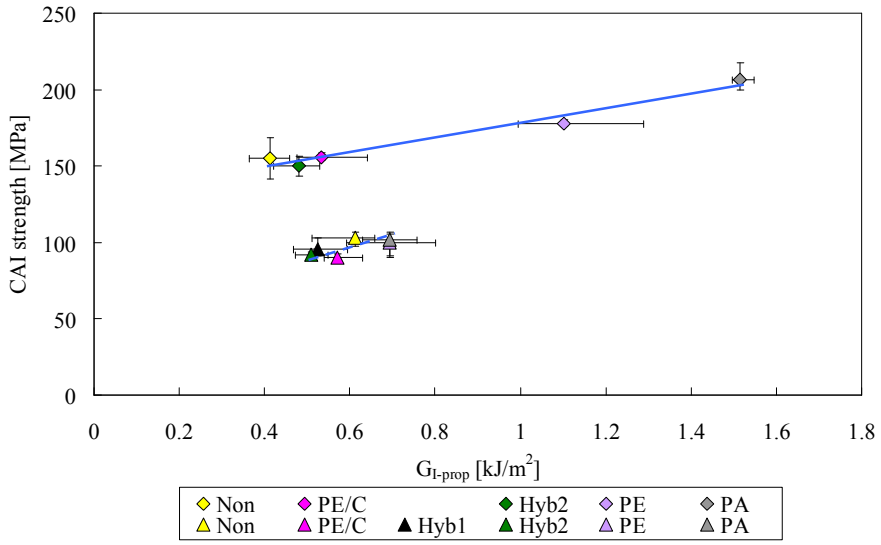

Figure 6.12 Relationship between $G_{I\text{-}prop}$ versus CAI strength (4J of impact energy) for both resin system specimens with error bars (Diamond is Ep2 system and Triangle is VE system)

The correlation between the Mode-II critical energy release rate values as against the CAI strengths is shown in Figure 6.13. The trend is almost the same as the Mode-I interlaminar toughness versus the CAI strength. In this case, all data for the Ep2 system fall along the line. Although the relationship between the Mode-I interlaminar toughness and the CAI resistance for the VE system specimens is over a narrow range, the correlation between the Mode-II interlaminar toughness and CAI strength can be seen clearly. Compared to the Ep2 system specimens, the difference in the CAI strength for the non-interleaved and interleaved samples is quite small and the relationship is flat.

In Figure 6.14 the relationship between the propagation values and the CAI strength is evaluated to see if there is a correlation. The tendency of both resin systems is almost the same as correlation between the Mode-II initial energy release rate and the post-impact compression resistance. For the Ep2 system, the $G_{II\text{-}prop}$ values are similar tendency to the $G_{IIC\text{-}NL}$ results. The VE resin composites are also spread widely for propagation values. Thus, the Mode-II energy release rate seems to be a better correlation of CAI resistance for the non-woven interleaved composites irrespective of the resin system. For both resin systems, a large improvement in the Mode-II energy release rate is realised through the non-woven interleaf veils, as compared with the Mode-I energy release rate.

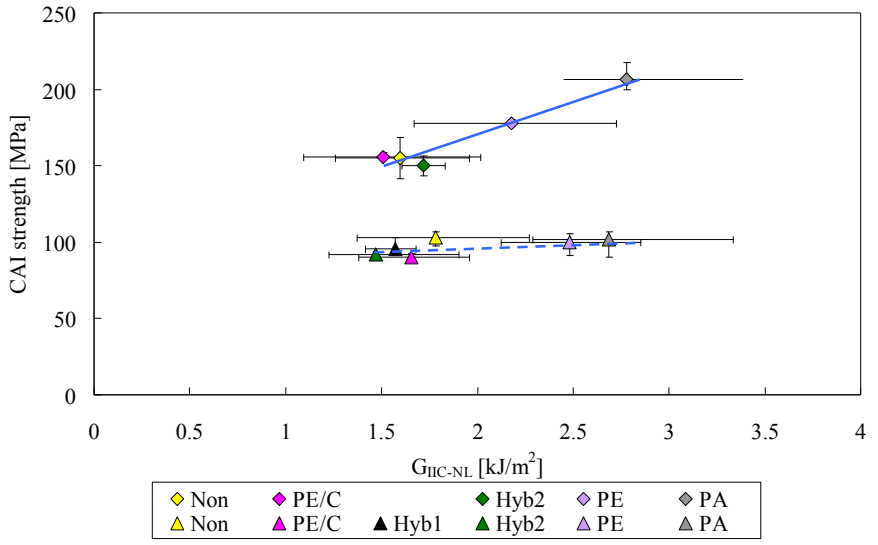

Figure 6.13 Relationship between $G_{IIC\text{-}NL}$ versus CAI strength (4J of impact energy) for both resin system specimens with error bars (Diamond is Ep2 system and Triangle is VE system)

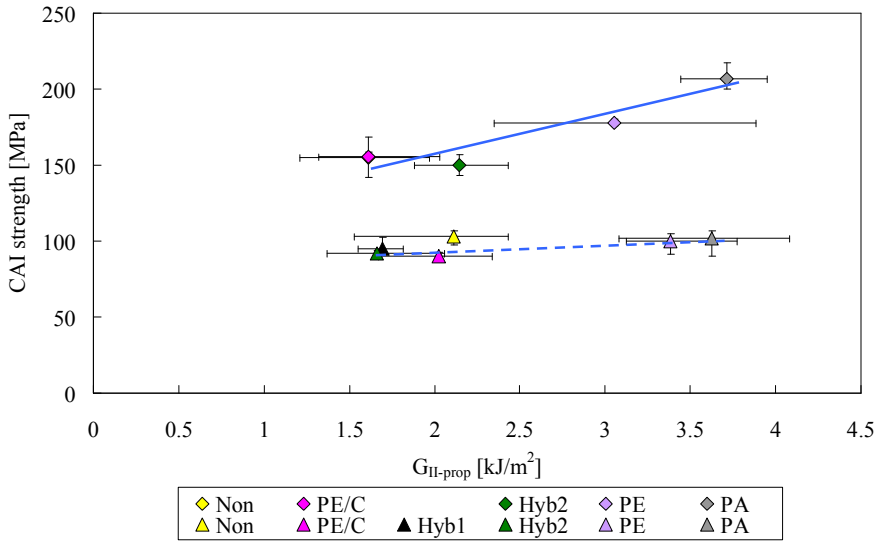

Figure 6.14 Relationship between $G_{II\text{-}prop}$ versus CAI strength (4J of impact energy) for both resin system specimens with error bars (Diamond is Ep2 system and Triangle is VE system)

For the Ep2 system, the G_{IC} and G_{IIC} values are improved significantly by the PE and PA veils. These interleaf veils also improve the CAI strength. For the VE system, although the Mode-II interlaminar toughness realises significant improvement by the interleaf veils, the CAI strength is hardly changed by interleaf veils. It appears that the composites with high Mode-I and Mode-II interlaminar toughness offer superior compression after impact strength.

In some publications, it was mentioned that there is a relationship between toughness and residual compressive resistance [214-215]. These papers, however, mainly used data by Masters. He mentioned that Mode-I interlaminar toughness and CAI strength give a poor correlation [143-144]. However, data from this research and reference [81] seem to show a linear relationship. The correlation between the G_{IC} and the CAI strengths may appear by an optimum combination of the fabric and the resin system. In the Mode-II interlaminar toughness, a clear correlation between the G_{IIC} and the CAI strength can be seen. Both of the Mode-I and Mode-II interlaminar toughness correlate with the CAI resistance. It is thought that the CAI behaviour is a combination of delamination and shear fracture modes. However, the references comparing the relationship between Mode-I and Mode-II interlaminar toughness, and CAI resistance are very few.

6.6 Correlation between Impact Damage Width and CAI Strength

Figure 6.15 plots the damage width as a function of the normalised CAI strength for the Ep2 system specimens. The damage width chosen is that caused by 4J of impact energy, and the CAI strength is normalised by undamaged compression strength. The relationship between the damage width and CAI strength appears to be linear for all composites. For the PE/C and Hyb2 veil interleaved laminates, although the CAI strength values for all impact energies are almost the same as the non-interleaved cases, the damage width has lower values than the non-interleaved composites. Therefore, the gradient of the fitted line is larger than that of the non-interleaved samples. In the Ep2 system, the PE/C and Hyb2 veils do not contribute to any improvement in the CAI resistance properties. For the PE veil interleaved specimens, the damage width has similar values to the control at all impact energies. In contrast, the CAI strength values are higher than the non-interleaved materials. Both the damage width and the CAI strength for the PA veil interleaved laminates are superior to the other interleaved laminates. It suggests that the PA veils can significantly contribute to the improvement of impact resistance and CAI strength. While the PE veils improved the CAI strength

only, the PE/C and Hyb2 veils could contribute to the suppression of the impact damage only.

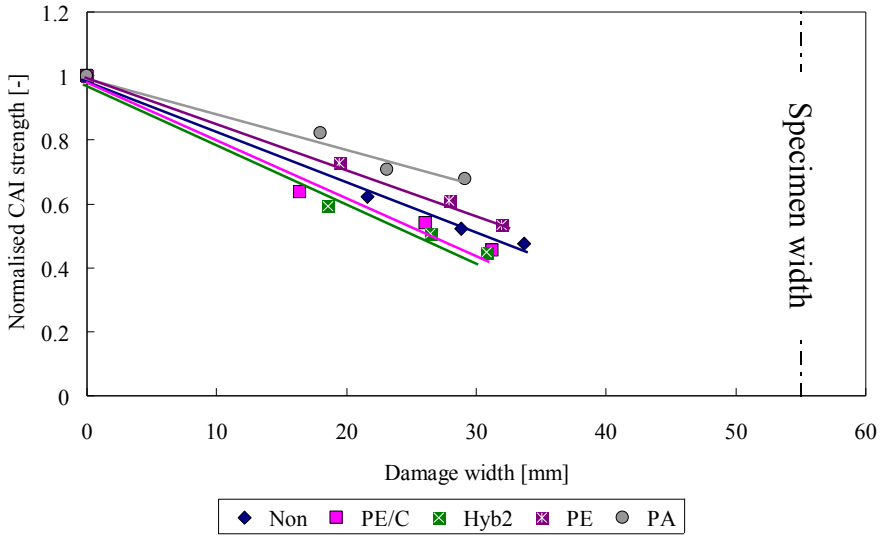

Figure 6.15 Compression after impact strength for non-interleaved and interleaved epoxy2 system specimens plotted as a function of damage width

Figure 6.16 shows the relationship between the damage width and the normalised CAI strength for the VE system with the fitted lines. Compared to the Ep2 system composites, the fitted lines show different behaviour. While the PE/C and Hyb2 veil interleaved specimens show a linear relationship between the damage width and the CAI strength, the non-interleaved and other interleaved laminates are different. In the PE/C and Hyb2 veil interleaved laminates, the CAI strength values at the lowest impact energy are lower than the other interleaved cases. However, the reduction of the CAI strength with the increase in impact energy is more gradual than the other interleaved samples. On the other hand, in the Hyb1, PE, and PA veil interleaved specimens the CAI strengths after the lowest impact energy possess moderately high values. However, the reduction of the CAI strength with increase of impact energy is larger than the PE/C and Hyb2 veil interleaved composites. In particular, the reduction from 8J to 12J is great. In the VE system, it seems that the reduction of the CAI strength with increase of impact energy is large compared with the Ep2 system laminates.

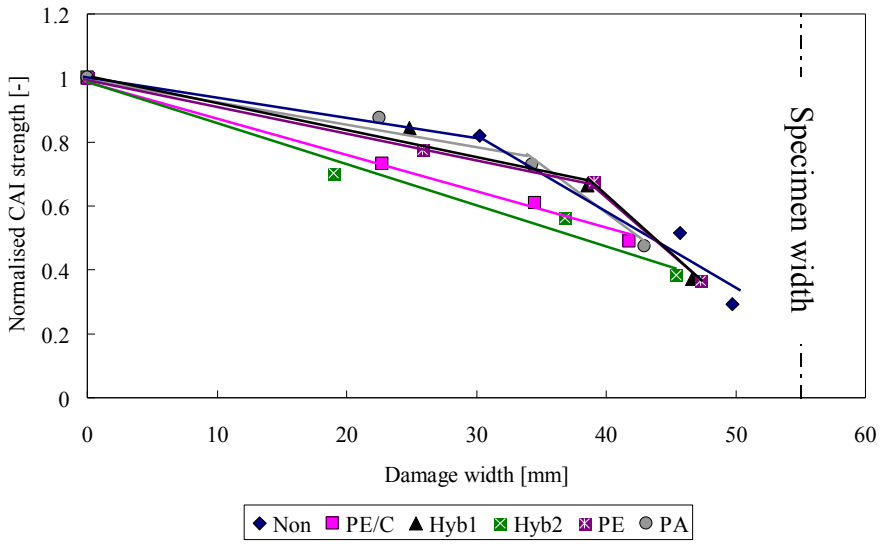

Figure 6.16 Compression after impact strength for non-interleaved and interleaved vinyl ester system specimens plotted as a function of damage width

6.7 Comparison of this research and previous works

Figure 6.17 shows range of the G_I and G_{II} values for this research with data from references. The range of G_I and G_{II} values in this study is 0.4 to 1.5kJ/m^2 and 0.5 to 5.8kJ/m^2, respectively. While the non-woven veils can improve moderately the Mode-I interlaminar toughness, the Mode-II interlaminar toughness exhibits a large range compared with the other toughening techniques. It is thought that the non-woven veils are valid for the improvement of the interlaminar toughness, in particular Mode-II interlaminar toughness. If an optimum combination of the resin and non-woven veil can be found, a considerable improvement in the interlaminar toughness may be able to be expected.

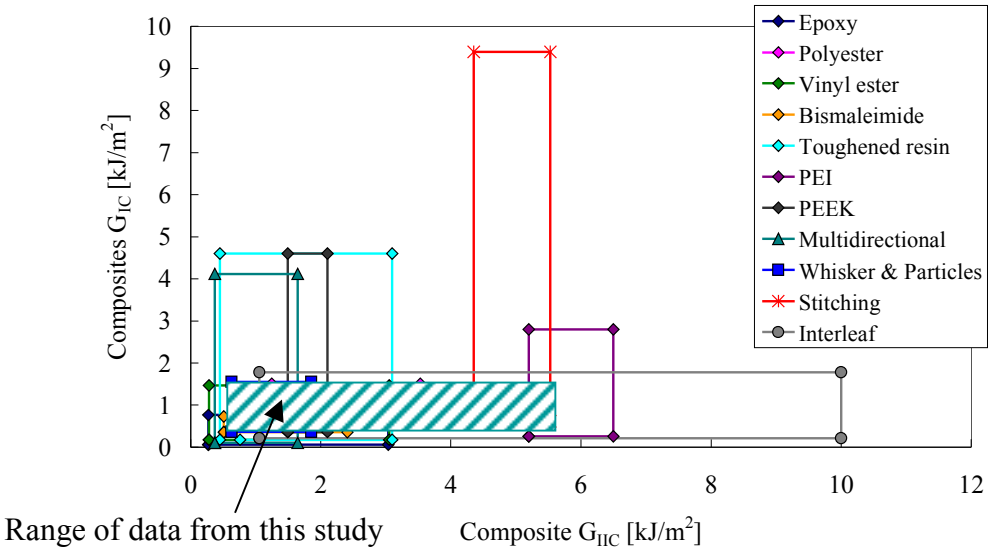

Figure 6.17 Comparison between this research and previous literatures for Mode-I and Mode-II energy release rates of composites [from Figure 2.20]

The relationship between the resin G_{IC} and the composite G_{IC} is plotted in Figures 6.18. Figure 6.19 indicates enlarged image of Figure 6.18 in low G_{IC} and G_{IIC} region. The data of the interleaved Ep2 system specimens takes a position near the long-chain line, as shown in Figure 6.19. The Ep2 system, which is the unmodified matrix, composites seem to show a good correlation in the brittle matrix region. On the other hand, laminates with the Ep1 system, which is the modified matrix, exhibit a poor correlation in the tougher matrix region. The PE and PA veils with the Ep2 system specimens have superior Mode-I interlaminar toughness compared with the other toughening techniques. Figure 6.20 shows the correlation of the resin G_{IC} and the composite G_{IIC} values. In data obtained by this study, there is no clear correlation. It can be confirmed that there is no correlation between the resin G_{IC} and composite G_{IIC}.

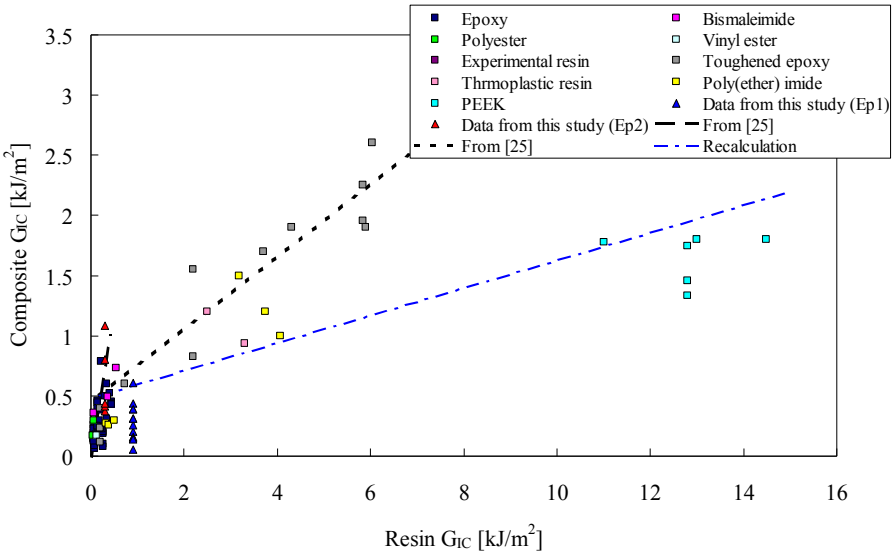

Figure 6.18 Relationship between resin G_{IC} and composite G_{IC} values in this work and previous researches [from Figure 2.21]

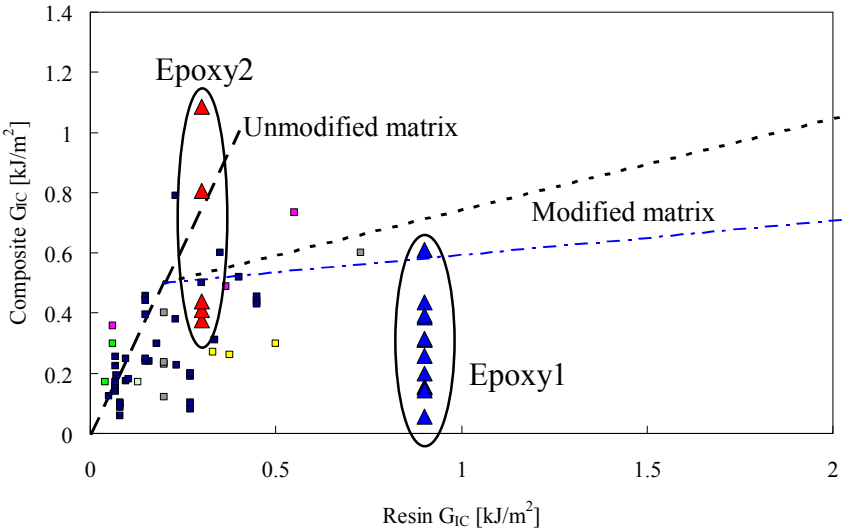

Figure 6.19 Enlarged illustration of Figure 6.19 (Marks and lines indicate the same as Figure 6.18)

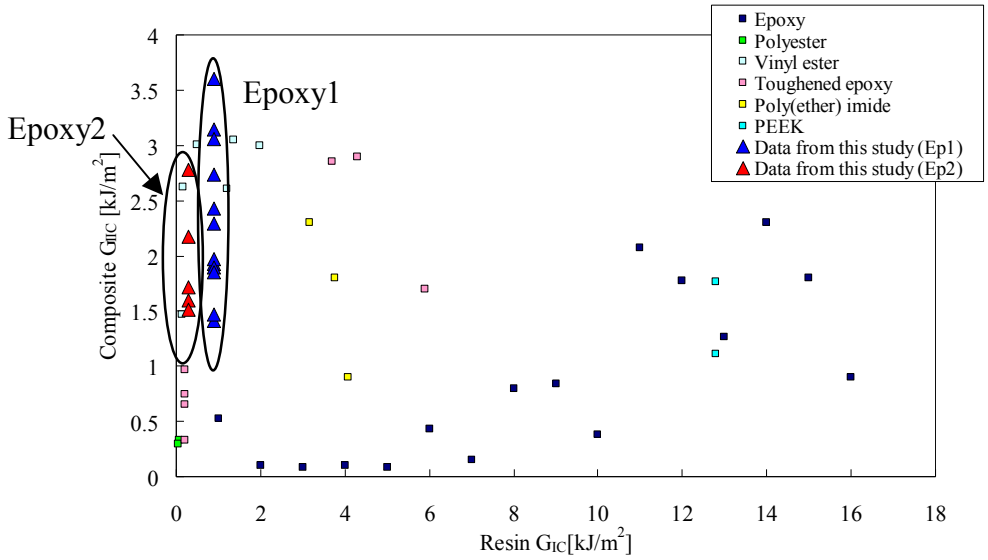

Figure 6.20 Relationship between resin G_{IC} and composite G_{IIC} values in this work and previous researches [from Figure 2.22]

Figure 6.21 compares the impact resistance properties of the CAI strength for this study and previous literatures. It can be seen that the damage width and the CAI strength are inversely proportional, as shown in Figure 6.21. The CAI strengths in the interleaved specimens are relatively lower than the data obtained from reference [143-144, 148]. In particular, the VE system laminates show the lowest CAI strength.

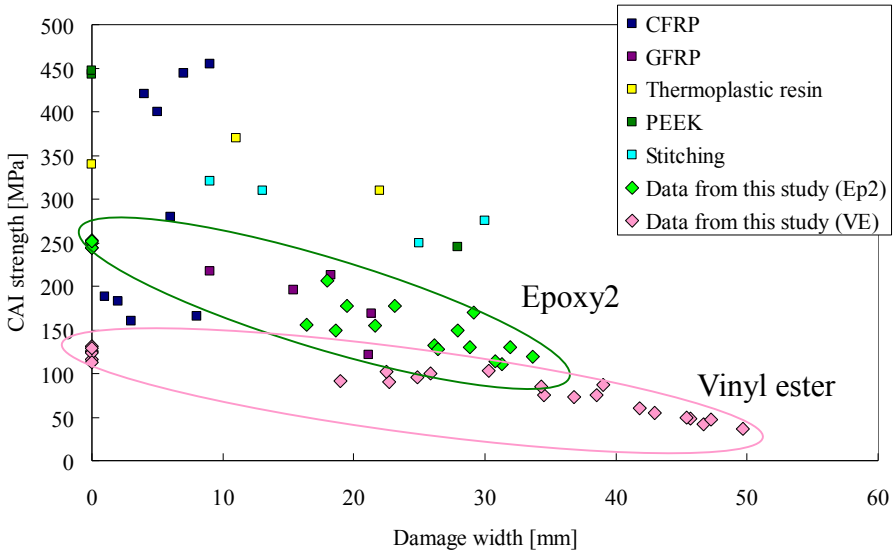

Figure 6.21 Diagram compares effect of impact resistance (damage width) on the CAI strength for this work and literatures [63, 166-168, 171]

The CAI strength between this study and previous works is compared in Figure 6.22. The impact energy range for post-impact properties is 4 to 6J. The range of the CAI strength in this work is around 100 to 220MPa. Compared to the other previous literatures, the non-woven interleaf veils can realise a moderate improvement of the post-impact resistance. An optimum combination between the resin and the fabric systems would realise more improvement of the post-impact compression strength.

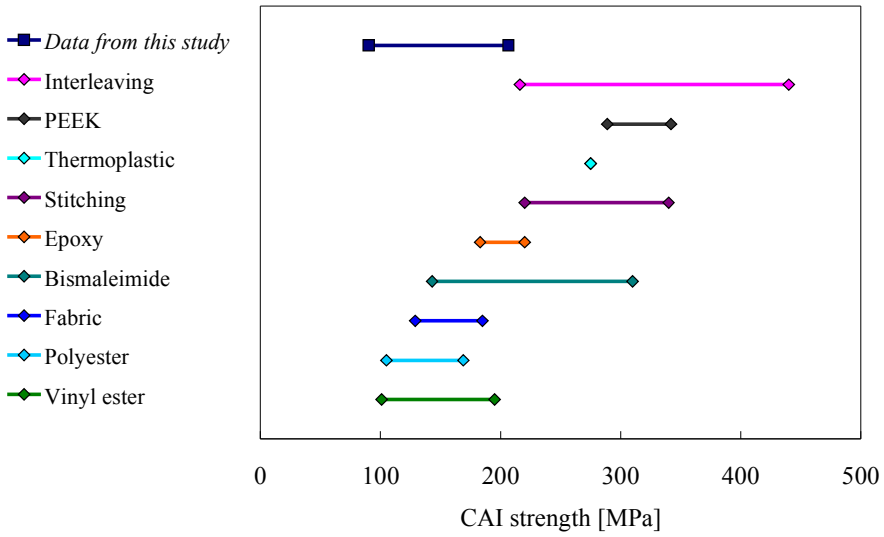

Figure 6.22 Comparison between this research and previous literatures for post-impact resistance of composites [63, 81, 95, 143, 148, 165-171]

6.8 Conclusion

The correlation between each fracture mode discussed in this chapter leads to the following conclusions.

(1) The correlation between the G_{IC} and G_{IIC} values of the composites is affected strongly by the resin and the fabric. For the woven fabric (satin and plain) and the Ep system, the relationship of G_{IC} and G_{IIC} values appeared to be linear. In the VE system, the relationship between G_{IC} and G_{IIC} values was flat. For the unidirectional specimens, there was no clear correlation between G_{IC} and G_{IIC} values. In particular, both modes of energy release rate values for the Ep1 system distributed over a wide range. On the other hand, the relationship between Mode-I and Mode-II interlaminar toughness for the VE system was in a narrow range.

(2) For the relationship between the interlaminar toughness and the impact resistance, the correlation did not appear clearly for each fracture mode. As a result, the fracture behaviour in the impact damage may not be a simple mode. In other words, the crack propagation for the impact fracture would be combined fracture modes, i.e. delamination and shear fracture modes, etc. It is thought that the impact damage and interlaminar fracture growth by DCB or 4ENF tests show a different behaviour. While the impact damage is a dynamic process, the interlaminar

fracture growth is static. Therefore, the correlation could not appear clearly.

(3) The relationship between the CAI and the interlaminar toughness is discussed. In both fracture modes, the correlation appeared linear unlike that between impact resistance and interlaminar toughness. The Ep2 system interleaved specimens had better fracture toughness than the VE system. The Mode-I and Mode-II interlaminar fractures would be similar in behaviour to the CAI fracture. The relationship between Mode-II interlaminar toughness and CAI strength had better compared with the Mode-I interlaminar toughness.

(4) The non-woven veils interleaved specimens can give various results according to the combination of the fabric and the resin system. The Mode-I and Mode-II interlaminar toughness for some interleaf veils could realise an improvement, compared with previous works. The impact and CAI resistance have also shown changes. From these results, it is thought that the non-woven interleaf veils are valuable for the interlaminar toughness of the composites. However, it is necessary to consider that the non-woven veil interleaved composites are affected by a combination of the resin and the fabric. Consequently, it is important in the improvement of the interlaminar toughness to find the optimum combinations between the fabric, resin, and interleaf veils.

Chapter 7

Summary of Conclusions and Future Work

7.1 Introduction

The objectives of this research are to evaluate and understand the mechanisms of the interlaminar toughening using non-woven veils and its influence on post-impact compression properties. Chapter 2 reviewed previous work for toughening composite materials, interlaminar toughness tests, and post-impact compression properties. Data form the literature, moreover, was summarised, and the effect on fracture toughness by different toughening methods was investigated. The mechanisms of Mode-I and Mode-II interlaminar toughening by non-woven veils were described and evaluated in Chapters 3 and 4. In Chapter 5, the impact and CAI resistance properties were investigated using non-woven veils as interleaf materials. Chapter 6 discussed the correlation between each toughness property. Furthermore, the effectiveness of the non-woven interleaf veils obtained in this research was evaluated by comparing previous work and data from this work. In this chapter, final conclusions of this thesis and future work are mentioned and suggested.

7.2 Conclusion on Fabrication of Specimens

The validation of non-woven veils for the VaRTM technique was indicated in previous works [129, 151-152]. In this work, it was confirmed that non-woven veils as interleaf materials were valid for the VaRTM method. Moulding of voidless panels could be realised. The fibre volume fraction of specimens was in a range of 45 to 61vol% (DCB/4ENF specimens) and 36 to 54vol% (CAI specimens).

7.3 Conclusion on Fracture Tests

Four tests for fracture toughness were used in this research. The DCB and 4ENF tests were selected as the Mode-I and Mode-II interlaminar toughness tests. The DCB test was carried out based on ASTM and ISO standards [178-179]. The 4ENF test, on the other hand, was referred to previous literatures [94, 192]. The specimens during the DCB test were not broken and gave realistic data. On the other hand, some of the plain weave specimens tended to undergo bending fracture when 4ENF tests were carried out.

It is thought that the thickness of specimen was thinner than the other fabric samples. Moreover, the fabric surface was coarse and the crack initiation and propagation seemed to be relatively slow. If bending fracture occurred, interlaminar cracks no longer propagated. Consequently, adequate stiffeners need to be attached to specimens for suppression of bending fracture.

For the impact and CAI tests, the miniaturised specimens which are called QMW size [171] were chosen. The impact test machines used were two different types, Dartvis and Fractovis Plus. Although the strikers on both machines were the same shape, specimen crimping was different. The former machine crimped the material under a ring mould by compressed air whereas the material was not clamped on the latter machine. The difference of damage width between both of impact machines was not seen using same samples. The specimens during CAI test fractured at the center, i.e. through the impact damage region. While the Ep2 system specimens tended to collapse catastrophically, the general trend of the VE system specimens was slow and gradual fracture.

7.4 Conclusion on Improvement by Non-Woven Veils as Interleaf Materials

In Chapter 3, the Mode-I interlaminar toughness mechanisms using non-woven veils were investigated and discussed. Three types of carbon fabrics and two resin systems were chosen as the base materials for this work. The PE veil improved the Mode-I interlaminar toughness in all fabric and resin system. Both hybrid veils showed a moderate improvement of the G_{IC} values. The non-woven veils, however, did not necessarily improve interlaminar toughness. In particular, the carbon veil interleaved specimens for all fabric and the Ep resin system had significantly poorer Mode-I interlaminar toughness than the non-interleaved laminates. The PA veil interleaved composites were affected strongly by fabric and resin system. While the satin weave and UD fabrics Ep1 system samples had significantly poor Mode-I interlaminar toughness, the plain weave fabric Ep2 system specimens were significantly increased G_{IC} values. It is thought that the adhesion between the matrix and veil fibres is an important factor for interlaminar fracture toughness. If the adhesion strength is weak, the veil fibres may pull out but work as bridging. This effect seems to contribute to the improvement of the interlaminar toughness. Many PE veil fibres were pulled out on the fracture surface and worked as fibre-bridging. Hence the PE veil interleaved laminates realised a significantly high Mode-I energy release rate. In contrast, the carbon veil fibres were embedded completely in the matrix. The veil fibres thus could not contribute to the Mode-I interlaminar toughness. The PA veils with the Ep resin system were not pulled out on the fracture surface but exposed. In this resin system, the PA veil may

contribute to the interlaminar toughness by adhesion between veil fibres and matrix. However, the PA veil for fracture toughness seems to be affected significantly by the resin system. On the other hand, the PA veil fibres for the VE system were different behaviour from the Ep system specimens. In the VE system, the PA veil fibres were deformed or elongated during crack propagation. This would contribute to moderate improvement of the Mode-I interlaminar toughness.

The influences on Mode-II interlaminar toughness mechanisms by interleaf veils were evaluated in Chapter 4. The base materials were the same as in Chapter 3. For the 5-harness satin weave and UD fabric Ep1 system specimens, the Hyb2 and PE veils significantly improved Mode-II interlaminar toughness properties. The PA veil contributed to the improvement of the propagation values. The carbon veil interleaved laminates had lower Mode-II interlaminar toughness compared with the other interleaved cases. The plain weave Ep2 resin composites were similar tendency to the Mode-I test results. For the VE system samples, the difference between each interleaved laminate was small compared with the Ep resin system specimens.

The post-impact compression resistance of CFRP using non-woven veils was discussed in Chapter 5. For the CAI resistance properties, the plain weave and two resins were examined. The impact damage resistance was improved using non-woven veils. In particular, the PA veils significantly contributed to the suppression of damage spread for the Ep2 system. In previous work, the PA veil with the VE system had superior impact resistance to the PE veil system [152]. In this research, the PA veil had also excellent damage resistance in both resin systems. The PE/C and hybrid veils had also good impact resistance. The PE veils showed only a slight improvement. The tendency of CAI strength differed from that of impact resistance. Reduction of the CAI strength for the PA veil interleaved samples was the smallest in all interleaved cases. The PE veil interleaved specimen had the highest CAI value. In contrast, the PE/C and hybrid were improved only slightly.

7.5 Suggestion for Future Work

It had already been mentioned that VaRTM is an attractive method in the academic and industrial areas. Some interleaving technique for the VaRTM, however, may restrict its use. However, this moulding method can be used enough by using appropriate interleaf materials. It is thought that the interleaf materials are not only non-woven veils but also that porous films may also be used as toughening materials.

In this study, Mode-I & II, impact, and CAI tests were undertaken for

evaluation of the interlaminar fracture toughness, but other mechanical tests such as flexural and tensile tests were not carried on. These properties would contribute to evaluate imterlaminar toughness. Furthermore, this research focuses mainly on experimental approaches for means of improving interlaminar toughness using non-woven veils. The modelling analysis as future work would produce more useful results. It is thought that the fracture mechanism would be clarified by evaluating the correlation of experimental and analytical approaches.

From the study, it was found that there were relationships between interlaminar fracture toughness and post-impact compressive resistance. However, there are few literatures, which mention the correlation between the interlaminar toughness and post-impact resistance. The literature by Maters is representative reference [143-144]. It is thought that evaluation of the relationship between each fracture toughness would get useful information for understanding interlaminar fracture toughness.

Appendix A

Load-Displacement Curves Obtained by DCB Tests

A.1 Load-Displacement Curve

In this chapter, results obtained by the DCB tests are given. The representative load-displacement curves are shown.

A.1.1 Non-interleaved Specimens

Figure A.1 shows results of the DCB test for the non-interleaved specimens with the Ep system. A typical load-displacement curve of the satin weave sample Ep1 system has a jagged shape (classifications of curve shapes are given in section 3.3.1). The maximum load and displacement are approximately 57N and 20mm, respectively. The crack propagation sharply jumped. A non-linear point appears after about 5mm of displacement, and is quite near the maximum load point.

The curve shape in the UD laminate is a bow type. In the linear region the load-displacement curve exhibited similar behaviour to the satin weave case. However, the crack initiation was later than the satin weave composite, at about 6mm of displacement. The maximum load and displacement values are around 60N and 30mm, respectively. The crack behaviour was different from the satin weave specimens. The crack propagated gradually, without jumping. Therefore, the curve is a smooth shape.

In the plain weave Ep2 resin composites, two types of areal weight fabrics were used in experiments. For the HAW plain weave specimen, the load increased until 40N. The load kept around 40N for a while, and then gradually decreased. The LAW plain weave specimen was similar in behaviour to the HAW case. However, the maximum load in the LAW specimen was lower than the HAW sample. Moreover, the gradient in linear region for the LAW laminate was smaller than that for the HAW laminate. The behaviour at the linear stage seemed to be influenced significantly by the areal weight of the fabric. The load increased to around 25N, afterwards gradually decreasing. The crack propagation speed was significantly slower than in the HAW composite.

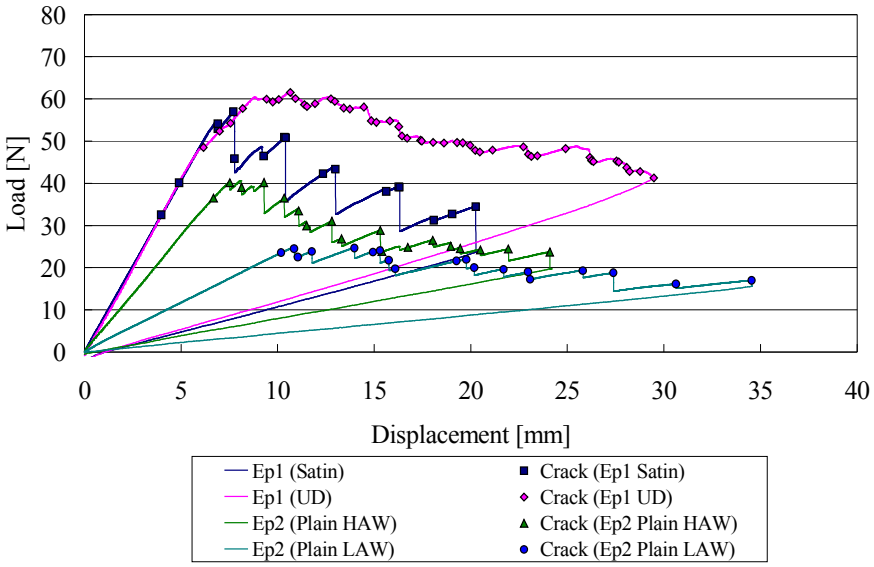

Figure A.1 Typical DCB load-displacement curves of non-interleaved specimens for epoxy resin system

Figure A.2 illustrates the typical load-displacement curves for the non-interleaved VE system composites. The crack in the VE system specimens propagated gradually, exhibiting slow growth. Compared to the satin weave Ep1 system specimens, the non-linear point appeared significantly early, about 3mm of displacement. The load increased until 11mm of displacement and then kept constant around 30N. The maximum load was significantly lower than the Ep1 system case which was about 57N.

In the UD laminate, the maximum load and displacement values are higher than the Ep1 system sample, which are 68N and 35mm. The crack growth in both resin system specimens was similar in behaviour, being gradual and slow propagation. The linearity in the UD fabric system was similar to the Ep1 system samples.

For the plain weave composite, the load increased up to 40N. Afterwards it gradually reduced until the test finishes. The slope in the linear region of the VE system laminate was similar to the HAW Ep1 system case. It is thought that the plain weave fabric has a coarser surface than the satin weave fabric. Hence, the crack initiation would be later than the satin composites. However, the crack propagation in both fabric specimens was quite similar. The condition of the fabric surface would affect the initiation only.

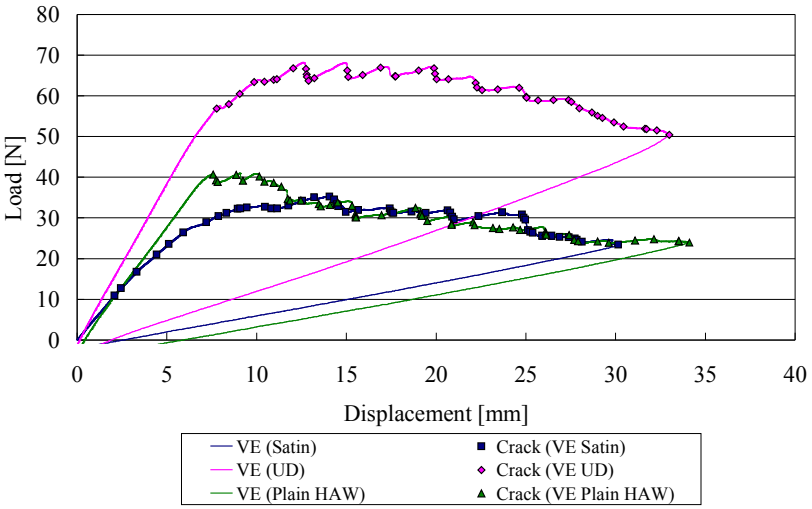

Figure A.2 Typical DCB load-displacement curves of non-interleaved specimens for vinyl ester resin system

A.1.2 Interleaved Specimens

A.1.2.1 Polyester/Carbon Veil Interleaved Specimens

Figure A.3 illustrates typical results of the DCB test for the PE/C veil interleaved specimens. For the plain weave specimens, the Ep2 system laminates used the LAW plain fabric. On the other hand, for the VE resin samples the HAW plain weave fabric were chosen. Although the load in the Ep2 system laminate fell slightly at 10mm, it increased to a maximum of 35N. Afterward the load dropped suddenly and kept around 20N to 25N until the test finished. The maximum load in the VE system sample, on the other hand, reached approximately 35N and the load was keeping up to 15mm of displacement. The rate of crack propagation for the Ep2 system laminate was significantly slower than that of the VE system. The slope at the linear stage for the Ep2 system specimen was smaller than the VE system specimen. This difference of the slope is due to the difference of the areal weight. The gradient at linear area would be affected by the areal weight of fabric in the same way as the non-interleaved cases.

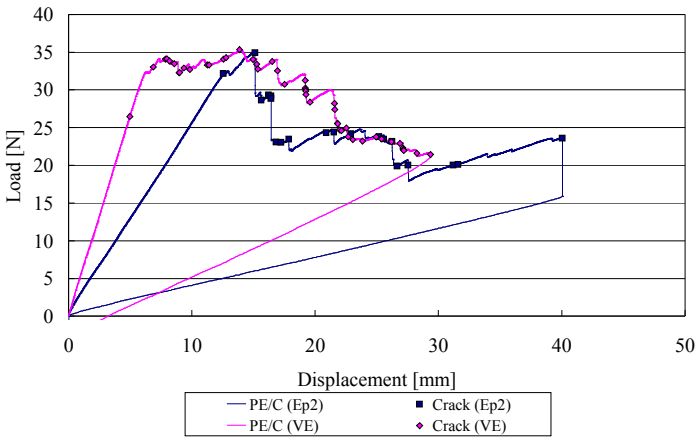

Figure A.3 Typical DCB load-displacement curves of PE/C (100/100) veil interleaved specimens for plain weave fabric with both resin systems

A.1.2.2 Polyester/Carbon (70:30) Hybrid Veil Interleaved Specimens

Figure A.4 shows results of the DCB test for the Hyb1 veil interleaved specimens. The load-displacement curve in the satin weave specimen has a jagged shape, as shown in Figure A.4 (a). The crack jumping was large compared with the non-interleaved case. The maximum load and displacement values were approximately 44N and 24mm, respectively. In the linear stage, the load increased quite linearly up to 32N. The load-displacement curve was linear throughout. Although the crack growth in Hyb1 veil interleaved specimens was slower than the non-interleaved sample, the maximum load was smaller.

For the UD fabric Ep1 system laminates, the crack growth behaviour exhibited significantly small jumps compared with the satin weave specimen, as shown in Figure A.4 (b). The maximum load and displacement values were about 60N and 25mm, respectively. For the VE system composite, the load-displacement curve is a bow shape. The crack propagation speed was slow and gradual compared with the Ep1 system case. The maximum load was almost the same as the Ep1 system laminates, however the displacement was larger, approximately 35mm.

In the plain weave VE resin laminates, the load-displacement curve is triangle shape, as illustrated in Figure A.4 (c). The maximum load and displacement were about 40N and 30mm, respectively. In this system, the gap between the non-linear point and maximum load point was small. The crack propagation was gradual. The maximum load is lower than the control.

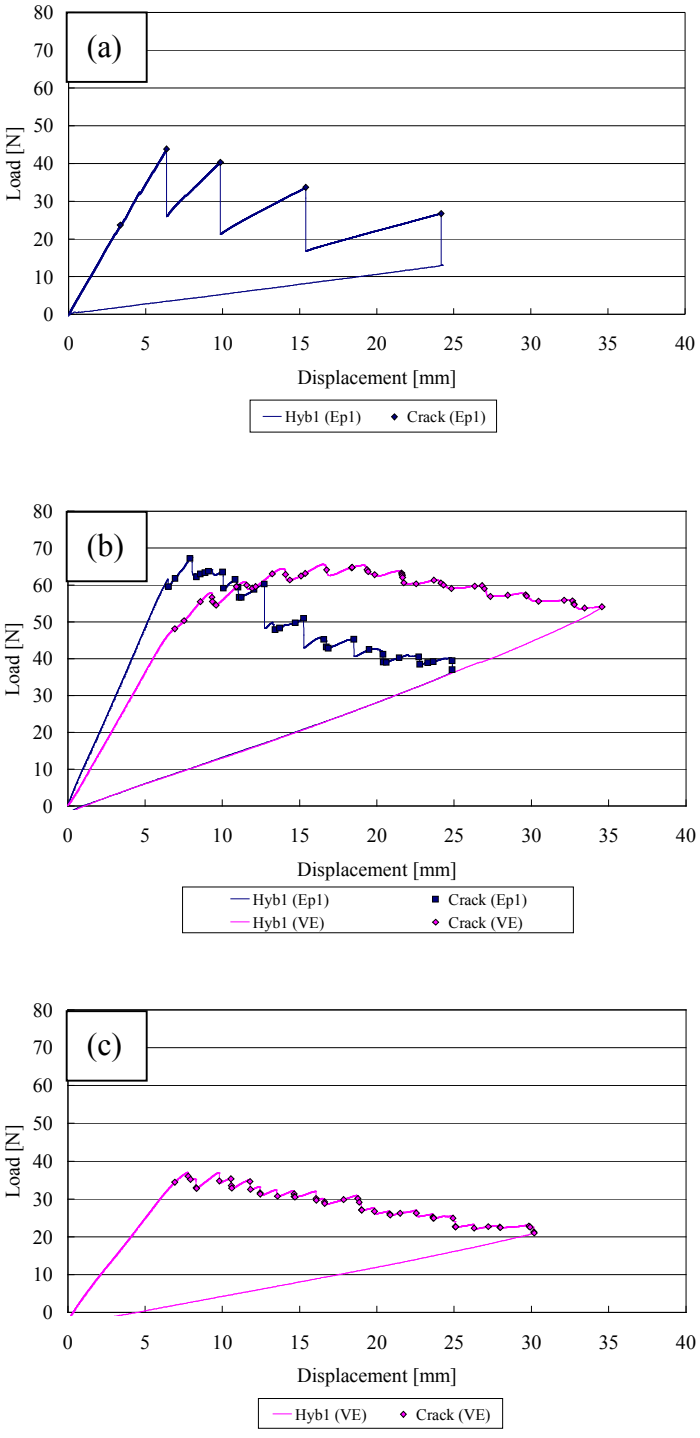

Figure A.4 Typical DCB load-displacement curves of PE/C (70:30) hybrid veil interleaved specimens with both resin systems: (a) 5-harness satin weave fabric, (b) Unidirectional fabric, (c) Plain weave fabric

A.1.2.3 Polyester/Carbon (80:20) Hybrid Veil Interleaved Specimens

Figure A.5 shows the load-displacement curves for the satin weave composites with both resin systems. The crack propagation was similar in behaviour to the Hyb1 veil interleaved samples. The maximum load and displacement were approximately 50N and 22mm, respectively. Although the maximum load is higher than the Hyb1 veil interleaved samples, the maximum displacement was lower. The crack propagation was faster compared with the Hyb1 veil interleaved laminates.

In the UD fabric Ep1 system composite, the Hyb2 veil interleaved laminate shows different behaviour from the Hyb1 veil interleaved cases. The crack propagation for the Ep1 system was slip-stick, as shown in Figure A.5 (b). The maximum load and displacement were around 60N and 23mm, respectively. Compared to the Hyb1 veil interleaved specimens, both maximum load and displacement had smaller values. On the other hand, the load-displacement curve for the VE system is a bow shape. The crack propagation was slow, stable and gradual. In the VE system, the crack growth was similar in behaviour to the Hyb1 veil interleaved case. The maximum load and displacement values were approximately 61N and 37mm, respectively.

In the plain weave Ep2 system specimen, the maximum load and displacement were about 30N and 35mm, respectively. The behaviour of the crack growth was completely different from the satin weave samples, as shown in Figure A.5 (a) and (c). The crack propagated slowly and gradually. For the VE system, the maximum load and displacement were 40N and 25mm, respectively. The initial rise of slope was swifter than the Ep2 system specimen.

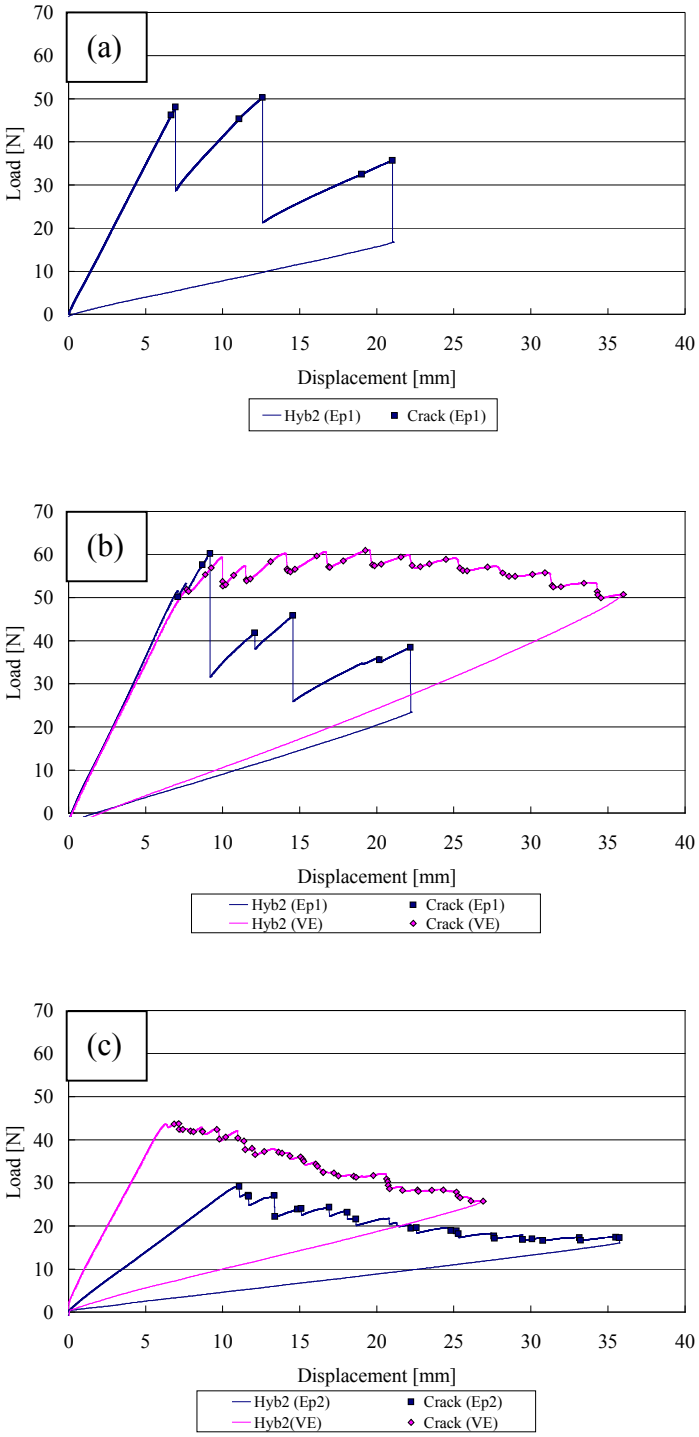

Figure A.5 Typical DCB load-displacement curves of PE/C (80:20) hybrid veil interleaved specimens with both resin systems: (a) 5-harness satin weave fabric, (b) Unidirectional fabric, (c) Plain weave fabric

A.1.2.4 Carbon Veil Interleaved Specimens

The typical load-displacement curves obtained by the DCB tests for the carbon veil interleaved specimens are shown in Figure A.6. The curve for the satin weave Ep1 system laminate is a jagged shape, as shown in Figure A.6 (a). Both the maximum load and displacement were significantly lower compared with the non-interleaved case. The maximum load and displacement were about 38N and 13mm, respectively. The crack propagation was quite rapid with large jumps. In the carbon veil interleaved samples, the cracks tended to propagate quite easily compared with the other interleaved cases.

The load-displacement curves in the UD fabric Ep1 and VE system composites showed different behaviour, as illustrated in Figure A.6 (b). For the Ep1 system, the crack growth was similar in behaviour to the satin weave laminates. The maximum load and displacement were almost the same values as the 5-harness satin specimen, approximately 34N of load and 13mm of displacement. The maximum load and displacement for the VE system, on the other hand, were significantly higher than those for the Ep1 system composite, approximately 60N and 33mm. The crack propagation for the VE system was slow and stable compared with the Ep1 system sample.

For the plain weave specimens, the crack propagation was similar in behaviour to the UD fabric VE system, which was stable growth, as shown in Figure A.6 (c). The maximum load and displacement were nearly 37N and 28mm, respectively. Compared to the UD fabric VE system composite, the increase of the load was lower, up to 40N.

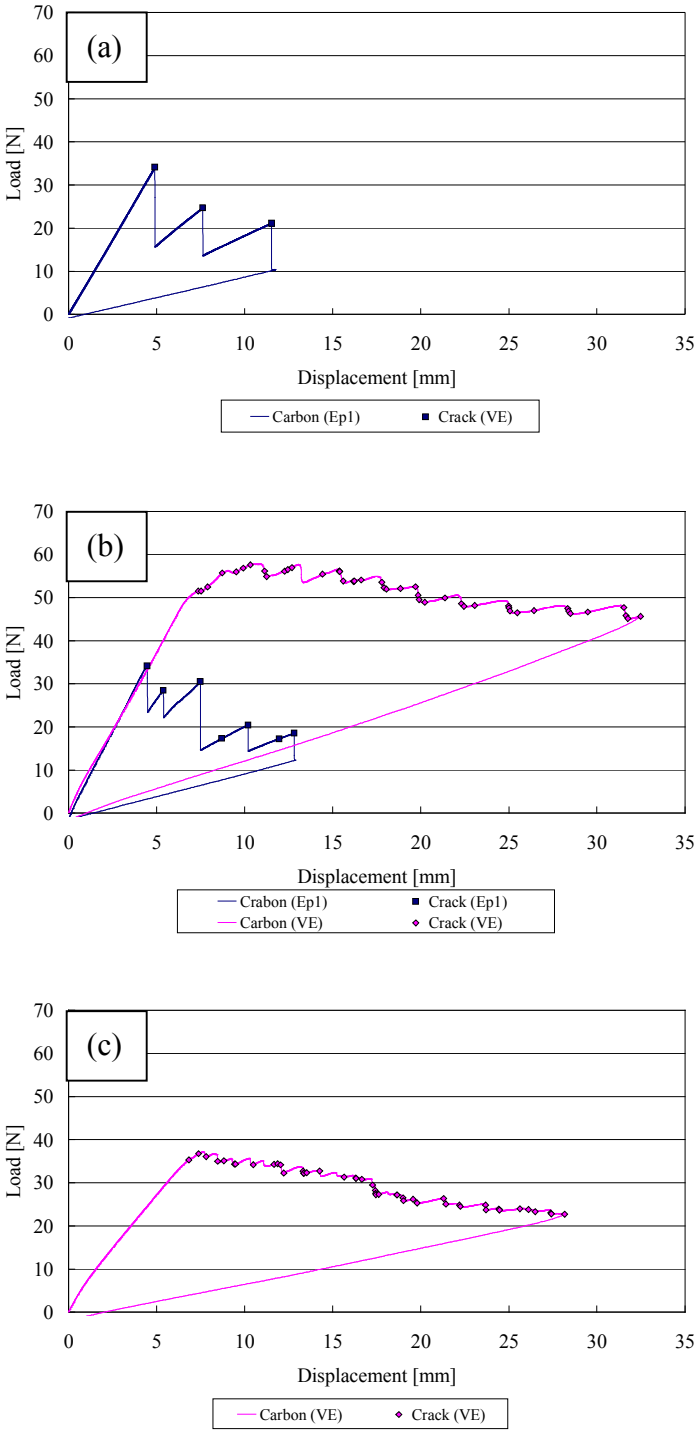

Figure A.6 Typical DCB load-displacement curves of carbon veil interleaved specimens with both resin systems: (a) 5-harness satin weave fabric, (b) Unidirectional fabric, (c) Plain weave fabric

A.1.2.5 Polyester Veil Interleaved Specimens

Figure A.7 shows representative load-displacement curves obtained by the DCB tests. The PE veil interleaved specimen, which is 5-harness satin fabric for the Ep1 resin system, is jagged in shape, as illustrated in Figure A.7 (a). The maximum load and displacement were larger than the other veil interleaved cases, about 55N and 32mm. When the crack propagated the PE veil fibre was pulled out from the fracture surface resulting in bridging. This effect would contribute to a significant increase of the maximum load and displacement. For the VE system, the maximum load was slightly lower than the Ep1 system laminate, approximately 42N. In contrast, the maximum displacement was almost the same value, 33mm. In the linear region, while the load for the Ep1 system laminate increased linearly until the first load drop, the non-linear point for the VE system sample appeared at an early stage.

For the UD specimens, the curves for both resin systems were similar shapes. The crack propagation for the Ep1 system was quite gradual, unlike the other interleaved samples. The maximum load and displacement for the Ep1 system were approximately 72N and 32mm. In the VE system sample, both maximum load and displacement were slightly larger than the Ep1 system case, about 75N and 36mm. In contrast, the non-linear point appeared earlier than the Ep1 resin composite.

In the plain weave specimens, the fracture progress was completely different from the other fabric with the Ep2 system samples. The crack propagation for the Ep2 system was significantly slow and gradual compared with the Ep1 system laminates. The maximum load and displacement are about 43N and 50mm, respectively. Compared to the satin weave specimens, the reduction of the load at each crack mini-jump was quite small, as shown in Figure A.7 (c). Moreover, the maximum displacement was significantly larger than the other fabric samples. For the VE system, the maximum load was almost the same value as the Ep2 system case, about 43N. In contrast, the displacement was smaller than the Ep2 system specimen, approximately 32mm. The crack propagation was gradual until the crack reached around 28mm of displacement. Although the slope for both resin systems was different, the increase of the load was similar in behaviour. The non-linear points of both resin systems were quite near to the maximum load point.

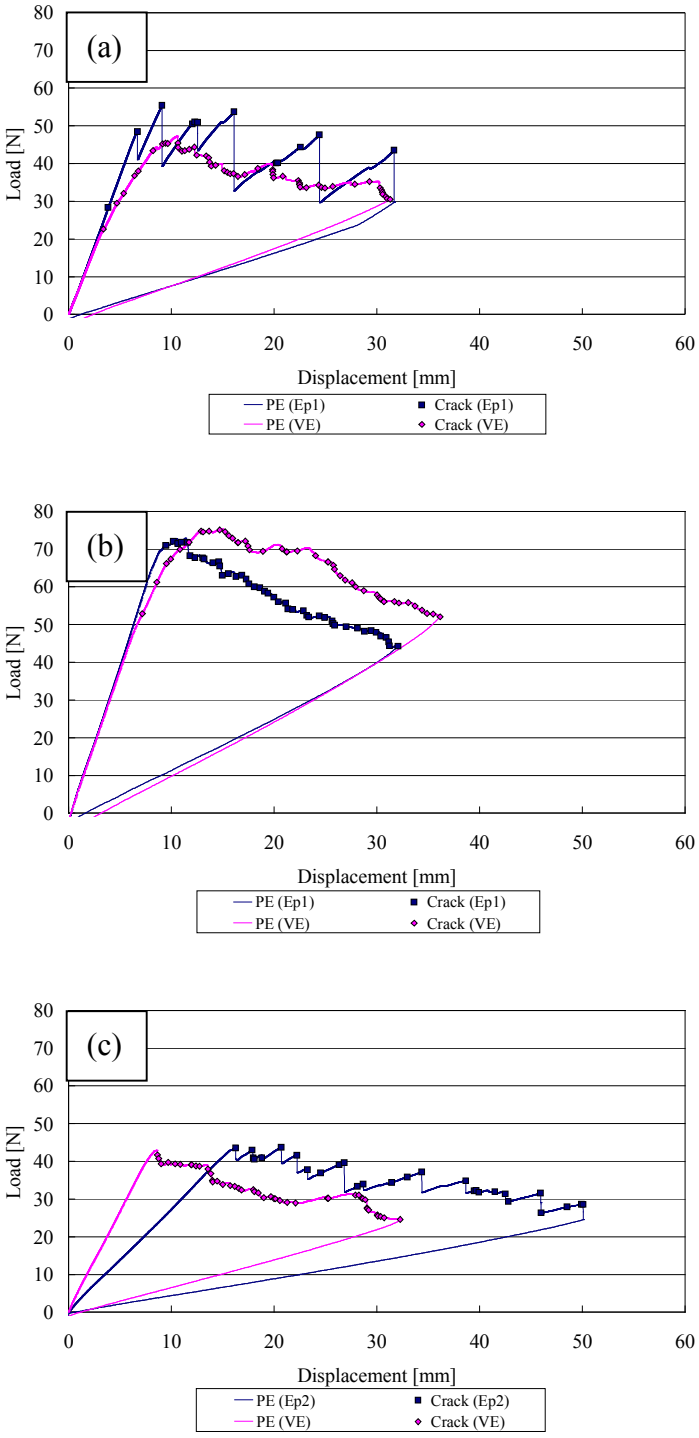

Figure A.7 Typical DCB load-displacement curves of PE veil interleaved specimens with both resin systems: (a) 5-harness satin weave fabric, (b) Unidirectional fabric, (c) Plain weave fabric

A.1.2.6 Polyamide Veil Interleaved Specimens

Figure A.8 illustrates the typical DCB test results for the PA veil interleaved specimens. The load-displacement curve in the satin weave Ep1 system laminate was similar in tendency to the carbon veils interleaved sample. The curve is jagged shape and crack propagation is large by jumping, as illustrated in Figure A.8 (a). The maximum load is nearly 40N. The maximum displacement was quite a short length, about 10mm. For the VE system, the crack propagation was similar in behaviour to the PE veil interleaved case (see in Figure A.7 (a)). The maximum load and displacement were around 40N and 32mm, respectively.

For the UD fabric Ep1 system, the crack propagation showed similar in behaviour to the satin weave laminate. The crack in the Ep1 system specimen propagated sharply and quickly, as shown in Figure A.8 (b). The maximum load and displacement were nearly 50N and 22mm. In particular, the displacement was substantially increased compared with the satin case. The graph of the VE system specimen, on the other hand, was similar to the other interleaved samples. The crack propagation was gradual and slow. The maximum load and displacement were approximately 70N and 40mm.

For the plain weave Ep2 system laminate, the crack propagation was similar in behaviour to the other fabric materials. The crack propagated quite sharply and jumped, as illustrated in Figure A.8 (c). However, the crack propagation speed was completely different from the other fabric cases. The crack propagated significantly slowly. Moreover, the crack initiation was suppressed longer than the Ep1 system laminates before a sharp jump. The maximum load and displacement were nearly 70N and 50mm, respectively. Some of the PA veil interleaved specimens exceeded displacements of 50mm. For the VE system, crack propagation was also slow and gradual. The growth showed similar in behaviour to the other fabric specimens. The maximum load and displacement were around 40N and 35mm, respectively. Compared to the Ep2 system composites, both maximum load and displacement values were considerably small.

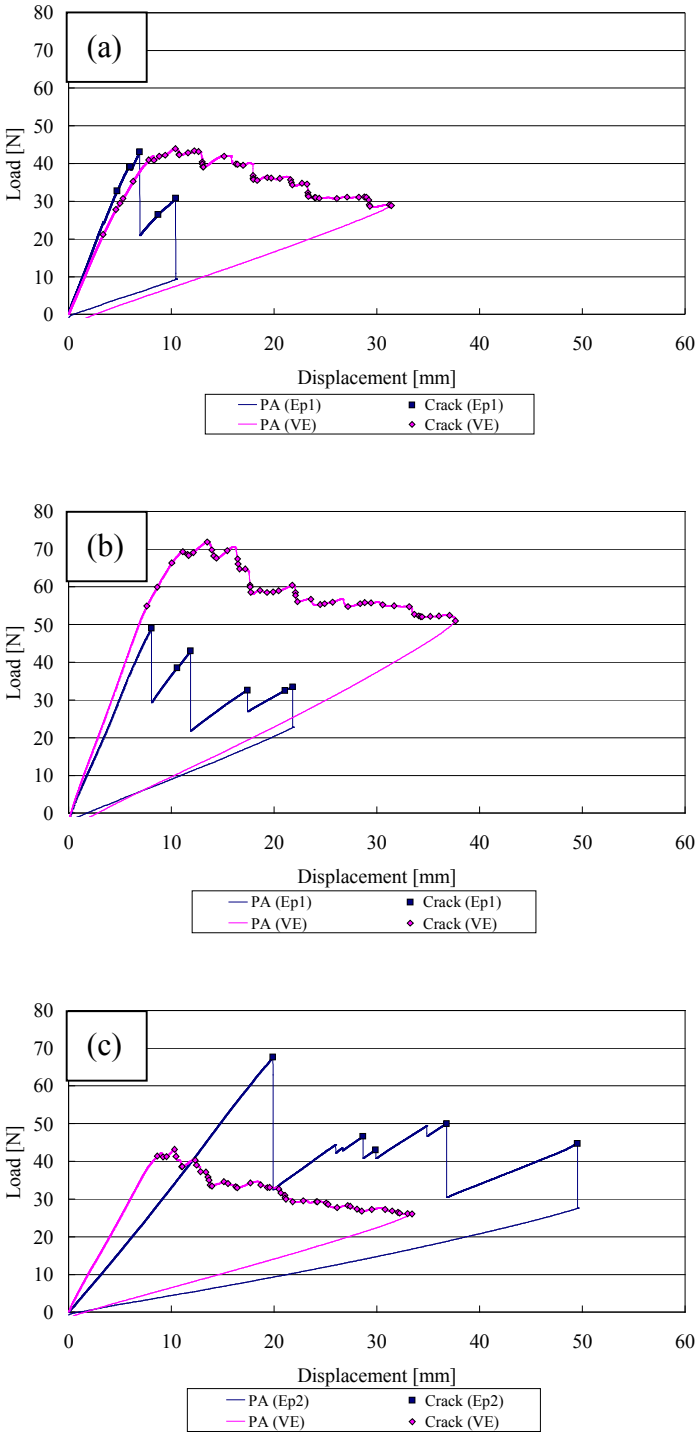

Figure A.8 Typical DCB load-displacement curves of PA veil interleaved specimens with both resin systems: (a) 5-harness satin weave fabric, (b) Unidirectional fabric, (c) Plain weave fabric

The crack propagation behaviour for the Ep system specimens was basically jumping. On the other hand, the crack growth for the VE system laminates was stable and gradual propagation. Tables A.1 to A.3 summarise the DCB test results for each fabric specimen. For Table A.3, the Ep2 system samples used the LAW fabric, and for the VE system specimens the HAW fabric was chosen. The non-interleaved composites with the Ep2 system are shown for both areal weight fabric specimens.

Table A.1 Summary of DCB test results for 5-haness satin weave fabric specimens (Load and displacement are maximum values)

	Epoxy1			Vinyl ester		
Interleaf	Crack	Load [N]	Displacement [mm]	Crack	Load [N]	Displacement [mm]
Non	Jump (S)$^{+}$	57	20	Stable$^{\$}$	35	30
Hyb1	Jump (L)$^{++}$	44	24	-$^{\#}$	-	-
Hyb2	Jump (L)	50	22	-	-	-
Carbon	Jump (L)	34	12	-	-	-
PE	Jump (S)	55	32	Stable	47	32
PA	Jump (L)	43	11	Stable	31	44

+: Crack jumps shortly, ++: Crack jumps largely, $: Crack propagates stable, #: Not examined

Table A.2 Summary of DCB test results for unidirectional fabric specimens (Load and displacement are maximum values)

	Epoxy1			Vinyl ester		
Interleaf	Crack	Load [N]	Displacement [mm]	Crack	Load [N]	Displacement [mm]
Non	Stable	62	29	Stable	68	33
Hyb1	Jump (L)	68	25	Stable	66	35
Hyb2	Jump (L)	60	22	Stable	61	36
Carbon	Jump (L)	34	13	Stable	59	33
PE	Stable	73	32	Stable	75	36
PA	Jump (L)	49	22	Stable	72	38

Table A.3 Summary of DCB test results for plain weave fabric specimens (Load and displacement are maximum values)

	Epoxy2			Vinyl ester		
Interleaf	Crack	Load [N]	Displacement [mm]	Crack	Load [N]	Displacement [mm]
Non	Jump (S)	25*/41**	35*/24**	Stable	41	34
PE/C	Jump (S)	35	40	Stable	35	29
Hyb1	-	-	-	Stable	37	30
Hyb2	Jump (S)	29	36	Stable	44	27
Carbon	-	-	-	Stable	37	28
PE	Jump (S)	44	50	Stable	43	32
PA	Jump (L)	68	50	Stable	43	33

*: LAW specimen, **: HAW specimen

Appendix B

Load-Displacement Curves Obtained by 4ENF Tests

B.1 Load-Displacement Curve

In this section, the results obtained by 4ENF tests are given. Representative load-displacement curves are shown.

B.1.1 Non-interleaved Specimens

The load-displacement curves for the non-interleaved specimens are shown in Figure B.1. The maximum load for the Ep1 system specimen is approximately 2kN. The crack initiation was quite late, over displacement of 3mm. The load kept constant at around 1.9kN. The load dropped slightly at a displacement of 4.1mm.

The UD specimen has a different load-displacement curve shape from the satin sample. The load dropped at a displacement of 4mm, afterwards it increased again until the test finished, as shown in Figure B.1. The maximum load and displacement values were approximately 2kN and 5.6mm, respectively. The maximum load was similar values to the satin weave case.

In the plain weave (HAW) Ep2 system, the maximum load and displacement were around 1.4kN and 6.4mm, respectively. Those of the LAW composite, on the other hand, gave a lower load value (0.8kN) than the HAW specimen, but the displacement was almost the same as the HAW case, about 6.5mm. The slope of the linear region for the LAW specimen was significantly smaller than that of the HAW laminate.

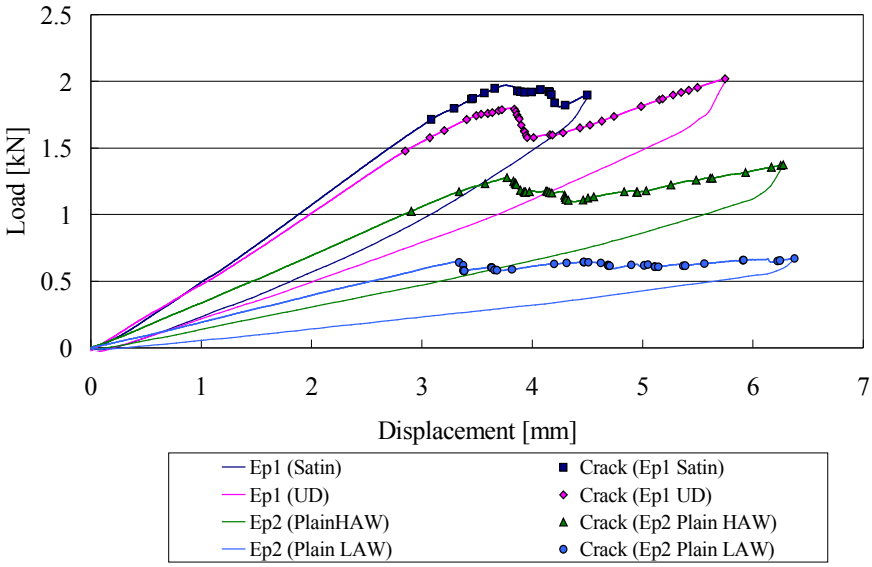

Figure B.1 Typical 4ENF load-displacement curves of non-interleaved specimens for epoxy resin systems

Figure B.2 shows the load-displacement curves for the VE system specimens. The maximum load and displacement values in the satin laminate were approximately 0.7kN and 3.3mm, respectively. Both of the maximum load and displacement values were significantly smaller compared with the Ep1 system composite. The crack velocity was quite faster than the Ep1 system specimens.

For the UD specimen, the maximum load and displacement values were about 1.9kN and 5.3mm, respectively. The curve shape was different from the Ep1 system sample. While the load in the Ep1 system specimen dropped once, for the VE system laminate it was increasing until the test finished. The slope in linear region was almost the same for both resin system laminates. However, the non-linear point for the VE system sample appeared earlier than the Ep1 system case.

In the plain weave specimen, only the HAW fabric was used. The maximum load and displacement were 0.7kN and 4.2mm, respectively. The maximum load was a similar value to the satin weave case. However, the crack propagation had a completely different behaviour. The crack propagation was quite slow. Moreover bending fracture started for some specimens during the 4ENF test. The crack could then propagate no longer.

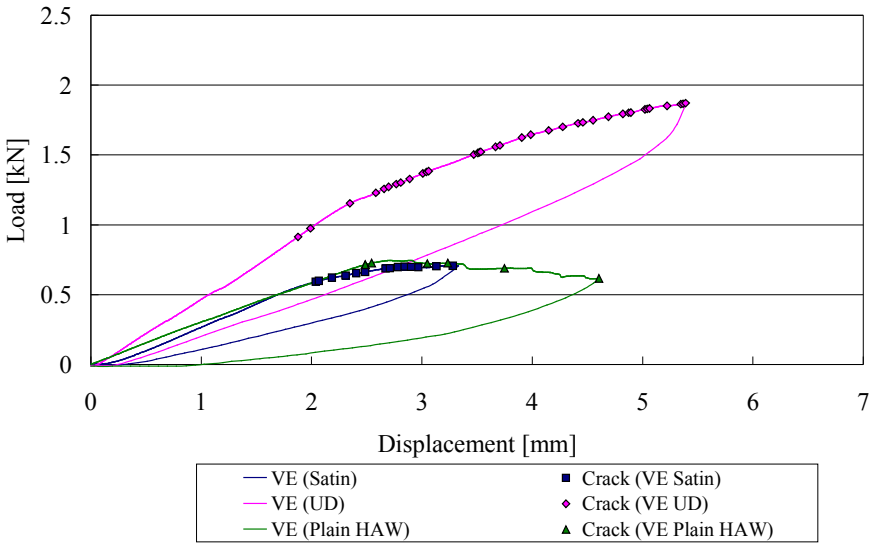

Figure B.2 Typical 4ENF load-displacement curves of non-interleaved specimens for vinyl ester resin system

B.1.2 Interleaved Specimens

B.1.2.1 Polyester/Carbon Veil Interleaved Specimens

The load-displacement curves for plain weave specimens are plotted in Figure B.3. The maximum load and displacement in the Ep2 system specimen were approximately 0.9kN and 6.7mm, respectively. In the Ep2 system laminate, the non-linear point appeared around 3.5mm. An increase of the load was slower than the VE system samples. The maximum load and displacement in the VE system specimen were 0.78kN and 4.4mm, respectively. The crack propagation speed of the Ep2 system specimen was slower than that of the VE system case. For both resin systems, the maximum load values were higher than the control.

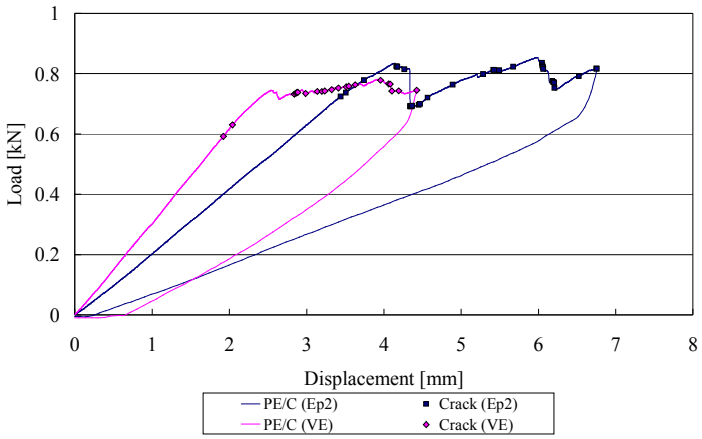

Figure B.3 Typical 4ENF load-displacement curves of PE/C (100:100) veil interleaved specimens for plain weave fabric specimens with both resin systems

B.1.2.2 Polyester/Carbon (70:30) Hybrid Veil Interleaved Specimens

Figure B.4 shows 4ENF test result for the Hyb1 veil interleaved specimens. The curve is similar to the control, as shown in Figure B.1 and B.4 (a). The maximum load and displacement in the satin laminate Ep1 system were about 1.8kN and 5.7mm, respectively. The load increased linearly up to 1.8kN. The load remained stable after the maximum load point. The maximum load was lower compared with the non-interleaved case.

For the UD specimens, the load-displacement curves for both resin system laminates have a completely different behaviour, as shown in Figure B.4 (b). The maximum load and displacement values for the Ep1 system specimen were larger than the VE system case. Both values for the Ep1 system specimen were approximately 2.4kN and 6.2mm, respectively. On the other hand, the maximum load and displacement for the VE system sample were around 1.6kN and 5mm, respectively. The crack initiation and non-linear point of the VE system laminate appeared earlier than those of the Ep1 system material. Moreover, the crack speed for the VE system composites was faster compared with the Ep1 system samples.

Figure B.4 (c) shows a result of the plain weave with the VE system specimen. The specimen in the plain weave composite gave 0.8kN of the load and 6.1mm of the displacement. The maximum load was the lowest value of all fabric samples. The crack propagation velocity was significantly slower than the other fabric specimens. After the displacement went beyond 5mm, the crack propagated no longer. Because bending fracture occurred.

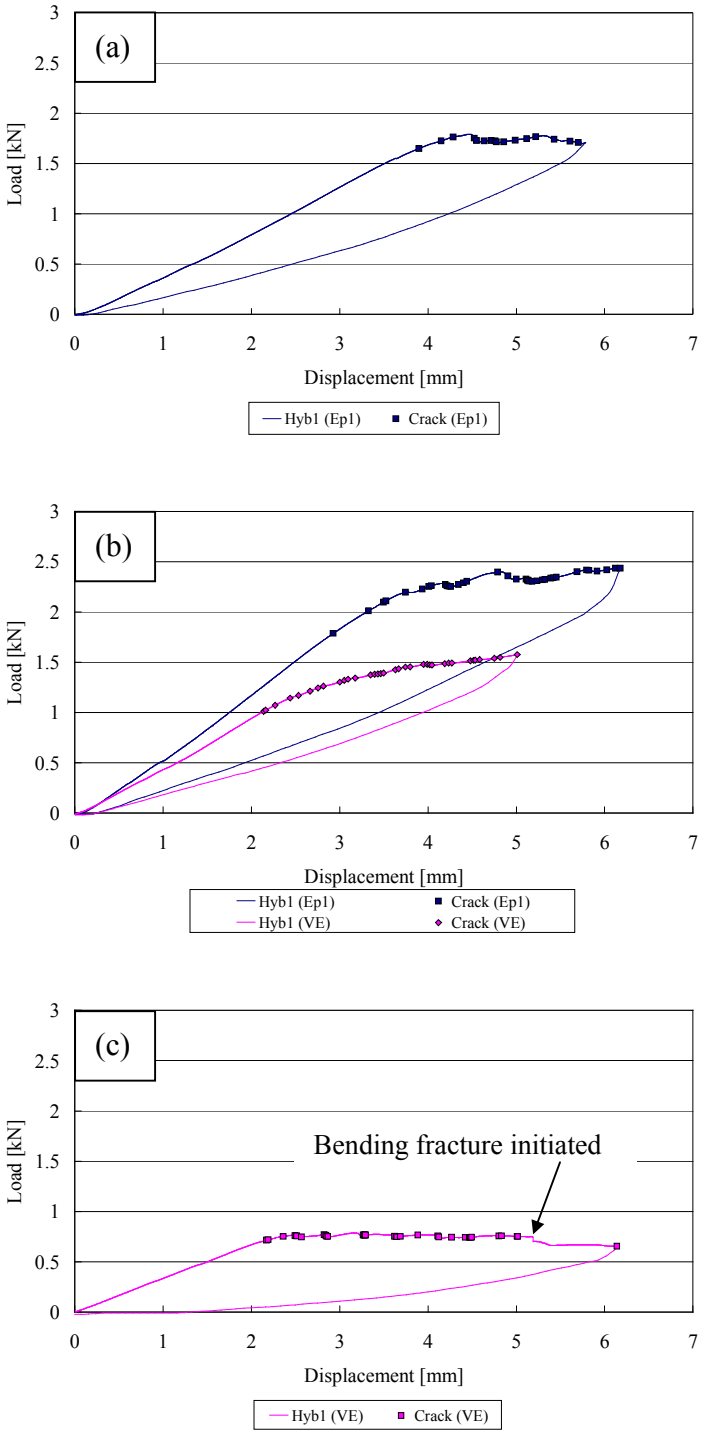

Figure B.4 Typical 4ENF load-displacement curves of PE/C (70:30) hybrid veil interleaved specimens with both resin systems: (a) 5-harness satin weave fabric, (b) Unidirectional fabric, (c) Plain weave fabric

B.1.2.3 Polyester/Carbon (80:20) Hybrid Veil Interleaved Specimens

The typical load-displacement curves for the Hyb2 veil interleaved specimens are plotted in Figure B.5. The maximum load and displacement values for the satin laminate Ep1 system were approximately 2.2kN and 6.7mm, respectively. Both values have larger than the Hyb1 veil interleaved case, as shown in Figure B.4 (a) and B.5 (a). The load kept constant over 5.2mm of displacement. Once the crack initiated, it propagated rapidly until the end of the test. The crack propagation behaviour was similar to the Hyb1 veil interleaved case.

In the UD laminates, the load-displacement curves in both resin systems have almost the same in behaviour as the Hyb1 veil interleaved samples, as shown in Figure B.4 (b) and B.5 (b). The Ep1 system specimen produced a significantly high maximum load and longer displacement, which were approximately 2.8kN and 7.1mm respectively. The VE system specimen, on the other hand, gave a maximum 1.5kN of load and 4.7mm of displacement. Both the maximum load and displacement values for the VE system specimen were significantly lower than the Ep1 system laminate. Moreover, the initiation of the crack propagation of the Ep1 system specimen was significantly later than the VE system case.

In the plain weave laminates, the maximum loads for both resin system specimens were similar values, approximately 0.98kN (Ep2) and 0.91kN (VE). The maximum load values for VE resin systems were slightly higher than the Hyb1 veil interleaved samples. The crack propagation behaviour for both resin system specimens, however, was different, as shown in Figure B.5 (c). The crack initiation of the Ep2 system composite was quite later than that of the VE system laminate. While the crack started for the Ep2 system around 3.5mm displacement, the crack for the VE system specimen initiated at about 2.2mm displacement. In both resin system specimens, the crack progressed constantly, and the propagation rate was almost the same.

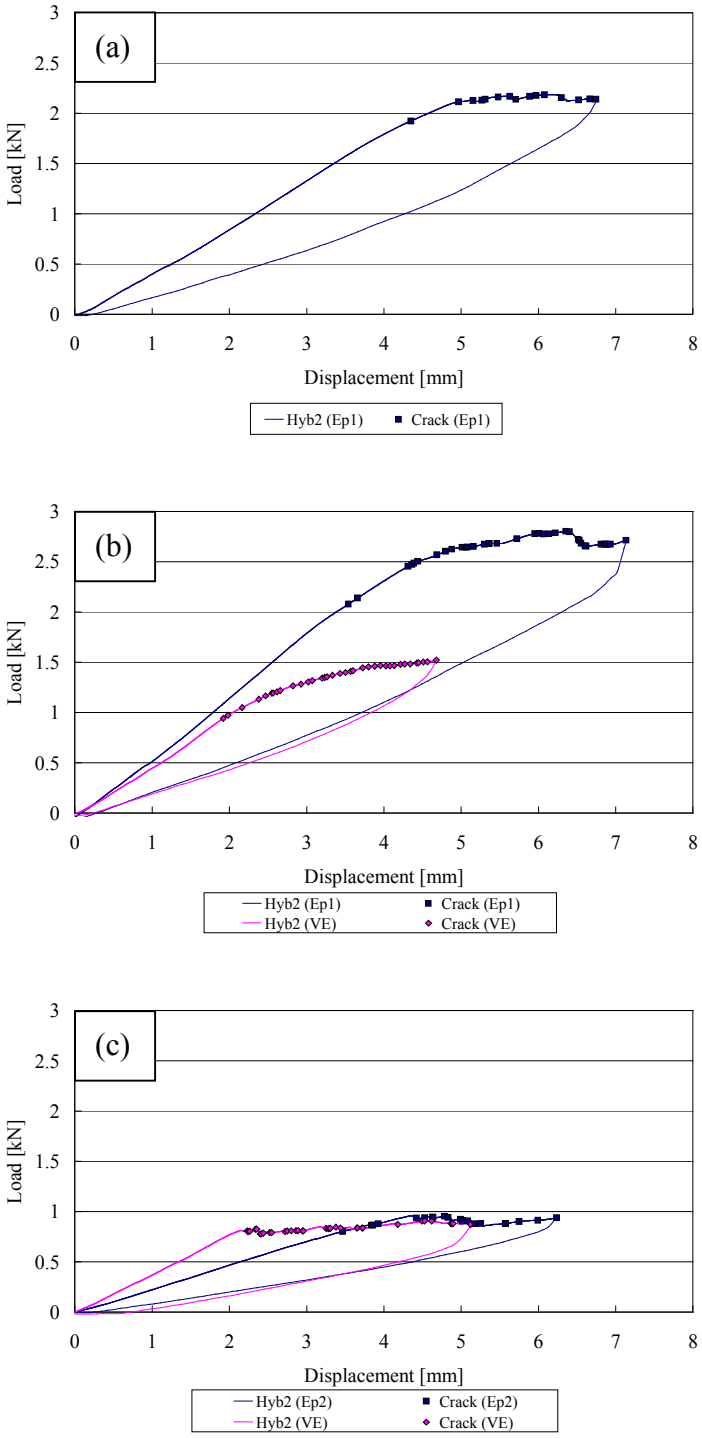

Figure B.5 Typical 4ENF load-displacement curves of PE/C (80:20) hybrid veil interleaved specimens with both resin systems: (a) 5-harness satin weave fabric, (b) Unidirectional fabric, (c) Plain weave fabric

B.1.2.4 Carbon Veil Interleaved Specimens

The typical load-displacement curves for the carbon veil interleaved composites are shown in Figure B.6. The maximum load and displacement values in the satin weave specimen were approximately 1.5kN and 4.4mm, respectively, as shown in Figure B.6 (a). The maximum load was lower than the non-interleaved case. Once the crack had initiated, the crack propagation was constant and fast. The crack initiation was earlier than the other interleaved specimens, except for the PA veil interleaved case.

In the UD laminates, the curve shapes for both resin system samples were similar, as illustrated in Figure B.6 (b). The maximum load and displacement in the Ep1 system specimen were around 2.1kN and approximately 5.4mm, respectively. The maximum load had slightly higher than for the non-interleaved material. The maximum load and displacement for the VE system composite were about 1.6kN and 4.7mm, respectively. The crack propagation for both system cases was constant over the non-linear point. The non-linear point of the VE system specimen appeared earlier than that of the Ep1 system laminate.

In the plain weave laminate, the maximum load value was approximately 0.9kN. The maximum load was similar in value to the hybrid veil interleaved samples. The crack no longer propagated after 4.5mm of displacement because bending fracture for 4ENF specimen was initiated. The crack propagation rate of the plain weave specimens was relatively slower than the other fabric samples.

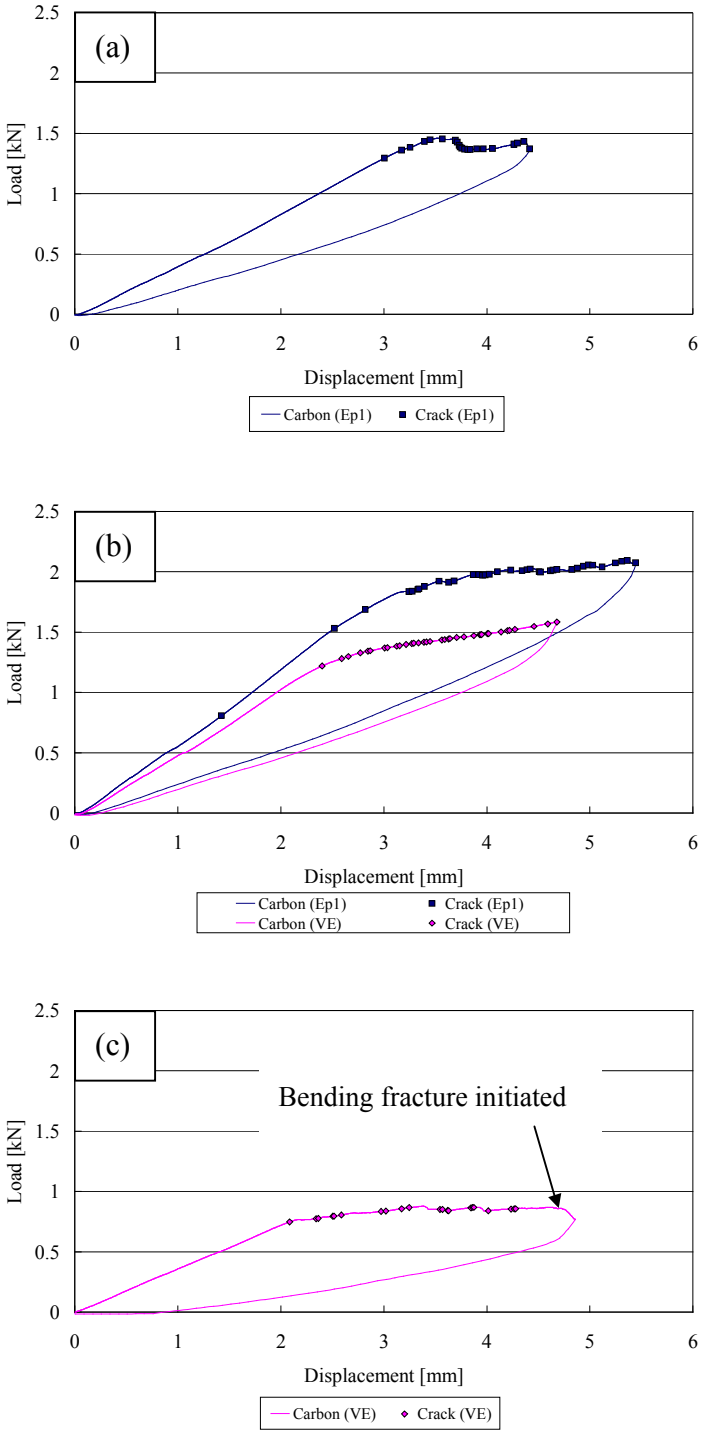

Figure B.6 Typical 4ENF load-displacement curves of carbon veil interleaved specimens with both resin systems: (a) 5-harness satin weave fabric, (b) Unidirectional fabric, (c) Plain weave fabric

B.1.2.5 Polyester Veil Interleaved Specimens

Typical load-displacement curves obtained by 4ENF test for the PE veil interleaved specimens are plotted in Figure B.7. The maximum displacement for both resin system specimens were similar, values around 6.3mm. On the other hand, the maximum load of the Ep1 system case was higher, nearly 2.0kN, than that of the VE system sample, approximately 1.3kN. The crack initiation for the Ep1 system laminate was slightly later than the VE system laminate. The crack propagation rate for both resin systems was similar.

For the UD specimens, although curve shapes in both resin systems were different, the crack propagation behaviour was similar, as illustrated in Figure B.7 (b). The Ep1 system specimen in the UD fabric gave 2.4kN of maximum load and 6.9mm of displacement. For the VE system composite, the maximum load and displacement were approximately 1.8kN and 4.9mm, respectively. The results of the VE system composites were similar to that of the control. The crack velocity of both resin systems seemed to be similar.

In the plain weave Ep2 system specimen, the maximum load and displacement values were around 1.2kN and 7.6mm, respectively. The crack propagated gradually up to 5.6mm displacement. Afterwards, it progressed rapidly until 7mm. The load dropped slightly at around 6.7mm displacement. The maximum load of the VE system laminate, on the other hand, was lower than that of the Ep2 system case, approximately 0.83kN. The crack propagation in the VE system sample was quite slow and did not grow over 3.2mm displacement due to the initiation of bending fracture, when the crack could propagate no longer.

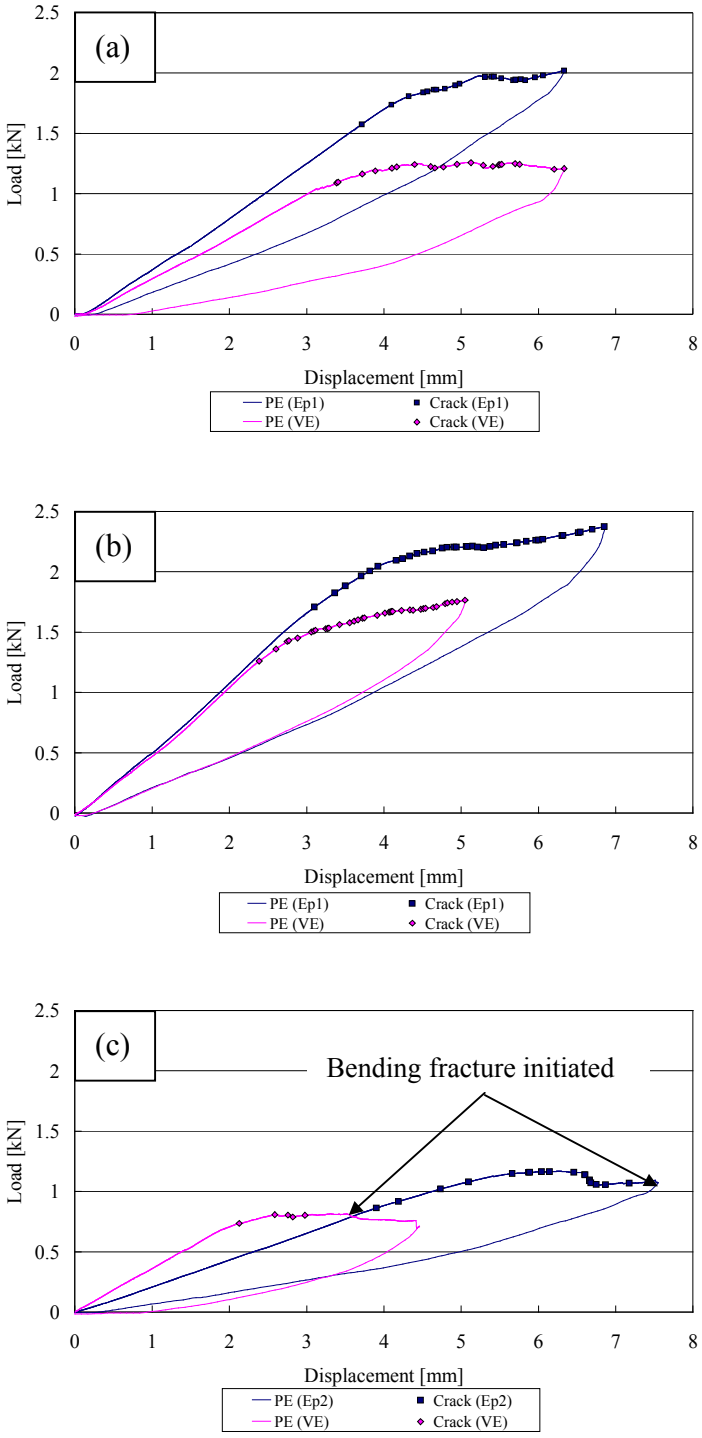

Figure B.7 Typical 4ENF load-displacement curves of PE veil interleaved specimens with both resin systems: (a) 5-harness satin weave fabric, (b) Unidirectional fabric, (c) Plain weave fabric

B.1.2.6 Polyamide Veil Interleaved Specimens

Typical load-displacement curves for the PA veil interleaved composites are shown in Figure B.8. The load kept increasing gradually over the non-linear point, as shown in Figure B.8 (a). The maximum load and displacement were around 1.7kN and 5.7mm, respectively. The maximum load obtained by the 4ENF test was moderately high, unlike the result of the DCB test. For the VE system, a load was constant over the maximum load point. The VE system case gave the maximum 1.2kN of load and 5.4mm of displacement. The curve shape was similar to that of the PE veil interleaved specimen.

In the UD laminate, the curve shapes for both resin systems are similar, as shown in Figure B.8 (b). The maximum load and displacement values for the Ep1 system sample were approximately 2.7kN and 7.6mm, respectively. Those of the VE system laminate, on the other hand, were lower than the Ep1 system case, nearly 2.2kN and 6.4mm. The crack propagation speed of the Ep1 system specimen was slower than that of the VE system material. In the VE system, the crack growth was constant and gradual.

In the plain weave composites, the crack propagation speed for both resin system specimens was significantly slow. For the Ep2 system specimen, the maximum load and displacement were 1.2kN and 6.4mm, respectively. The Ep2 system sample initiated bending fracture at around 6.3mm displacement and finally underwent at 6.4mm, as illustrated in Figure B.8 (c). The VE system laminate gave a maximum load of 0.8kN and displacement of 4.5mm. Bending fracture initiated at a displacement over 3.2mm. Once bending fracture started, the crack could grow no longer and therefore data points were significantly less.

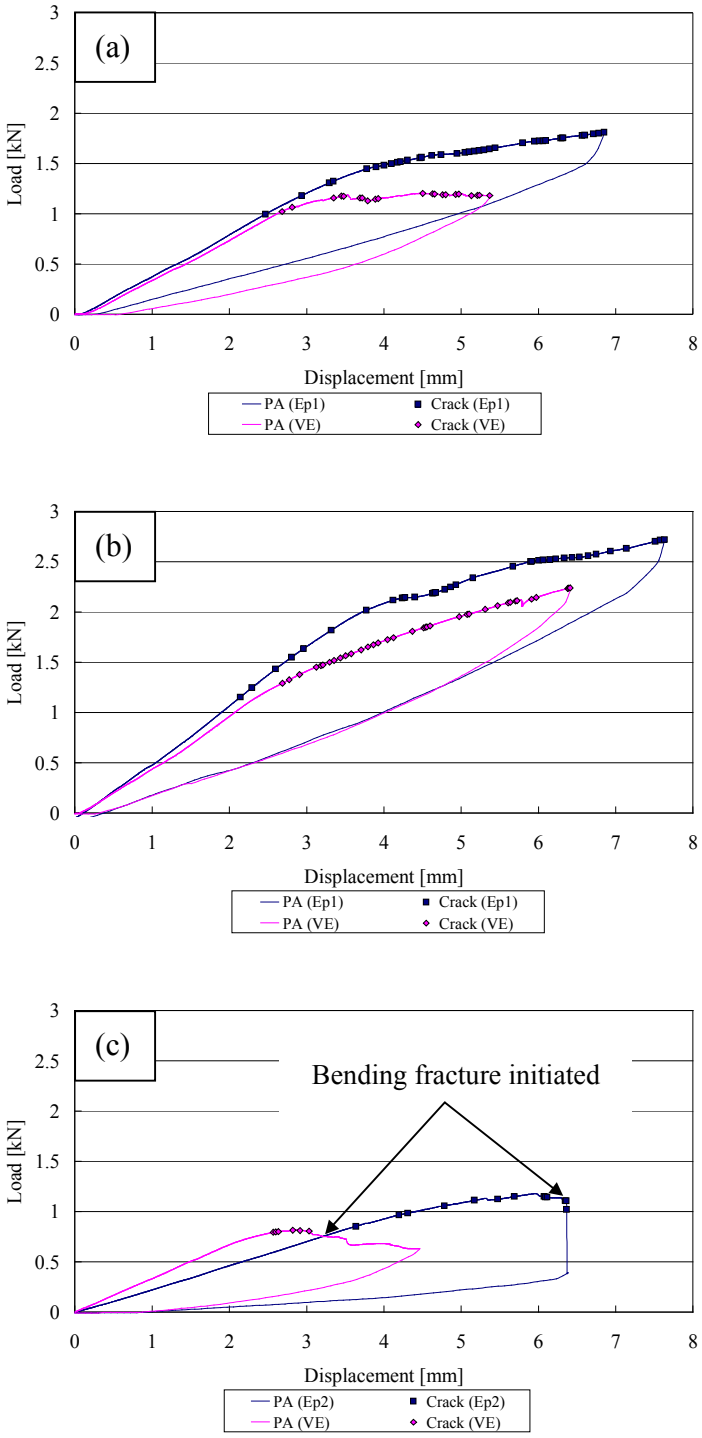

Figure B.8 Typical 4ENF load-displacement curves of PA veil interleaved specimens with both resin systems: (a) 5-harness satin weave fabric, (b) Unidirectional fabric, (c) Plain weave fabric

The crack growth in the Mode-II interlaminar fracture test was normally stable propagation. The maximum load and displacement for the Ep system laminates were higher than the VE system specimens. The VE system samples tended to show the non-linear point earlier than the Ep system cases. For the plain weave materials, the crack propagation speed was significantly slower compared with the other fabric cases. Moreover, some plain weave interleaved samples underwent bending fracture during 4ENF tests. Tables B.1 to B.3.5 show the summaries of the results for the 4ENF test.

Table B.1 Summary of 4ENF test results for 5-haness satin weave fabric specimens (Load and displacement are maximum values)

	Epoxy1		Vinyl ester	
Interleaf	Load [kN]	Displacement [mm]	Load [kN]	Displacement [mm]
Non	2.0	4.5	0.7	3.3
Hyb1	1.8	5.8	-#	-
Hyb2	2.2	6.8	-	-
Carbon	1.5	4.4	-	-
PE	2.0	6.3	1.3	6.3
PA	1.8	6.9	1.2	5.4

#: Not examined

Table B.2 Summary of 4ENF test results for unidirectional fabric specimens (Load and displacement are maximum values)

	Epoxy1		Vinyl ester	
Interleaf	Load [kN]	Displacement [mm]	Load [kN]	Displacement [mm]
Non	2.0	5.8	1.9	5.4
Hyb1	2.4	6.2	1.6	5.0
Hyb2	2.8	7.1	1.5	4.7
Carbon	2.1	5.5	1.6	4.7
PE	2.4	6.9	1.8	5.1
PA	2.7	7.6	2.2	6.4

Table B.3 Summary of 4ENF test results for plain weave fabric specimens (Load and displacement are maximum values)

	Epoxy2		Vinyl ester	
Interleaf	Load [N]	Displacement [mm]	Load [N]	Displacement [mm]
Non	0.7*/1.4**	6.4*/6.3**	0.7	4.6
PE/C	0.9	6.8	0.8	4.4
Hyb1	-	-	0.8	6.1
Hyb2	1.0	6.2	0.9	5.1
Carbon	-	-	0.9	4.9
PE	1.2	7.5	0.8	4.5
PA	1.2	6.4	0.8	4.5

*: LAW specimen, **: HAW specimen

Appendix C

Damage Area Obtained by Impact Tests

C.1 Introduction

Damage areas for all impacted specimens were measured by C-scan. In this section, correlations between the damage area and other mechanical properties are indicated and discussed.

C.2 Correlation between Mode-I and Mode-II Interlaminar Toughness, and Impact Damage Area

Diagrams of the correlation between the Mode-I initial and propagation values as a function of the damage area are shown in Figures C.1 and C.2, respectively. For the Ep2 resin system, the correlation between the $G_{IC\text{-}NL}$ and damage area does not appear clearly, as shown in Figure C.1. The trend of the correlation is different from the relationship between G_{IC} values and damage width (see in Figure 6.7). There is no clear correlation between $G_{I\text{-}prop}$ values and the damage area. For the VE resin system, the relationship between $G_{IC\text{-}NL}$ values and the damage area is similar to the correlation between $G_{IC\text{-}NL}$ values and the damage width (see in Figure 6.7). However, there is no correlation between $G_{I\text{-}prop}$ values and the damage area, as shown in Figure C.2. It can be seen that there is no clear relationship between Mode-I interlaminar toughness and the damage area in both resin systems, unlike the relationship between Mode-I interlaminar toughness and the damage width.

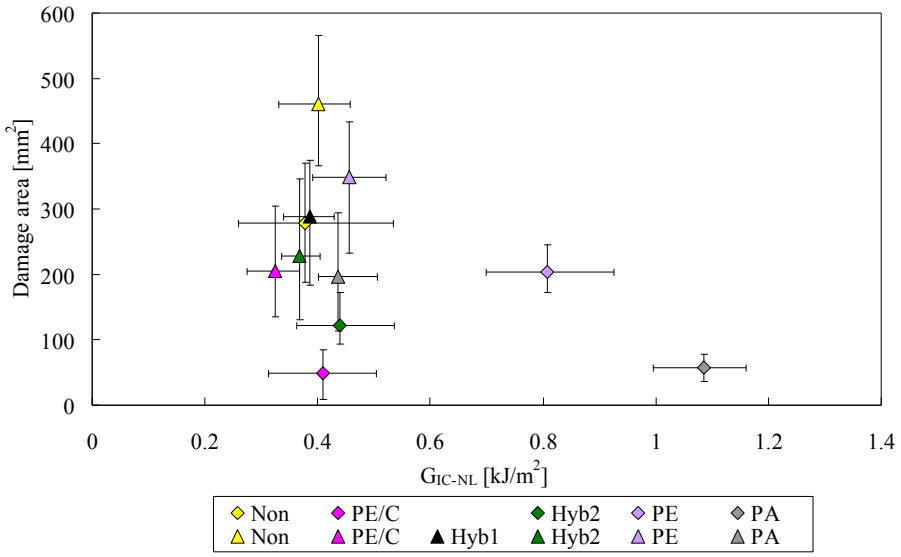

Figure C.1 Relationship between $G_{IC\text{-}NL}$ versus damage area (4J of impact energy) for both resin systems with error bars (Diamond is Ep2 system and Triangle is VE system)

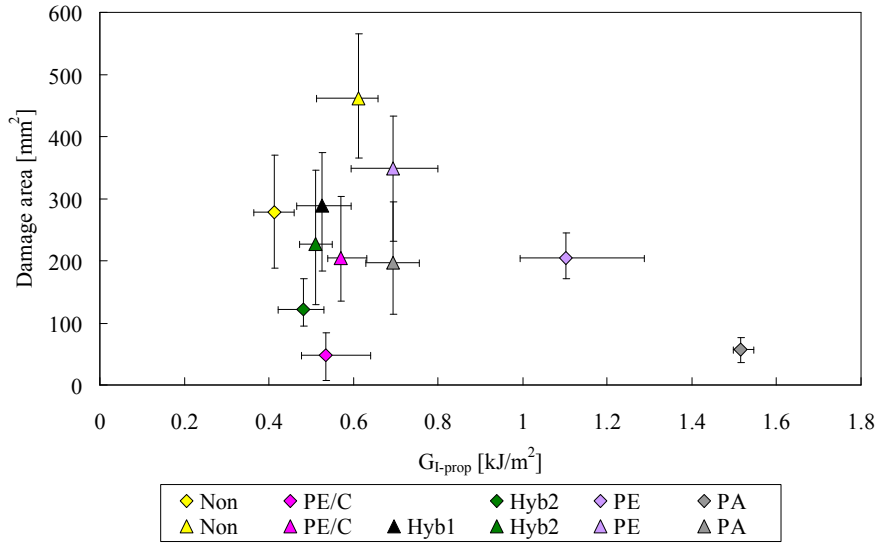

Figure C.2 Relationship between $G_{I\text{-}prop}$ versus damage area (4J of impact energy) for both resin systems with error bars (Diamond is Ep2 system and Triangle is VE system)

Figures C.3 and C.4 show the comparison of the relationship between the Mode-II initial and propagation values, and damage area. In the Ep2 system, the correlation between Mode-II interlaminar toughness and damage area is similar to the relationship between the Mode-II interlaminar toughness and damage width, as shown in Figure 6.9 and C.3. However, data spread in the damage area is larger than the damage width. For the VE system, the correlation is also quite similar to the relationship between $G_{IIC\text{-}NL}$ values and the damage width (see in Figure 6.9 and C.3). For the propagation values, the tendency of the correlation is almost the same as the initial values. There is no clear relationship between $G_{II\text{-}prop}$ values and damage area for both resin systems. The correlation between interlaminar toughness and damage area does not appear clearly. When the relationship between the interlaminar toughness and impact resistance is discussed, the damage width may be more suitable than the damage area, It is thought that the damage width would indicate the impact damage more clearly compared with the damage area.

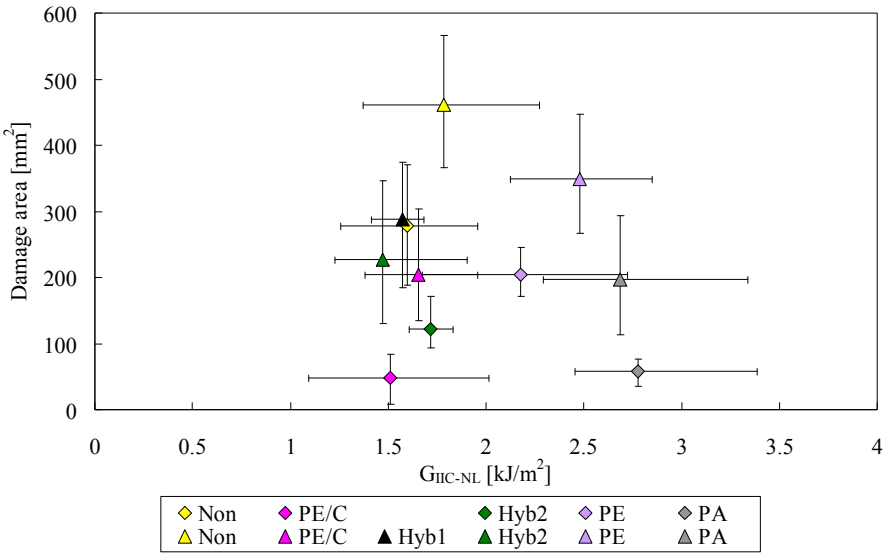

Figure C.3 Relationship between $G_{IIC\text{-}NL}$ versus damage area (4J of impact energy) for both resin systems with error bars (Diamond is Ep2 system and Triangle is VE system)

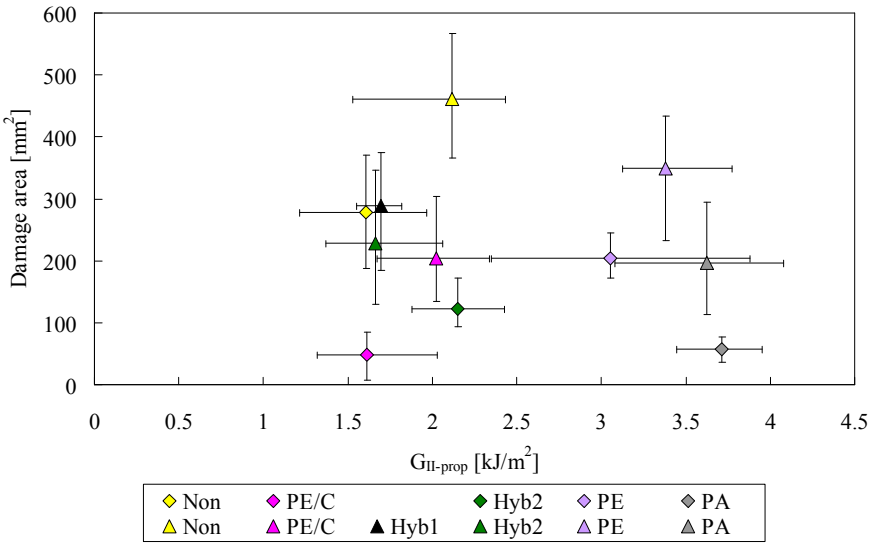

Figure C.4 Relationship between $G_{II\text{-}prop}$ versus damage area (4J of impact energy) for both resin systems with error bars (Diamond is Ep2 system and Triangle is VE system)

C.3 Correlation between Impact Damage Area and CAI Strength

Figure C.5 plots the impact damage area as a function of normalised CAI strength for the Ep2 system specimens. The CAI strengths are normalised by compression strength for undamaged composites. While the relationship between damage width and CAI strength is linear (see in Figure 6.15), the correlation between damage area and CAI strength is a non-linear relationship, as shown in Figure C.5. The damage width increases largely at the lowest impact energy. Thereafter the increase in the damage width is small with increase in impact energies. On the other hand, the increase in the damage area is different from the increase in the width. For the PE/C, Hyb2, and PA veil interleaved composites, the increase in the damage area at the lowest energy is small. Thereafter, an increase in the damage area grows steadily. In contrast, an increase of the damage area for the control and PE veils interleaved samples becomes small as the impact energy increases.

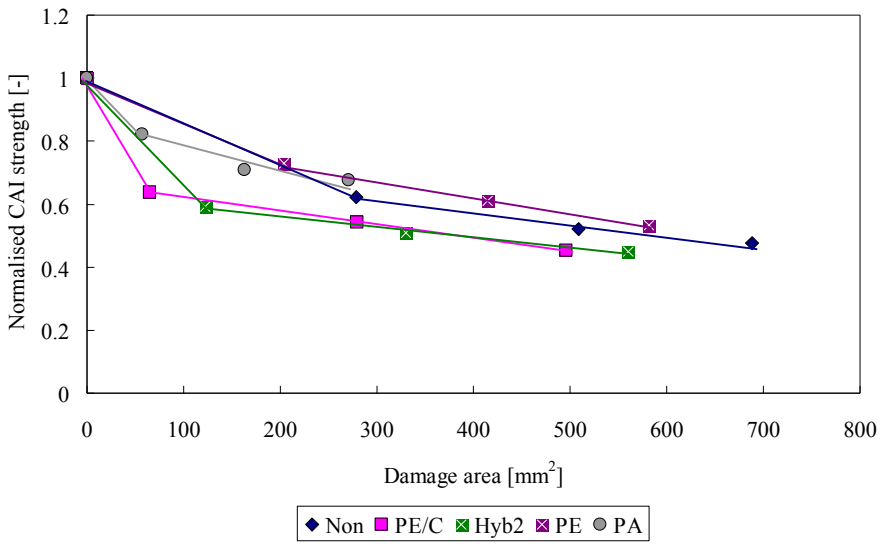

Figure C.5 Compression after impact strength for non-interleaved and interleaved epoxy2 system specimens plotted as a function of damage area

Figure C.6 shows the relationship of the damage area as a function of the normalised CAI strength for the VE systems. Compared to the Ep2 system specimens, the increase of the damage area shows a different behaviour. On the other hand, the relationship between the damage area and CAI strength is similar to the correlation between the damage width and CAI strength, except for the PE/C and Hyb2 veils interleaved cases (see in Figure 6.16 and C.6). The increase of the damage area tended to be small from 0J to 4J and 8J to 12J. However, the damage area increased largely from 4J and 8J of impact energy. The increase of damage area for the PA veil interleaved materials is quite smaller than the other interleaved samples. Moreover, the reduction of CAI strength is relatively small. On the other hand, while CAI strength for the PE/C veil interleaved samples reduces large at 4J impact energy, the reduction in higher energies is smaller than the other interleaved materials. For the Hyb2 veil interleaved samples, although the damage area are smaller than the other interleaved cases, the CAI strengths are lower. Compared to the relationship between damage width and CAI strength, it is seemed that the correlation between damage area and CAI strength is not good.

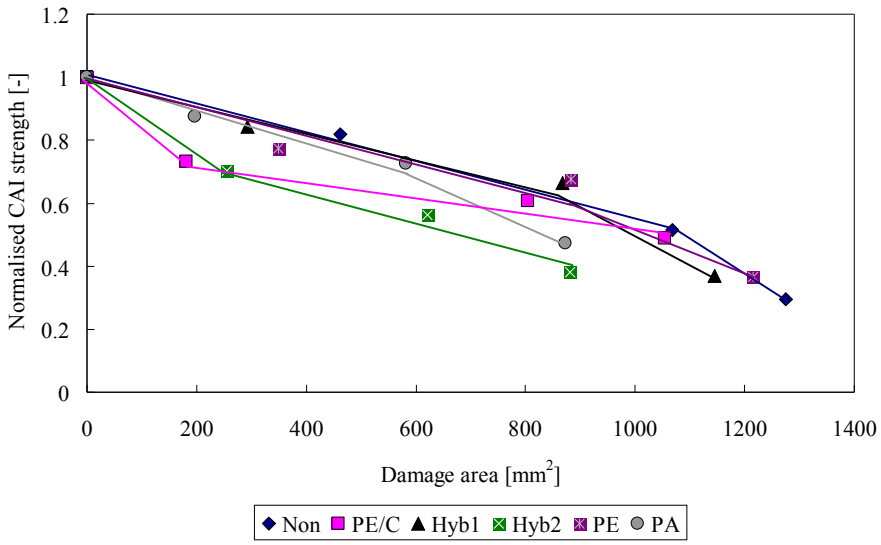

Figure C.6 Compression after impact strength for non-interleaved and interleaved vinyl ester system specimens plotted as a function of damage area

C.4 Comparison of this research and previous works

Figure C.7 compares the influence of the impact damage area on CAI strength for this study and previous other researches. The relationship between the damage area and CAI strength from previous literatures is similar to this study's finding. The CAI strength at the lowest impact energy dropped rapidly. However, reduction of the CAI strength at higher impact energies is small. The damage area of the specimens in this work is relatively smaller than the other data in the literature, in particular the Ep2 system composites. In contrast, the CAI strength is poor compared with previous literatures, in particular the VE system laminates.

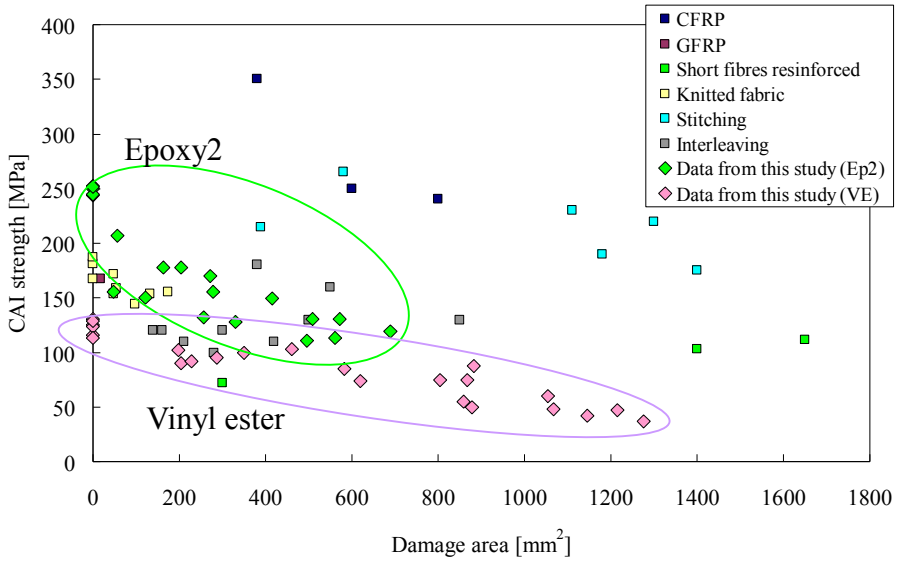

Figure C.7 Diagram compares effect of impact resistance (damage area) on the CAI strength for this work and literatures [57, 77, 88, 95, 148, 163]

References

[1] Ashby M.F., Jones D.R.H., (1998), "Engineering Materials 2: An Introduction to Microstructures, Processing and Design Second Edition", *Butterworth Heinemann*, **Chapter 25**, pp.252-265

[2] Miki M., Fukuda T., Motoki S., Hojo M., (1997), "Fukugouzairyou (Japanese)", *Kyouritsu Publicatio*, **Chapter 2**, pp.27-61

[3] Nihon Kikai Gakkai, (1990), "Sentan Fukugou Zairyou (Japanese)", *Gihoudou Publication*, **Chapter 1**, pp.1-12

[4] Callister Jr., W. D., (2003), "Materials Science and Engineering An Introduction Sixth Edition", *John Wiley & Sons, Inc.*, **Chapter 16**, pp.527-568

[5] Kawasetsu N., Shindo K., Takita K., Kato E., (2004), "Behaviour of resin flow during VaRTM process for FRP structure", *Procedure of 12th The Japan Society of Mechanical Engineering Materials and Processing*, pp.137-138

[6] Ashby, M.F., (1999), "Materials Selection in Mechanical Design Scond Edition", *Butterworth-Heinemann*, **Chapter 1**, pp.1-7

[7] Miki M., Fukuda T., Motoki S., Hojo M., (1997), "Fukugouzairyou (Japanese)", *Kyouritsu Publicatio*, **Chapter 1**, pp.1-26

[8] Zako, M., (2004), *Journal of the Textile Machinery Society of Japan*, **57**, pp.11-16

[9] Hillermerier, R.W., Hayes, B.S., Seferis, J.C., (1999), "Processing of highly elastomeric toughened cyanate esters through a modified resin transfer molding technique", *Polymer Composites*, **20**(1), pp.517-524

[10] Hillermeier, R.W., Seferis, J.C., (2001), "Interlayer toughening of resin transfer molding composites", *Composites Part A*, **32**, pp.155-165

[11] Miyairi, H., (2003), *Plastics (Japan)*, **54**(1), pp.168-177

[12] Williams, C., Summerscales, J., Grove, S., (1996), "Resin infusion under flexible tooling (RIFT): a review", *Composites Part A*, **27A**, pp.721-729

[13] Kelkar, A.D., Tate, J.S., Chaphalkar, P., (2006), "Performance evaluation fo VARTM manufactured textile composites for the aerospace and defense applications", *Materials Science and Engineering B*, **132**, pp.525-534

[14] Heider, D., Simacek, P., Dominausks, A., Deffor, H., Advani, S., Gillespie Jr., J.W., (2007), "Infusion design methodology for thick-section, low-permeability preforms using inter-laminar flow media", *Composites Part A*, **38**, pp.126-128

[15] Nalla, A.R., Fuqua, M., Glancey, J., Lelievre, B., (2007), "A multi-segment injection line and real-time adaptive, model-based controller for vacuum assisted resin transfer molding", *Composites Part A*, **38**, pp.1058-1069

[16] Kuentzer, N., Simacek, P., Advani, S.G., Walsh, S., (2007), "Correlation of void distribution to VARTM manufacturing techniques", *Composites Part A*, **38**, pp.802-813

[17] Johnson, R.J., Pitchumani, R., (2007), "Flow control using localized induction heating in a VARTM process", *Composites Science and Technology*, **67**, pp.669-684

[18] Simacek, P., Advani, S.G., (2007), "Modeling resin flow and fiber tow saturation induced by distribution media collapse in VARTM", *Composites Science and Technology*, **67**, pp.2757-2769

[19] Miki M., Fukuda T., Motoki S., Hojo M., (1997), "Fukugouzairyou (Japanese)", *Kyouritsu Publication*, **Chapter 6**, pp.159-185

[20] Sela, N., Ishai, O., (1989), "Interlaminar fracture toughness and toughening of laminated composite materials: a review", *Composites*, **20**(5), pp.423-435

[21] Abrate, S., (1998), "Impact on composite structures", *Cambridge University Press*, **Chapter 4**, pp.135-160

[22] Richardson, M.O.W., Wisheart, M.J., (1996), "Review of low-velocity impact properties of composite materials", *Composites Part A*, **27A**, pp.1123-1131

[23] Chan, W.S., (1991), "Design approaches for edge delamination resistance in laminated composites", *Journal of Composites Technology & Research*, **14**(2), pp.91-96

[24] Scott, J.M., Phillips, D.C., (1975), "Carbon fibre composites with rubber toughened matrices", *Journal of Materials Science*, **10**, pp.551-562

[25] Hunston, D.L., (1984), "Composite interlaminar fracture: effect of matrix fracture energy", *Composites Technology Review*, **6**(4), pp.176-180

[26] Zulkifli, R., Fatt, L.K., Azhari, C.H., Sahari, J., (2002), "Interlaminar fracture properties of fibre reinforced natural rubber/polypropylene composites", *Journal of Materials Processing Technology*, **128**, pp.33-37

[27] Kim, J., Baillie, C., Poh, J., Mai, Y.–W., (1992), "Fracture toughness of CFRP with modified epoxy resin matrices", *Composites Science and Technology*, **43**, pp.283-297

[28] Gao, B., Kim, J.–K., Leung, C.K.Y., (2003), "Effect of rubber modifier on interlaminar fracture toughness of CFRP-concrete interface", *Composites Science and Technology*, **63**, pp.883-892

[29] Takeichi, T., Saito, Y., Agag, T., Muto, H., Kawauchi, T., (2008), "High-performance polymer alloys of polybenzoxazine and bismaleimide", *Polymer*, **49**, pp.1173-1179

[30] Chou, S., Chen, H.–C., Wu, C.–C., (1992), "BMI resin composites reinforced with 3D carbon-fibre fabrics", *Composites Science and Technology*, **43**, pp.117-128

[31] Wilkinson, S.P., Ward, T.C., McGrath, J.E., (1993), "Effect of thermoplastic modifier variables on toughening a bismaleimide matrix resin for high-performance composite materials", *Polymer*, **34**(4), pp.870-884

[32] Boogh, L., Pettersson, B., Manson, J.–A.E., (1999), "Dendritic hyperbranched polymer as tougheners for epoxy resins", *Polymer*, **40**, pp.2249-2261

[33] Mezzenga, R., Boogh, L., Manson, J.–A.E., (2001), "A review of dendritic hyperbranched polymer as modifiers in epoxy composites", *Composites Science and Technology*, **61**, pp.787-795

[34] DeCarli, M., Kozielski, K., Tian, W., Varley, R., (2005), "Toughening of a carbon fibre reinforced epoxy anhydride composite using an epoxy terminated hyperbranched modifier", *Composites Science and Technology*, **65**, pp.2156-2166

[35] Verrey, J., Winkler, Y., Michaud, V., Manson, J.–A.E., (2005), "Interlaminar fracture toughness improvement in composites with hyperbranched polymer modified resin", *Composites Science and Technology*, **65**, pp.1527-1536

[36] Friedrich, K., Hou, M., (1998), "On stamp forming of curved and flexible geometry components from continuous glass fiber/polypropylene composites", *Composites Part A*, **29A**, pp.217-226

[37] Nowacki, J., neitzel, M., (2000), "Thermoforming of reinforced thermoplastic stiffened structure", *Polymer Composites*, **21**(4), pp.531-538

[38] Frassine, R., Pavan, A., (1995), "Viscoelastic effects on the interlaminar fracture behaviour of thermoplastic matrix composites: I. Rate and temperature dependence in unidirectional PEEK/carbon-fibre laminates", *Composites Science and Technology*, **56**, pp.1253-1260

[39] Davies, P., Cantwell, W., Moulin, C., Kausch, H.H., (1989), "A study of the delamination resistance of IM6/PEEK composites", *Composites Science and Technology*, **36**, pp.153-166

[40] Bradsky, G. von, Chivers, R.A., Crick, R.A., Turner, R.M., (1993), "Interlaminar fracture toughness of a range of continuous fibre PEEK composites", *Composites Science and Technology*, **47**, pp.75-81

[41] Frassine, R., Pavan, A., (1995), "Viscoelastic effects on the interlaminar fracture behaviour of thermoplastic matrix composites: II. Rate and temperature dependence in unidirectional PEI/carbon-fibre laminates", *Composites Science and Technology*, **54**, pp.193-200

[42] Kim, K.–Y., Ye, L., (2004), "Interlaminar fracture toughness of CF/PEI composites at elevated temperatures: roles of matrix toughness and fibre/matrix adhesion", *Composites Part A*, **35**, pp.477-487

[43] Hashemi, S., Kinloch, A.J., Williams, J.G., (1990), "Mechanics and mechanisms of delamination in a Poly(ether sulphone) - Fibre composite", *Composites Science and Technology*, **37**, pp.429-462

[44] Hine, P.J., Brew, B., Duckeet, R.A., Ward, I.M., (1992), "Failure mechanism in carbon-fibre-reinforced poly(ether sulphone)", *Composites Science and Technology*, **43**, pp.37-47

[45] Kuboki, T., Jar, P.–Y.B., Forest, T.W., (2003), "Influence of interlaminar fracture toughness on impact resistance of glass fibre reinforced polymers", *Composites Science and Technology*, **63**, pp.943-953

[46] Venderbosch, R.W., Peijs, T., Meijer, H.E.H., Lemstra, P.L., (1996), "Fibre-reinforced composites with tailored interphases using PPE/epoxy blends as a matrix system", *Composites Part A*, **27A**, pp.895-905

[47] Perrin, F., Bureau, M.N., Denault, J., Dickson, J.I., (2003), "Mode I interlaminar crack propagation in continuous glass fiber/polypropylene composites: temperature and molding condition dependence", *Composites Science and Technology*, **63**, pp.597-607

[48] Azimi, H.R., Pearson, R.A., Hertzberg, R.W., (1995), "Role of crack tip shielding mechanisms in fatigue of hybrid epoxy composites containing rubber and solid glass spheres", *Journal of Applied Polymer Science*, **58**, pp.449-463

[49] Spanoudakis, J., Young, R.J., (1984), "Crack propagation in a glass particle-filled epoxy resin Part 1. effect of particle volume fraction and size", *Journal of Materials Science*, **19**, pp.473-486

[50] Spanoudakis, J., Young, R.J., (1984), "Crack propagation in a glass particle-filled epoxy resin Part 2. effect of particle-matrix adhesion", *Journal of Materials Science*, **19**, pp.487-496

[51] Boyce, M.E., Argon, A.S., Parks, D.M., (1987), "Mechanical properties of compliant composite particles effective in toughening glassy polymers", *Polymer*, **28**, pp.1680-1694

[52] Derkowski, B.J., Sue, H.–J., (2003), "Morphology and compression-after-impact strength relationship in interleaved toughened composites", *Polymer Composites*, **24**(1), pp.158-170

[53] Srivastava, V.K., Hogg, P.J., (1998), "Damage performance of particles filled quasi-isotropic glass-fibre reinforced polyester resin composites", *Journal of Materials Science*, **33**, pp.1119-1128

[54] Jang, B.Z., Liau, J.Y., Hawng, L.R., Shih, W.K., (1990), "Particulate and whisker modifications of matrix resin for improved toughness of fibrous composites", *Journal of Reinforced Plastic and Composites*, **9**(July), pp.314-334

[55] Xiong, Z., Geng, L., Yao, C.K., (1990), "Investigation of high-temperature deformation behavior of a SiC whisker reinforced 6061 aluminium composite", *Composites Science and Technology*, **39**, pp.117-125

[56] Wang, W.X., Takao, Y., Matsubara, T., Kim, H.S., (2002), "Improvement of the interlaminar fracture toughness of composite laminates by whisker reinforced interlamination", *Composites Science and Technology*, **62**, pp.767-774

[57] Sohn, M.S., Hu, X.Z., Kim, J.K., Walker, L., (2000), "Impact damage characterisation of carbon fibre/epoxy composites with multi-layer reinforcement", *Composites Part B*, **31**, pp.681-691

[58] Low, I.–M., Mai, Y.–W., Bandyopadhayay, S., (1992), "Effects of temperature and rate on fracture toughness of short-alumina-fibre-reinforced epoxies", *Composites Science and Technology*, **43**, pp.893-902

[59] Choi, N.S., Takahashi, K., (1992), "Stress fields on and beneath the surface of short-fiber-reinforced composites and their failure mechanisms", *Composites Science and Technology*, **43**, pp.237-244

[60] Walker, L., Sohn, M.–S., Hu, X.–Z., (2002), "Improving impact resistance of carbon-fibre composites through interlaminar reinforcement", *Composites Part A*, **33**, pp.3-12

[61] Yamashita, S., Hatta, H., Takei, T., Sugano, T., (1992), "Interlaminar reinforcement of laminated composites by addition of oriented whiskers in the matrix", *Journal of Composite Materials*, **26**(9), pp.1254-1268

[62] Siddiqui, N.A., Woo, R.S.C., Kim, J.–K., Leung, C.C.K., Munir, A., (2007), "Mode I interlaminar fracture behavior and mechnical properties of CFRPs with nanoclay-filled epoxy matrix", *Composites Part A*, **38**, pp.449-460

[63] Lee, S.M., (1992), "Influence of fiber/matrix interfacial adhesion on composite fracture behavior", *Composites Science and Technology*, **43**, pp.317-327

[64] Suzuki, T., Miyajima, T., Sakai, M., (1994), "The role of the fiber/matrix interface in the first matrix cracking of fiber-reinforced brittle-matrix composites", *Composites Science and Technology*, **51**, pp.283-289

[65] Hu, X.–Z., Mai, Y.–W., (1993), "Mode I delamination and fibre bridging in carbon-fibre/epoxy composites with and without PVAL coating", *Composites Science and Technology*, **46**, pp.147-156

[66] Albertsen, H., Ivens, J., Peters, P., Wevers, M., Verpoest, I., (1995), "Interlaminar fracture toughness of CFRP influenced by fibre surface treatment: Part 1. Experimental results", *Composites Science and Technology*, **54**, pp.133-145

[67] Ivens, J., Albertsen, H., Wevers, M., Verpoest, I., Peters, P., (1995), "Interlaminar fracture toughness of CFRP influence by fibre surface treatment: Part 2. Modelling of the interface effect", *Composites Science and Technology*, **54**, pp.147-159

[68] Hirai, Y., Hamada, H., Kim, J.–K., (1998), "Impact response of woven glass-fabric composites - I. Effect of fibre surface treatment", *Composites Science and Technology*, **58**, pp.91-104

[69] Hirai, Y., Hamada, H., Kim, J.–K., (1998), "Impact response of woven glass-fabric composites - II. Effect of temperature", *Composites Science and Technology*, **58**, pp.119-128

[70] Vickers, P.E., Boniface, L., Pricket, A., Watts, J.F., (2000), "The effect of siloxane-type molecules on the interlaminar toughness of CFRP", *Composites Part A*, **31**, pp.559-569

[71] Kim, J., Mai, Y.–W., (1991), "Effects of interfacial coating and temperature on the fracture behaviours of unidirectional Kevlar and carbon fibre reinforced epoxy resin composites", *Journal of Materials Science*, **26**, pp.4702-4720

[72] Johnson, W.S., Mangalgiri, P.D., (1987), "Investigation of fiber bridging in double cantilever beam specimens", *Journal of Composites Technology & Research*, **9**(1), pp.10-13

[73] Huang, X.N., Hull, D., (1989), "Effects of fibre bridging on G_{IC} of a unidirectional glass/epoxy composite", *Composites Science and Technology*, **35**, pp.283-299

[74] Madhukar, M.S., Drzal, L.T., (1992), "Fiber-matrix adhesion and its effect on composite mechanical properties: IV. Mode I and Mode II fracture toughness of graphite/epoxy composites", *Journal of Composite Materials*, **26**(7), pp.936-968

[75] Naik, N.K, Shembekar, P.S., Hosur, M.V., (1991), "Failure behavior of woven fabric composites", *Journal of Composites Technology & Research*, **13**(1), pp.107-116

[76] Alif, N., Carlsson, L.A., Boogh, L., (1998), "The effect of weave pattern and crack propagation direction on mode I delamination resistance of woven glass and carbon composites", *Composites Part B*, **29B**, pp.603-611

[77] Naik, N.K., Borade, S.V., Arya, H., Sailendra, M., Prabhu, S.V., (2002), "Experimental studies on impact behaviour of woven fabric composites: Effect of impact parameters", *Journal of Reinforced Plastic and Composites*, **21**(15), pp.1347-1362

[78] Kim, J.–K., Sham, M.–L., (2000), "Impact and delamination failure of woven-fabric composites", *Composites Science and Technology*, **60**, pp.745-761

[79] Briscoe, B.J., Court, R.S., Williams, D.R., (1993), "The effects of fabric weave and surface texture on the interlaminar fracture toughness of aramid/epoxy laminates", *Composites Science and Technology*, **47**, pp.261-270

[80] Kim, J., Shioya, M., Kobayashi, H., Kaneko, J., Kido, M., (2004), "Mechanical properties of woven laminates and felt composites using carbon fibers. Part 1: in-plane properties", *Composites Science and Technology*, **64**, pp.2221-2229

[81] Kim, J., Shioya, M., Kobayashi, H., Kaneko, J., Kido, M., (2004), "Mechanical properties of woven laminates and felt composites using carbon fibers. Part 2: interlaminar properties", *Composites Science and Technology*, **64**, pp.2231-2238

[82] Bradley, L.R., Bowen, C.R., McEnaney, B., Johnson, D.C., (2007), "Shear properties of a carbon/carbon composite with non-woven felt and continuous fibre reinforcement layers", *Carbon*, **45**, pp.2178-2187

[83] Lee, L., Rudov–Clark, S., Mouritz, A.P., Bannister, M.K., Herszberg, I., (2002), "Effect of weaving damage on the tensile properties of three-dimensional woven composites", *Composite Structures*, **57**, pp.405-413

[84] Bannister, M., Herszberg, I., Nicolaidis, A., Coman, F., Leong, K.H., (1998), "The manufacture of glass/epoxy composites with multilayer woven architectures", *Composites Part A*, **29A**, pp.293-300

[85] Mouritz, A.P., Baini, C., Herszberg, I., (1999), "Mode I interlaminar fracture toughness properties of advanced textile fibreglass composites", *Composites Part A*, **30**, pp.859-870

[86] Callus, P.J., Mouritz, A.P., Bannister, M.K., Leong, K.H., (1999), "Tensile properties and failure mechanisms of 3D woven GRP composites", *Composites Part A*, **30**, pp.1277-1287

[87] Rudov–Clark, S., Mouritz, A.P., Lee, L., Bannister, M.K., (2003), "Fibre damage in the manufacture of advanced three-dimensional woven composites", *Composites Part A*, **34**, pp.963-970

[88] Khondker, O.A., Herszberg, I., Hamada, H., (2004), "Measurements and prediction of the compression-after-impcat strength of glass knitted textile composites", *Composites Part A*, **35**, pp.145-157

[89] Kim, K.–Y., Curiskis, J.I., Ye, L., Fu, S.–Y., (2005), "Mode-I interlaminar fracture behaviour of weft-knitted fabric reinforced composites", *Composites Part A*, **36**, pp.954-964

[90] Dransfield, K., Baillie, C., Mai, Y.–W., (1994), "Improving the delamination resistance of CFRP by stitching – A review", *Composites Science and Technology*, **50**, pp.305-317

[91] Mouritz, A.P., Leong, K.H., Herszberg, I., (1997), "A review of the effect of stitching on the in-plane mechanical properties of fibre-reinforced polymer composites", *Composites Part A*, **28A**, pp.979-991

[92] Jain, L.K., Mai, Y.–W., (1994), "On the effect of stitching on Mode I delamination toughness of laminated composites", *Composites Science and Technology*, **51**, pp.331-345

[93] Guenon, V.A., Chou, T.–W., Gillespie Jr., J.W., (1989), "Toughness properties of a three-dimensional carbon-epoxy composite", *Journal of Materials Science*, **24**, pp.4168-4175

[94] Savona, S.C., (2003), "Energy absorbing composites for crash energy management", *PhD thesis*, **Queen Mary, University of London**

[95] Aymerich, F., Priolo, P., (2008), "Characterization of fracture modes in stitched and unstitched cross-ply laminates subjected to low-velocity impact and compression after impact loading", *International Journal of Impact Engineering*, **35**, pp.591-608

[96] Byun, J.–H., Gillespie Jr., J.W., Chou, T.–W., (1990), "Mode I delamination of a three-dimensional fabric composite", *Journal of Composite Materials*, **24**, pp.497-518

[97] Shu, D., Mai, Y.–W., (1993), "Effect of stitching on interlaminar delamination extension in composite laminates", *Composites Science and Technology*, **49**, pp.165-171

[98] Jain, L.K., Mai, Y.–W., (1994), "Analysis of stitched laminated ENF specimens for interlaminar mode II fracture toughness", *International Journal of Fracture*, **68**, pp.219-244

[99] Jain, L.K., Mai, Y.–W., (1995), "Determination of Mode II delamination toughness of stitched laminated composites", *Composites Science and Technology*, **55**, pp.241-253

[100] Tanzawa, Y., Watanabe, N., Ishikawa, T., (2001), "FEM simulation of a modified DCB test for 3-D orthogonal interlocked fabric composites", *Composites Science and Technology*, **61**, pp.1097-1107

[101] Brandt, J., Drechsler, K., Arendts, F.–J., (1996), "Mechanical performance of composites based on various three-dimensional woven-fibre performs", *Composites Science and Technology*, **56**, pp.381-386

[102] Velmurugan, R., Solaimurugan, S., (2007), "Improvements in Mode I interlaminar fracture toughness and in-plane mechanical properties of stitched glass/polyester composites", *Composites Science and Technology*, **67**, pp.61-69

[103] Herakovich, C.T., (1989), "Failure modes and damage accumulation in laminated composites with free edge", *Composites Science and Technology*, **36**, pp.105-119

[104] Hunston, D.L., Bascom, W.D., (1983), "Effects of lay-up, temperature, and loading rate in double cantilever beam tests of interlaminar crack growth", *Composites Technology Review*, **5**(Winter), pp.118-119

[105] Laksimi, A., Benzeggagh, M.L., Jing, G., Hecini, M., Roelandt, J.M., (1991), "Mode I interlaminar fracture of symmetrical cross-ply composites", *Composites Science and Technology*, **41**, pp.147-164

[106] Robinson, P., Song, D.Q., (1992), "A modified DCB specimen for Mode I testing of multidirectional laminates", *Journal of Composite Materials*, **26**(11), pp.1554-1577

[107] Polaha, J.J., Davidson, B.D., Hudson, R.C., Pieracci, A., (1996), "Effects of mode ratio, ply orientation and precracking on the delamination toughness of a laminted composite", *Journal of Reinforced Plastic and Composites*, **15**(February), pp.141-173

[108] Chou, I., (1998), "Effect of fiber orientation and moisture absorption on the interlaminar fracture toughness of CFRP laminates", *Advanced Composite Materials*, **7**(4), pp.377-394

[109] Rhee, K.Y., Koh, S.K., Lee, J.H., (2000), "Mode I fracture resistance characteristics of graphite/epoxy laminated composites", *Polymer Composites*, **21**(2), pp.155-164

[110] de Morais, A.B., Moura, M.F., Marques, A.T., de Castro, P.T., (2002), "Mode-I interlaminar fracture of carbon/epoxy cross-ply composites", *Composites Science and Technology*, **62**, pp.679-686

[111] Pereira, A.B., de Morais, A.B., (2004), "Mode I interlaminar fracture of carbon/epoxy multidirectional laminates", *Composites Science and Technology*, **64**, pp.2261-2270

[112] Shi, Y.B., Hull, D., Price, J.N., (1993), "Mode II fracture of +θ/-θ angled laminate interfaces", *Composites Science and Technology*, **47**, pp.173-184

[113] Bazhenov, S.L., (1995), "Interlaminar and intralaminar fracture modes in 0/90 cross-ply glass/epoxy laminate", *Composites*, **26**, pp.125-133

[114] Lagace, P., Brewer, J., Kassapoglou, C., (1987), "The effect of thickness on interlaminar stresses and delamination in straight-edged laminates", *Journal of Composites Technology & Research*, **9**(3), pp.81-87

[115] Jayatheertha, C., Webber, J.P.H., (1994), "Effects of stacking sequence and thickness on the interlaminar stresses for quasi-isotropic laminated plates with a hole", *Composites Science and Technology*, **51**, pp.601-611

[116] Zhou, G., Davies, G.A.O., (1995), "Impact response of thick glass fibre reinforced polyester laminates", *International Journal of Impact Engineering*, **16**(3), pp.357-374

[117] Found, M.S., Howard, I.C., Paran, A.P., (1997), "Size effects in thin CFRP panels subjected to impact", *Composite Structures*, **38**(1-4), pp.599-607

[118] Agrawal, A., Jar, P.–Y.B., (2003), "Analysis of specimen thickness effect on interlaminar fracture toughness of fibre composites using finite element models", *Composites Science and Technology*, **63**, pp.1393-1402

[119] Naik, N.K., Joglekar, M.N., Arya, H., Borade, S.V., Ramakrishna, K.N., (2004), "Impact and compression after impact characteristics of plain weave fabric composites: effect of plate thickness", *Advanced Composite Materials*, **12**(4), pp.1115-1137

[120] Yokozeki, T., Aoki, Y., Ogasawara, T., (2008), "Experimental characterization of strength and damage resistance properties of thin-ply carbon fiber/toughened epoxy laminates", *Composite Structures*, **82**, pp.382-389

[121] Cantwell, W.J., Morton, J., (1989), "Geometrical effects in the low velocity impact response of CFRP", *Composite Structures*, **12**, pp.39-59

[122] Manders, P.W., Bader, M.G., (1981), "The strength of hybrid glass/carbon fibre composites Part 1 Failure strain enhancement and failure mode", *Journal of Materials Science*, **16**, pp.2233-2245

[123] Manders, P.W., Bader, M.G., (1981), "The strength of hybrid glass/carbon fibre composites Part 2 A statistical model", *Journal of Materials Science*, **16**, pp.2246-2256

[124] French, M.A., Prithard, G., (1993), "The fracture surfaces of hybrid fibre composites", *Composites Science and Technology*, **47**, pp.217-223

[125] Hwang, S.–F., Shen, B.–C., (1999), "Opening-mode interlaminar fracture toughness of interply hybrid composite materials", *Composites Science and Technology*, **59**, pp.1861-1869

[126] Jang, B.Z., Chen, L.C., Wang, C.Z., Lin, H.T., Zee, R.H., (1989), "Impact resistance and energy absorption mechanisms in hybrid composites", *Composites Science and Technology*, **34**, pp.305-335

[127] Woods, D.W., Hine, P.J., Ward, I.M., (1994), "The impact properties of hybrid composites reinforced with high-modulus polyethylene fibres and glass fibres", *Composites Science and Technology*, **52**, pp.397-405

[128] Thanomsilp, C., Hogg, P.J., (2003), "Penetration impact resistance of hybrid composites based on commingled yarn fabrics", *Composites Science and Technology*, **63**, pp.467-482

[129] Hogg, P.J., (2005), "Toughening of thermosetting composites with thermoplastic fibres", *Materials Science and Engineering A*, **412**, pp.97-103

[130] Lee, S.–H., Lee, J.–H., Cheong, S.–K., Noguchi, H., (2008), "A toughening and strengthening technique of hybrid composites with non-woven tissue", *Journal of Materials Processing Technology*, **207**, pp.21-29

[131] Dhakal, H.N., Zhang, Z.Y., Richardson, M.O.W., Errajhi, O.A.Z., (2007), "The low velocity impact response of non-woven hemp fibre reinforced unsaturated polyester composites", *Composite Structures*, **81**, pp.559-567

[132] Hojo, M., Ando, T., Tanaka, M., Adachi, T., Ochiai, S., Endo, Y., (2006), "Modes I and II interlaminar fracture toughness and fatigue delamination of CF/epoxy laminates with self-same epoxy interleaf", *International Journal of Fatigue*, **38**, pp.1154-1165

[133] Lu, W.H., Liao, F.S., Su, A.C., Kao, P.W., Hsu, T.J., (1995), "Effect of interleaving on the impact response of a unidirectional carbon/epoxy composite", *Composites*, **26**, pp.215-222

[134] Kishi, H., Kuwata, M., Matsuda, S., Asami, T., Murakami, A., (2005), "Damping performance of thermoplastic-elastomer interleaved CFRP - Effect of viscoelasticity of the interlaminar films and stiffness of the intra-laminar region", *Advanced Composites Letters*, **14**(2), pp.97-104

[135] Ishai, O., Rosenthal, H., Sela, N., Drukker, E., (1988), "Effect of selective adhesive interleaving on interlaminar fracture toughness of graphite/epoxy composite laminates", *Composites*, **19**(1), pp.49-54

[136] Sela, N., Ishai, O., Banks–Sills, L., (1989), "The effect of adhesive thickness on interlaminar fracture toughness of interleaved CFRP specimens", *Composites*, **20**(3), pp.257-264

[137] Rechak, S., Sun, C.T., (1990), "Optimal use of adhesive layers in reducing impact damage in composite laminates", *Journal of Reinforced Plastic and Composites*, **9**, pp.569-582

[138] Altus, E., Ishai, O., (1990), "The effect of soft interleaved layers on the combined transverse cracking/delamination mechanisms in composite laminates", *Composites Science and Technology*, **39**, pp.317-348

[139] Matsuda, S., Hojo, M., Ochiai, S., Moriya, K., Murakami, A., Usui, Y., Ando, M., (1998), "Mode I interlaminar fracture toughness of ionomer interleaved CFRP laminates", *Journal of the Society of Materials Science (Japan)*, **47**(11), pp.1125-1130

[140] Matsuda, S., Hojo, M., Ochiai, S., Murakami, A., Akimono, H., Ando, M., (1999), "Effect of ionomer thickness on mode I interlaminar fracture toughness for ionomer toughened CFRP", *Composites Part A*, **30**, pp.1311-1319

[141] Matsuda, S., Hojo, M., Murakami, A., Ochiai, S., Moriya, K., Akimoto, H., Ando, M., (2000), "Mode II interlaminar fracture toughness of ionomer interleaved carbon fiber/epoxy laminates", *Journal of the Adhesion Society of Japan*, **37**(2), pp.45-52

[142] Ozdil, F., Carlsson, L.A., (1992), "Mode I interlaminar fracture of interleaved graphite/epoxy", *Journal of Composites Materials*, **26**(3), pp.432-459

[143] Masters, J.E., (1987), "Correlation of impact and delamination resistance in interleafed laminates", *Proceeding of the 6th ICCM/2nd ECCM*, **London, UK**, pp.3.96-3.107

[144] Masters, J.E., (1989), "Improved impact and delamination resistance through interleafing", *Key Engineering Materials*, **37**, pp.13-27

[145] Aksoy, A., Carlsson, L.A., (1992), "Interlaminar shear fracture of interleaved graphite/epoxy composites", *Composites Science and Technology*, **43**, pp.55-69

[146] Hojo, M., Matsuda, S., Tanaka, M., Ochiai, S., Murakami, A., (2006), "Mode I delamination fatigue properties of interlayer-toughened CF/epoxy laminates", *Composites Science and Technology*, **66**, pp.665-675

[147] Carroll, B., (1988), "Improved toughness of carbon fiber composites via the use of thermoplastic interplies", *33rd International SAMPE Symposium*, **March**, pp.78-90

[148] Duarte, A., Herszberg, I., Paton, R., (1999), "Impact resistance and tolerance of interleaved tape laminates", *Composite Structures*, **47**, pp.753-758

[149] Lee, S.–H., Noguchi, H., Kim, Y.–B., Cheong, S.–K., (2002), "Effect of interleaved non-woven carbon tissue on interlaminar fracture toughness of laminated composites: Part I - Mode I", *Journal of Composite Materials*, **36**(18), pp.2153-2168

[150] Lee, S.–H., Noguchi, H., Kim, Y.–B., Cheong, S.–K., (2002), "Effect of interleaved non-woven carbon tissue on interlaminar fracture toughness of laminated composites: Part II - Mode II", *Journal of Composite Materials*, **36**(18), pp.2169-281

[151] Tzetzis, D., (2003), "Feasibility study on the vacuum infusion of composite to composite in-field repairs", *PhD thesis*, **Queen Mary, University of London,**

[152] Kuwata, M., Matsuda, S., Kishi, H., Murakami, A., Hogg, P.J., (2007), "Impact resistance of interleaved FRP using non-woven fabric as interleaf materials", *Journal of the Japan Society for Composite Materials*, **33**(2), pp.55-61

[153] Fracasso, R., Rink, M., Pavan, A., Frassine, R., (2001), "The effects of strain-rate and temperature on the interlaminar fracture toughness of interleaved PEEK/CF composites", *Composites Science and Technology*, **61**, pp.57-63

[154] Jorgensen, O., Horsewell, A., (1997), "On the indentation failure of carbon-epoxy cross-ply laminates, and its suppression by elasto-plastic interleaves", *Acta Materialia*, **45**(8), pp.3431-3444

[155] Singh, S., Partridge, I.K., (1995), "Mixed-mode fracture in an interleaved carbon-fibre/epoxy composite", *Composites Science and Technology*, **55**, pp.319-327

[156] Fujimoto, J., Tanaka, T., Kimpara, I., Tanimoto, T., (1994), "Damping properties under flexural vibration for CFRP/damping materials laminates", *Journal of Japanese Society Composite Materials*, **20**(4), pp.144-153

[157] Fujimoto, J., Tanaka, T., Kimpara, I., Tanimoto, T., (1994), "Damping properties under longitudinal vibration for CFRP/damping materials laminates", *Journal of Japanese Society Composite Materials*, **20**(4), pp.154-161

[158] Akimoto, A., Shonaike, G.O., Usui, Y., Aoki, Y., Murakami, A., Matsuda, S., (2000), "Fracture and damping of ionomer interleaved epoxy composites", *Journal of Thermoplastic Composite Materials*, **13**, pp.314-325

[159] Kishi, H., Kuwata, M., Matsuda, S., Asami, T., Murakami, A., (2004), "Damping properties of thermoplastic-elastomer interleaved carbon fiber-reinforced epoxy composites", *Composites Science and Technology*, **64**, pp.2517-2523

[160] Friedrich, K., Walter, R., Carlsson, L.A., Smiley, A.J., Gillespie Jr., J.W., (1989), "Mechanisms for rate effects on interlaminar fracture toughness of carbon/epoxy and carbon/PEEK composites", *Journal of Materials Science*, **24**, pp.3387-3398

[161] Compston, P., Jar, P.–Y.B., Burchill, P.J., Takahashi, K., (2001), "The effect of matrix toughness and loading rate on the mode-II interlaminar fracture toughness of glass-fibre/vinyl-ester composites", *Composites Science and Technology*, **61**, pp.321-333

[162] Compston, P., Jar, P.–Y.B., Davies, P., (1998), "Matrix effect on the static and dynamic interlaminar fracture toughness of glass-fibre marine composites", *Composites Part B*, **29B**, pp.505-516

[163] Cartie, D.D.R., Irving, P.E., (2002), "Effect of resin and fibre properties on impact and compression after impact performance of CFRP", *Composites Part A*, **33**, pp.483-493

[164] Deng, S., Ye, L., Mai, Y.–W., (1999), "Influence of fibre cross-sectional aspect ratio onmechanical properties of glass-fibre/epoxy composites II. Interlaminar fracture and impact behaviour", *Composites Science and Technology*, **59**, pp.1725-1734

[165] Altstadt, V., Gerth, D., Stangle, M., Recker, H.G., (1993), "Interlaminar crack growth in third-generation thermoset prepreg systems", *Polymer*, **34**(4), pp.907-909

[166] Bibo, G.A., Hogg, P.J., Backhouse, R., Mills, A., (1998), "Carbon-fibre non-crimp fabric laminates for cost-effective damage-tolerant structures", *Composites Science and Technology*, **58**, pp.129-143

[167] Abe, M., Hogg, P.J., (2004), "A minituarized post-impact compression test for curved composites", *11th ECCM 31 May - 3 June*, **Rhodes, Greece**

[168] Bibo, G.A., Hogg, P.J., Kemp, M., (1995), "High-temperature damage tolerance of carbon fibre-reinforced plastics: 2. Post-impact compression properties", *Composites*, **26**, pp.91-102

[169] Davies, G.A.O., Hitchings, D., (1996), "Impact damage and residual strengths of woven fabric glass/polyester laminates", *Composites Part A*, **27A**, pp.1147-1156

[170] Ishikawa, T., Sugimoto, S., Matsushima, M., Hayashi, Y., (1995), "Some experimental findings in compression-after-impact (CAI) tests of CF/PEEK (APC-2) and conventional CF/Epoxy flat plates", *Composites Science and Technology*, **55**, pp.349-363

[171] Prichard, J.C., Hogg, P.J., (1990), "The role of impact damage in post-impact compression testing", *Composites*, **21**, pp.503-511

[172] Sutherland, L., Guedes Soares, C., (2005), "Impact on low fibre-volume glass/polyester rectangular plates", *Composite Structures*, **68**, pp.13-22

[173] Davies, P., Blackman, B.R.K., Brunner, A.J., (1998), "Standard test methods for delamination resistance of composite materials: Current status", *Applied Composite Materials*, **5**, pp.345-364

[174] Kinloch, A.J., (1987), "Adhesion and Adhesives Science and Technology", *Chapman and Hall*, **Chapter 7**, pp.264-337

[175] Hojo, M., Kageyama, K., Tanaka, K., (1995), "Prestandardization study on mode I interlaminar fracture toughness test for CFRP in Japan", *Composites*, **26**, pp.243-255

[176] de Morais, A.B., de Moura, M.F.S.F., (2005), "Assessment of initiation criteria used in interlaminar fracture tests of composites", *Engineering Fracture Mechanics*, **72**, pp.2615-2627

[177] JIS K 7086, (1993), "Testing methods for interlaminar fracture toughness of carbon fiber reinforced plastics"

[178] ASTM D 5528 - 94D, (1994), "Standard test method for Mode I interlaminar fracture toughness of unidirectional fiber-reinforced polymer matrix composites"

[179] ISO 15024, (2001), "Fibre-reinforced plastic composites - Delamination of mode I interlaminar fracture toughness, G_{IC}, for unidirectionally reinforced materials"

[180] Davies, P., Moulin, C., Kausch, H.H., (1990), "Measurement of G_{IC} and G_{IIC} in carbon/epoxy composites", *Composites Science and Technology*, **39**, pp.193-205

[181] Davies, P., Kausch, H.H., Williams, J.G., Kinloch, A.J., Charalambides, M.N., Pavan, A., Moore, D.R., Prediger, R., Robinson, I., Burgoyne, N., Friedrich, K., Wittich, H., Rebelo, C.A., Torres Marques, A., Ramsteiner, F., Melve, B., Fischer, M., Roux, N., Martin, D., Czarnocki, P., Neville, D., Verpoest, I., Goffaus, B., Lee, R., Walls, K., Trigwell, N., Partidge, I.K., Jaussaud, J., Andersen, S., Giraud, Y., Hale, G., McGrath, G., (1992), "Round-robin interlaminar fracture testing of carbon-fibre-reinforced epoxy and PEEK composites", *Composites Science and Technology*, **43**, pp.129-136

[182] O'Brien, T.K., Martin, R.H., (1993), "Round robin testing for Mode I interlaminar fracture toughness of composite materials", *Journal of Composites Technology & Research*, **15**(4), pp.269-281

[183] Reeder, J.R., Demarco, K., Whitley, K.S., (2004), "The use of doubler reinforcement in delamination toughness testing", *Composites Part A*, **35**, pp.1337-1344

[184] Williams, J.G., (1988), "On the calculation of energy release rates for cracked laminates", *International Journal of Fracture*, **36**, pp.101-119

[185] Hashemi, S., Kinloch, A.J., Williams, J.G., (1989), "Corrections needed in double-cantilever beam tests for assessing the interlaminar failure of fibre-composites", *Journal of Materials Science Letters*, **8**, pp.125-129

[186] Caprino, G., (1990), "The use of thin DCB specimens for measuring Mode I interlaminar fracture toughness of composite materials", *Composites Science and Technology*, **39**, pp.147-158

[187] Olsson, R., (1992), "A simplified improved beam analysis of the DCB specimen", *Composites Science and Technology*, **43**, pp.329-338

[188] Ozdil, F., Carlsson, L.A., (1999), "Beam analysis of angle-ply laminate DCB specimens", *Composites Science and Technology*, **59**, pp.305-315

[189] Ye, L., (1992), "Evaluation of Mode-I interlaminar fracture toughness for fiber-reinforced composite materials", *Composites Science and Technology*, **43**, pp.49-54

[190] Tanaka, K., Kageyama, K., Hojo, M., (1995), "Prestandardization study on mode II interlaminar fracture toughness test for CFRP in Japan", *Composites*, **26**, pp.257-267

[191] Davies, P., Sims, G.D., Blackman, B.R.K., Brunner, A.J., Kageyama, K., Hojo, M., Tanaka, K., Murri, G., Rousseau, C., Gieseke, B., Martin, R.H., (1999), "Comparison of test configurations for determination of mode II interlaminar fracture toughness results from international collaborative test programme", *Plastics, Rubber and Composites*, **28**(9), pp.432-437

[192] Martin, R.H., Davidson, B.D., (1999), "Mode II fracture toughness evaluation using four point bend, end notched flexure test", *Plastics, Rubber and Composites*, **28**(8), pp.401-406

[193] Todo, M., Jar, P.–Y.B., Takahashi, K., (2000), "Initiation of a mode-II interlaminar crack from an insert film in the end-notched flexure composite specimen", *Composites Science and Technology*, **60**, pp.263-272

[194] Schuecker, C., Davidson, B.D., (2000), "Evaluation of the accuracy of the four-point bend end-notched flexuretest for Mode II delamination toughness determination", *Composites Science and Technology*, **50**, pp.2137-2146

[195] Davies, P., Casari, P., Carlsson, L.A., (2005), "Influence of fibre volume fraction on Mode II interlaminar fracture toughness of glass/epoxy using the 4ENF specimen", *Composites Science and Technology*, **65**, pp.295-300

[196] Zile, E., Tamuzs, V., (2005), "Mode II delamination of a unidirectional carbon fiber/epoxy composite in four-point bend end-notched flexure tests", *Mechanics of Composite Materials*, **41**(5), pp.383-390

[197] Gillespie Jr., J.W., Carlsson, L.A., Simley, A.J., (1987), "Rate-dependent Mode I interlaminar crack growth mechanisms in graphite/epoxy and graphite/PEEK", *Composites Science and Technology*, **28**, pp.1-15

[198] Mall, S., Law, G.E., Katouzian, M., (1987), "Loading rate effect on interlaminar fracture toughness of a thermoplasitc composite", *Journal of Composite Materials*, **21**, pp.569-579

[199] Smiley, A.J., Pipes, R.B., (1987), "Rate effects on Mode I interlaminar fracture toughness in composite materials", *Journal of Composite Materials*, **21**, pp.670-688

[200] Hashemi, S., Kinloch, A.J., Williams, J.G., (1990), "The effects of geometry, rate and temperature on the Mode I, Mode II and Mixed-Mode I/II interlaminar fracture toug carbon-fibre/Poly(ether-ther ketone) composites", *Journal of Composite Materials*, **24**, pp.918-956

[201] Kinloch, A.J., Shaw, S.J., Tod, D.A., Hunston, D.L., (1983), "Deformation and fracture behaviour of a rubber-toughened epoxy: 1. Microstructure and fracture studies", *Polymer*, **24**, pp.1341-1354

[202] Szekrenyes, A., (2006), "Prestressed fracture specimen for delamination testing of composites", *International Journal of Fracture*, **139**, pp.213-237

[203] Szekrenyes, A., Uj, J., (2006), "Comparison of some improved solutions for mixed-mode composite delamination coupons", *Composite Structures*, **72**, pp.321-329

[204] ASTM D 6671 - 01, (2001), "Standard test method for mixed Mode I - Mode II interlaminar fracture toughness of unidirectional fiber reinforced polymer matrix composites"

[205] Ozdil, F., Carlsson, L.A., (1999), "Beam analysis of angle-ply laminate mixed-mode bending specimens", *Composites Science and Technology*, **59**, pp.937-945

[206] Yan, A.–M., Marechal, E., Nguyen–Dang, H., (2001), "A finite-element model of mixed mode-delamination in laminated composites with an R-curve effect", *Composites Science and Technology*, **61**, pp.1413-1427

[207] Tracy, G.D., Feraboli, P., Kedward, K.T., (2003), "A new mixed mode test for carbon/epoxy composite systems", *Composites Part A*, **34**, pp.1125-1131

[208] Szekrenyes, A., Uj, J., (2004), "Beam and finite element analysis of quasi-unidirectional composite SLB and ELS specimens", *Composites Science and Technology*, **64**, pp.2393-2406

[209] Becht, G., Gillespie Jr., J.W., (1988), "Design and analysis of the crack rail shear specimen for Mode III interlaminar fracture", *Composites Science and Technology*, **31**, pp.143-157

[210] ASTM D 4255 / D 4255M - 01, (2007), "Standard test method for in-plane shear properties of polymer matrix composite materials by the rail shear method"

[211] Nihon Kikai Gakkai, (1990), "Sentan Fukugou Zairyou (Japanese)", *Gihoudou Publication*, **Chapter 15**, pp.179-195

[212] Donaldson, S.L., (1988), "Mode III interlaminar fracture characterization of composite materials", *Composites Science and Technology*, **32**, pp.225-249

[213] Robinson, P., Song, D.Q., (1994), "The development of an improved Mode III delamination test for composites", *Composites Science and Technology*, **52**, pp.217-233

[214] Cantwell, W.J., Morton, J., (1991), "The impact resistance of composite materials - a review", *Composites*, **22**, pp.347-362

[215] Hull, D., Shi, Y.B., (1993), "Damage mechanism characterization in composite damage tolerance investigations", *Composite Structures*, **23**, pp.99-120

[216] Bibo, G.A., Hogg, P.J., (1996), "Review: The role of reinforcement architecture on impact damage mechanisms and post-impact compression behaviour", *Journal of Materials Science*, **31**, pp.1115-1137

[217] Zhou, G., (1998), "The use of experimentally-determined impact froce as a damage measure in impact damage resistance and tolerance of composite structures", *Composite Structures*, **42**, pp.375-382

[218] Christoforou, A.P., (2001), "Impact dynamics and damage in composite structures", *Composite Structures*, **52**, pp.181-188

[219] Baker, A.A., Jones, R., Callinan, R.J., (1985), "Damage tolerance of graphite/epoxy composites", *Composite Structures*, **4**, pp.15-44

[220] Prevorsek, D.C., Chin, H.B., Bhatnagar, A., (1993), "Damage tolerance: design for structural integrity and penetration", *Composite Structures*, **23**, pp.137-148

[221] Sutherland, L., Guedes Soares, C., (2005), "Impact characterisation of low fibre-volume glass reinforced polyester circular laminated plates", *International Journal of Impact Engineering*, **31**, pp.1-23

[222] ASTM E 23, "Standard test methods for notched bar impact testing of metallic materials"

[223] JIS K7077, "Testing method for charpy impact strength of carbon fiber reinforced plastics"

[224] ASTM D2563 - 08, "Standard practice for classifying visual defects in glass-reinforced plastic laminate parts"

[225] Nihon Kikai Gakkai, (1990), "Sentan Fukugou Zairyou (Japanese)", *Gihoudou Publication*, **Chapter 16**, pp.197-210

[226] Ahmadnia, A., (2000), "Energy Absorption of Macrocomposite Laminates", *PhD thesis*, **Queen Mary, University of London**

[227] Summerscales, J., (1990), "Non-destructive Testing of Fibre-reinforced Plastics Composites Volume 2", *Elsevier Applied Science*, **Chapter 2**, pp.55-160

[228] Girshovich, S., Gottesman, T., Rosenthal, H., Drukker, E., Steinberg, Y., (1992), "Impact damage assessment of composites, Damage Detection in Composite Materials", ASTM STP 1128, *American Society for Testing and Materials*, **Philadelphia**, pp.183-199

[229] Abrate, S., (1998), "Impact on composite structures", *Cambridge University Press*, **Chapter 6**, pp.172-214

[230] "Standard tests for toughened resin composites", (1982), *NASA reference publication 1092*

[231] "CRAG test methods for the measurement of the engineering properties of fibre reinforced plastics", (1988), *RAE TR 88012*

[232] "Advanced composite compression test", (1982), *Boeing specification support standard BSS 7620*

[233] "Test method for compression after impact properties of oriented fibre resin composites", (1988), *SRM 2-88*

[234] Uehara, M., Kunoo, K., Uda, N., Ono, K., (2002), "Mechanical consideration of specimen size effect in CFRP's compression after impact (CAI) test", *The Proceeding of The 51st Nat. Cong. Of Theoretical & Applied Mechanics*, pp.465-466

[235] de Freitas, M., Reis, L., (1998), "Failure mechanisms on composite specimens subjected to compression after impact", *Composite Structures*, **42**, pp.365-373

[236] Short, G.J., Guild, F.J., Pavier, M.J., (2002), "Post-impact compressive strength of curved GFRP laminates", *Composites Part A*, **33**, pp.1487-1495

[237] Short, G.J., Guild, F.J., Pavier, M.J., (2002), "Delaminations in flat and curved composite laminates subjected to compressive load", *Composite Structures*, **58**, pp.249-258

[238] JIS K7089, "Testing method for compression after impact properties of carbon fibre reinforced plastic"

[239] ASTM D7137 / D7137M - 07, "Standard Test Method for Compressive Residual Strength Properties of Damaged Polymer Matrix Composite Plates"

[240] Caprino, G., (1984), "Residual strength prediction of impacted CFRP laminates", *Journal of Composite Materials*, **18**, pp.508-518

[241] Hull, D., Clyne, T.W., Miyairi, H., Ikegami, K., Kimpara, I., (2003), "An Introduction to Composite Materials (Japanese Edition)", *Baifukan*, **Chapter 7**, pp.112-133

[242] Cantwell, W.J., Morton, J., (1985), "Detection of impact damage in CFRP laminates", *Composite Structures*, **3**, pp.241-257